Inaugural dissertation

for

obtaining the doctoral degree

of the

Combined Faculty of Mathematics, Engineering, and Natural Sciences

of the

Ruprecht - Karls - University

Heidelberg

Presented by

M.Sc. Lucas Til Arendholz

Born in Bad Saarow-Pieskow, Germany

Oral examination on 29th of April 2024

The role of EBI2 in inflammatory skin diseases

Referees

Prof. Dr. Ana Martin-Villalba

Prof. Dr. Alexander Enk

Table of Contents

Summary

Epstein-Barr virus-induced gene 2 (EBI2), also known as G protein-coupled receptor 183 (GPR183), is a chemotactic receptor. Its ligand 7α,25-dihydroxycholesterol (7α,25-OHC) is an oxysterol and is produced by the enzymes cholesterol 25-hydroxylase (CH25H) and cytochrome P450 family 7 subfamily B member 1 (CYP7B1). The EBI2-oxysterol axis has been shown to be critical for the correct development and microanatomical positioning of immune cells in primary and secondary lymphoid organs (SLOs). It is part of the chemotactic network that guides the intricate intranodal migration of B cells, T cells, and dendritic cells. Deficiency in EBI2 or CH25H leads to impaired B- and T cell priming. In line with its chemotactic function in SLOs, the EBI2-oxysterol axis has been associated with several disease pathologies. There, it was shown to be involved in the recruitment of pathogenic cells and formation of tertiary lymphoid structures in diseases affecting the joints, the lung, the central nervous system, and the intestine. Recent reports also suggest a contribution of the EBI2-oxysterol axis in the pathogenesis of inflammatory skin diseases; however, conclusive studies are missing. Tissue-resident memory T (T_{RM}) cells are known drivers of peripheral diseases. They are especially well described in the skin, where they mediate site-specific relapses of chronic inflammatory disorders. To date, nothing is known about the connection between the EBI2-oxysterol axis, inflammatory skin diseases and T_{RM} cells.

Here I show that EBI2 expression is a characteristic feature of T_{RM} cells. Utilizing an EBI2-enhanced green fluorescent protein (EGFP) knock-in mouse line that functions both as a reporter and a knock-out, I found that murine T_{RM} cell progenitor cells upregulate EBI2 during differentiation to T_{RM} cells in the skin. Consequently, murine skin T_{RM} cells highly express EBI2. In contrast, only minor proportions of circulating $CD8^+$ naïve and memory T cells express EBI2. This induction of EBI2 on T_{RM} cells suggests a functional relevance. Similarly, I found that the majority of T_{RM} cells from healthy human skin also expresses EBI2. I therefore launched a clinical study to analyze skin biopsies from psoriasis patients using high parameter flow cytometry. While T_{RM} cells from non-lesional and lesional skin showed similar EBI2 expression, I found that the EBI2 expression level was associated with a functional dichotomy. $EBI2^{high}$ T_{RM} cells showed higher proportions of effector molecule-producing cells than $EBI2^{low}$ T_{RM} cells. They were further enriched in cells producing granzyme B, interferon-γ, interleukin-10, and Ki-67 and decreased in cells expressing the exhaustion marker CD101. This suggests that EBI2 is part of the $T_{RM}1$ phenotype, shown to be an important mediator of vitiligo and host defense. It will therefore be interesting to investigate the role of the EBI2-oxysterol axis in vitiligo pathogenesis and viral infection. However, in mice, EBI2 deficiency had no impact on T_{RM} cell generation, retention, subset distribution, or on allergic contact dermatitis and psoriasis mouse models. Collaboration partners showed that EBI2 is also expressed by human lung and colon T_{RM} cells. Elucidating the role of EBI2 on T_{RM} cells and its involvement in T_{RM} cell-mediated host defense and skin disease pathogenesis is therefore an interesting topic for future investigations with potential therapeutical implications.

Zusammenfassung

Epstein-Barr Virus-induziertes Gen 2 (EBI2), auch bekannt als G Protein-gekoppelter Rezeptor 183 (GPR183), ist ein chemotaktischer Rezeptor. Sein Ligand 7α,25-Dihydroxycholesterin (7α,25-OHC) ist ein Oxysterol und wird von den Enzymen Cholesterin 25-Hydroxylase (CH25H) und Cytochrom P450 Familie 7 Unterfamilie B Mitglied 1 (CYP7B1) produziert. Es wurde gezeigt, dass die EBI2-Oxysterol-Achse wichtig für die korrekte Entwicklung und mikroanatomische Positionierung von Leukozyten in den primären und sekundären lymphatischen Organen (SLO) ist. Sie ist Teil des chemotaktischen Netzwerks, das die komplexe intranodale Migration von B-Zellen, T-Zellen und dendritischen Zellen steuert. EBI2- oder CH25H-Defizienz führt zu einer verminderten Aktivierung naiver B- und T-Zellen. Darüber hinaus wurde die EBI2-Oxysterol-Achse mit vielen Krankheits-pathologien in Verbindung gebracht. Analog zu ihrer chemotaktischen Funktion in den SLO wurde gezeigt, dass die EBI2-Oxysterol-Achse bei bestimmten Erkrankungen der Lunge, der Gelenke, des zentralen Nervensystems und des Darms für die Rekrutierung pathogener Zellen und / oder die Bildung tertiärer lymphatischer Strukturen verantwortlich ist. Jüngste Studien suggerierten außerdem eine Beteiligung der EBI2-Oxysterol-Achse bei der Pathogenese inflammatorischer Hautkrankheiten. Dies ist bis heute jedoch nicht eindeutig nachgewiesen. Weiterhin ist bekannt, dass gewebe-residente Gedächtnis-T-Zellen (englisch: *tissue-resident memory T cells*, T_{RM}-Zellen) eine Vielzahl von Erkrankungen in peripheren Geweben vermitteln. Sie sind besonders gut in der Haut charakterisiert und dort für die lokale Persistenz von chronischen Krankheiten verantwortlich. Es ist bis heute nicht bekannt, ob es eine Verbindung zwischen der EBI2-Oxysterol-Achse, entzündlichen Hauterkrankungen und T_{RM}-Zellen gibt.

In dieser Arbeit zeige ich, dass EBI2 Expression ein charakteristisches Merkmal von T_{RM}-Zellen ist. Unter Verwendung einer EBI2-EGFP (englisch: *enhanced green fluorescent protein*) Knock-in-Mauslinie, die sowohl als Reporter als auch als Knock-out fungiert, habe ich herausgefunden, dass murine T_{RM}-Zell-Vorläuferzellen EBI2 während ihrer Differenzierung zu T_{RM}-Zellen in der Haut hochregulieren. Infolgedessen exprimieren murine T_{RM}-Zellen stark EBI2. Im Gegensatz dazu exprimiert nur ein geringer Anteil der zirkulierenden $CD8^+$ naiven und Gedächtnis-T-Zellen EBI2. Die Induktion von EBI2 auf Haut-T_{RM}-Zellen suggeriert somit eine funktionelle Relevanz. Gleichermaßen habe ich in gesunder menschlicher Haut beobachtet, dass nahezu alle T_{RM}-Zellen EBI2 exprimieren. Daher habe ich eine klinische Studie initiiert, um Hautbiopsien von Psoriasis Patienten mittels hochparametrischer Durchflusszytometrie zu charakterisieren. Obwohl T_{RM}-Zellen aus nicht-läsionaler und läsionaler Haut eine ähnliche EBI2 Expression aufwiesen, stellte ich fest, dass eine unterschiedliche Expressionsstärke von EBI2 mit einer funktionellen Dichotomie der T_{RM}-Zellen verbunden war. Stark-EBI2-exprimierende T_{RM}-Zellen wiesen höhere Anteile an Effektormolekül-produzierenden Zellen auf als niedrig-EBI2-exprimierende T_{RM}-Zellen. Sie waren angereichert in Granzym-B-, Interferon-γ-, Interleukin-10- und Ki-67-exprimierenden Zellen, und wiesen weniger Zellen auf, die den *Exhaustion*-Marker CD101 exprimierten. Dies deutet darauf hin, dass EBI2 Teil des

T_{RM}1 Phänotyps ist, der nachweislich eine wichtige Rolle bei Vitiligo und der Wirtsabwehr darstellt. Es sollte es interessant sein die Rolle der EBI2-Oxysterol-Achse bei der Vitiligo-Pathogenese und bei Virusinfektionen zu untersuchen. Eine Defizienz von EBI2 in Mäusen hatte jedoch weder Einfluss auf die Bildung von T_{RM}-Zellen, ihre Retention, ihre Subgruppen Generierung, oder auf den Grad der Entzündung bei allergischen Kontaktekzem- und Psoriasis-Mausmodellen. Kooperationspartner zeigten außerdem, dass EBI2 auch von T_{RM}-Zellen der Lunge und des Dickdarms exprimiert wird. Der Nachweis einer potenziellen Funktion von EBI2 auf T_{RM}-Zellen sowie die Klärung der Frage, wie die EBI2-Oxysterol-Achse an der T_{RM}-Zell-vermittelten Wirtsabwehr und Pathogenese von Hautkrankheiten beteiligt ist, stellt daher ein interessantes Thema für künftige Forschung mit potenziell therapeutischer Anwendung dar.

List of Abbreviations

#	number
%	percent
°C	degrees Celsius
µg	micro gram
µL	microliter
25-OHC	25-hydroxycholesterol
7TM	seven transmembrane
7α,25-OHC	7α,25-dihydroxycholesterol
Å	ångström
A. dest	*Aqua destillata*
A	adenine
a.U.	arbitrary units
ACD	allergic contact dermatitis
ACK	ammonium-chloride-potassium
AD	atopic dermatitis
AF	Alexa Fluor
AMP	antimicrobial peptide
APC	antigen-presenting cell or allophycocyanine
ATP	adenosine triphosphate
AUC	area under the curve
Blimp1	B-lymphocyte-induced maturation protein 1
BMDCs	bone marrow-derived dendritic cells
BMI	body mass index
BSA	bovine serum albumin
BUV	brilliant ultraviolet
BV	brilliant violet
C	carbon or cytosine
CAD	chronic atopic dermatitis
cAMP	cyclic adenosine monophosphate
CD	cluster of differentiation
CD4SP	CD4 single positive
cDC	conventional dendritic cell
cDNA	complementary deoxyribonucleic acid
CH25H	cholesterol 25-hydroxylase
CHS	contact hypersensitivity
CLA	cutaneous lymphocyte antigen
cm	centimeter
CNS	central nervous system
COPD	chronic obstructive pulmonary disease
Covid-19	coronavirus disease 2019
CRTAM	class I-restricted T cell-associated molecule
CTL	cytotoxic T lymphocyte
CTRL	control
Cy	cyanine
CYP7B1	cytochrome P450 family 7 subfamily B member 1
d	day
Da	Dalton
DAMP	danger-associated molecular pattern
dATP	deoxyadenosine triphosphate
DC	dendritic cell
dCTP	deoxycytidine triphosphate
dDC	dermal dendritic cell
dds	DESeq2 data set
DEG	differentially expressed gene
DETC	dendritic epidermal T cell
dGTP	deoxyguanosine triphosphate
dLN	draining lymph node
DMSO	dimethyl sulfoxide
DNA	deoxyribonucleic acid
DNFB	2,4-dinitrofluorobenzene
dNTP	deoxynucleotide triphosphate
doi	digital object identifier
DTH	delayed-type hypersensitivity
dTTP	deoxythymidine triphosphate
DUSP6	dual-specificity phosphatase 6
e.g.	*exempli gratia*
EAE	experimental autoimmune encephalitis
EBI2	Epstein-Barr virus-induced gene 2
EBV	Epstein-Barr virus
ECM	extracellular matrix
edLN	ear-draining lymph node
EDTA	ethylenediaminetetraacetic acid
EM	electron microscopy
et al.	*et alia*
EtOH	ethanol

FACS	fluorescence-activated cell sorting
Fc	fragment crystallizable (of an Ig)
FCS	fetal calf serum
FDC	follicular dendritic cell
FDE	fixed drug eruption
FITC	fluorescein-5-isothiocyanate
fl	floxed
FMO	fluorescence minus one
FRC	follicular reticular cell
frt	flippase recognition target
FSC-A	forward scatter - area
FTY720	fingolimod
g	gram or gravitational constant
G	gauge or guanine
GC	germinal center
GDP	guanosine diphosphate
GEO	gene expression omnibus
GOI	gene of interest
GPCR	G protein-coupled receptor
GPR183	G protein-coupled receptor 183
GRK	GPCR kinases
GTP	guanosine triphosphate
GV-SOLAS	*Gesellschaft für Versuchstierkunde* / Society of Laboratory Animal Science
GWAS	genome-wide association study
GZMB	granzyme B
h	hour
H	hydrogen
HCl	hydrochloric acid
HEPES	4-(2-hydroxyethyl)-1-piperazineethanesulfonic acid
het	heterozygote
HEV	high endothelial venule
HIV	human immunodeficiency virus
Hobit	homolog of Blimp-1 in T cells
hom	homozygote
HSB3B7	C_{27} 3β-HSD7, 3β-hydroxysteroid dehydrogenase type 7
HSV	herpes simplex virus
i.e.	*id est*
i.p.	intraperitoneal
i.v.	intravenous
iBALT	inducible bronchus-associated lymphoid tissue
IBD	inflammatory bowel disease
IBF	interfaculty biomedical research department
ICAM1	intercellular adhesion molecule 1
ICOSL	inhibitor of co-stimulation ligand
ID	identification number
IEC	intestinal epithelial cell
IFN-γ	interferon γ
Ig	immunoglobulin
IgA	immunoglobulin A
IGA	investigator's global assessment score
IL	interleukin
ILC	innate lymphoid cell
ILC2	type 2 innate lymphoid cells
iLNs	inguinal lymph node
IMQ	Imiquimod
iSALT	inducible skin-associated lymphoid tissue
ITEM	Institute for Toxicology and Experimental Medicine
JAK	Janus kinase
K	potassium
KCl	potassium chloride
kg	kilogram
KLF	Kruppel-like factor
KLRG1	killer cell lectin-like receptor G1
KO	knock-out
L	lesional or liter
LF	lymphoid follicle
LFA-1	lymphocyte function-associated protein 1
LN	lymph node
LPS	lipopolysaccharide
M	molar (mol/L)
mAB	monoclonal antibody
MAIT	mucosal-associated invariant T cell
MEM	minimum essential medium
MFI	mean fluorescence intensity
mg	milligram
MGI	mouse genome informatics
$MgCl_2$	magnesium chloride

MHC	major histocompatibility complex
mL	milliliter
MLC	memory lymphocyte cluster
mm	millimeter
MP	memory progenitor
MPEC	memory progenitor effector cell
MRC	marginal reticular cells
mRNA	messenger ribonucleic acid
MS	multiple sclerosis
mTEC	medullary thymic epithelial cells
mTOR	mammalian target of rapamycin
M-Mulv	Moloney murine leukemia virus
mV	millivolt
MZ	marginal zone
N_2	nitrogen
n	number
NaN_3	sodium azide
NaOH	sodium hydroxide
NeoR	neomycin resistance gene
NaCl	sodium chloride
NF-κB	nuclear factor κ-light-chain-enhancer of activated B cells
ng	nanogram
NKT	natural killer T cell
NL	non-lesional
nM	nanomolar
O_2	oxygen
OCP	osteoclast progenitor cell
OHC	mono/dihydroxycholesterol
PASI	psoriasis area and severity index
PBL	peripheral blood leukocyte
PBMC	peripheral blood mononuclear cell
PBS	phosphate-buffered saline
PCA	principal component analysis
PCLS	precision-cut lung slices
PD-1	programmed cell death protein 1
pDC	plasmacytoid dendritic cell
PE	phycoerythrin
Pen/ Strep	penicillin/ streptomycin
PerCP	Peridinin-Chlorophyll-Protein
PKA	protein kinase A
PMA	phorbol 12-myristate 13-acetate
pMHC	peptide:MHC complex
pmol	picomole
PRR	pattern recognition receptor
qRT-PCR	quantitative reverse transcription polymerase chain reaction
RORγt	RAR-related orphan receptor γ t
RPMI	Roswell Park Memorial Institute
RT	room temperature
Runx3	RUNX family transcription factor 3
S1P	sphingosine 1 phosphate
$S1P_1$	sphingosine 1 phosphate receptor 1
scFv	single chain variable fragment
scRNAseq	single-cell ribonucleic acid sequencing
sdLN	skin-draining lymph node
SDS	sodium dodecyl sulfate
SLEC	short-lived effector cell
SLO	secondary lymphoid organ
SNP	single nucleotide polymorphism
SPF	specific-pathogen free
SSC-A	side scatter - area
T	thymine
TAE	Tris-acetate-EDTA
T17 cells	T cells type 17
T_C1 cells	cytotoxic T lymphocytes type 1
T_C17 cells	cytotoxic T lymphocytes type 17
T_{CM} cells	central memory T cell
TCR	T cell receptor
TCRV	TCR variable chain
T_H17 cells	helper T lymphocytes type 17
T_E	terminal effector cell
T_{EM} cells	effector memory T cell
T_{EMRA} cells	effector memory T cell re-expressing CD45RA
T_{FH}	follicular helper T cell
TGF-β	transforming growth factor β

TIL	tumor-infiltrating lymphocyte
TLS	tertiary lymphoid structure
T_N cells	naive T cell
TNCB	2,4,6-trinitrochlorobenzene
TNF-α	tumor-necrosis factor α
TRC	T zone reticular cell
T_{RM} cells	tissue-resident memory T cell
$T_{RM}1$ cells	T_{RM} cells of type 1
$T_{RM}17$ cells	T_{RM} cells of type 17
TSLP	thymic stromal lymphopoietin
U	unit
UMAP	uniform manifold approximation and projection
VCAM-1	vascular cell adhesion molecule 1
VD3	vitamin D3
WT	wild type
Δ	delta (deleted / knock-out)

Figures

Tables

1. Introduction

1.1. T cell memory generation

1.1.1 Priming of naïve T cells in secondary lymphoid organs

T cells and B cells constitute the adaptive immune system. A hallmark of adaptive immunity is the ability to form immune memory. For this, mature naïve lymphocytes are primed in specialized organs called secondary lymphoid organs (SLOs), which include the spleen and lymph nodes. Mature naïve lymphocytes travel through the blood, enter the SLOs through specialized vasculature only found in SLOs, called high endothelial venules (HEVs), and then exit the lymphatic system again into the blood[1]. This process is called recirculation. L-selectin (CD62L) is expressed on recirculating cells and interacts with a sulfated mucin-like glycoprotein 6-sulfo sialyl Lewis^X on the endothelium. Slowed down and tethered to the endothelium by this interaction, lymphocytes recognize chemokines like CCL19 and CCL21 displayed by the endothelial cells[1,2]. Recirculating lymphocytes express CCR7, the receptor for CCL19 and CCL21, on their surface, and CCR7 signaling activates integrins on the lymphocytes. The most prominent integrin activated in this way is the lymphocyte function-associated antigen 1 (LFA-1). It interacts with the intercellular adhesion molecule 1 (ICAM-1) on the HE vs Ultimately, this leads to firm adhesion and transendothelial migration into the SLO[1]. Therefore, lymphocytes capable of recirculating through the SLOs can be identified by expression of CD62L and CCR7.

Chemokines organize the SLOs by attracting different cell types to different microanatomical niches. The main producers of these chemokines are stromal cells, particularly follicular reticular cells (FRCs) and follicular dendritic cells (FDCs). FRCs produce CCL19 and CCL21, attracting T cells to the T zone through CCR7[3]. FDCs produce CXCL13, which is recognized by B cells through CXCR5, and directs them into the B cell follicle, where the FDCs are situated[4]. This spatial segregation enhances the efficiency with which B- and T cells find their cognate antigen presented by dendritic cells (DCs). DCs, as professional antigen-presenting cells (APCs), capture antigen in the periphery, shuttle it to the SLOs, and break down protein antigens into peptides. The peptides are then presented to T cells on major histocompatibility complex (MHC) class I or II molecules. CD4$^+$ T cells are restricted to recognize peptides in the context of MHC class II, and CD8$^+$ T cells are restricted to MHC class I. Recognition of their cognate peptide:MHC (pMHC) complex induces firm adhesion of the T cells to the DCs and allows the formation of the immunological synapse. This is an intricately organized molecular structure, which concentrates important molecules on the cell surfaces in one location. It consists of adhesion molecules (T cell: LFA-1 and DC: ICAM1), co-stimulatory molecules (T cell: CD28 and DC: CD80/CD86), and multiple T cell receptor (TCR)-pMHC complexes[5].

Activation of a T cell induces the rapid expression of CD69[6] within the first hours after antigen contact. CD69 is one of the most widely used markers to assess lymphocyte activation in SLOs. Its upregulation serves the purpose of inhibiting the sphingosine-1-phosphate (S1P)-mediated tissue egress. A constant gradient of the chemoattractant S1P originates from the blood and lymph. It is sensed by lymphocytes through S1P receptors and predominantly through S1P

receptor 1 ($S1P_1$). This is a universal system, directing all recirculating lymphocytes from tissues (including SLOs) into the blood. However, because lymphocyte activation is a process that takes many days, lymphocytes need to suppress this immediate egress. CD69 acts as a direct inhibitor of $S1P_1$ causing its downregulation through direct interaction[7]. After differentiation lymphocytes downregulate CD69, allowing cell surface upregulation of $S1P_1$ and ultimately to the egress of differentiated B- and T cells into the blood.

1.1.2 Differentiation of primed naïve T cells into memory and effector T cells

Activation of a T_N (naïve T) cell by a professional APC induces epigenetic and transcriptional changes in the T cell. Epigenetic remodeling allows access of the transcription machinery to the different genes and initiates transcription and translation into a protein. This process is called differentiation and it stably alters the properties of the T cell[8–10].

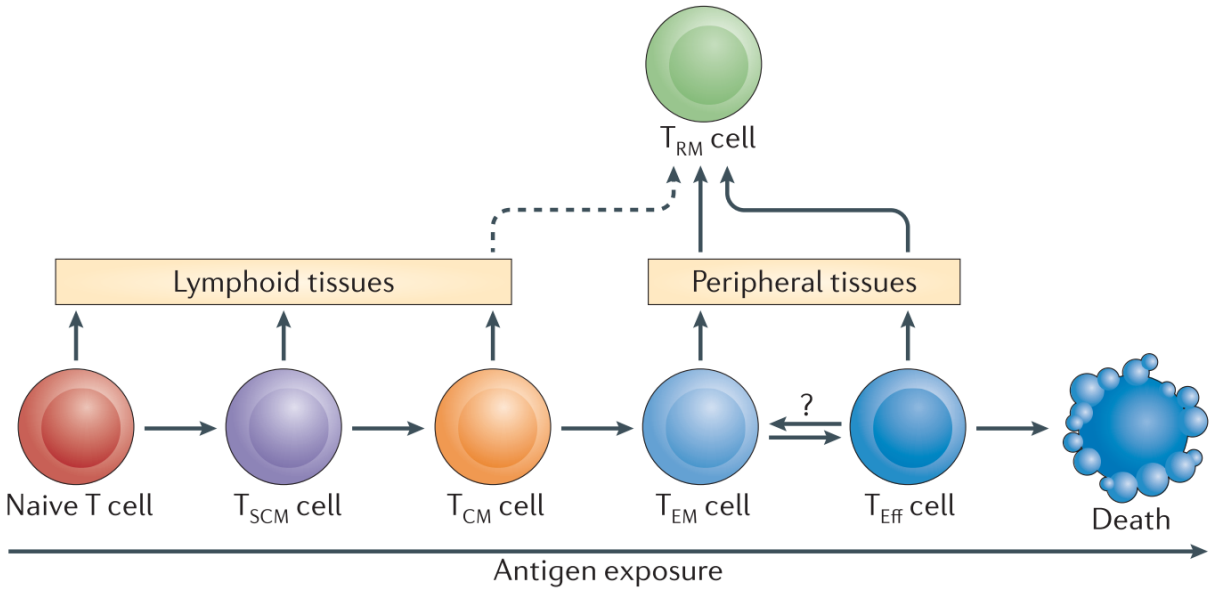

Figure 1. Linear model of memory T cell generation. From Farber, Yudanin *et al*., 2014[11]. Linear, progressive, or hierarchical model of memory T cell generation. Increasing extent of activation and signaling intensity by antigen exposure drives the differentiation of naïve T cells towards different memory T cell subtypes. In this linear model, progressive differentiation correlates with decreasing ability to differentiate into different memory populations and with increasing effector function and peripheral tissue tropism. Follicular T helper (T_{FH}) cells would arise from T_{SCM} cells or progenitor T_{CM} cells[12]. Dotted line: T_{RM} cells were found to reside also in SLOs; it is possible that T_{CM} cells can give rise to these SLO T_{RM} cells[8,13]. T_{SCM}: stem cell memory T cell; T_{CM}: central memory T cell; T_{EM}: effector memory T cell; T_{EFF}: effector T cell; T_{RM} cell: tissue-resident memory T cell.

Primed T_N cells give rise to effector and memory T cells. However, the way how different memory and effector subsets are generated from T_N cells remains a point of active discussion and research[9,14,15]. The linear differentiation model (also progressive or hierarchical differentiation model), originally proposed by Sallusto and Lanzavecchia in 2002 (Figure 1)[16],

is supported by many experimental evidences and regarded as the most likely model by many researchers[8,9,14]. However, there are also strong supporting data for other differentiation models like the asymmetric cell division model. It states that through inaccuracies in cell division, the two daughter cells are provided with unequal sets of proteins and other factors, which leads to initiation of different differentiation programs[9]. Many of the experimental approaches used to study memory T cell generation employed adoptive transfer of sorted memory T cell populations, tracing of the transferred cells, and evaluation of their ability to reconstitute the memory T cell pool and to fend off infection.

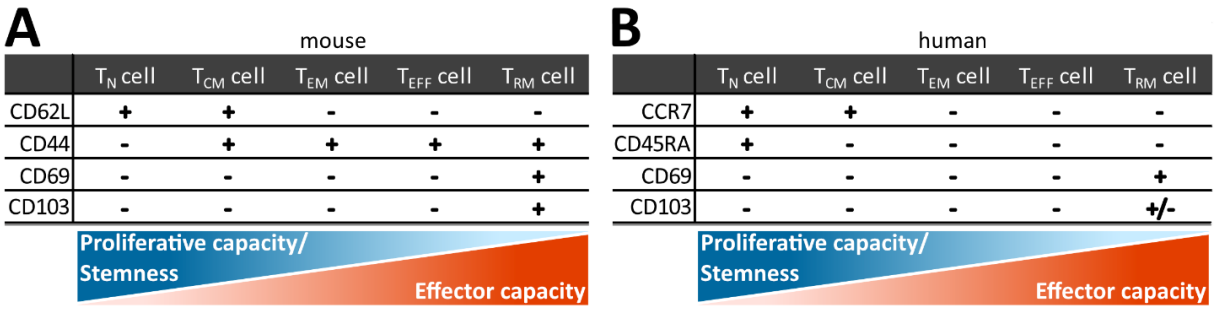

Figure 2. Characteristics of memory T cell subsets in mouse and human. A Murine and **B** human T cells are categorized into circulating and T_{RM} cells, based on their expression of CD69. CD62L / CCR7 expression indicates a T cell's ability to recirculate from the blood through SLOs. CD44 is a marker of antigen-experienced T cells, i.e. memory T cells. CD45RA is an isoform of the CD45 antigen, which is expressed by naïve T cells. Memory T cells express the alternatively spliced form CD45RO. Mouse T_{RM} cells are generally regarded to express CD103, while CD103 expression in human T_{RM} cells is dependent on their tissue of origin[17]. Proliferation capacity / stemness refers to a cells' potential to undergo clonal expansion and to generate different types of progenies. Effector capacity refers to a cells' potential to produce effector molecules and directly contribute to host defense. T_N: naïve T cell, T_{CM}: central memory T cell; T_{EM}: effector memory T cell; T_{EFF}: effector T cell; T_{RM} cell: tissue-resident memory T cell.

The different memory T cell subsets are characterized based on their expression of trafficking molecules and based on their proliferative or respective effector capacity **(**Figure 2). T_N cells (mouse: $CD62L^+CD44^-$, human: $CCR7^+CD45RA^+$) possess the greatest proliferative capacity and limited ability to produce effector molecules. Their purpose is to circle through the SLOs, find their antigen, become activated, and generate memory and effector T cells that are capable of defending the host[8,9,16].

Central memory T (T_{CM}) cells (mouse: $CD62L^+CD44^+$, human: $CCR7^+CD45RA^-$) still have great potential to readily proliferate and to differentiate into effector memory T (T_{EM}) cells upon a secondary antigen encounter. However, their capabilities to produce effector molecules and to actively contribute to host defense are limited. They represent a reservoir to mount a rapid immune response. T_{CM} cells recirculate constantly through the whole body. They can briefly enter peripheral tissues but do not become sessile. They follow the S1P gradient back into the

blood and then continue to recirculate. By this, T_{CM} cells scan the body for any foreign agents to immediately initiate a secondary host defense response, faster than the primary response[8,9,16,18].

T_{EM} cells (mouse: $CD62L^{-}CD44^{+}$, human: $CCR7^{-}CD45RA^{-}$) possess very limited proliferative capabilities upon secondary antigen encounter[9,18]. Their lack of expression of SLO homing molecules is indicative of their tropism. T_{EM} cells patrol peripheral tissues, but, like T_{CM} cells, eventually exit them. They are unable to recirculate through the SLOs and their tropism is therefore blood and tissue confined[19]. They are specialized in producing effector molecules such as cytokines, granzymes, and perforins[8,18]. However, T_{EM} cells possess some degree of stemness as they are regarded as progenitor cells for tissue-resident memory T (T_{RM}) cells[20-22]. T_{RM} cells are non-recirculating memory T cells, that reside in peripheral tissue for decades and are marked by the expression of CD69. This is a hallmark of T_{RM} cells, as CD69 promotes their tissue retention by downregulation of $S1P_1$ and thereby inhibiting their tissue egress[23]. Furthermore, T_{RM} cells have been shown to undergo *in situ* proliferation after antigen encounter, which is thought to contribute to their longevity and host defense[24]. T_{RM} cells are discussed in more detail in section 1.3. Lastly, effector T (T_{EFF}) cells are terminally differentiated cells. They show virtually no ability to proliferate or give rise to other types of cells. T_{EFF} cells are essential in mediating rapid host defense, but are short-lived, as they undergo cell death after a few days. Due to their short-lived nature and lack of SLO homing molecules, their sole purpose seems to be to trafficking to inflamed tissue and exertion of effector function[8,25].

1.2. The skin immune system

The skin is the largest organ of the human body. It is challenged every day by microorganisms and environmental factors and constitutes the first line of defense against them. Fittingly, the skin is lined by immune cells, surveilling it to readily act against foreign agents. It was estimated that approx. 2×10^{10} T cells reside in the skin, which is almost double as much as in the circulation[26]. The skin is made up of three layers: the epidermis, the dermis, and the subcutis (Figure 3). The subcutis harbors most of the larger blood vessels in the skin. It is made up of adipocytes, fibroblasts, and stromal cells and only a few immune cells reside there. Those that do are mainly innate and adaptive lymphocytes[27].

The majority of skin immune cells are located in the dermis (Figure 3). The extracellular matrix (ECM) and the connective tissue of the dermis are made up mostly of collagen and elastic fibers, mainly synthesized by fibroblasts[28]. Fibroblasts are the most abundant cell type of the dermis, and they play various roles in skin homeostasis, wound healing, and inflammation. It is therefore not surprising, that there is considerable heterogeneity amongst fibroblasts, with subsets mediating different functions[29]. In addition to fibroblasts, blood vessels, lymph vessels, and neurons are present in the dermis, along with glands, sensory structures, and hair follicles. The epidermis is the outermost layer of the skin (Figure 3). It is made up of keratinocytes, melanocytes, and immune cells[27]. Basal keratinocytes and melanin-producing

melanocytes, which confer pigmentation to the skin, make up the stratum basale and mediate the contact and adhesion to the dermis. As keratinocytes mature, they gain different functional properties and make up the stratum granulosum. The superficial layer of the epidermis is the stratum corneum, which consists of a cornified layer of dead keratinocytes.

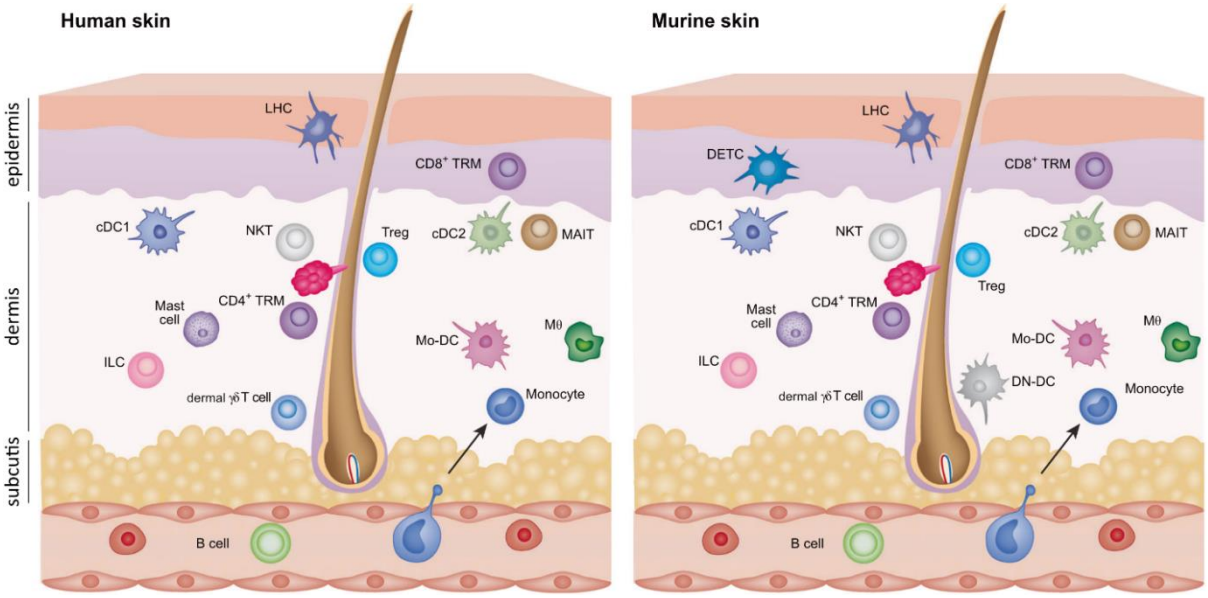

Figure 3. Comparison of the immune cell landscape of human and murine skin. Adapted from Zhang *et al*., 2022[27]. Humans and mice share many resident immune cell types. cDC1s, cDC2s, and Mo-DCs represent DC populations present in both species. Also shared are monocytes, macrophages, Langerhans cells, and mast cells. Shared lymphocyte populations are $CD4^+$ and $CD8^+$ T_{RM} cells, T_{reg} cells, ILCs, dermal γδ T cells, and unconventional T cells like NKT and MAIT cells. Exclusive to the murine skin are DN-DCs and DETCs. However, this represents a simplified overview and quantities of shown cell populations differ between human and mouse skin. Dermal γδ T cells are e.g. more abundant in murine than in human skin and take over different functions[30]. cDC: conventional DC, DETC: dendritic epidermal T cell, DN-DC: double-negative DC, ILC: innate lymphoid cell, LHC: Langerhans cell, MAIT: mucosal-associated invariant T cell, Mo-DC: monocyte-derived DC, Mθ: macrophage, NKT: natural killer T cell, T_{reg}: regulatory T cell, T_{RM}: tissue-resident memory T cell.

In addition to the physical barrier provided by the skin, there are other mechanisms to keep microorganisms at bay. Antimicrobial peptides (AMPs), lipids, and an acidic layer further enhance protection against the outside world and are secreted into the stratum corneum of the epidermis[27]. The skin is colonized by bacteria, viruses, and fungi that collectively constitute the skin microbiome[31]. It consists of non-pathogenic and opportunistically pathogenic microorganisms and is beneficial for the host in many ways. It has important functions in the defense against pathogens, breaking up natural products, and educating the immune system[31].

While there are some species-specific differences, most types of immune cells are found in the skin of both humans and mice (Figure 3). Many populations of professional APCs reside in the skin. Langerhans cells are specialized APCs in the epidermis. Together with various dermal DC populations, such as conventional DC 1 (cDC1), cDC2, and monocyte-derived DC, they function as vigilant sensors[27]. After recognizing invading pathogens and foreign agents they capture them, migrate to the skin-draining lymph nodes (sdLNs), and present the antigens to T cells. $CD103^{-}CD11b^{-}$ double negative DCs are another dermal DC population exclusive in murine skin. Other myeloid sensor cells in the skin of humans and mice are macrophages and mast cells[27].

In addition to the myeloid compartment, there are abundant lymphoid cells present in the dermis (Figure 3). ILCs (innate lymphoid cells), and the unconventional T cell populations natural killer T (NKT) cells, mucosal-associated invariant T (MAIT) cells, and dermal γδ T cells also populate the dermis but are less abundant than conventional T cells[27]. In mice, γδ T cells are more frequent than in humans. Due to this difference, they are key players in some murine disease models but not in the human equivalent disease. One example of this is the IMQ (imiquimod)-induced psoriasis-like dermatitis model. In mice, interleukin (IL)-17 producing dermal γδ T cells play pivotal roles in the exacerbation of the psoriasis-like dermatitis, but their role in human psoriasis is minor[32,33].

$CD4^{+}$ and $CD8^{+}$ T_{RM} cells are the most abundant immune cell types in the skin of humans and mice. $CD4^{+}$ T_{RM} cells preferentially reside in the dermis, while $CD8^{+}$ T_{RM} cells are confined to the epidermis[27]. Among $CD4^{+}$ T_{RM} cells are also $FoxP3^{+}$ regulatory T_{RM} cells. They make up 10-30 % of the murine skin $CD4^{+}$ T cells and 20-60 % of the human ones[34,35]. In the murine skin exists another population of γδ T cells, called dendritic epidermal T cells (DETCs). These cells are localized to the epidermis and play important roles in wound healing and keratinocyte homeostatic proliferation[36]. In humans, $CD8^{+}$ T_{RM} cells are thought to take over these roles[27]. The skin immune system not only protects the skin itself, but also plays a major role in establishing systemic defenses. It was shown that smallpox infection via the lung is efficiently controlled by the typical upper skin layer scratch vaccination scheme used for example with the smallpox vaccination for administration of the vaccinia virus[37,38]. Skin vaccination induced T_{RM} cells capable of protecting against viral challenge. These also seeded distant tissues like the lung and conferred enhanced anti-viral protection[37,38].

1.3. Tissue-resident memory T cells

1.3.1 Tissue-resident memory T cell biology and characterization

T_{RM} cells are a subset of memory T cells that are resident in peripheral, non-lymphoid tissue. T_{EM} cells were found in 2001 to be preferentially localized in peripheral tissue[19]. The authors described a T cell population that would later be coined as T_{RM} cells. Like T_{EM} cells, T_{RM} cells express CD44 and lack CD62L (Figure 2). Thomas Gebhardt and colleagues introduced the concept of T_{RM} cells in 2009[39]. They investigated memory T cells in the skin of mice and described them as a non-recirculating, resident population that mediates long-term protection against secondary infections at the forefront of pathogen encounters. The authors also first described the hallmark surface markers that are still used to identify T_{RM} cells. Those being CD69 and CD103 in the mouse. However, early studies of T_{RM} cells focused on $CD8^+$ T_{RM} cells[21,40–43] and while $CD4^+$ T_{RM} cells have been described first in 2011[11,44] they remained controversial for a long time.

Longevity is a defining characteristic of T_{RM} cells. They seed the peripheral tissues early in life and a stable pool is maintained into old age[45]. Murine T_{RM} cells were shown to persist in tissues for over a year after antigen-specific induction[46]. While it is difficult to track human cells *in vivo*, transplant studies are a useful tool for studying T_{RM} cells. As passenger cells in the grafted organ, they can be distinguished from host cells and their fate can be analyzed at later time points. Human intestinal graft studies have revealed that T_{RM} cells persisted in the grafted organ (small intestine) for at least five years[47]. T_{RM} cells have been shown to reside in the brain, salivary glands, tonsils, lungs, lymph nodes (LNs), liver, spleen, intestine, female reproductive tract, and skin[45]. In recent years, more evidence has arisen that proves the existence of T_{RM} cells not only in the peripheral organs but also in primary and secondary lymphoid organs[13,45]. However, their function in lymphoid organs is not yet fully understood[45].

The fact that T_{RM} cells are present in the periphery at the forefront of pathogen encounters suggested that they could provide quick protection against invading pathogens. And indeed, not only were T_{RM} cells shown to be transcriptionally and functionally distinct from their circulating counterparts[11,39,43], but they were also shown to mediate enhanced protection against various types of infections in different organs, including the lung, skin, and vaginal mucosa[11,39,43,44]. Moreover, a substantial population of tumor-infiltrating lymphocytes (TILs) in various tumors of human patients resemble T_{RM} cells by expression of CD69, CD103, and CD49a. These tumor-associated T_{RM} cells correlate with good clinical outcomes and are thought to facilitate the success of immune checkpoint inhibition therapy[48].

In vivo live imaging techniques provided insights into their behavior and function. It clearly showed that $CD8^+$ T_{RM} cells are confined to the epidermis of mice and continuously patrol it, to rapidly respond to an infection[40,46]. In contrast, $CD4^+$ T_{RM} cells preferentially localize to the dermis and, in fact, represent the most abundant T_{RM} cell population in human skin[49]. Once T_{RM} cells encounter their antigen, they lose their motility and dendritic shape and become stationary[40,42,50]. T_{RM} cells activated by cognate antigen rapidly secrete interferon (IFN)-γ, tumor necrosis factor (TNF)-α, IL-2, and chemokines. The T_{RM} cell-derived cytokines induce a

pathogen alert state in the surrounding cells and tissue[42] and activate skin-resident innate immune cells and the endothelium[51]. Chemokines secreted from T_{RM} cells rapidly recruit other memory T cells to the site of antigen encounter, to enhance immunity in a site-specific manner[41]. In addition to their ability to efficiently encounter pathogens, alarm the surrounding tissue, and recruit additional cells, they also possess direct killing capacity[19].

The development of $CD8^+$ T_{RM} cells was analyzed in detail by Laura Mackay and colleagues in 2013[21]. The authors found that killer cell lectin-like receptor G1 $(KLRG1)^-$ skin-infiltrating T_{EM} cells gave rise to $CD8^+$ $CD69^+CD103^+$ intraepithelial bona fide T_{RM} cells. Additionally, it was shown that CD69 and CD103 expression was imperative for T_{RM} cell development and survival[21,52]. Skin infiltrating $KLRG1^-$ T_{EM} cells follow a chemokine gradient into the epidermis. The lodgment in the epidermis was shown to be an essential part of their developmental pathway. Furthermore, IL-15 and transforming growth factor-β (TGF-β) were established as key cytokines involved in the formation and / or survival of skin T_{RM} cells[21]. Indeed, TGF-β was later found to be activated and presented by skin DCs in mice and humans and to induce the expression of CD103 on T_{RM} cells, thereby mediating their tissue lodgment[53,54]. *Ex vivo* TGF-β stimulation even induced changes in gene expression of $CD8^+$ murine T cells that showed 50 % overlap with the core T_{RM} cell gene signature *in vivo*[21,55].

The T_{RM} cell core signature was established in 2013 for murine and in 2017 for human T_{RM} cells (Figure 4)[21,56]. These transcripts distinguish T_{RM} cells from circulating T cells and show considerable overlap between humans and mice. Transcripts prominently enriched in T_{RM} cells are responsible for tissue retention and, in line with this, decreased gene transcripts are associated with tissue exit[21,56]. Enriched gene transcripts code for CD69, CD103, CD49a, class I-restricted T cell-associated molecule (CRTAM), and CXCR6. Decreased gene transcripts code for the transcription factor Kruppel-like transcription factor 2 (KLF2) and KLF3. In line with this, expression of genes controlled by these transcription factors was also downregulated. These include CD62L, $S1P_1$, $S1P_5$, and CX3CR1. Notably, T_{RM} cells also express several inhibitory molecules such as programmed cell death protein 1 (PD-1), CD101, dual-specificity phosphatase 6 (DUSP6), and IL-10. In combination with the reduced expression of Ki-67, this strongly hints towards a tight regulation of T_{RM} cell activation and activity, which is readily available upon activation shown by their expression of IL-2, IL-17, and IFN-γ[21,56].

Homolog of Blimp-1 in T cells (Hobit) and B-lymphocyte-induced maturation protein 1 (Blimp1) were identified as master transcription factors that regulate a universal tissue-residency program found not only in T_{RM} cells but also in other skin resident lymphocytes like NKT cells and liver-resident natural killer (NK) cells in the mouse[57]. Moreover, the transcription factor RUNX family transcription factor 3 (Runx3) is responsible for the instruction of the TGF-β-responsiveness program in $CD8^+$ T cells and therefore indispensable for $CD8^+$ T_{RM} cell development[58]. However, Runx3 is dispensable for $CD4^+$ T_{RM} cell development. Interestingly, forced Runx3 expression in $CD4^+$ T cells instructed a $CD8^+$ T_{RM} cell-like program. $CD4^+$ T_{RM} cell development is partially mediated by Runx1 but does not solely depend on it[58].

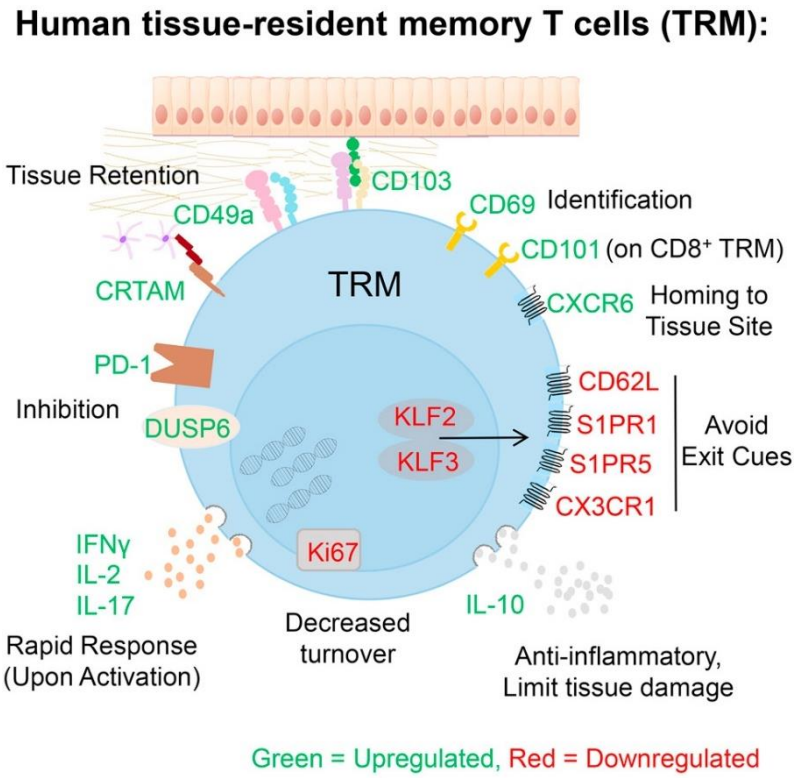

Figure 4. Core signature of human T_{RM} cells. From Kumar *et al*., 2017[56]. The bulk transcriptome of human $CD69^+$ vs $CD69^-$ T cells from the lung and spleen was sequenced and a combined T_{RM} cell-specific signature was identified for $CD4^+$ and $CD8^+$ T_{RM} cells, that distinguished tissue-resident from circulating T cells. Upregulated genes are involved in residency and homing (CD69, CD103, CD49a, CXCR6, and CRTAM) as well as inhibitory molecules (PD-1, CD101, and DUSP6). Specific cytokines are enriched in T_{RM} cells (IL-10, IFN-γ, IL-2, and IL-17). Downregulated genes are mainly associated with avoidance of tissue exit (the transcription factors KLF2, KLF3, and consequently CD62L, $S1P_1$, $S1P_5$, CX3CR1), in addition to Ki-67, signifying decreased turnover. CRTAM: class I-restricted T cell-associated molecule, DUSP6: dual-specificity phosphatase 6, KLF2/3: Kruppel-like transcription factor 2/3.

1.3.2 T_{RM} cell heterogeneity and implication in skin diseases

T_{RM} cells show remarkable heterogeneity. The human skin is populated by different T_{RM} cell subtypes, specifically T_{RM} cells of type 1 and type 17 ($T_{RM}1$ and $T_{RM}17$ cells)[59,60]. These subtypes were identified in a study by Cheuk *et al*. in 2017[59]. $CD69^+$ $T_{RM}1$ cells were marked by CD103 and CD49a expression and $CD69^+$ $T_{RM}17$ cells expressed CD103 and CCR6. Further characterization on the transcriptional level revealed that $CD103^+CD49a^+$ T_{RM} cells expressed genes highly associated with a type 1 immune response. Many of those genes encoded for type 1 associated effector molecules like perforin, granzyme B, and IFN-γ[59], whereas $CD103^+CD49a^-$ T_{RM} cells were enriched in type 17 immune response associated transcripts of IL-17F, RAR-related orphan receptor γ t (RORγt), IL-23, and CCR6[59].

Their constant presence in tissues, together with their ability to produce cytokines and generate rapid strong immune responses make T_{RM} cells a prime target for investigation regarding the etiology of human diseases. Indeed, T_{RM} cells have been found in many tissues

and are thought to contribute to a plethora of diseases associated with infection, cancer, autoimmunity, transplantation, and overall inflammatory disorders, including skin diseases[59,61–63]. Due to their longevity and resilience, they are especially involved in chronic inflammatory disorders. In the skin, T_{RM} cell-mediated disorders are characterized by site-specific lesions that persist or recur over decades[64–66].

1.3.2.1. T_{RM} cells and psoriasis

Psoriasis is a T cell-mediated disease[67]. More specifically, IL-17-producing cytotoxic T lymphocytes type 17 (T_C17) and helper T lymphocytes type 17 (T_H17) cells are the key mediators in humans and show a T_{RM} cell phenotype[68,69]. They are induced by skin-resident DCs, which are activated by environmental factors and trauma, capture autoantigens in the skin, and migrate to the dLNs (draining lymph nodes). There, they prime naïve T cells and produce IL-23, IL-6, and TGF-β, which drives the expression of RORγt in the differentiating T cells and skews them towards T lymphocytes type 17 (T17) cells[66,70,71]. T_C17 and T_H17 cells migrate into the skin, where they are again activated by DC-derived proinflammatory cytokines. This induces IL-17, IL-22 and IFN-γ-secretion in T cells[68,71]. These cytokines are the key effector molecules in psoriasis pathogenesis, as they recruit neutrophils to the skin, drive epidermal remodeling, and keratinocyte proliferation and activation, which further amplifies the inflammation[32,66,72].

T_{RM} cells are known to reside in psoriasis lesions and even persist in clinically healed leasions[69,73,74]. The most effective and most common treatment options for psoriasis are monoclonal antibodies, (so-called biologics) that target and neutralize key effector cytokines. There are anti-IL-17 antibodies (Secukinumab, Ixekizumab, Brodalumab, and Bimekizumab), an anti-IL-12/IL-23 antibody (Ustekinumab, targets the IL-12/IL-23-shared subunit p40 and thereby neutralizes both cytokines), anti-IL-23 antibodies (Guselkumab, Tildrakizumab, Risankizumab, and Mirikizumab), and anti-TNF-α antibodies (Etanercept, Infliximab, Adalimumab, Certolizumab). However, while neutralizing T_{RM} cell effector cytokines and thereby inhibiting inflammation, none of these treatment strategies aims to eliminate the source of the cytokines, the T_{RM} cells. Clinically healed psoriasis lesions therefore often relapse after the treatment is stopped[66,71]. Characterization of healed psoriasis lesions revealed epidermal T_C17 ($CD8^+CLA^+CCR6^+IL\text{-}23R^+CD103^+$) (CLA, cutaneous lymphocyte-associated antigen) and T_H22 ($CD4^+$) to reside in ex-lesions and to readily respond to *ex vivo* stimulation with IL-17 or IL-22-production respectively. T_{RM} cells in active psoriatic lesions are of the $T_{RM}17$ subtype and are characterized as $CD8^+CD69^+CD103^+CD49a^-CCR6^+ROR\gamma t^+$ and produce IL-17[59]. Interestingly, in mice, $T_{RM}17$ cells are be induced by colonization with *Staphylococcus epidermidis,* and steady-state commensal-specific $T_{RM}17$ cells are poised for a type 2 immune response. Tissue injury and alarmins trigger the release of the type 2 immune mediators IL-13 (which mediates tissue repair) and IL-5 (which recruits eosinophils) and co-expression of RORγt and GATA3[60]. Critically, a recent study in mice showed that anti-IL-23 treatment reduced $CD69^+CD103^+$ T_{RM} cells from the skin[75]. This implies that patients treated

with anti-IL-23 biologics could experience long-term therapeutic benefits in T17-mediated cutaneous inflammatory diseases.

1.3.2.2. T_{RM} cells and vitiligo

Vitiligo is another inflammatory skin disease, mediated by T_{RM} cells[66,76–78]. It is an autoimmune disease, where T_{RM} cells react against melanocyte-derived antigens, which leads to progressive depigmentation of the skin[66,76,77]. Melanocytes of vitiligo patients are especially fragile and susceptible to oxidative stress. Melanocyte death through environmental triggers activates skin-resident DCs, which prime T cells in sdLNs. $CD8^+$ T_{EM} cells then migrate to the skin and kill melanocytes, which releases more antigens and creates a vicious cycle[66,76–78]. T_{EM} cells then differentiate into T_{RM} cells, which reside locally for decades. Treatment strategies in vitiligo face similar problems as in psoriasis. Treatments used topically and systemically are broadly anti-inflammatory, immune inhibiting agents like glucocorticoids, calcineurin inhibitors, and Janus-kinase (JAK)-inhibitors with considerable side effects[79]. T_{RM} cells are suppressed but not depleted by these treatments and consequently, vitiligo patients often experience site-specific relapses after treatment stop[66,78]. T_{RM} cells in vitiligo lesions are $T_{RM}1$ cells characterized as $CD8^+CD69^+CD103^+CD49a^+CXCR3^+$ and produce IFN-γ and granzyme B[59,76,78].

1.3.2.3. T_{RM} cells and atopic dermatitis

Like psoriasis and vitiligo, atopic dermatitis (AD) is a chronic inflammatory skin disease. It is also mediated by T_{RM} cells and therefore shows characteristic site-specific recurring lesions. However, AD is a type 2 immune response mediated disease and is often associated with other atopic comorbidities[66,80]. In most cases, AD is caused by barrier defects and a dysregulated type 2 immune response[66,80,81]. Barrier defects are often caused by a loss-of-function mutation in the filaggrin gene, which leads to higher permeability of the skin for foreign agents that act as allergens and can cause damage to keratinocytes[80]. This triggers the release of epidermal alarmins like IL-25, IL-33, and thymic stromal lymphopoietin (TSLP) which causes a local type 2 promoting milieu. DCs and type 2 innate lymphoid cells (ILC2s) are activated and in turn release IL-5 and IL-13, which, together with IL-4, are key effector cytokines of type 2 immunity[66,80,81]. This polarizes allergen-specific T cells in sdLNs towards a type 2 phenotype. Allergen-specific skin T_{RM} cells ultimately cause the hallmark clinical symptoms itch and inflammation[66,80,81].

While there exists clear evidence for T_{RM} cells to play a critical role in the pathogenesis of AD, type 2 T_{RM} cells are less well defined as $T_{RM}1$ and $T_{RM}17$ cells, likely because they do not commonly reside in the skin[66,82,83]. They are also not directly targeted by current treatment strategies, which involve neutralizing antibodies and broadly immunosuppressing agents. An effective monoclonal antibody in the treatment of many AD patients is Dupilumab, which targets the IL-4Rα chain that is shared between the IL-4 and IL-13 receptors and therefore

serves a dual purpose in silencing the key axis in this disease[66,80]. Further treatments include glucocorticoids and JAK inhibitors[66,80,84]. T_{RM} cells remain dysfunctional for the duration of the respective treatment but cause flare-up relapses once treatment is stopped.

1.3.2.4. T_{RM} cells and allergic contact dermatitis

Allergic contact dermatitis (ACD) is a frequent occupational disease and patients experience strong allergic skin reactions when they come in contact with allergens contained in cosmetics, rubber, and metals. It is characterized as a type 4 delayed type hypersensitivity (DTH) reaction by classification after Gell and Coombs[64,85]. A subclinical sensitization phase marks the beginning of the pathogenic cascade, typical for DTH reactions and atopic diseases. Details of the pathogenesis of DTH reactions and ACD are described in detail in the following section 1.4.3. Briefly, first contact with the allergen induces priming of allergen-specific T cells in the dLNs by skin-resident DCs. The primed T cells differentiate into T_{CM} cells and T_{EM} cells and infiltrate the skin upon secondary antigen encounter. They then mediate the challenge or elicitation phase by production of effector molecules like IFN-γ, which in turn also activates keratinocytes and local skin-resident myeloid cells to secrete TNF-α and IL-1β. This generates a strong inflammation that shows as swelling, redness, heat, and pain and can even lead to painful blister formation[64,86–88]. T_{EM} cells in the skin then differentiate into T_{RM} cells which reside locally and mediate even stronger re-call responses upon successive antigen encounter[64,88]. T_{RM} cells have been shown to mediate key features of ACD. Due to their persistence in the tissue and their longevity, they cause lesions that are clearly defined, recurrent, and site-specific. Also, repeated antigen exposure leads to the accumulation of T_{RM} cells, and the number of epidermal T_{RM} cells has been shown to correlate with the magnitude of the clinical response[64,89].

The first treatment regimen in the management of ACD is allergen avoidance. Patch tests are the gold standard for the diagnosis of ACD and the identification of allergens for each patient. There, multiple potential allergens are applied onto the skin of a patient in defined areas. A DTH reaction after 48-72 h indicates the allergens for the respective patient[90]. Clinical symptoms are addressed by application of topical immunosuppressive glucocorticoids and calcineurin inhibitors. In severe cases, oral glucocorticoids are used[90]. However, evidence for the role of biologics in the treatment of severe chronic ACD accumulates. The biologics in clinical testing are Dupilumap and Ustekinumab, and those show only mild success[90]. As discussed in previous sections, T_{RM} cells in the skin persist through most, if not all, treatment options. Therefore, when patients are not under active treatment, T_{RM} cells mediate recurring and worsening flare-up reactions[64].

Treatment strategies that target T_{RM} cells in the skin are being explored and some show promising results in animal models[64]. They could prove to be used in many inflammatory skin disease models, irrespective of the underlying type of immune response and etiology of the disease, as long as T_{RM} cells play a critical part in disease exacerbation. For example, anti-CD122 (IL-15 receptor subunit) application acutely reduced IFN-γ production by T_{RM} cells and

was found to reduce T_{RM} cell numbers in lesional skin in long-term administration. This conferred durable healing and reversion of vitiligo lesions in a mouse model[91]. Furthermore, Lefevre *et al*. suggested that the application of low doses of antigen could be useful in attempts of desensitization, as well as pharmacological inhibition of lipid metabolism and mTOR (mammalian target of rapamycin) signaling, which is both critical for T_{RM} cells[64]. However, the authors also advise care in the complete depletion or inhibition of T_{RM} cells in the skin in hindsight of their important role in defense against invading pathogens.

1.4. The contact hypersensitivity reaction as a model for allergic contact dermatitis

The murine contact hypersensitivity (CHS) reaction is used as a model for the human inflammatory skin disease ACD. It is a DTH reaction type 4 after the classification of hypersensitivity reactions by Coombs and Gell in 1963[85,92]. The DTH reaction is mediated by cytotoxic T cells[85,86,88,92]. It is one of the best characterized immunological disease models and has been extensively used for more than 60 years[93]. Haptens are the most widely used class of substances to induce the CHS reaction in animal models. These are low molecular weight (<1000 Da) chemicals that are not immunogenic themselves. Four haptens are typically used in animal models, TNCB (2,4,6-trinitrochlorobenzene), DNFB (2,4-dinitrofluorobenzene), oxazolone, and FITC (fluorescein-5-isothiocyanate), whereas countless other haptens and substances can induce ACD in humans[88].

1.4.1 The sensitization phase/ immunization

The CHS reaction occurs in two phases. The first phase is known as the initiation or sensitization phase and typically happens without clinical symptoms[88]. It marks the first contact with the hapten/ antigen (here: TNCB) and is therefore also referred to as immunization. The hapten is solved in a formulation of an organic solvent and oil (here: acetone and Mygliol 812) and is applied onto the shaved skin. In this formulation, the hapten penetrates the skin and persists in the epidermis for weeks[94]. Haptens are highly reactive and elicit immune responses by covalently binding to (haptenizing) and thereby altering host proteins. Importantly, haptens exert considerable toxicity, and application onto the skin elicits a general non-antigen-specific inflammation, which is referred to as irritant reaction. Through cell death, DAMPs (danger-associated molecular patterns) are released, which are sensed by keratinocytes and APCs through PRRs (pattern recognition receptors). Consequently, they secrete pro-inflammatory cytokines like TNF-α and IL-1β, which in turn activate skin-resident APCs and induce their maturation[88,95]. Epidermal Langerhans cells, Langerin$^+$ dermal DCs (dDCs), CD11b$^+$ dDCs, and double-negative dDCs in mice have all been shown to take on redundant roles in the sensitization phase of the CHS reaction[96,97].

Activated skin-resident APCs mature and by that lose their sessile characteristics and become migratory. They start to express CCR7 and travel through dermal lymphatic vessels into the dLNs, shuttling haptenized proteins[96,98,99]. In the dLNs, they prime neoepitope-reactive naïve T cells recognizing haptenized peptides in complex with MHC molecules[96,99,100]. These 'hapten-specific' T cells become activated and differentiate into effector and memory T cells. They then exit the lymph node and enter the bloodstream, from which they can home to the site of inflammation and infiltrate the skin in case of a subsequent skin challenge. This is a critical step, as demonstrated by experiments with fingolimod (FTY720)[101]. The $S1P_1$ agonist induces its downregulation, thereby sequestering lymphocytes in SLOs[102,103]. Recirculating T_N cells and T_{CM} cells are trapped in the SLOs, causing lymphopenia in naïve mice treated with FTY720. In sensitized mice, FTY720 treatment prevents freshly generated T_{EM} cells from exiting the LNs. The elicitation phase of the CHS is thereby significantly impaired, as ear-infiltrating T_{EM} cells are the main mediators of it[101].

1.4.2 The challenge phase/ acute reaction

The second phase of the CHS reaction is the elicitation or challenge phase. A second application of the hapten, typically three to five days post sensitization, leads to the recruitment of sensitization-induced T_{EM} cells into the site of challenge. The challenge is conducted on a naïve skin site and mice are usually sensitized on the shaved abdomen and challenge is carried out on the ear pinnae. The inguinal LNs (iLNs) drain the abdomen, which is why T cell priming during sensitization happens primarily there. Three pairs of LNs drain the face, head, and ears of mice. After nomenclature of van den Broeck *et al*., 2006, they are referred to as mandibular, accessory mandibular and superficial parotid LNs[104].

The acute CHS reaction, or flare-up, is caused by skin-infiltrating hapten-specific T_{EM} cells. The irritant properties of the hapten lead to a rapid inflammation upon challenge, analogous to the sensitization. Keratinocyte- and skin-resident APC-derived TNF-α and IL-1β activate the local endothelium to express the adhesion molecules E-selectin, P-selectin, ICAM-1, and vascular cell adhesion molecule 1 (VCAM-1). Recently generated T_{EM} cells and neutrophils in the blood interact with the adhesion molecules of the activated endothelium, thereby selectively extravasating into the inflamed skin site within the first hours after hapten application. In the challenge phase, antigen-presentation is required for T cell function and happens in the skin. However, instead of professional APCs, keratinocytes and other skin-resident immune cells like macrophages are thought to present haptenized peptides to T cells, as T_{EM} cell function does not require co-stimulation by professional APCs[105–107].

The main effector cells during the challenge phase are $CD8^+$ T_{EM} cells. While $CD4^+$ T_{EM} cells also infiltrate the skin upon challenge, they are thought to play a regulating role. This was demonstrated by *in vivo* depletion experiments and by the use of MHC class I deficient mice. There, the MHC class I-restricted $CD8^+$ T cell response but not the MHC class II-restricted $CD4^+$ T cell response is abrogated. These mice did not develop an acute flare-up reaction[88]. $CD8^+$ T_{EM} cells in the challenged skin are of type 1 ($CXCR3^+$ cytotoxic T lymphocytes type 1, T_C1 cells)

and produce IFN-γ. This leads to further activation of keratinocytes, which produce more inflammatory mediators and chemokines, entering a positive feedback loop. This results in vasodilation and consequently edema formation that can be measured as a change of skin thickness. Importantly, the extent of ear swelling directly reflects the magnitude of the underlying immune response. An alteration in the ear swelling is therefore proof of an altered immune reaction in either the sensitization or challenge phase. After the characteristic peak of the acute CHS response at 24 - 48 h post challenge, the flare-up subsides gradually over the next 7 - 14 days. The resolution of the CHS reaction is mediated by local regulatory T (T_{reg}) cells[88].

1.4.3 The re-challenge phase/ memory reaction

Already in 1983, it was understood that local hapten challenge induces long-term immune memory in the skin and that a re-challenge of a healed (previously challenged) site weeks after the challenge induces a stronger flare-up reaction than the original one[87]. It is now known, that T_{RM} cells are induced by hapten challenge, reside in the challenged site, and mediate a stronger re-call memory response[108,109]. T_{RM} cells in healed CHS skin are derived from effector progenitor T cells that infiltrated the skin during the challenge. The largest part of the T_{EM} cell pool contracts within days after the acute inflammation, this process is especially characterized in $CD8^+$ T cells. So-called short-lived effector cells (SLEC) are characterized by their expression of the terminal differentiation marker KLRG1 and by the lack of expression of the memory/ memory precursor marker CD127 (IL-7Rα chain). However, memory progenitor effector cells (MPEC), being $KLRG1^-CD127^+$, do not contract and through IL-7 and IL-15 mediated signaling survive and become memory T cells, specifically T_{RM} cells[20,21,25]. T_{RM} cell fate decision is made even prior to peripheral tissue infiltration and was shown to be imprinted during T cell priming in SLOs by cross-presentation-proficient $BATF3^+$ DCs[20,110].

Antigen challenge of healed skin in the CHS model (and in ACD patients in the context of patch-tests) leads to a quicker and more severe flare-up reaction, than antigen challenge of naïve skin. This is mediated by T_{RM} cells and highlights their function as the first line of defense[64]. Even though hapten moieties on haptenized host proteins were proven to persist in the skin for weeks, T_{RM} cell lodgment in the skin and longevity are independent of antigen presence[44]. Similar to the T_{EM} cells during the acute challenge, T_{RM} cells do not rely on professional APCs for their reactivation, as also non-hematopoietic cells are capable of activating them[111].

1.5. The Epstein-Barr virus-induced gene 2 (EBI2)-oxysterol axis

EBI2 is a chemotactic receptor expressed on the cell surface[112]. It was originally discovered as one of the highest upregulated genes in an Epstein-Barr virus (EBV) infected B cell line, hence its name[113]. Other EBV-induced genes discovered in this study included EBI1 and EBI3, which are now known as CCR7 and IL-27 subunit β. Further characterization showed that EBI2 is a 7 trans-membrane (7TM) domain-containing G protein-coupled receptor (GPCR) (Figure 5 A)[112,113]. Its gene *GPR183* is located on the minus strand of the human chromosome 13 (exact position: 13q32.3) and contains 12,861 bases (GeneCards.org). The structure of EBI2 was resolved in 2022 and gave valuable insights into the ligand binding site[114].

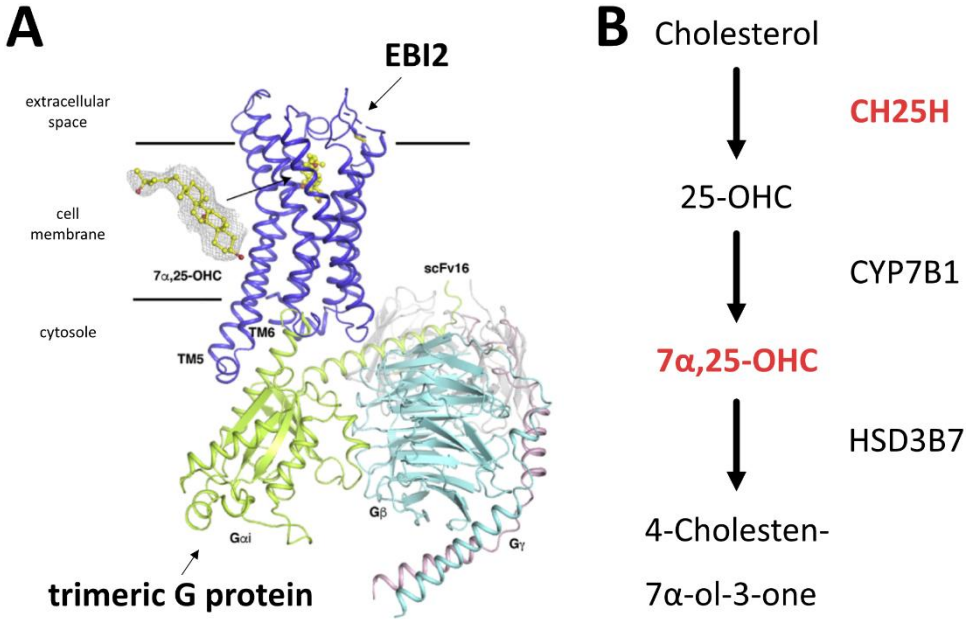

Figure 5. Structure of human EBI2 with trimeric G protein and synthesis pathway of 7α,25-OHC. A Adapted from Chen *et al*. 2022[114]. Cryo-EM (electron microscopy) structure of the EBI2-G_i complex, 7α,25-dihidroxycholesterol (7α,25-OHC), and single-chain variable fragment 16 (scFv16) at 3.1 Å-resolution. The scFv is not naturally associated with EBI2 or the G protein but is a remnant of the methodological approach to resolving the structure. **B** Synthesis pathway of 7α,25-OHC from cholesterol. CH25H (cholesterol 25-hydroxylase) is marked in red as the rate-limiting enzyme in the reaction. Sequential hydroxylation of cholesterol by CH25H and CYP7B1 (cytochrome P450 family 7 subfamily B member 1) synthesized the EBI2 ligand 7α,25-OHC. HSD3B7 (C_{27} 3β-HSD7, or 3β-hydroxysteroid dehydrogenase type 7) degrades it, rendering it inactive in terms of EBI2 binding.

1.5.1 The EBI2 ligand 7α,25-dihydroxycholesterol

Despite its potential role in EBV infection, EBI2 remained an orphan receptor (receptor with an unknown ligand) for a long time. 18 years after its discovery, in 2011, two groups using similar approaches independently discovered that EBI2 binds oxysterols (oxidated derivatives of cholesterol)[115,116]. They tested oxysterols extracted from porcine spleen[116] and from a peritonitis-induced sepsis model sheep liver[115] for their EBI2 binding and signaling induction

potency. Several oxysterols were shown to bind to EBI2: 7α,25-dihydroxycholesterol (7α,25-OHC), 7α,27-OHC, 7β-OHC, 7β,25-OHC, and 7β,25-OHC. Of these, 7α,25-OHC showed the highest binding affinity and signal induction potency and was therefore the strongest ligand for EBI2[115,116]. This was not only confirmed by signaling analysis but 7α,25-OHC also showed the highest potency in inducing EBI2-specific migration of whole splenocytes, B cells, $CD4^+$ T cells, and bone marrow-derived DCs (BMDCs)[115,116].

7α,25-OHC synthesis is part of the bile acid synthesis pathway[117]. It is generated via sequential hydroxylation of cholesterol (Figure 5 B). Cholesterol is an essential part of the plasma membrane of mammalian cells and is ubiquitously present in tissues[118,119]. Most mammalian cells can synthesize it endogenously[118,119]. Cholesterol is first converted to 25-hydroxycholesterol (25-OHC) and the enzyme catalyzing this reaction is cholesterol 25-hydroxylase (CH25H)[117]. This is the rate-limiting reaction in the synthesis of the EBI2 ligand. Hence, CH25H expression correlates with 7α,25-OHC levels and is commonly used as a surrogate marker for its availability, because the direct quantification of the oxysterol is difficult and requires special equipment and expertise[115,116,120]. The mitochondrial enzyme CYP7B1 then catalyzes a subsequent hydroxylation of 25-OHC, synthesizing 7α,25-OHC. The enzyme C_{27} 3β-HSD7, or 3β-hydroxysteroid dehydrogenase type 7 (HSD3B7) further metabolizes 7α,25-OHC[117]. This degradation generates a product (4-cholesten-7α-ol-3-one) that is unable to induce EBI2-specific migration. Interestingly, HSD3B7 expression was shown to be necessary for the functioning of the EBI2-oxysterol axis by constraining the 7α,25-OHC gradient generated by CH25H and CYP7B1[121]. EBI2 and its ligand-producing and -degrading enzymes are collectively referred to as the EBI2-oxysterol axis[122,123].

Recognizing its important function in mounting an immune response, two small molecule EBI2 inhibitors were synthesized and characterized. GSK682753A was developed in 2013[124] and NIBR189 was developed in 2014[125]. Both were demonstrated to inhibit EBI2 signaling and EBI2-mediated migration of B cells and monocytes respectively[124,125].

1.5.2 G protein-coupled receptor and EBI2 signaling

EBI2 is a GPCR (Figure 5 A), which constitute the largest family of proteins in humans[126]. They are made up of characteristic 7TM domains that anker them into the plasma membrane. Their intracellular domains provide a binding site for G proteins. These are heterotrimers of an α, β, and γ subunit that mediate the signaling of GPCRs[126,127]. They show great heterogeneity, as there exist 16 Gα, 5 Gβ, and 13 Gγ subunits in humans, each with different downstream signaling properties. The β and γ subunits always remain in a heterodimer conformation, while the Gα subunit confers downstream signaling on its own[128]. The activation of a GPCR induces a conformational change and enables the interaction with the G protein, which is dissociated from the GPCR in its inactive state. Guanosine diphosphate (GDP) is bound by the resting G protein. Association with the GPCR catalyzes the exchange of GDP with guanyl triphosphate (GTP). This leads to dissociation of the trimeric G protein complex from the GPCR and releases the $G\alpha_i$ monomer and the Gβγ heterodimer, which each mediate downstream signaling.

EBI2 was shown to signal via $G\alpha_i$[112,129]. In line with this, EBI2-mediated cell migration towards 7α,25-OHC was shown to be sensitive to pertussis toxin (toxin derived from the bacterium *Bordetella pertussis*), which inhibits signaling of certain GPCR classes, including $G\alpha_i$[112,130]. Both $G\alpha_i$ and $G\alpha_s$ subunits signal via modulation of adenylate cyclases. These enzymes catalyze the production of the second-messenger cyclic adenosine monophosphate (cAMP) from adenosine triphosphate (ATP). $G\alpha_i$ subunits inhibit the cAMP production by the adenylate cyclases and $G\alpha_s$ subunits stimulate it[131]. High cAMP levels open ion channels and activate protein kinase A (PKA), which propagates signaling in a wide range of biochemical mechanisms[128]. In fact, the reduction of cellular cAMP levels, next to the incorporation of radiolabeled GTP (^{35}SGTP-γS), is an assay used for the investigation of EBI2 signaling activity[112,116,129].

GPCR signaling is terminated via proteins called β-arrestins. After ligand-mediated activation of the GPCR, GPCR kinases (GRKs) phosphorylate the intracellular C-terminal part of the receptor[127,132]. This recruits β-arrestins, which in turn inhibits G protein binding to the receptor and thereby stops signaling. Furthermore, β-arrestin binding leads to clathrin-dependent internalization (desensitization) of the GPCR. This represents a characteristic feature of GPCRs and shows that they possess a memory of prior activation[132]. After internalization, the GPCRs can be subjected to recycling to the surface (resensitization) or lysosomal degradation (downregulation).

1.6. The EBI2-oxysterol axis in immune responses

1.6.1 The role of the EBI2-oxysterol axis in B cell biology

Due to its discovery in EBV-infected B cells, research revolving around EBI2 focused on its function on B cells for a long time. In 2009, while still an orphan receptor, two groups independently reported a critical role of EBI2 in the priming of B cells[122,123]. Using KO (knock-out) mice and adoptive transfer models, they showed that EBI2 expression by B cells is required for their optimal intranodal position during activation (Figure 6)[122,123]. Multiple chemokine-receptor-axes work together in orchestrating the intricate microanatomical migratory processes that maneuver B cells through the SLOs. CCL19 and CCL21, produced by TRC (T zone reticular cells), draw B cells from the blood through the HEVs into the lymph node (see section 1.1.1)[133]. From there, they quickly migrate into the lymphoid follicles (LFs), following the CXCL13 gradient generated by FDCs, situated in the LF, and marginal reticular cells (MRCs), situated in the marginal zone (MZ). CXCR5 is the receptor for CXCL13 and it is expressed by naïve B cells, amongst other cells[4,134,135].

Once B cells encounter their cognate antigen, EBI2 is upregulated in an nuclear factor κ-light-chain-enhancer of activated B cells (NF-κB)-dependent manner[136] and was shown to regulate the CXCL13-CXCR5 axis. EBI2 forms heterodimers with CXCR5 on activated B cells, which reduces the binding of CXCL13 to CXCR5 and thereby downregulates CXCR5-mediated signaling[137]. This CXCR5-CXCL13-axis suppression was shown to be necessary for the activated

B cells to be able to migrate to the B-T zone border, where they co-localize with helper T (T_H) cells. Not all B cell responses require B-T cell interactions and such that do not are called T-independent B cell responses[4,135]. In T-dependent responses, B cells are required to meet T_H cells at the B-T zone border to receive help via CD40/ CD40 ligand (CD40L) interaction. This is mandatory for B cells to proliferate and engage in the germinal center (GC) reaction, ultimately leading to class switching and differentiation into memory and plasma cells[4,135]. The migration to the outer follicular regions has been shown to be mediated by EBI2 (Figure 6) and its ligand.

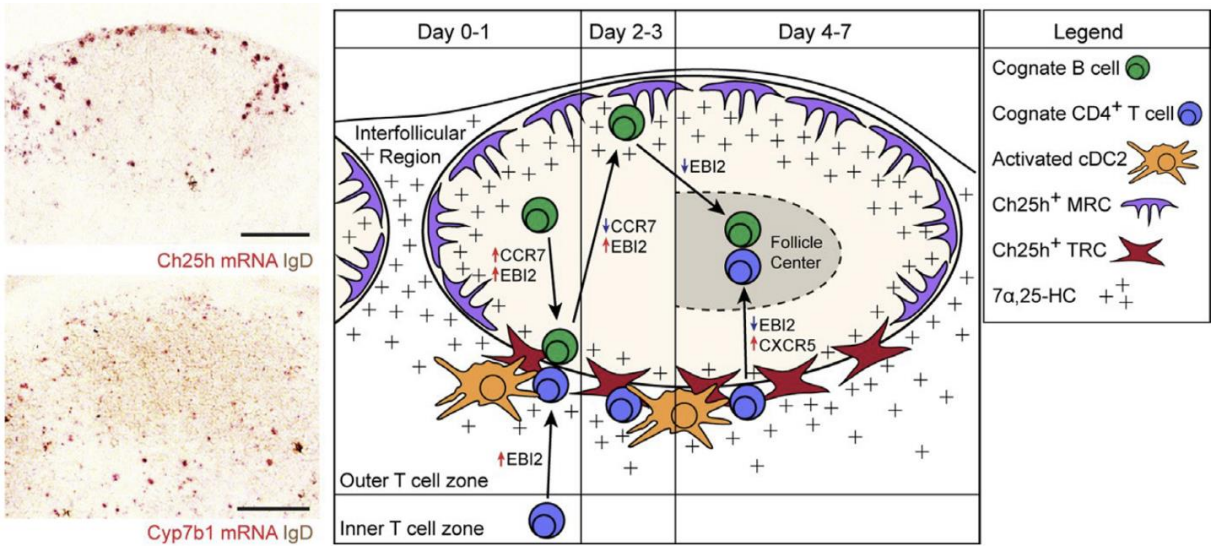

Figure 6. Distribution and function of the EBI2-oxysterol axis in intranodal B cell migration. From Lu & Cyster, 2019[141]. Left: RNAScope of murine spleen sections, showing in red *Ch25h* (top) and *Cyp7b1* (bottom) mRNA expression, together with IgD (brown, naïve B cells). Right: Regulation of EBI2 and CCR7 expression on naïve B cells regulates their positioning in the B cell zone during activation. 7α,25-OHC availability is indicated by crosses. 7α,25-OHC: 7α,25-dihydroxycholesterol; CH25H: cholesterol 25-hydroxylase; IgD: immunoglobulin D; cDC2: conventional dendritic cell 2; MRC marginal zone reticular cells; TRC: T zone reticular cells.

CH25H is expressed by lymph node stromal cells, which line the LF (Figure 6)[115,116,121]. Specifically, MRCs and CCL19^{lo} TRCs show the highest expression of CH25H, as established by single-cell ribonucleic acid sequencing (scRNAseq)[138]. CH25H and 7α,25-OHC production is induced in the spleen upon lipopolysaccharide (LPS) stimulation and can be inhibited by administration of the pharmacological CH25H-inhibitor clotrimazole[115,116,139]. This highlights the role of the EBI2-oxysterol axis in mounting an immune response against invading pathogens. Despite CH25H being the rate-limiting enzyme in the synthesis of 7α,25-OHC, CYP7B1, and HSD3B7 have been shown to be all important in the organization of the LN architecture and orchestration of T-dependent B cell responses[121]. Deficiency in any of the four parts of the EBI2-oxysterol axis leads to essentially the same phenotype of a distorted LN architecture[121–123]. Importantly, HSD3B7 mediated inactivation of 7α,25-OHC was demonstrated to contribute critically to the formation of the 7α,25-OHC gradient that guides

B- and T cells[121]. It constrains the ligand gradient, focusing the migration target area and thereby increasing the efficiency of the EBI2-oxysterol axis.

After receiving T cell help, B cells downregulate CCR7 and continue to express EBI2, which facilitates migration to MRCs along a 7α,25-OHC gradient (Figure 6). BCL-6-mediated downregulation of EBI2 occurs 3-4 days post activation and allows CXCR5 signaling, which guides B cells into the GC[122,123,140]. In conclusion, EBI2 guides naïve activated B cells to the outer follicular regions, to receive T cell help. Consequently, EBI2 deficient mice show an impaired early antibody response in T-dependent immune reactions, as well as an impaired early plasmablast response, which also occurs in the extrafollicular regions[122,123].

However, the study of the role of EBI2 in B cell biology is, for the most part, confined to the SLOs and its role on plasma cells in the periphery and memory B cells remained unknown for a long time. Recently, a study reported that dietary cholesterol influenced the EBI2-oxysterol axis and that this interplay regulated intestinal plasma cell positioning and immunoglobulin A (IgA) secretion into the gut lumen[142]. The authors report CH25H expression by intestinal epithelial cells (IEC) and production of 7α,25-OHC from dietary cholesterol. Gut microbiota induced packing of 7α,25-OHC by bile acids into chylomicrons, which were shuttled to the lymphatic vessels. EBI2 was shown to be expressed by spleen and gut plasma cells. Dietary cholesterol metabolism led to intestinal plasma cell re-localization near the lymphatic vessels, away from the lumen, thereby limiting the secretion of IgA into the gut lumen[142]. The authors discussed this role of the EBI2-oxysterol axis as a mechanism to limit microbiota targeting IgA secretion by intestinal plasma cells[142].

1.6.2 The role of the EBI2-oxysterol axis in dendritic cell biology

In addition to B cells, the EBI2-oxysterol axis was also shown to be critical for the development of DC subsets in the spleen of mice. Two groups showed that splenic $CD4^+$ DCs, but not $CD8^+$ DCs, express high levels of EBI2[143,144]. The $CD4^+$ DC subset is normally situated in the MZ bridging channels of the spleen. It was strongly reduced in numbers in mice deficient for either EBI2, CH25H, CYP7B1, or HSD3B7[144]. The MZ is a specialized region of the spleen, where blood and therefore blood-born antigens are released from the blood vessels into the spleen. The MZ bridging channels lead the blood from the MZ finally into the spleen. $CD4^+$ DCs are situated in these MZ bridging channels, and efficiently capture particulate blood-borne antigens. This activates them, inducing CCR7 expression and migration to the B- T zone border where they mediate $CD4^+$ T cell and B cell responses[143,144]. In addition to the strong reduction in the abundance of the $CD4^+$ DCs in the spleen, both groups showed that the few $CD4^+$ DCs present in the EBI2-oxysterol axis deficient mice failed to locate in the MZ bridging channels. Moreover, $CD4^+$ T cell- and B cell responses to particulate blood-borne antigen were impaired, when mice lacked EBI2 in DCs[143,144]. $CD8^+EBI2^-$ DCs were not affected by the lack of EBI2 or other members of the EBI2-oxysterol axis. This demonstrated that the EBI2-oxysterol axis is critically involved in the microanatomical positioning in SLOs of cells beyond just B cells and that it is imperative to a functional immune system[144].

Interestingly, the EBI2-oxysterol axis seems to not only modulate the migration of cells but has also been shown to modulate signaling. A subset of DCs, plasmacytoid DCs (pDCs), are among the most important sources of type 1 IFNs and therefore important in antiviral immune responses. Upon activation, they rapidly produce large amounts of IFN-β and IFN-α, as well as type 3 IFNs, like IFN-λ or IL-28/ IL-29[145]. However, EBI2 deficient pDCs as well CD11b$^+$ myeloid cells show a heightened ability to produce type 1 IFNs, compared to wild type (WT) ones *in vitro* and *in vivo*[146]. They also failed to localize to the spleen and peritoneal cavity from blood[146]. Similarly, another group showed that CH25H-deficient murine macrophages displayed an elevated IL-1 family cytokine secretion and that CH25H-deficient mice were more susceptible to septic shock and experimental autoimmune encephalomyelitis (EAE)[147]. Moreover, EBI2 was shown to induce B cell proliferation upon inverse agonist treatment[148]. All these reports demonstrate that EBI2-mediated signaling may have broader physiological implications than solely chemotactic migration.

1.6.3 The role of the EBI2-oxysterol axis in T cell biology

EBI2 gene expression by human T cells was recognized soon after its identification[112]. Due to the lack of specific anti-mouse EBI2 mAbs, reporter mice were used to verify ubiquitous expression in CD4$^+$ T cells and low expression in CD8$^+$ T cells, mirrored in human[120,122,149]. Corresponding to expression levels, EBI2 deficiency had an impact on murine CD4$^+$ T cells, but only indirectly on CD8$^+$ T cells[120,150,151]. The EBI2-oxysterol axis modulates T cell activation and fate decisions. Closely related to its role in B cells as a gatekeeper for GC entry, the EBI2-oxysterol axis was found to be implicated in follicular T helper (T_{FH}) cell generation[151]. Upregulated on activated CD4$^+$ T cells, EBI2 and 7α,25-OHC mediate migration towards the B-T zone border, where 7α,25-OHC is produced by FRCs see 1.6.1. There, they co-localize and interact with DCs expressing inhibitor of co-stimulation ligand (ICOSL) and CD25. Both of these are factors driving T_{FH} cell fate decision and EBI2- or CD25 deficient mice show reduced T_{FH} cell abundance[151].

Later, Baptista *et al*. discovered an even broader physiological function of EBI2 on T cells[150]. In their study, the authors showed that intranodal positioning of naïve CD4$^+$ T cells depends at least partially on the EBI2-oxysterol axis. EBI2 expression facilitated their localization of the edges of the T zone, in close proximity to cDC2s, which preferentially activate naïve CD4$^+$ T cells. In line with this, the positioning of cDC2s also relied on their EBI2 expression[152]. In contrast, naïve CD8$^+$ T cell positioning was not influenced by EBI2 deficiency and they localized preferentially in the T zone center, in close proximity to cDC1s, capable of cross-priming and therefore specialized CD8$^+$ T cell activators[150]. In line with this, cDC1 positioning in the T zone center was independent of the EBI2-oxysterol axis and their HSD3B7 expression led to ligand degradation and exclusion of cDC2s from the T zone center[152]. Furthermore, the CD4$^+$ T cell priming deficiency in EBI2 KO mice led to a delayed CD4$^+$ T cell-mediated immune response and a delayed CD4$^+$ T cell help-dependent CD8$^+$ T cell-mediated response[150].

Thymic development of αβ-TCR$^+$ and γδ-TCR$^+$ T cells has also been shown to be at least partially mediated by the EBI2-oxysterol axis[153,154]. CD4 single positive (CD4SP) thymocytes and CD4$^+$CD8$^+$ double positive (DP) thymocytes that have undergone thymic selection, are conventional αβ-TCR$^+$ T cell precursors and were shown to express EBI2, as well as thymic DCs[153]. CH25H, responsible for the 7α,25-OHC gradient generation, was expressed by a subset of medullary thymic epithelial cells (mTECs)[153] later further characterized by scRNAseq as SOX4$^+$ mTEC1[154]. EBI2 deficiency therefore led to an impaired ability of CD4SP thymocytes to migrate to the thymic medulla, where the mTECs are situated, and consequently to an impaired negative selection. The authors furthermore described alterations in the TCR repertoire, but no big impact on the thymocyte abundance and subset frequencies[153]. Moreover, Franscoli *et al*. showed that the EBI2-oxysterol axis regulates the maturation of EBI2 expressing γδ thymocytes and that EBI2 deficiency leads to a reduced accumulation of γδ T cells in the skin of mice[154]. These dermal γδ T cells were also shown to be functionally sensitive to dietary oxysterols in an EBI2-dependent manner[154].

Lastly, also CH25H was found to be inducible on CD4$^+$ T cells and to modulate their function[155]. IL-27 was shown to induce CH25H expression in CD4$^+$ T cells, which was further enhanced by TGF-β. IL-27 and TGF-β stimulated CH25H$^+$ CD4$^+$ T cells modulated extracellular 25-OHC production. Accumulation of 25-OHC had inhibitory paracrine effects on T cell activation and proliferation. Being an important mediator of skin inflammation, IL-27, but also CH25H deficient mice showed stronger disease courses in autoimmune and hapten-induced skin disease models[155].

1.6.4 The EBI2-oxysterol axis in disease pathologies

Next to its association with immune responses against viruses (i.e. EBV)[113,136,140,150] and bacteria[116,139,150], the EBI2-oxysterol axis was shown to drive certain disease pathologies. For example, EBI2 was reported to promote central nervous system (CNS) infiltration by encephalitogenic T cells in an EAE model[120,156]. Co-transfer of equal numbers of EBI2 KO and EBI2 WT EAE-mediating T cells, showed an advantage of the WT cells to infiltrate the CNS and elicit EAE. Transfer of EBI2-KO encephalitogenic T cells led to a delayed onset of the disease[120]. CH25H-deficient mice, however, showed conflicting EAE phenotypes in two studies. Reboldi *et al*. investigated EAE in CH25H deficient mice and reported a more severe disease progression compared to WT controls[147]. The authors attributed this phenotype to increased IL-1 family cytokine production. Chalmin *et al*. reported one year later a reduced EAE disease phenotype in CH25H KO mice[156]. The mechanism they revealed revolved around EBI2-oxysterol axis sensing by memory CD4$^+$ T cells and migration into the CNS, where monocyte-derived DCs expressed CH25H[156]. Similar findings were presented by my group[120]. This shows that more studies are needed to investigate the role of the EBI2-oxysterol axis and specifically CH25H deficiency in the EAE model. Interestingly, EBI2 was found highly expressed by T cells in the lesions of multiple sclerosis (MS) patients. This further suggests a migratory and pro-

inflammatory role[120]. In addition to MS, genome-wide association studies (GWAS) linked mutations in the CH25H gene to the development of Alzheimer's disease in humans[157,158].

Apart from the CNS, diseases affecting different organs are also associated with a pathogenic role of the EBI2-oxysterol axis. Nevius *et al*. showed in their study that EBI2 is expressed by osteoclast precursor cells (OCPs) and that it enhanced their fusion and thereby the formation of large osteoclasts in addition to mediating osteoclast migration to the bone surface[159]. Male mice showed increased bone mass and female mice were protected from hormone and age-associated osteoporosis when EBI2 signaling was absent[159].

A strong connection is also seen between the EBI2-oxysterol axis and the lung. The disease pathology of a smoke-induced chronic obstructive pulmonary disease (COPD) model was dependent on the EBI2-oxysterol axis. Lymphoid tissue organization by the EBI2-oxysterol axis was shown to be critical for disease pathogenesis, similar to its function in SLOs. Airway epithelium in COPD patients and mice revealed elevated expression of CH25H and CYP7B1 compared to healthy controls. In the mouse model, this induced the formation of TLS in the lung. The inducible bronchus-associated lymphoid tissue (iBALT) was essential for disease progression and was reduced in EBI2 or CH25H-deficient mice. Furthermore, its formation was therapeutically reversible by administration of the CH25H pharmacological inhibitor clotrimazole[160]. Moreover, multiple studies report additional lung disease pathologies to be associated with the EBI2-oxysterol axis such as acute and severe coronavirus disease 2019 (Covid-19) pneumonia[161–163], *Mycobacterium tuberculosis* infection[164–166], and allergic airway reaction[167,168]. All studies described the recruitment of myeloid cell populations (macrophages or eosinophils) to the lung, which was mediated at least partially by the EBI2-oxysterol axis.

In addition to CNS and lung, the EBI2-oxysterol axis was shown to be important in intestine physiology[142] and pathology. Two GWAS' linked an increased risk for the development of inflammatory bowel disease (IBD) to mutations in the CH25H and EBI2 gene[169,170]. Indeed, Wyss *et al*. found elevated levels of EBI2, CH25H, and CYP7B1 mRNA in the inflamed colons of IBD patients and of mice in an IBD model[171]. Interestingly, EBI2 deficient mice showed only a decreased inflammation in an IL-10 deficiency-induced IBD model but not in a dextran sulfate sodium-induced model. However, the authors reported reduced inflammation-induced colonic lymphoid structures in the mucosa of EBI2-deficient mice in both models and at baselinel[171].

Recently, three studies connected skin inflammation and disease pathology to the EBI2-oxysterol axis. Ruiz *et al*. found that a gain-of-function mutation in the EBI2 gene led to increased surface expression by $CCR6^+$ T_H17 cells in the circulation, which was accompanied by an increased risk of developing psoriasis in a swiss IBD cohort[172]. In line with this, Frascoli *et al*. showed that IL-17 producing γδ T cells in the skin of mice express EBI2 and are reduced in EBI2 deficient mice[154]. These cells are known to be the main mediators of the IMQ-induced psoriasis-like dermatitis model, a mouse model for psoriasis[33]. Although γδ T cells are not critical in human psoriasis pathogenesis[32], both studies showed an association between psoriasis and the EBI2-oxysterol axis. However, it remains unanswered how αβ T cells, which

mediate human psoriasis, are connected to the EBI2-oxysterol axis. Contradictory to this skin inflammation-promoting role by the EBI2-oxysterol axis in the previous studies, Takashi *et al*. showed an increased skin inflammation in a DNFB-induced CHS model in CH25H deficient mice. The authors attributed this phenotype to reduced production of IL-1 family cytokines, as previously mentioned[155]. This demonstrates that the role of the EBI2-oxysterol axis in skin inflammation is still not fully understood and requires more investigation. Furthermore, T_{RM} cells have been shown to mediate many disease pathologies, including skin diseases like psoriasis[74,173], and their connection with the EBI2-oxysterol axis is completely unknown and was not discussed in the aforementioned studies.

1.7. Aims of this work

The EBI2-oxysterol axis mediates microanatomical positioning of B cells, T cells, and DCs in primary and SLOs, contributing to immune cell activation and the orchestration of the immune response in a broad sense[122,123,141,150,153,174,175]. Moreover, pathologies affecting many different peripheral organs like the CNS, the lungs, and the gut are associated with contributions of the EBI2-oxysterol axis in human disease and animal models[142,161,169,174,176-178]. This is strong evidence that the EBI2-oxysterol axis is involved in the regulation of the immune response also outside of lymphoid organs and thereby at virtually all sites of the body. Either recruitment into the target organ or microanatomical positioning and TLS formation were shown to be at least partially mediated by it[120,156,160,163].

Recently, links between the EBI2-oxysterol axis and skin disease pathologies were made in psoriasis patients and animal models of psoriasis and ACD[154,155,172]. However, these reports showed partially contradicting results, and an additional layer of complexity was introduced, as dietary cholesterol was shown to modulate the function of the EBI2-oxysterol axis[154,155]. Overall, the importance of the EBI2-oxysterol axis in physiology and pathology is evident but especially its connection to diseases affecting the skin was unclear and its role on αβ T cells in this context was largely unexplored and required more investigation.

The aim of my thesis was to elucidate the role of EBI2 in inflammatory skin diseases. The focus was put on αβ T cells and how EBI2 is involved in their function and contribution to murine skin disease models. In detail, my aim was to analyze the impact of EBI2 deficiency in the TNCB-induced CHS model and the IMQ-induced psoriasis-like dermatitis model. High parameter flow cytometry, high dimensional data analysis, bioinformatical analysis of public data sets, and EBI2 reporter mice were aimed to be utilized in order to characterize αβ T cells and the EBI2-oxysterol axis in steady-state and inflammatory processes in the skin.

T_{RM} cells are critical mediators of many disease pathologies and have been especially well characterized in the skin. Whether they express EBI2 or react to oxysterols was not known. Another aim of this work was to elucidate whether there exists a connection between the EBI2-oxysterol axis and T_{RM} cells in the skin. Due to their well-known importance in human skin diseases and animal models thereof, this also held translational potential.

2. Materials and Methods

2.1. Materials

2.1.1 Chemicals and reagents

Table 1. Reagents, chemicals, kits, enzymes, and other substances. 7α,25-OHC: dihydroxycholesterol, BSA: bovine serum albumin, cDNA: complementary deoxyribonucleic acid, DMSO: dimethyl sulfoxide, EDTA: ethylenediaminetetraacetic acid, FCS: fetal calf serum, HEPES: 4-(2-hydroxyethyl)-1-piperazineethanesulfonic acid, MEM: minimum essential medium, PBMC: peripheral blood mononuclear cell, PCR: polymerase chain reaction, PMA: phorbol 12-myristate 13-acetate, RPMI: Roswell Park Memorial Institute, SDS: sodium dodecyl sulfate, TNCB: 2,4,6-trinitrochlorobenzene.

Substance	Company
100 bp+ DNA ladder	Fermentas, Life Science, Waltham, MA, USA
2-propanol	AppliChem, Darmstadt, Germany
^{3}H-thymidin	Hartmann Analytics, Braunschweig, Germany
7α,25-OHC	Sigma-Aldrich, St. Louis, MO, USA
Acetic acid, 100 %	Carl Roth, Karlsruhe, Germany
Acetone	Carl Roth, Karlsruhe, Germany
Aldara® 5 % creme	Meda Pharma, Solna, Sweden
Brefeldin A	Sigma-Aldrich, St. Louis, MO, USA
BSA	Sigma-Aldrich, St. Louis, MO, USA
CCL19	BioLegend, San Diego, CA, USA
CCL21	BioLegend, San Diego, CA, USA
Chloroform	Carl Roth, Karlsruhe, Germany
Collagenase type IV	Worthington, Lakewood, NJ, USA
DMSO	Sigma-Aldrich, St. Louis, MO, USA
DNAse I	Sigma-Aldrich, St. Louis, MO, USA
DreamTaq™ PCR Master Mix (2X)	Thermo Fisher Scientific, Waltham, MA, USA
EDTA	Sigma-Aldrich, St. Louis, MO, USA
Ethanol 100 % p.a.	Carl Roth, Karlsruhe, Germany
FCS	Gibco® life technologies™, Grand Island, NY, USA
First-strand cDNA synthesis kit	Thermo Fisher Scientific, Waltham, MA, USA
FoxP3/Transcription Factor Staining kit	Thermo Fisher Scientific, Waltham, MA, USA
FTY720	Sigma-Aldrich, St. Louis, MO, USA
HEPES	Gibco® life technologies™, Grand Island, NY, USA
Histopaque® -1083	Sigma-Aldrich, St. Louis, MO, USA
Ionomycin	PromoCell, Heidelberg, Germany
L-Glutamine	Gibco® life technologies™, Grand Island, NY, USA
Liberase	F. Hoffmann-La Roche AG, Basel, Switzerland
MEM	Gibco® life technologies™, Grand Island, NY, USA
Midori Green Advance	NIPPON Genetics, Düren, Germany
Moisturizing cream (5 % dexpanthenol)	Bepanthen, Bayer, Leverkusen, Germany
Mygliol 812	Caesar & Loretz, Hilden, Germany
NaN_3	AppliChem, Darmstadt, Germany
NaOH	Carl Roth, Karlsruhe, Germany
NIBR189	Sigma-Aldrich, St. Louis, MO, USA
Nuclease-free water	Thermo Fisher Scientific, Waltham, MA, USA
PBMC spin medium	pluriSelect, Leipzig, Germany

Penicillin	Gibco® life technologies™, Grand Island, NY, USA
PMA	PromoCell, Heidelberg, Germany
Proteinase K	Sigma-Aldrich, St. Louis, MO, USA
REDTaq®ReadyMix™ PCR Reaction Mix	Sigma-Aldrich, St. Louis, MO, USA
ROTI®Histofix (4 %)	Carl Roth, Karlsruhe, Germany
RPMI 1640	PAN-BioTech, Aidenbach, Germany
SDS	Serva Electrophoresis, Heidelberg, Germany
Sham cream (stearic acid, cetyl stearyl alcohol, white vaseline, polysorbate, glycerol, benzyl alcohol, water)	homemade by the pharmacy of the Medical Center of the Johannes Gutenberg-University, Mainz, Germany
Sodium Pyruvate	Gibco® life technologies™, Grand Island, NY, USA
Streptomycin	Gibco® life technologies™, Grand Island, NY, USA
SYBR green 2 x master mix	Thermo Fisher Scientific, Waltham, MA, USA
TNCB	Hartmann Analytics, Braunschweig, German
Tris	Carl Roth, Karlsruhe, Germany
TriZol	Thermo Fisher Scientific, Waltham, MA, USA
Trypan Blue	Gibco® life technologies™, Grand Island, NY, USA
Trypsin/EDTA (10x)	GE Healthcare, Chicago, IL, USA
ULTRAPure™ Agarose	Invitrogen, Waltham, MA, USA
Veet® sensitive depilation cream	Reckitt Benckiser, Mannheim, Germany
β-Mercaptoethanol	Sigma-Aldrich, St. Louis, MO, USA

2.1.2 Primer

Table 2. Oligo DNA primer used for genotyping or qRT-PCR. DNA: deoxyribonucleic acid, qRT-PCR: quantitative reverse transcription polymerase chain reaction, GPR183: g protein-coupled receptor 183, WT: wild type, KO: knock-out, flox: loxP-flanked, TBP: TATA-binding protein, A: adenine, C: cytidine, G: guanine, T: thymine.

Purpose	Target	Primer Name	Direction	Sequence
geno-typing	β-actin	Actin for	sense	TGT TAC CAA CTG GGA CGA CA
		Actin rev	anti-sense	GAC ATG CAA GGA GTG CAA GA
	GPR183 WT	EBI2 WT for	sense	CTC TTC AGG ACT GCC AAG CAG
		EBI2 WT rev	anti-sense	GCT GTG CTG TGA AGT CCC AAG
	GPR183 KO	EBI2 delta for	sense	AGT CTA ACG CCT GTC TAG AAT
		EBI2 delta rev	anti-sense	CTC CTG GAC GTA GCC TTC GG
	GPR183 flox	EBI2 delta for new	sense	AGT CTA ACG CCT GTC TAG AAT GT
		EBI2 flox rev	anti-sense	TTGCCATGAGACGTTGCCAGT
	CD4-Cre	CD4-Cre for	sense	CCC AAC CAA CAA GAG CTC
		CD4-Cre rev	anti-sense	CCC AGA AAT GCC AGA TTA CG
	Uni-Cre	Uni-Cre for	sense	GCA CTG ATT TCG ACC AGG TT
		Uni-Cre rev	anti-sense	CCC GGC AAA ACA GGT AGT TA
qRT-PCR	GPR183	mm_FW_Gpr183_BLAST1	sense	CAA ACA CGG ACT GCC ACA AC
		mm_REV_Gpr183_BLAST1	anti-sense	GTT GCC AGT GGG GTA GTG AA
	TBP	mm_FW_Tbp_Eissa	sense	ACC GTG AAT CTT GGC TGT AAA C
		mm_REV_Tbp_Eissa	anti-sense	GCA GCA AAT CGC TTG GGA TTA

2.1.3 Laboratory equipment

Table 3. Laboratory equipment and devices.

Device	Specification	Company
Brightfield microscope	Leica DM IRB	Leica, Wetzlar, Germany
Caliper	IP67, digital	Kroeplin, Schlüchtern, Germany
Cell freezing block	Mr. Frosty	Thermo Fisher Scientific, Waltham, MA, USA
Centrifuge	Multifuge 3 S-R	Heraeus, Hanau, Germany
Counting chamber	Neubauer Improved	Marienfeld Superior, Lauda-Königshofen, Germany
Eppi centrifuge	Z 216 MK	Hermle, Gosheim, Germany
Eppi shaker	neoMix	neoLab Migge, Heidelberg, Germany
Fine scale	SNR 49608372	Sartorius, Göttingen, Germany
Flow cytometer	Gallios 4L FACSymphony A3	Beckmann Coulter, Brea, CA, USA Becton Dickinson, Franklin Lakes, NJ, USA
Gel imager	iBright FL1000	Thermo Fisher Scientific, Waltham, MA, USA
Hair trimmer	Isis	Aesculap, Tuttlingen, Germany
Incubator	MCO-20AIC	Sanyo, Moriguchi, Osaka, Japan
NanoDrop	DS-11 FX+	DeNovix, Wilmington, Germany
pH meter	pH 211	Sigma-Aldrich, St. Louis, MO, USA
Power supply	Power Pac Basic	Bio-Rad, Hercules, CA, USA
qRT-PCR cycler	StepOnePlus	Applied Biosystems, Waltham, MA, USA
Sterile hood	HeraSafe, KS 15	Thermo Fisher Scientific, Waltham, MA, USA
Thermo cycler	Biometra TRIO	Analytik Jena, Jena, Germany
Tissue homogenizer	gentleMACS IKA® T10 basic ULTRA TURRAX	Miltenyi Biotec, Bergisch Gladbach, Germany IKA, Staufen, Germany
Vacuum aspirator	Vacusafe	Integra Biosciences, Zizers, Switzerland
Vortexer	Vortex Mixer	VWR International, Radnor, PA, USA
Water bath	WB 22	neoLab Migge, Heidelberg, Germany

2.1.4 Consumables

Table 4. Specific laboratory consumables.

Consumable	Specification	Company
96-well V bottom plate	costar® Assay Plate	Corning, Corning, NY, USA
Cannula	22 G, BD Microlance	Becton Dickinson
Cell strainer	40 µm/ 70 µm	Corning, Corning, NY, USA
Counting Beads	Trucount Beads	Becton Dickinson
EDTA blood collection tube	S-Monovette, 9 mL	Sarstedt, Nümbrecht, Germany
Flow Cytometry Staining Buffer	Brilliant Stain Buffer	Becton Dickinson
Homogenizer tube	gentleMACS ™ C Tube	Miltenyi Biotec
HTS transwell plate	HTS Transwell®-96 Permeable Supports with 5 µm pore size	Corning, Corning, NY, USA
Injection syringe	Omnican® F, 1 mL	Braun, Melsungen, Germany
Li-Hep blood collection tube	1 mL	Sarstedt, Nümbrecht, Germany

2.1.5 Buffers and Media

Table 5. Components of buffers and media. ACK: ammonium chloride-potassium, BSA: bovine serum albumin, DMSO: dimethyl sulfoxide, EDTA: ethylenediaminetetraacetic acid, FACS: fluorescence-activated cell sorting, FCS: fetal calf serum, HEPES: 4-(2-hydroxyethyl)-1-piperazineethanesulfonic acid, MEM: minimum essential medium, PBS: phosphate-buffered saline, TAE: Tris, acetic acid, EDTA.

Buffer/ Medium	Components	Final Concentration
ACK buffer (10X) pH 7.2	NH_4Cl	1.5 mM
	$KHCO_3$	100 mM
	Triplex111 (EDTA-2Na)	10 mM
FACS buffer I	PBS	
	BSA	1 % (w/v)
	NaN3	0.1 % (w/v)
FACS buffer II	PBS	
	BSA	1 % (w/v)
	NaN3	0.1 % (w/v)
	EDTA, pH 8.0	20 mM
Freezing medium	DMSO	10 % (v/v)
	FCS	90 % (v/v)
Lysis buffer	Tris-HCl, pH 8.0	50 mM
	NaCl	100 mM
	SDS	1 % (w/v)
	EDTA, pH 8.0	100 mM
PBS/ 2 % FCS	PBS	
	FCS	2 % (v/v)
R10 medium	RPMI 1640	
	FCS	10 % (v/v)
	Penicillin	100 U/mL
	Streptomycin	100 µg/ mL
	L-Glutamine	2 mM
	MEM	1 % (v/v)
	Sodium Pyruvate	1 mM
	HEPES	10 mM
	β-Mercaptoethanol	50 µM
Skin medium	RPMI 1640	
	FCS	10 % (v/v)
	Penicillin	100 U/mL
	Streptomycin	100 µg/ mL
	L-Glutamine	2 mM
	HEPES	10 mM
TAE buffer	Tris	40 mM
	Acetic acid	40 mM
	EDTA	1 mM

2.1.6 Antibodies

Table 6. Anti-mouse monoclonal antibodies used in flow cytometry, *in vitro,* and *in vivo*. Antibodies and reagents were purchased from BioLegend (BioLegend, San Diego, CA, USA), BD (Becton Dickinson, Franklin Lakes, NJ, USA), or Thermo Fisher Scientific (Thermo Fisher Scientific, Waltham, MA, USA). Antibodies, with concentrations provided, were used for *in vitro* activation of T cells and concentrations are final. CD45.2 conjugated to biotin and was used for intravascular labeling, see 2.2.1.1. AF: Alexa Fluor, APC: allophycocyanin, BB: brilliant blue, BUV: brilliant ultraviolet, BV: brilliant violet, Cy: cyanine, FITC: fluorescein isothiocyanate, IL-7Rα: interleukin-7 receptor chain α, IFN-γ: interferon-γ, KLRG1: killer cell lectin-like receptor G1, PE: phycoerythrin, PerCP: Peridinin-Chlorophyll-Protein, TCR: T cell receptor, TCRV: T cell receptor variable chain, V: violet, *: after Heilig & Tonegawa, 1986.

Target	Conjugate	Clone/ Reagent	Use	Location	Company
Biotin	PE-Cy5	Streptavidin	1:400	-	BioLegend
CD103	BUV563 AF647	2E7 M290	1:200	Surface	BioLegend BD
CD11b	AF700 APC-Cy7 PE-Cy7	M1/70	1:200	Surface	BioLegend
CD127 (IL-7Rα)	BV786	SB/199	1:200	Surface	BD
CD19	PE AF700 APC-Cy7	6D5	1:200	Surface	BioLegend
CD28	/	37.51	1 µg/ mL	Surface	BioLegend
CD3ε	BV786	145-2C11	1:200	Surface	BioLegend
CD3ε	/	145-2C11	3 µg/ mL	Surface	BioLegend
CD4	FITC BV421	GK1.5	1:100	Surface	BioLegend
CD44	AF700 PE	IM7	1:400	Surface	BioLegend Thermo Fisher
CD45	BUV805 BV421 BV510 PE-Cy7	30-F11	1:100	Surface	BD BioLegend BioLegend BioLegend
CD45.2	Biotin	104	3 µg	Surface	BioLegend
CD49a	BV650 PE	Ha31/8 HMa1	1:200	Surface	BD BioLegend
CD62L	APC BV605	MEL-14	1:400	Surface	BioLegend
CD69	PE-Cy7	H1.2F3	1:100	Surface	BioLegend
CD8	APC BV510 PE	53-6.7	1:100	Surface	BioLegend
dead cells	eFluor 780	Fixable Viability Dye	1:1000	Surface/ Intracellular	Thermo Fisher
IFN-γ	APC	XMG1.2	1:100	Intracellular	BioLegend
Ki-67	PE	16A8	1:200	Intranuclear	BioLegend
KLRG1	BB700	2F1	1:400	Surface	BD
Ly6C	V450	AL-21	1:200	Surface	BD

Ly6G	Biotin FITC	1A8	1:400	Surface	BioLegend
TCRVγ4*	APC	UC3-10A6	1:200	Surface	BioLegend
TCRVδ4*	PE	GL2	1:200	Surface	BioLegend
TCRβ	PE-Dazzle 594®	H57-597	1:200	Surface	BioLegend
TCRγδ	PerCP-eF710	GL3	1:400	Surface	Thermo Fisher
Ter-119	APC-Cy7 APC-eFluor 780	Ter-119	1:200	Surface	BioLegend Thermo Fisher

Table 7. Anti-human monoclonal antibodies used in flow cytometry. Antibodies and reagents were purchased from BioLegend (BioLegend, San Diego, CA, USA), BD (Becton Dickinson, Franklin Lakes, NJ, USA), or Thermo Fisher Scientific (Thermo Fisher Scientific, Waltham, MA, USA). AF: Alexa Fluor, BUV: brilliant ultraviolet, BV: brilliant violet, Cy: cyanine, EBI2: Epstein-Barr virus-induced gene 2, FITC: fluorescein isothiocyanate, IL-7Rα: interleukin-7 receptor chain α, PE: phycoerythrin, PerCP: Peridinin-Chlorophyll-Protein, TCR: T cell receptor.

Target	Conjugate	Clone/ Reagent	Dilution	Location	Company
CD103	PE-Dazzle 594®	Ber-ACT8	1:50	Surface	BioLegend
CD127 (IL-7Rα)	PerCP-Cy5.5	A019D5	1:100	Surface	BioLegend
CD3ε	Pacific Blue	HIT3a	1:100	Surface	BioLegend
CD4	BV421 PE-Cy7	RPA-T4 OKT4	1:100 1:200	Surface	BioLegend
CD45	BUV805 BV421	HI30	1:40	Surface	BD BioLegend
CD45RA	FITC	HI100	1:40	Surface	Thermo Fisher
CD69	PE-Cy7	FN50	1:50	Surface	BioLegend
CD8	BV510	RPA-T8	1:100	Surface	BD
dead cells	eFluor 780	Fixable Viability Dye	1:1000	Surface/ Intracellular	Thermo Fisher
EBI2	AF647	SA313E4	1:12.5	Surface	BioLegend
TCR α/β	PE	IP26	1:50	Surface	BioLegend

Table 8. Anti-human monoclonal antibodies used for human psoriasis patient skin biopsy analysis. Antibodies and reagents were purchased from BioLegend (BioLegend, San Diego, CA, USA), BD (Becton Dickinson, Franklin Lakes, NJ, USA), or Thermo Fisher Scientific (Thermo Fisher Scientific, Waltham, MA, USA). CD: cluster of differentiation, EBI2: Epstein-Barr virus-induced gene 2, IFN-γ: interferon-γ, IL: interleukin, PD-1: programmed cell death protein 1, TCR: T cell receptor, PE: phycoerythrin, Cy: cyanine, BUV: brilliant ultraviolet, BV: brilliant violet, FITC: fluorescein isothiocyanate, APC: allophycocyanine, AF: Alexa Fluor.

Target	Conjugate	Clone	Dilution	Company
CCR7	PE-Cy5	G043H7	1:20	BioLegend
CD101	BUV563	V7.1	1:20	BD
CD103	PE-Dazzle	Ber-ACT8	1:50	BioLegend
CD4	BUV395	SK3	1:20	BD
CD45	BUV805	HI30	1:20	BD
CD45RA	FITC	HI100	1:100	Thermo Fisher Scientific
CD49a	BUV615	SR84	1:20	BD
CD69	PE-Cy7	FN50	1:50	BioLegend
CD8	BUV496	RPA-T8	1:20	BD
dead cells	APC-Cy7	Fixable Viability Dye	1:1000	Thermo Fisher Scientific
EBI2	AF647	SA313E4	1:12.5	BioLegend
Granzyme B	BV510	GB11	1:20	BD
IFN-γ	BV605	B27	1:20	BD
IL-10	R718	JES3-19F1	1:50	BD
IL-13	BV711	JES10-5A2	1:20	BD
IL-17A	BV750	N49-653	1:20	BD
IL-22	BB700	MH22B2	1:20	BD
IL-4	BUV737	MP4-25D2	1:20	BD
Ki-67	BV786	B56	1:20	BD
PD-1	BV421	EH12.1	1:20	BD
TCR α/β	PE	IP26	1:50	BioLegend

2.1.7 Software and bioinformatic tools

Table 9. Software and bioinformatical tools used for data analysis, statistics, and visualization.

Software	Version	Supplier
Affinity Designer 2	2.2	Serif, West Bridgford, UK
FlowJo Treestar	10.9	Becton Dickinson, NJ, USA
GraphPad Prism	10	GraphPad Software, CA, USA
Microsoft Office	Microsoft Office 365	Microsoft, WA, USA
Python	3.11	Python Software Foundation, DE, USA
R Statistical Software and R Studio	4.2.1 2022-06-23 ucrt	R Core Team, IN, USA
StepOne Software	2.3	Applied Biosystems, MA, USA

2.1.8 Mice

Housing: All mice were housed at the Heidelberg IBF (interfaculty biomedical research department) under specific pathogen-free (SPF) conditions. The mice were housed in type II conventional cages with semi-open tops, ABEDD LT-E-001 litter, 12 h/ 12 h light/ dark-rhythm, 22°C ± 2°C room temperature, 50 % - 60 % humidity and were fed *ad libitum* with water and Altromin Rod 16 or Rod 18. The cages were enriched with Crincklet's Nest Pads and the mice were housed according to the GV-SOLAS (*Gesellschaft für Versuchstierkunde*/ Society of Laboratory Animal Science) recommendations. Unless otherwise stated, mice of both sexes and all ages were used for the preparation of single-cell suspensions from tissues and for *in vivo* mouse models.

$EBI2^{EGFP}$ strain: This strain carries either an EBI2 WT allele ($EBI2^{+}$) or an EGFP minigene as a knock-in in place of the EBI2 gene on mutated alleles ($EBI2^{EGFP}$). In homozygous knock-in conformation ($EBI2^{EGFP/EGFP}$), this results in a whole-body EBI2 KO and instead EGFP expression under the control of the endogenous EBI2 promoter. Heterozygous knock-in conformation ($EBI2^{+/EGFP}$) results in dual expression of EBI2 and EGFP, both at approximately half the quantity compared to respective homozygotes. The original $EBI2^{fl\text{-}EGFP}$ mouse was created by Dr. Stefano Casola (Milan, Italy) (Figure 7). The name of this strain in the Mouse Genome Informatics (MGI) online repository is $GPR183^{tm1.2Scla}$, MGI ID:7265061. For this, targeted embryonic stem cells (ES, line: IB10/E14IB10) from the 129P2/OlaHsd strain of origin were injected into C57BL/6J blastocysts. Germline-transmitted offspring was crossed to a Cre recombinase expressing deleter strain, to delete the floxed allele. The resulting $EBI2^{EGFP}$ mice were crossed to a flippase (FLP)-expressing deleter strain to delete the neomycin resistance cassette. Afterward, the strain was crossed to the C57BL/6 background.

$EBI2^{flox\text{-}EGFP}CD4^{Cre}$ strain: This strain is a conditional EBI2 KO in all αβ T cells. The EBI2 locus of this strain resembles the one depicted in Figure 7, A, center ($EBI2^{flox}$, not crossed to the Cre- and FLP-deleter strains) or the WT locus (top) respectively. The EBI2 gene is transcribed under the control of the endogenous promoter and transcription should be abrogated on the indicated TGA stop codon. As a result, the EGFP gene should not be transcribed, when there is no Cre-recombinase expressed and EBI2 expression would therefore be WT-like. Additionally, this strain carries the Cre-recombinase gene under the control of the CD4 promoter. Because of transient CD4 promoter activity during thymic maturation, Cre-mediated deletion of the EBI2 single coding exon, together with the stop codon, occurs in all αβ T cells. In $EBI2^{+/+}$, $EBI2^{+/fl}$, $EBI2^{fl/fl}$, and $EBI2^{+/+}CD4^{Cre}$ mice, no recombination takes place and all cells should behave WT-like. In Cre-expressing mice, the expression of the floxed EBI2 allele determines the phenotype. In heterozygous conformation ($EBI2^{+/fl}CD4^{Cre}$), all αβ T cells should show a heterozygous EBI2 KO and EGFP reporter expression. In homozygous conformation ($EBI2^{fl/fl}CD4^{Cre}$) all αβ T cells should show a homozygous EBI2 KO and EGFP reporter expression.

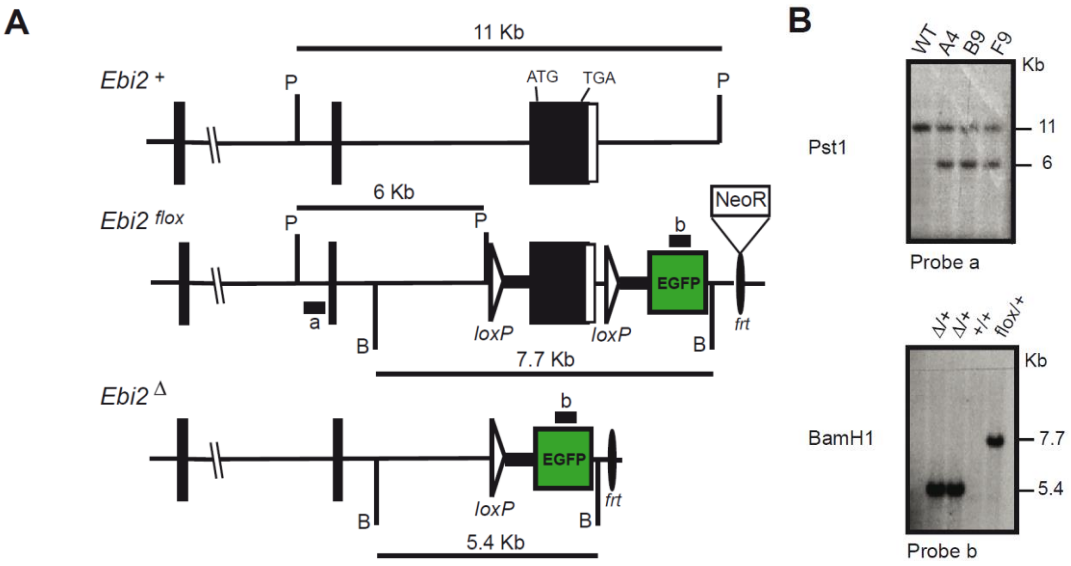

Figure 7. EBI2 locus of the EBI2^{EGFP} (Gpr183$^{tm1.2Scla}$) mouse strain. From Wanke *et al.*, 2017[120]. **A** The EBI2 locus in different states during the generation of the EBI2^{EGFP} mouse strain. Top: WT locus (EBI2^{+}). ATG: start codon, TGA: stop codon. P: Pst1 restriction enzyme recognition site. Center: floxed EBI2 gene with enhanced green fluorescent protein (EGFP) insertion (EBI2^{flox}). The EBI2-knock-in gene construct was inserted into the EBI2 locus, replacing the WT gene. The construct contains different Pst1 recognition sites and additional BamH1 restriction enzyme recognition sites (B). It also holds the EBI2 single-coding exon, flanked by loxP sites. The segment containing the intronic region upstream of the exon (fat section) and the loxP sequence, was cloned upstream of an EGFP reporter minigene, followed by a NeoR (neomycin resistance) cassette, flanked by frt (flippase recognition target) sites, which was subsequently cloned downstream of the EBI2^{fl} sequence. Fat lines with a and b indicate southern blot probe annealing sites. Bottom: EBI2 KO locus (EBI2$^{\Delta}$). Product of Cre-mediated deletion of content between loxP sites, resulting in an EBI2 knock-out (EBI2$^{\Delta}$ or EBI2^{EGFP}) and EGFP-reporter activity. Flippase-mediated recombination resulted in the deletion of the NeoR cassette between frt-sites. **B** Southern blot of DNA from different ES clones stained with probe a (top, digested with Pst1) or of DNA from EBI2^{EGFP} mice of indicated genotypes stained with probe b (bottom, digested with BamH1).

Controls: If not otherwise indicated, control animals were sex and age-matched littermates.

EBI2 WT mice: Different strains were used as EBI2 WT mice. Those were either commercially acquired C57BL6/J or EBI2 WT mice whose genetic background had no apparent or anticipated impact on the outcome of the experiment. This included mice of the following genotypes: Ly5.1^{hom} or Ly5.1^{het}, Thy1.1^{hom} or Thy1.1^{het}, IL-17Aind$^{fl/fl}$, IL-17RA$^{fl/fl}$, RiboTag$^{fl/fl}$, without Cre expression.

2.1.9 Human skin biopsies

Study design: I was solely responsible for conceptualizing the study, writing the ethics proposal, and coordinating the on-site implementation of the study. This involved coordination with the doctors, the surgical department, the study ambulance, and the hospital administration staff. I also prepared, measured, and analyzed the samples. I designed the high-parameter flow cytometry panel with 23 parameters. Prof. Dr. Knut Schäkel acted as advisor for the study planning and ethics proposal writing and mediator for the on-site implementation, Dr. Florian Kurschus functioned as advisor for all steps. Patients were included in the study when they presented with or were in-house diagnosed with psoriasis. Patients who met any of the following criteria were excluded from the study: under systemic immunomodulatory treatment, below 18 years of age, pregnant or breastfeeding, and had human immunodeficiency virus (HIV) or hepatitis B or C virus infections. After informed written consent, blood was drawn from the patients, and two 6 mm punch biopsies were taken under local anesthesia by a physician.

Punch biopsies of psoriatic skin: Two 6 mm punch biopsies were taken from psoriasis patients and kept in a sterile bandage, wetted with 0.9 % NaCl. One punch biopsy from lesional skin and one from non-lesional skin. Biopsies originated from varying body parts, but patient-matched samples were always from the ipsi- or contralateral body part. Non-lesional skin sites were at least 10 cm apart from a lesion. After removal, the biopsies were kept at 4°C and processed within 4 h.

Biopsies of healthy skin: Healthy skin removed during surgery was obtained from the surgical department of the University Hospital Heidelberg, Dermatology. The samples were of varying sizes, original body parts, and patient's sex and age. The skin samples were either Burow's triangles or split skin and were processed within 4 h after surgery. Burow's triangles are full-thickness skin samples that are comprised of hypodermis, dermis, and epidermis. Split skin is comprised of a thin layer of dermis and the whole epidermis and is taken using a dermatome.

2.2. Methods

2.2.1 *In vivo* mouse models

2.2.1.1. TNCB-induced contact hypersensitivity model

For sensitization, mice were shaved on the lower abdomen on day (d) -5 and painted with 15 µL of a 1 % TNCB solution solved in acetone:mygliol 812 (4:1) or just the solvent as control. On d0, the baseline ear thickness was measured using a digital caliper. The mice were then challenged for acute CHS by application of 10 µL of 0.5 % TNCB or solvent on each side of the ear pinnae. For investigation of the immune response in the edLNs and for consistency reasons, here, the superficial parotid LNs were used for analysis and referred to as edLNs after nomenclature from van den Broeck *et al*.[104]. The ear thickness was subsequently monitored for the time points indicated in the respective experiments. After a minimum of 30 days, re-challenge for the memory CHS was conducted as the challenge on the indicated ears. For chronic CHS, after the acute challenge on d0, the mice were challenged every 48 h for a total of 5 times with 0.5 % TNCB on the indicated ears, and ear swelling was monitored every 24 h. During the treatment, the mice were anesthetized by inhalation of an isoflurane/O_2 mixture, and their eyes were covered in a moisturizing cream containing 5 % dexpanthenol.

Labeling of vascular leukocytes: In indicated experiments, 3 µg biotin-labeled anti-mouse CD45.2 monoclonal antibody (mAb) was injected i.v. into the mice through the tail vein 3 min before sacrifice. This labels the intravascular leukocytes to distinguish them from tissue-resident ones.

NIBR189 intraperitoneal administration: In indicated experiments, mice were injected with 2 mg/ kg NIBR189 in phosphate buffered saline (PBS) or corresponding amounts of dimethyl sulfoxide (DMSO) in PBS intraperitoneal (i.p.) every 12 h, starting 1 h before the challenge.

FTY720 intraperitoneal administration: In indicated experiments, mice were administered 2.4 mg/ kg body weight FTY720 solved in ethanol (EtOH) and diluted in PBS, or equal amounts of EtOH in PBS as control. Administration was done from 49 h before challenge or re-challenge and until sacrifice, every 24 h by i.p. injection.

2.2.1.2. IMQ-induced psoriasis-like dermatitis

Female seven weeks old mice were used. The lower back was shaved on d-2. Additionally, the shaved area was depilated using Veet® sensitive depilation cream, which was applied onto the shaved area and was thoroughly removed after 2 min of incubation. After one day of rest, on d0, 50 mg of 5 % IMQ-containing Aldara® cream or sham cream as control was applied onto the shaved and depilated back skin area and 5 mg on each side of the ears. The cream was re-applied every 24 h for 5 days. The sham cream was custom-made by the pharmacy of the Medical Center of the Johannes Gutenberg University and was formulated to resemble the Aldara® cream as closely as possible, without the IMQ. On each day before the treatment, the mice were evaluated for parameters, that are based on the psoriasis area and severity index (PASI), which is used to clinically evaluate the severity of psoriasis in patients. Assessed

parameters included µm thickness of the back skin fold (measured with a digital caliper), and, ranked on a scale from 0 to 4, back skin erythema and back skin scaling (Table 10). These single scores were summed up to yield the cumulative score, indicating the severity of the IMQ-induced psoriasis-like dermatitis. During the treatment, the mice were anesthetized by inhalation of an isoflurane/O_2 mixture, and their eyes were covered in a moisturizing cream containing 5 % dexpanthenol.

Table 10. Scoring system for the IMQ-induced psoriasis-like dermatitis. *: increase of back skin fold thickness relative to d0, #: size and texture of the scales.

Score	Thickness*	Erythema	Scaling#
0	< 20 %	no	no
1	20 % - 40 %	light red	small
2	40 % - 60 %	red	medium, rough
3	60 % - 80 %	dark red	large, hard
4	> 80 %	dark red - violet	very large, plate-like

2.2.2 Genotyping of mice

Isolation of genomic DNA: Mice were genotyped by polymerase chain reaction (PCR). For this, genomic deoxyribonucleic acid (DNA) was isolated from tail pieces by overnight digestion in lysis buffer, containing Tris-hydrochloric acid (Tris-HCl, 50 mM, pH 8.0), NaCl (100 mM), sodium dodecyl sulfate (SDS, 1 %), ethylenediaminetetraacetic acid (EDTA, 100 mM), and proteinase K (0.5 mg/ mL), at 56°C, shaking. Debris was then pelleted at 18516.316 x g for 10 min at room temperature (RT). The supernatant was added to 2-propanol and was vigorously shaken to precipitate the DNA. The DNA was then pelleted at 18516.316 x g for 20 min, washed twice in 70 % EtOH, dried, and then solved in *Aqua destillata* (*A. dest*).

PCR: Two PCR master mixes were used: REDTaq®ReadyMix™ PCR Reaction Mix (Sigma-Aldrich) or DreamTaq™ PCR Master Mix (2X) (Thermo Fisher Scientific). Both contained a deoxynucleoside triphosphate (dNTP) mix (dATP, dCTP, dGTP, dTTP, 0.4 mM each) and $MgCl_2$ (4 mM), while the REDTaq®ReadyMix™ also contained Tris-HCl (20 mM, pH 8.3), KCl (100 mM), gelatin (0.002 %), *Taq* DNA Polymerase (0.06 U/ µL), as well as stabilizers and the DreamTaq™ mix contained DreamTaq buffer. The reaction was prepared in 25 µL total reaction volume, containing 10 µL REDTaq®ReadyMix™ or 12.5 µL DreamTaq™ mix, approx. 100 ng DNA template, and 10 pmol of each primer, and was filled up with water included in the kit. The primers are listed as part of Table 2. PCRs were run in the Biometra TRIO thermo cycler (Analytik Jena) with the following program: initial denaturation (95°C, for 5 min), 37 cycles of denaturation (95°C, for 30 s), annealing (58°C, for 30 s), and elongation (72°C, for 1 min), and a final elongation (72°C, for 10 min). The PCR products were stored at 4°C until used.

Agarose gel electrophoresis: For analysis of PCR product size, a 1.5 % agarose gel was prepared by adding Tris-acetate-EDTA (TAE) buffer (40 mM Tris, 40 mM acetic acid, 1 mM EDTA) to ULTRAPure™ Agarose (Invitrogen) and heating until dissolved. DNA staining dye Midori Green

Advance (NIPPON Genetics) was added at 5 µL/ 100 mL gel after cooling it at RT (room temperature) for 30 s. Marker DNA 100 bp+ DNA ladder (Fermentas) was used, and electrophoresis was performed at 120 mV. Imaging of the stained and separated DNA bands was performed using iBright FL1000 (Thermo Fisher Scientific).

2.2.3 Quantitative reverse-transcription polymerase chain reaction

RNA purification: For quantitative reverse transcription PCR (qRT-PCR), spleens from indicated mice were snap-frozen in liquid N_2 immediately after harvest. Total messenger ribonucleic acid (mRNA) extraction was done using Trizol® (Thermo Fisher Scientific), following the manufacturer's instructions. Briefly, the frozen organs were cut to use 50 mg - 100 mg of tissue per reaction. The tissue was thawed in Trizol at RT, homogenized using a tissue homogenizer, and incubated for 5 min at RT to dissociate nucleotide complexes. Chloroform was then added to the samples for cell lysis and incubated for 2 min. The lysate was then centrifuged at 12000 x g for 15 min at 4°C, the RNA-containing supernatant was collected, and 2-propanol was added for RNA precipitation. After centrifugation to purify the precipitate, the RNA was further purified by washing with 75 % EtOH, dried, and then solved in RNAse-free water. The concentration and purity were determined spectrometically using the NanoDrop® (DeNovix).

RT-PCR: Complementary DNA (cDNA) was reverse transcribed from isolated total RNA using the First Strand cDNA Synthesis kit (Thermo Fisher Scientific). Briefly, reverse transcription (RT)-PCR reaction components were prepared in PCR tubes as follows:

Table 11. Components for RT-PCR using the First Strand cDNA Synthesis kit. RNA: ribonucleic acid, U: unit, dNTP: deoxynucleoside triphosphate, M-Mulv: Moloney murine leukemia virus, *A. dest.*: *Aqua destillata.*

Per Reaction	Component
1 µg	RNA (1:10 prediluted in RNAse-free water)
1 µL	Random Hexamer Primers
4 µL	5 x Reaction Buffer
1 µL	RiboLock RNase Inhibitor (20 U/ µL)
2 µL	10 mM dNTP Mix
2 µL	M-MuLV Reverse Transcriptase (20 U/ µL) **OR** 2 µL *A. dest.* for no-enzyme control
9 µL	RNAse-free Water
20 µL	total

The RT-PCR mix was placed in a thermocycler and incubated for 5 min at 25°C, then at 37°C for 60 min, and finally for 5 min at 70°C to terminate the reaction. The resulting cDNA was then used for qPCR.

qPCR: For qPCR, the SYBR™ Green PCR Mastermix (Applied Biosystems, Table 12) was used. All measurements were done in triplicates and measured on the StepOnePlus Real-Time PCR cycler using the cycling program depicted in Table 13. Gene expression fold change of the gene of interest (GOI) was normalized to housekeeping genes using the $2^{-\Delta\Delta CT}$ method. It was calculated as:

$$gene\ expression\ fold\ change_{GOI} = 2^{-\Delta\Delta CT} = 2^{\Delta CT_{GOI} - \Delta CT_{housekeeping\ gene}}$$

Table 12. Components for qPCR per reaction. PCR: polymerase chain reaction, cDNA: complementary deoxyribonucleic acid. The primers are listed as part of Table 2.

Per Reaction	Component
10 µL	2 x SYBR™ Green PCR Mastermix
2 µL	primer forward + primer reverse (1 µM each)
4 µL	cDNA template (pre-diluted 1:10) OR RNAse-free water for no-template control
4 µL	RNAse-free water
20 µL	total volume

Table 13. Cycler program on StepOnePlus for qPCR with SYBR™ Green.

Step	Temperature	Duration	Cycles
activation	50°C	120 s	
initial denaturation	95°C	600 s	
denaturation	95°C	15 s	40 cylces
annealing + elongation	60°C	60 s	
final denaturation	95°C	15 s	
melting curve	60°C - 90°C	15 s	0.3°C increments

2.2.4 Preparation of single-cell suspensions from murine tissues

LN and spleen single-cell suspensions: LNs or spleens were harvested into 4°C PBS/ 2 % fetal calf serum (FCS), minced through a 40 µm cell strainer, pelleted at 300 x g at 4°C and assessed for viability, and counted using Neubauer Improved Counting Chamber and 0.1 % trypan blue (gibco).

Skin single-cell suspensions: Ears were harvested and stored in 4°C PBS. After drying, the ears were separated into ventral and dorsal ear lobes, minced with iris scissors, and digested in 0.5 mg/ mL Liberase (Sigma) with 0.05 mg/ mL DNase I (Sigma) in Roswell Park Memorial Institute 1640 (RPMI 1640, PAN-BioTech) for 1 h, shaking at 37°C. The ear was then dissociated by aspirating and expelling into a syringe through a 22 G cannula until aspirating without resistance. The cell suspension was then filtered through a 40 µm cell strainer and pelleted at 400 x g for 20 min.

Dermis and epidermis separation and single-cell suspensions: Separated ventral and dorsal ear lobes were obtained as described above. Prewarmed separation solution was added into wells of a 12-well plate. Due to different tissue content and thickness, the separation solution varied for each ear lobe. For ventral ear lobe: 0.5 % trypsin/ 0.2 % EDTA in PBS with 0.05 mg/ mL DNAse I, for dorsal ear lobe: 0.2 % trypsin/ 0.08 % EDTA with 0.05 mg/ mL DNAse I. Ventral and dorsal ear lobes were then placed floating on the separation solution with the dermis submerged in the separation solution and the epidermal side at air. After 30 min of incubation at 37°C and 5 % CO_2, 50 µL FCS was added to inhibit the enzymatic activity of the trypsin, and the plate was transferred onto ice. The ear lobes were washed with cold PBS and dried. The epidermis was peeled off the dermis using forceps and both parts were washed in cold PBS and digested as described for skin single-cell suspension above, except the digestion time was shortened to 30 min.

PBL (peripheral blood leukocyte) single-cell suspension: Blood was drawn by heart puncture and harvested into a lithium heparin (Li-Hep) collection tube to inhibit coagulation. The weight of the tube was taken before and after blood collection, to assess the volume of drawn blood. The whole blood was then diluted in PBS at RT and layered carefully on top of Histopaque®-1083 (density: 1.083 g/ mL, Sigma-Aldrich). After density centrifugation, the interface ring was harvested into PBS/ 2 % FCS, washed, assessed for viability, and counted using Neubauer Improved Counting Chamber and 0.1 % trypan blue.

2.2.5 Preparation of single-cell suspension from human tissues

Human skin single-cell suspensions: After removal of subcutaneous fat, the skin was cut into smaller pieces using a scalpel and transferred into a C-tube (Merck) in 1 mL of skin medium, containing RPMI 1640, FCS (10 %), Penicillin/ Streptomycin (Pen/Strep, 100 U/ mL and 100 µg/ mL), L-glutamine (2 mM), and 4-(2-hydroxyethyl)-1-piperazineethanesulfonic acid (HEPES, 10 mM). The skin was further minced to increase the surface area for digestion by cutting with scissors. DNase I (0.02 mg/ mL) and collagenase type IV (0.8 mg/ mL) were added, as well as 4 mL of skin medium. For digestion, the tissue was incubated for 14 h at 37°C, 5 % CO_2. To stop the digestion, the tissue was put on ice and subsequently dissociated using the gentleMACS™ (Merck) dissociator with program Multi_B01. The cells were then passed over a 100 µm cell strainer, washed with PBS/ 2 % FCS, passed over a 40 µm cell strainer again, and washed with PBS/ 2 % FCS.

PBMC single-cell suspensions: 9 mL of human full blood was drawn into EDTA tubes, to inhibit coagulation. The blood was kept at 4°C and processed within 4 h, where it was diluted with PBS to a total volume of 35 mL and layered on top of 15 mL peripheral blood mononuclear cell (PBMC) spin medium (density: 1.077 g/ mL, pluriSelect). After density centrifugation for 25 min at 1500 x g at RT with centrifuge acceleration set to 3 and break turned off, the interface ring was harvested into PBS/ 2 % FCS, washed, and assessed for viability, and counted using Neubauer Improved Counting Chamber and 0.1 % trypan blue.

Freezing and thawing of PBMCs: PBMC pellets from healthy donors were resuspended in 90 % FCS/ 10 % DMSO freezing medium, aliquoted at 1 x 10^6 cells per vial, transferred into RT Mr. Frosty™ (Thermo Fisher Scientific) and subsequently to -80°C. The 2-propanol-filled Mr. Frosty facilitated a gradual freezing of the cells at a rate of approx. -1°C/ min. The next day, frozen cells were transferred and submerged in liquid N_2 for long-term storage. For thawing, cells were retrieved from liquid N_2 and immediately swirled in a 37°C water bath. As soon as only minimal ice was left, warm PBS/ 2 % FCS was added, and the suspension was transferred dropwise into 37°C PBS/ 2 % FCS, then pelleted and assessed for viability and counted using Neubauer Improved Counting Chamber and 0.1 % trypan blue.

2.2.6 Erythrocyte lysis

When murine spleen or bone marrow was handled, erythrocytes were lysed in ammonium chloride-potassium (ACK) buffer. For this, the cell suspension was pelleted and resuspended in 2 mL ACK-lysis buffer and incubated on ice for 2 min. Afterwards, 8 mL PBS/ 2 % FCS were added, and the suspension was pelleted. The procedure was repeated until the pellet appeared white.

2.2.7 Transwell migration assay (Boyden chamber)

Murine single-cell suspensions from LNs or spleen were generated as described in 2.2.4. The cells were pelleted and resuspended in R10 medium, containing RPMI 1640, FCS (10 %), Pen/ Strep (100 U/ mL, 100 µg/ mL), L-glutamine (2 mM), HEPES (10 mM), and β-Mercaptoethanol (50 µM). The cell suspension was then transferred into wells of a 12-well plate and activated either overnight with soluble anti-mouse CD3 mAb (1 µg/ mL) and anti-mouse CD28 mAb (6 ng/ mL) or with 50 µg/ mL phorbol 12-myristate 13-acetate (PMA) and 500 ng/ mL ionomycin for 3 h at 37°C and 5 % CO_2 as indicated. After the activation, the cells were harvested and adjusted to 1.34 x 10^6 cells/ mL (so that 75 µL contained 1 x 10^5 cells) in R10 medium. Attractant media were prepared using R10 medium supplemented with either indicated concentrations of 7α,25-OHC (Novartis), or equal amounts of DMSO as control or with CCL19/ CCL21 (50 ng/ mL each, BioLegend). 235 µL of prewarmed attractant media were added to each well of a 96-well receiver plate. A 96-well inlet with membranes that contain 5 µm pores was inserted into the receiver plate (Corning™ Costar™ HTS Transwell™). Due to specific volumes and surface tension, the attractant media touched but did not penetrate the membranes of the inlets. Finally, 75 µL cell suspension were added carefully into the top chamber on top of each membrane and the cells were left migrating into the bottom chamber for 3 h at 37°C and 5 % CO_2. As an 'input' reference, 75 µL cell suspension was added to a control plate with respective attractant media, without an inlet. Finally, the cells were incubated for 20 min at 4°C to stop the migration and centrifuged for 3 min at 180 x g at 4°C to release all cells that had migrated through the membrane but were still attached to the inlet. Cells from the bottom well are referred to as 'migrated' and cells from the input plate as

'input' and both were analyzed by flow cytometry. Accurate cell numbers were determined using Trucount Beads (Becton Dickinson) (section 2.2.8).

2.2.8 Flow Cytometry

Single-cell suspensions were generated as described in 2.2.4 and 2.2.5, transferred into a 96-well V-bottom plate (Corning®), and pelleted.

Re-activation: In cases where intracellular/ intranuclear staining was to be conducted, cell pellets were resuspended in R10 medium, containing PMA (50 ng/ mL), ionomycin (500 ng/ mL), and Brefeldin A (1 µg /mL) for 4 h at 37°C and 5 % CO_2. The cells were subsequently pelleted.

Surface staining: Pellets were resuspended in rat anti-mouse CD16 mAb and incubated for 10 min to minimize fragment crystallizable (Fc)-mediated unspecific binding. The mAbs used for surface staining as well as Fixable Viability Dye (Thermo Fisher Scientific) were diluted together in FACS buffer I, containing PBS, bovine serum albumin (BSA, 0.5 %), and NaN_3 (0.1 %). This master mix was added to the cells and incubated for a minimum of 30 min at 4°C, dark. The cells were washed twice in FACS I. Staining was performed in 96-well V bottom plates.

Biotin-Streptavidin staining: When biotin-labeled mAbs were used for surface staining, streptavidin-fluorochrome conjugates were diluted in FACS buffer I, added after washing of the surface-stained cells, and incubated for 15 min at 4°C in the dark. The cells were then washed twice in FACS buffer I.

Intracellular/ intranuclear staining: Re-activated and surface-stained cells were fixated by pelleting and resuspending in 2 % ROTI®Histofix (4 % ROTI®Histofix, Carl Roth, diluted 1:2 in PBS) and incubation for 40 min (for intracellular stainings) or 60 min (for intranuclear stainings) on ice in the dark[179]. The cells were then washed, resuspended in 1X permeabilization buffer (10X concentrate diluted in *A. dest.*, from FoxP3/Transcription Factor Staining kit, eBioscience), and pelleted again, to make the cell membrane permeable for the staining reagents. Intracellular/ intranuclear staining mAbs were diluted in 1X permeabilization buffer, added to the cells, and incubated for a minimum of 1 h. After this, the cells were washed twice in 1 x permeabilization buffer.

For acquisition, the cells were transferred into 5 mL tubes in fluorescence-activated cell sorting (FACS) buffer II and acquired at Beckmann Coulter Gallios or BD FACSymphony A3.

Counting beads: When cell counts are displayed, the samples were measured in FACS buffer II with BD Trucount Absolute Counting beads. The lyophilized beads were reconstituted in 1.5 mL FACS buffer II, vigorously vortexed and 100 µL were added to each tube. Each lot contained a defined number of beads. The beads for every sample were gated and corrected cell counts were calculated as follows:

$$beads\ per\ tube = \frac{total\ number\ of\ beads\ in\ 1.5\ mL}{15}$$

$$bead\ factor = \frac{beads\ per\ tube}{bead\ count\ measured}$$

$$corrected\ cell\ count = cell\ count\ measured\ \times bead\ factor$$

2.2.9 Bioinformatic analysis of public bulk RNA-sequencing data set

The investigated public data set was published by Tsoi *et al.* in 2019 in the Journal of Investigative Dermatology (doi: 10.1016/j.jid.2018.12.018, PubMedID: PMID: 30641038) included in their study 'Atopic Dermatitis Is an IL-13-Dominant Disease with Greater Molecular Heterogeneity Compared to Psoriasis'[180]. The data set is deposited in the Gene Expression Omnibus (GEO) Database under the Accession Number GSE121212. It was submitted there on October 14th, 2018, and the study was published on January 18th, 2019. This is a disclaimer, that all credit until publication goes to the authors. The analysis published here in this dissertation was done by me independently and does not claim to be involved in the generation of this data set nor the analysis published in the original study[180]. The differential gene expression analysis in this dissertation was done using R and R Studio. Gene counts were normalized using the DESeq2 method[181]. The workflow was according to the DESeq2 vignette, made available by the developers of DESeq2 under https://bioconductor.org/packages/devel/bioc/vignettes/DESeq2/inst/doc/DESeq2.html. Briefly: I imported the count matrix from the GEO repository, containing the number of aligned reads per gene, as well as the metadata file. I excluded one sample from the analysis, because this was the only non-matched singular sample (no sample pair of non-lesional and lesional skin of this patient). I constructed the dds (DEseq2DataSet) using the design formula 'design = ~ patient.ID + condition'. I normalized large batch effects with the surrogate variable method[182]. I conducted quality control using the pheatmap function from the pheatmap package, as well as the plotPCA function and the ggplot2 package to visualize the principal component analysis (PCA). I used shrunken log_2 fold change values, from the lfcShrink function on the comparison 'PSORIASIS_lesional vs CTRL_healthy' to construct the heatmap. I plotted the PCA from raw counts that were transformed by using the vst (variance-stabilizing transformation) function on the dds object, which contained raw counts, including only the top 5000 genes. Differential gene expression analysis was done using the DESeq2 function on the dds object and I made pair-wise comparisons manually using the results function in the DESeq2 results object, specifying the contrasts, i.e., the pairs of samples to compare, and using the Benjamini-Hochberg method to correct for multiple testing. I imported the results from the differential

gene expression analysis into Python to generate scatterplots and volcano plots with a custom script. The script, along with accessory files, is available at: https://github.com/theTcellGuy/GSE121212-Tsoi_et_al_2019 - in the GitHub repository 'GSE121212-Tsoi_et_al_2019'.

2.2.10 Statistical analysis

Statistical analysis was done using Excel (Microsoft) for the normalization of gene expression values from qRT-PCR using the $2^{-\Delta\Delta CT}$ method. I generated the AUC values of CHS ear swelling measurements with a custom Python (Python Software Foundation) script, using the trapezoidal method (trapz function) from the open-source library NumPy[183] and conducted statistical analysis thereof in GraphPad Prism 10. I also used a custom Python script to create scatter and volcano plots (Figure 8, Figure 9). I did all other statistical analyses in GraphPad Prism 10 with the indicated tests and test details. All graphs, besides the ones made in Python and the flow cytometry dot plots, were made in GraphPad. I conducted the differential gene expression analysis in R and R Studio, using the DESeq2 package, as described in section 2.2.9.

3. Results

3.1. EBI2-oxysterol axis genes are upregulated in inflamed skin in a public bulk transcriptome sequencing dataset.

In 2012, a single nucleotide polymorphism (SNP) in the *GPR183* (EBI2) gene was associated with an increased risk of developing IBD in a GWAS[170]. Following up on this, a study published in 2021 by Ruiz *et al*. found strong evidence that the EBI2-oxysterol axis is also implicated in the disease pathology of psoriasis[172]. They had observed that a cohort with the rs9513593-G SNP in the *GPR183* gene had elevated EBI2 surface expression on peripheral blood T cells that also expressed CCR6 or CCR9 and were therefore linked to T_H17 cells and IBD. This was the first association of the EBI2-oxysterol axis with skin disease pathogenesis. Moreover, another study from 2021 linked a SNP in the *CH25H* gene to increased risk for IBD development as well, further highlighting the potential involvement of the EBI2-oxysterol axis in IBD pathogenesis[169].

Intrigued by this finding, public bulk transcriptome sequencing data of healthy skin and matched non-lesional and lesional skin from psoriasis, AD, and CAD (chronic AD) patients, published in the study by Tsoi *et al*. in 2019 (GEO data accession number: GSE121212, doi: 10.1016/j.jid.2018.12.018)[180], was analyzed in R and python to specifically investigate the expression pattern of genes of the EBI2-oxysterol axis. As quality control measures, PCA and heatmaps were created, which indeed showed clustering by the top genes according to disease state (Figure 8 A, B). Furthermore, the genes *IL17A*, *IL13,* and *IL22*, which are known to be important in the pathogenesis of either psoriasis or AD, showed increased gene counts in the respective lesional skin samples (Figure 8 D). This validates the normalization script generated, using DESeq2 for gene count normalization[181]. Strikingly, gene counts for *CH25H* were also elevated slightly in lesional compared to non-lesional skin from psoriasis patients, and even more pronounced for AD and CAD (Figure 8 E). *CYP7B1* counts showed elevated counts in all three conditions, but especially for psoriasis lesional skin. These are the first indications that the enzymes that generate the EBI2 ligand 7α,25-OHC, are upregulated in lesional skin of psoriasis and AD. In line with this, the ligand-degrading enzyme *HSB3B7* did not show increased gene expression in any condition, further strengthening the assumption that 7α,25-OHC is synthesized and enriched in lesional skin and not degraded. Additionally, the counts for the *GPR183* gene were also increased in lesional compared to non-lesional skin in all three conditions.

Differential expression analysis using DESeq2 then enabled statistical analysis to explore up- or downregulation of the genes. The threshold for up- and downregulated expression of genes was set to a 2-fold increase or decrease respectively, considering only significantly differently expressed genes with an adjusted p-value < 0.05. However, even though these thresholds are the ones chosen in the original study, they are arbitrarily set. Fold changes > 2 therefore do not guarantee biological relevance, and fold changes < 2 likewise can also be biologically meaningful.

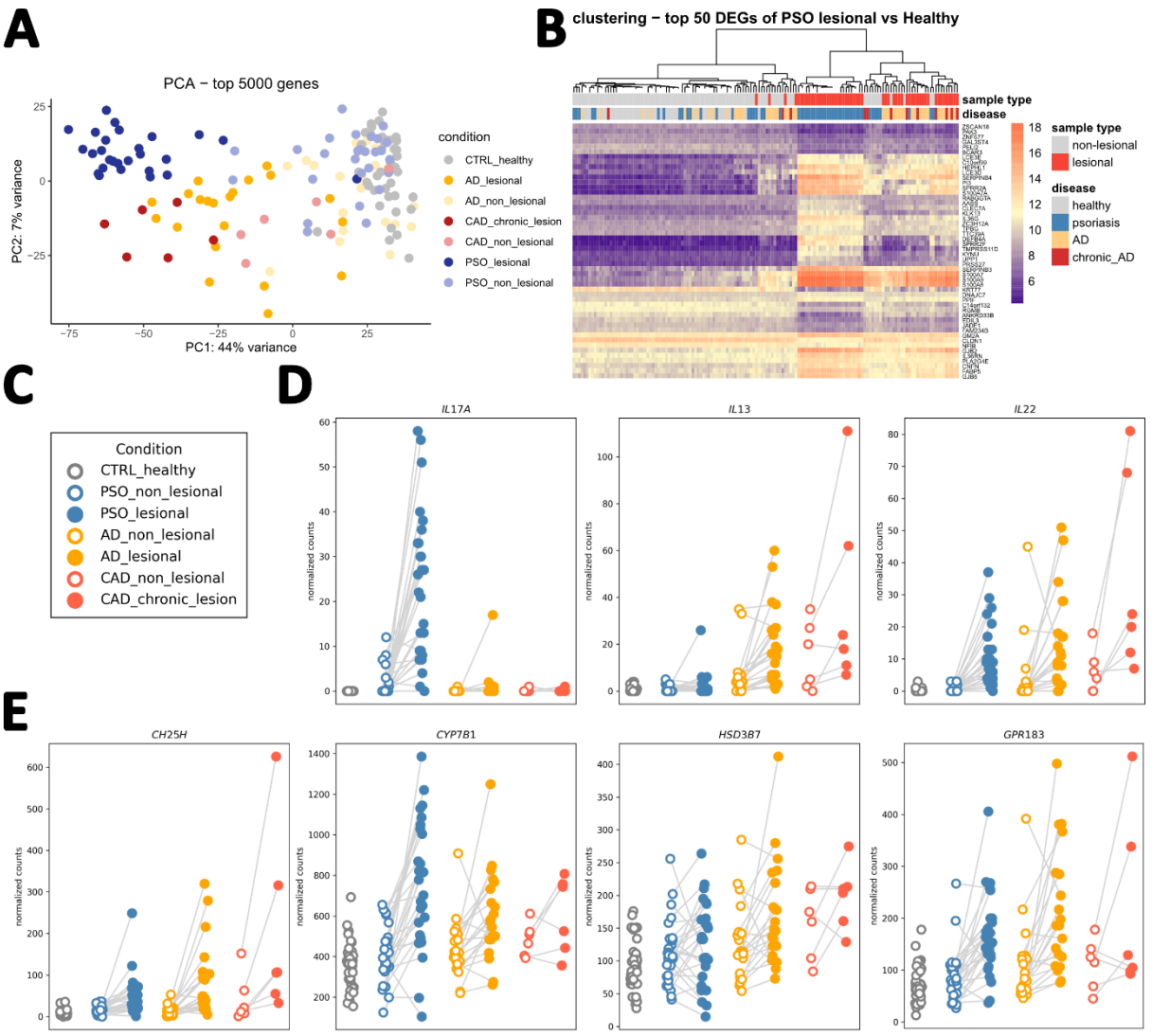

Figure 8. EBI2-oxysterol axis gene expression in human skin diseases - analysis of bulk RNA seq data set GSE121212 from Tsoi *et al*. Normalization and differential gene expression analysis were conducted in R using the DESeq2 package[181]. In their study, Tsoi *et al.* conducted bulk RNA-sequencing on skin punch biopsies of healthy control donors (CTRL_healthy, H, n = 38), psoriasis patients - matched non-lesional (PSO_non_lesional) and lesional skin (PSO_lesional, PSO_L, n = 28), and atopic dermatitis (AD) patients - matched non-lesional (AD_non_lesional) and lesional skin (AD_lesional, n = 21) as well as chronic AD - matched non-lesional (CAD_non_lesional) and lesional skin (CAD_chronic_lesion, n = 6)[180]. **A-B** Quality control, figures created in R. **A** Principal component analysis (PCA) using the top 5000 genes. **B** Heatmap using the top 50 differentially expressed genes (DEGs) when comparing PSO_lesional with CTRL_healthy. Top 50 DEGs with the highest p-value from Wald-test adjusted with the Benjamini-Hochberg procedure. The scale indicates variance-stabilizing transformed normalized counts. **C-E** Targeted analysis for the indicated genes. **C** Legend for **D-E**. Shown are scatter plots created in Python from the normalized counts obtained in R. Matched samples are connected by a grey line. **D** Genes associated with either psoriasis or AD disease pathogenesis. **E** Genes of the EBI2-oxysterol-axis.

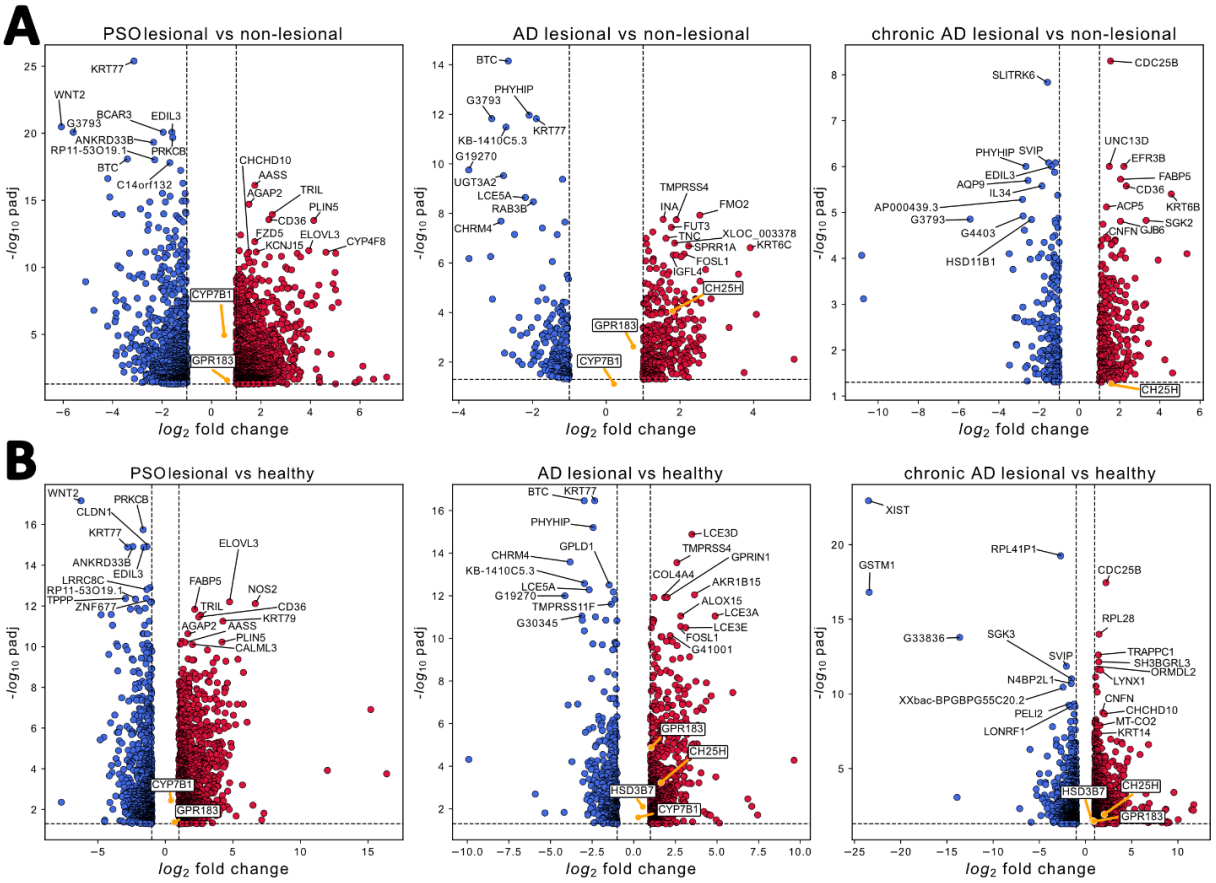

Figure 9. Differential expression analysis of normalized read counts from bulk RNAseq data set GSE121212 from Tsoi *et al*. Normalization and differential gene expression analysis were conducted in R using the DESeq2 package[181]. In their study, Tsoi *et al.* conducted bulk RNA-sequencing on skin punch biopsies of healthy donors (CTRL_healthy, n = 38), psoriasis patients - matched non-lesional (PSO_non_lesional) and lesional skin (PSO_lesional, n = 28), and atopic dermatitis (AD) patients - matched non-lesional (AD_non_lesional) and lesional skin (AD_lesional, n = 21) as well as chronic AD - matched non-lesional (CAD_non_lesional) and lesional skin (CAD_chronic_lesion, n = 6)[180]. Volcano plots, showing differentially expressed genes in the indicated comparisons between **A** matched lesional and non-lesional skin biopsies and **B** not matched lesional and healthy skin biopsies. Shown are -log10 of adjusted p-value (padj) vs log2 fold change in gene expression from the differential expression analysis for all genes with a padj ≤ 0.1. The threshold for differential gene expression was set to padj ≤ 0.05 (corresponding to -log10 of 1.3). Genes were considered upregulated with a fold change of ≥ 2 (corresponding to a log2 fold change of 1) and downregulated with a fold change > 2 (log2 fold change of -1).

Comparing lesional skin to matched non-lesional skin (Figure 9 A), *CYP7B1* and *GPR183* were differentially expressed in psoriasis but showed only a slight increase in expression. In AD, *CH25H* was highly upregulated and *GPR183* was differentially expressed, but not upregulated, considering the threshold. In chronic AD, no genes of the EBI2-oxysterol axis were differentially expressed. Comparing lesional skin to not matched healthy skin, the differences were more extreme for genes of the EBI2-oxysterol axis and *GPR183* as well as *CH25H* showed significant upregulation in AD skin, *CH25H* also in CAD.

Taken together, I wrote an R script for the normalization and differential expression analysis of a public data set, which passed the quality control measures. Importantly, using this script, I found that the genes of the EBI2-oxysterol axis were differentially expressed and upregulated in skin lesions of psoriasis and AD patients, especially in the lesional skin of AD patients. In many other comparisons, differential expression was apparent, but the upregulation did not cross the 2-fold threshold.

Interestingly, these results are in line with previous results from Julius Schwingen from my group. He showed in mice, that TNCB-application onto the ear skin (causing rather severe inflammation in the skin) led to a significant upregulation of the *Ch25h* and *Cyp7b1* mRNA in the ear, but not of *Hsd3b7* (dissertation submitted for review, 2023) when compared to solvent-treated ears. He observed upregulation of *Ch25h* already 12 h post application and of both EBI2 ligand-generating enzymes 24 h post application. Taken together, his results and my targeted analysis suggest an induction of the EBI2-oxysterol axis enzymes early at the site of inflammation and thereby the generation and accumulation of 7α,25-OHC, building up a ligand gradient in mouse and human skin. EBI2-expressing cells in the immediate vicinity would be able to sense this gradient and migrate to the epicenter of the inflammation.

3.2. The role of T cells and EBI2 in inflammatory skin disease mouse models.

3.2.1 Characterization of the EBI2^{flox}CD4^{Cre} strain as a conditional EBI2 KO in T cells.

Because there were strong indications that the EBI2-oxysterol axis could play a role in inflammatory skin disease pathologies and that T cells might be involved in this[172], a T cell-specific conditional preclinical KO mouse model would enable a targeted and detailed investigation of this matter. For this, the EBI2$^{fl/fl}$CD4^{Cre} line was to be used, where Cre-recombinase expression is under the control of the endogenous CD4 promoter. After Cre-mediated recombination, the floxed *Gpr183* single coding exon is excised and an EGFP minigene is inserted in place expressed under the control of the EBI2 promoter. This transgenic mouse line therefore serves a dual purpose, as a conditional EBI2 KO and reporter for EBI2 expression. Due to CD4 expression in all T cells at the double-positive state during thymic development, this should generate an αβ T cell-specific KO of EBI2 after thymic development. Studying EBI2 in mice still poses a serious challenge, due to the lack of a functional antibody that targets the murine form, despite 88 % sequence homology to the human homolog for which mAbs are available.

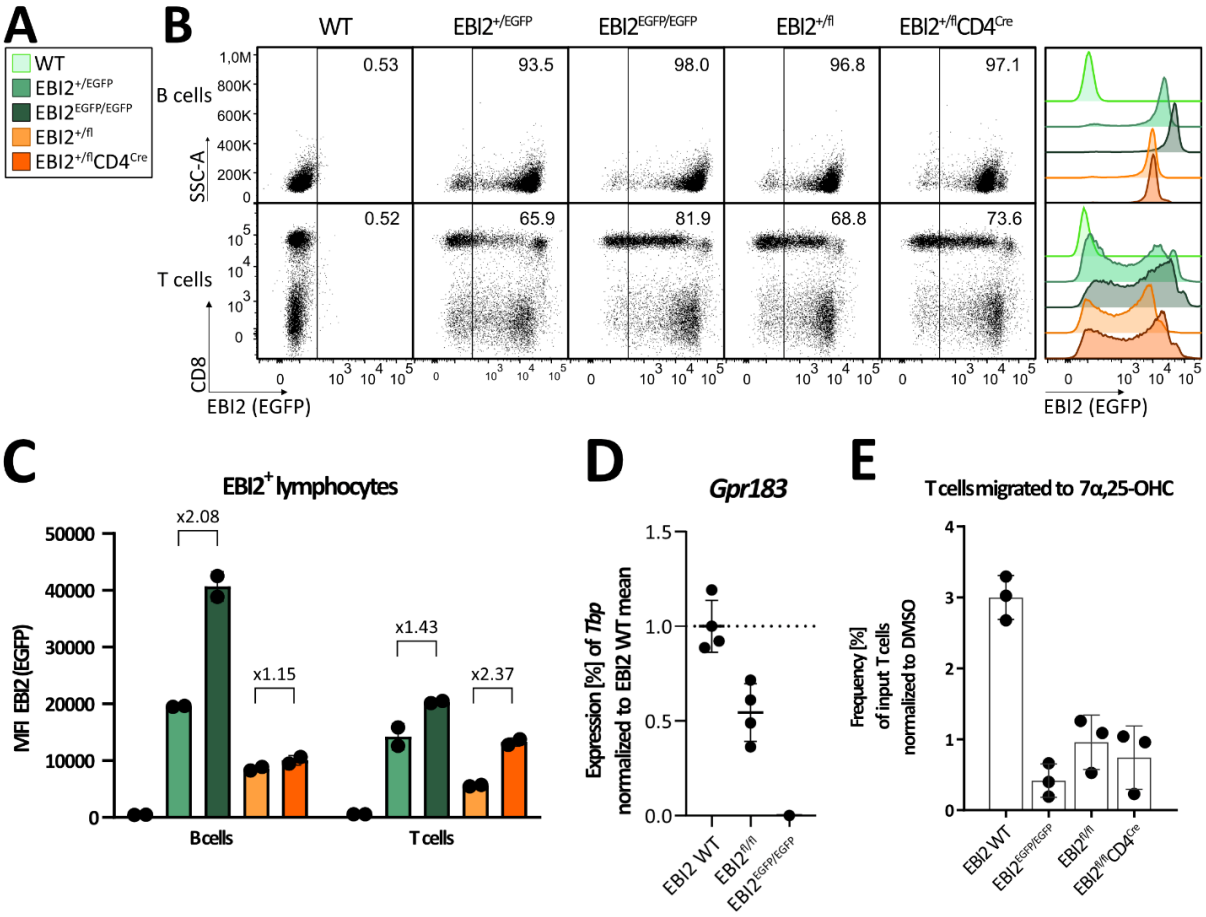

Figure 10. Phenotypical and functional characterization of the EBI2 expression in EBI2^{flox}CD4^{Cre} mice. **A-C** Flow cytometric analysis of B cells (top) and T cells (bottom) of pooled inguinal and brachial LNs from mice of indicated genotype (n = 2 each). **A** Legend for **B-C. B** Shown are representative dot plots and frequencies of EBI2 (EGFP)$^{+}$ fractions. **C** MFI of EBI2 (EGFP) of B- and T cells from **B**. **D** Relative gene expression of the murine EBI2 gene *Gpr*183 in spleen lysate of mice of indicated genotypes, measured by qRT-PCR. Relative expression was calculated as the percent of *Tbp* for all samples individually and then normalized to the mean relative expression of EBI2 WT mice (shown as a dotted line) using the $2^{-\Delta\Delta CT}$ method. Pooled from two individual experiments. The experiment conducted by me involved the comparison of EBI2 WT, EBI2$^{fl/fl,}$ and EBI2$^{EGFP/EGFP}$ (n = 1 each). The other experiment was conducted by intern Zeina Salloum, comparing EBI2 WT and EBI2$^{fl/fl}$ (n = 3 each). Dots represent individual mice with mean ± SD. **E** Boyden chamber transwell migration assay of LN cells from pooled superficial LNs of mice of indicated genotypes (n = 1 each). LN single-cell suspensions were seeded in the top chamber on top of a membrane with 5 µm pores or seeded in a separate plate as input control. The EBI2-ligand 7α,25-OHC (10 nM) was added to the bottom chamber as an attractant, and cells were left migrating for 3 h. Shown are migrated T cells in the bottom chamber as a percentage of input, quantified via flow cytometry. Dots represent technical replicates of n = 1 with bars depicting the mean ± SD. TBP: TATA-binding protein.

The EBI2$^{fl/fl}$CD4^{Cre} mouse was analyzed flow cytometrically to verify correct targeting and the EBI2 (EGFP) signal was compared to EBI2$^{+/EGFP}$ and EBI2$^{EGFP/EGFP}$ mice (Figure 10 A-C). As expected, WT mice showed no EGFP signal and EBI2$^{+/EGFP}$ mice showed a strong EGFP signal in B cells and T cells, much in line with previously reported frequencies of EBI2-expressing lymphocytes[122] with B cells being nearly uniformly EBI2^{+} and T cells expressing EBI2 differently

depending on the lineage ($CD4^+$ or $CD8^+$). Since the EBI2 (EGFP) mean fluorescence intensity (MFI) doubled nearly perfectly from $EBI2^{+/EGFP}$ to $EBI2^{EGFP/EGFP}$, the fraction of EBI2-positive-gated cells increased with the same gating applied to both. Unexpectedly, the $EBI2^{+/fl}$ mouse showed EGFP expression despite the absence of Cre. Additionally, EGFP expression was apparent in B cells. In fact, the signal was even comparable to the signal from $EBI2^{+/EGFP}$ mice. This indicated a Cre-independent, so-called 'leaky' expression of EGFP. Interestingly, with Cre expression present in the $EBI2^{+/fl}CD4^{Cre}$ mouse, the EBI2 (EGFP) signal increased, but only in T cells and not in B cells, suggesting correct targeting of the Cre-mediated recombination.

Leaky expression of the downstream EGFP could mean that the *Gpr183* mRNA produced was altered and might not have produced a functional protein. To investigate this, qRT-PCR was performed for quantification of the *Gpr183* mRNA (Figure 10 D). A two-fold reduction of the *Gpr183* mRNA was observed, comparing $EBI2^{fl/fl}$ to WT. Negligible amounts of *Gpr183* mRNA were detected in the $EBI2^{EGFP/EGFP}$ mice. Whether the *Gpr183* mRNA was expressed at lower levels or altered in a way that the primers were unable to bind their target, could not be discriminated at this point and was not further investigated.

A Boyden Chamber transwell migration assay was established in order to investigate the EBI2-specific migratory capacity of LN suspensions. WT LN suspensions showed specific migration towards the EBI2 ligand 7α,25-OHC in the bottom chamber, with a 3-fold higher number of cells migrating towards it compared to DMSO as an attractant (Figure 10 E). Expectedly, $EBI2^{EGFP/EGFP}$ LN suspensions showed near baseline levels of migratory cells, verifying that $EBI2^{EGFP/EGFP}$ cells were unable to sense and respond to 7α,25-OHC and verifying the assay. In line with the previous results, LN suspensions from $EBI2^{fl/fl}$ and $EBI2^{fl/fl}CD4^{Cre}$ mice showed a decreased ability to specifically migrate towards 7α,25-OHC. The migrated fraction of the $EBI2^{fl/fl}$ LN cells was slightly higher than the one from $EBI2^{EGFP/EGFP}$ LN cells, suggesting residual EBI2 expression.

Taken together, I could show that the $EBI2^{fl/fl}$ and $EBI2^{fl/fl}CD4^{Cre}$ mouse strains did not show a conditional T cell-specific KO of EBI2, but rather a leaky expression of EGFP. This was in conjunction with reduced detection of the *Gpr183* mRNA, likely creating an aberrant *Gpr183* mRNA that might have fused with the *EGFP* mRNA. In any case, this resulted in the expression of a detectable EGFP, as demonstrated by flow cytometry, with strongly decreased levels of the functional EBI2 protein, as both lines showed a drastically impaired ability to migrate specifically towards 7α,25-OHC. Hence, these mouse strains were not utilized in further experiments. Of note the $EBI2^{EGFP}$ strain was not affected by this 'leaky expression' and EBI2 expression of all genotypes ($EBI2^{+/+}$, $EBI2^{+/EGFP}$, and $EBI2^{EGFP/EGFP}$) was validated and deemed as expected. The WT alleles in this strain are purely WT and not floxed or willingly altered in any way. The KO alleles are recombined and have EGFP in place of EBI2.

3.2.2 The role of EBI2 in the TNCB-induced CHS reaction as a model of ACD.

To elucidate the involvement of EBI2 in inflammatory skin disease models in mice, the TNCB-induced CHS reaction was utilized (introduced in section 1.4, method described in section 2.2.1.1). Since T cell-, specifically $CD4^+$ T cell, responses have been shown to rely at least partially on EBI2 (see section 1.6.3), it was reasonable to assume that a deficiency of EBI2 may lead to a milder phenotype in the CHS model. However, no difference in the ear swelling reaction between $EBI2^{EGFP/EGFP}$ and $EBI2^{+/EGFP}$ mice was observed, neither in the acute phase (d0-d2 post challenge) nor in the memory phase (d30-d32 post challenge) (Figure 11 A, B). In line with previous reports, the re-call reaction was indeed stronger than the acute reaction. Additionally, the question arose whether the magnitude of the acute ear swelling reaction dictates the magnitude of the memory reaction in individual mice. A stronger acute response would thereby lead to a more robust memory formation and therefore to a stronger re-call response. However, no correlation between the area under the curve (AUC) of the acute and memory phase was observed (Figure 11 C).

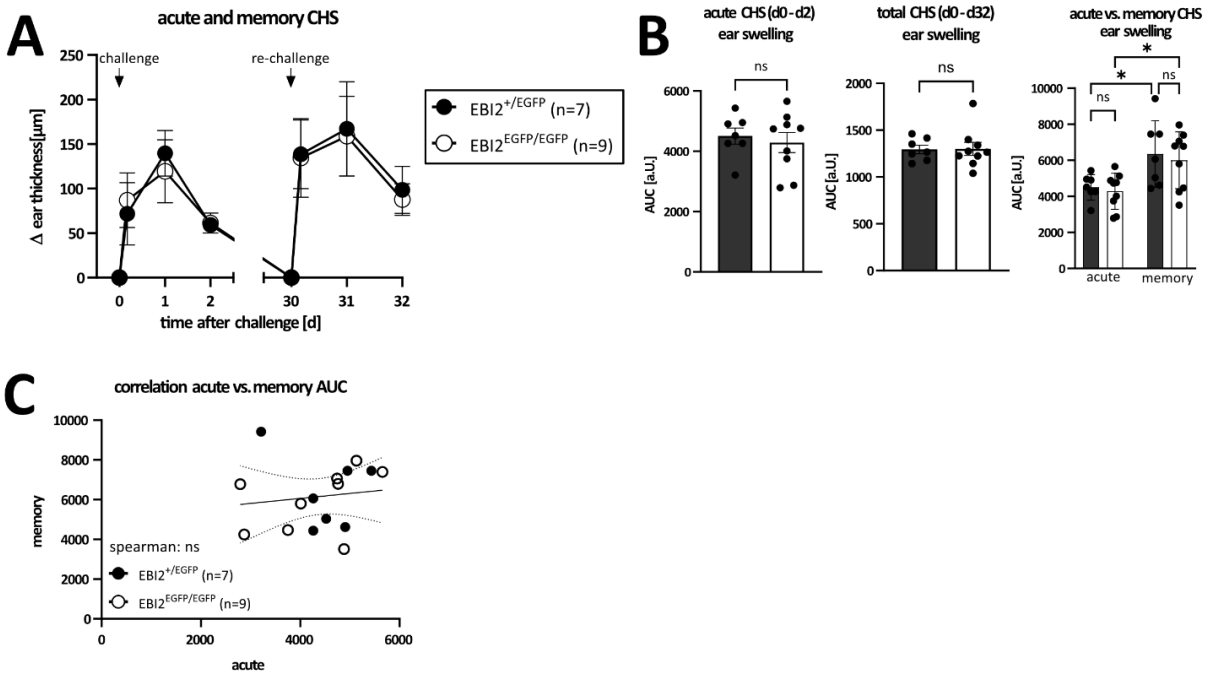

Figure 11. The role of EBI2 in acute and memory TNCB-induced CHS. A Ear swelling reaction in acute and memory CHS of $EBI2^{+/EGFP}$ (n = 7) and $EBI2^{EGFP/EGFP}$ (n = 9) mice. Mice were sensitized on the shaved abdomen with 1 % TNCB on d-5. For acute CHS, the mice were challenged on d0 with 0.5 % TNCB on both ears. For memory CHS, the mice were re-challenged on d30 with 0.5 % TNCB on the ears. Arrows indicate TNCB application. Shown is the mean ± SD. **B** Area under the curve (AUC) in arbitrary units (a.U.) for the ear swelling reaction shown in **A**. Left: calculation only done on curves from d0 to d2. Center: calculation done on the whole time from d0 to d32. Right: comparison of the AUCs calculated for acute (d0-d2) vs memory (d30-d32). AUCs were calculated for each mouse individually in python using the composite trapezoidal rule with the NumPy.trapz function. Dots represent individual mice with bars depicting the mean ± SD. Two-tailed Mann-Whitney test. **C** Correlation of the acute vs memory AUC for each mouse from **B** right panel. Dots represent individual mice, the straight line shows linear regression, and dotted lines indicate 95 % confidence intervals. Two-tailed Spearman correlation tested. ns: not significant, * $p < 0.05$.

In conclusion, full-body EBI2 KO did not lead to a reduced CHS flare-up reaction, neither in the acute nor in the memory phase of the TNCB-induced CHS model. Also, the strength of the memory response was independent of the strength of the acute response.

Another variation of the CHS model is the chronic CHS reaction. There, instead of a singular application of the antigen to elicit the acute or memory response, the antigen is applied repeatedly onto the skin, every 48 h for a total of five times[184,185]. This model is also dependent on T cells which are continuously stimulated by repeated antigen applications. As EBI2 deficiency was reported to cause a delay in B- and T cell priming in the LNs[123,150], rather than a complete abrogation of the priming, a singular challenge might not be sensitive enough to visualize an underlying delay of the T cell response.

The ear swelling increased after every challenge and increased over the level of peak acute ear swelling at 24 h post first challenge (Figure 12 A). However, no significant difference in the chronic flare-up reaction between $EBI2^{+/EGFP}$ and $EBI2^{EGFP/EGFP}$ mice was observed (Figure 12 B). The reaction to the irritant solvent solution of acetone and Mygliol (solvent control, left ear) was apparent but not strong and did not increase over time, despite repeated application (Figure 12 C). A hint towards an underlying priming deficiency of $EBI2^{EGFP/EGFP}$ mice was observed when analyzing the cell counts in the draining lymph nodes on d9, where the $EBI2^{EGFP/EGFP}$ mice showed significantly reduced numbers of LN suspension cells compared to the $EBI2^{+/EGFP}$ mice (Figure 12 D). However, this was not reflected in the B- and T cell numbers in the edLNs determined by flow cytometric analysis (Figure 12 E), nor did it affect the proportions of T cell populations (T_N, T_{EM}, T_{CM} cells, data not shown) in the edLNs.

Unexpectedly, the $EBI2^{EGFP/EGFP}$ mice did not show a deficit in any of the TNCB-induced CHS models. It is known that complete full-body knockouts can lead to genetic compensatory mechanisms[186–188]. Genetic compensation is a phenomenon where the deletion of a gene would induce the upregulation of genes whose product could compensate for the loss of the originally deleted gene. Such compensatory mechanisms in the $EBI2^{EGFP/EGFP}$ line could be accounted for by either a conditional KO or by pharmacological inhibition. Since it was not possible to utilize the conditional $EBI2^{fl}CD4^{Cre}$ line, EBI2 was pharmacologically inhibited in EBI2 WT mice. NIBR189 is an EBI2-specific inhibitor from Novartis, Basel, Switzerland[125].

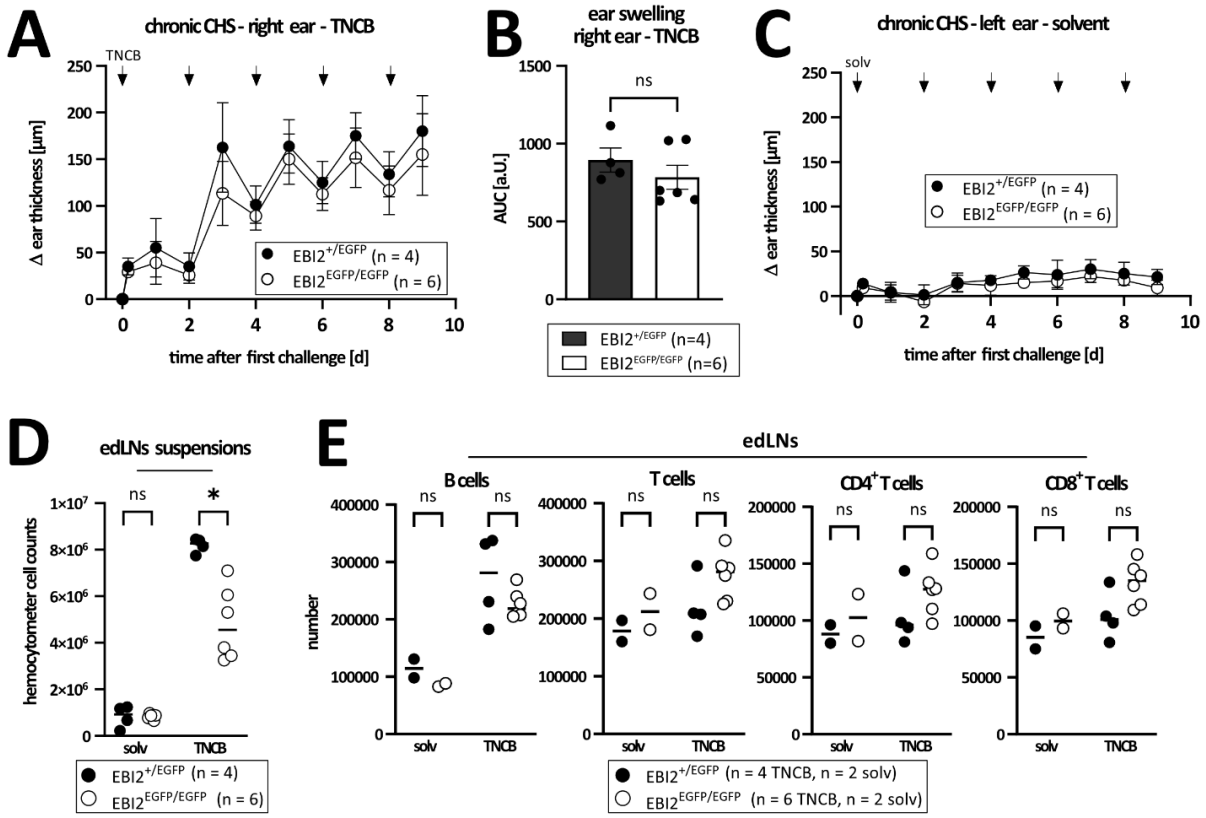

Figure 12. The role of EBI2 in chronic TNCB-induced CHS. A Ear swelling reaction in chronic CHS of EBI2$^{+/EGFP}$ (n = 4) and EBI2$^{EGFP/EGFP}$ (n = 6) mice. Mice were sensitized on the shaved abdomen on d-5 with 1 % TNCB and challenged with solvent (left) on one ear and with 0.5 % TNCB (right) on the other ear on d0. They received four additional TNCB- or solvent challenges respectively on d2, d4, d6, and d8. Shown is the mean ± SD. Arrows indicate solvent or TNCB-application times respectively. **B** Area under the curve (AUC) in arbitrary units (a.U.) for the ear swelling reaction shown in **A** (d0-d9). AUCs were calculated for each mouse individually in python using the composite trapezoidal rule with the NumPy.trapz function. Dots represent individual mice with bars depicting the mean ± SD. Two-tailed Mann-Whitney test. **C** Ear swelling reaction of the solvent-treated ears. **D** Number of live LN single-cell suspension cells from ear-draining (ed) LNs from **A** at d9 from either the solvent-treated side (solv) or the TNCB-treated side (TNCB), counted using hemocytometer and 0.1 % Trypan Blue. Dots represent individual mice. Two-tailed Mann-Whitney test. **E** Number of B- and T cells in edLN suspensions from **D** determined by flow cytometry. Dots represent individual mice and horizontal bars indicate the mean. Two-tailed Mann-Whitney test. ns: not significant, * $p < 0.05$.

Treatment of EBI2 WT mice with NIBR189 had no impact on the acute ear swelling reaction, compared to DMSO (Figure 13 A). There was also no significant difference in the number of LN suspension cells in general or specifically in the number of T cells in either the ear or the edLNs (Figure 13 B-D). The ratio of CD4$^+$ to CD8$^+$ T cells was also unchanged when the mice were treated with the EBI2 inhibitor. EBI2 deficiency has been described to differentially impact CD4$^+$ and CD8$^+$ T cell priming[150], but such an increase in the proportion of CD8$^+$ T cells was not observed in this experiment; neither in the edLNs nor in the isolated ear skin infiltrating cells.

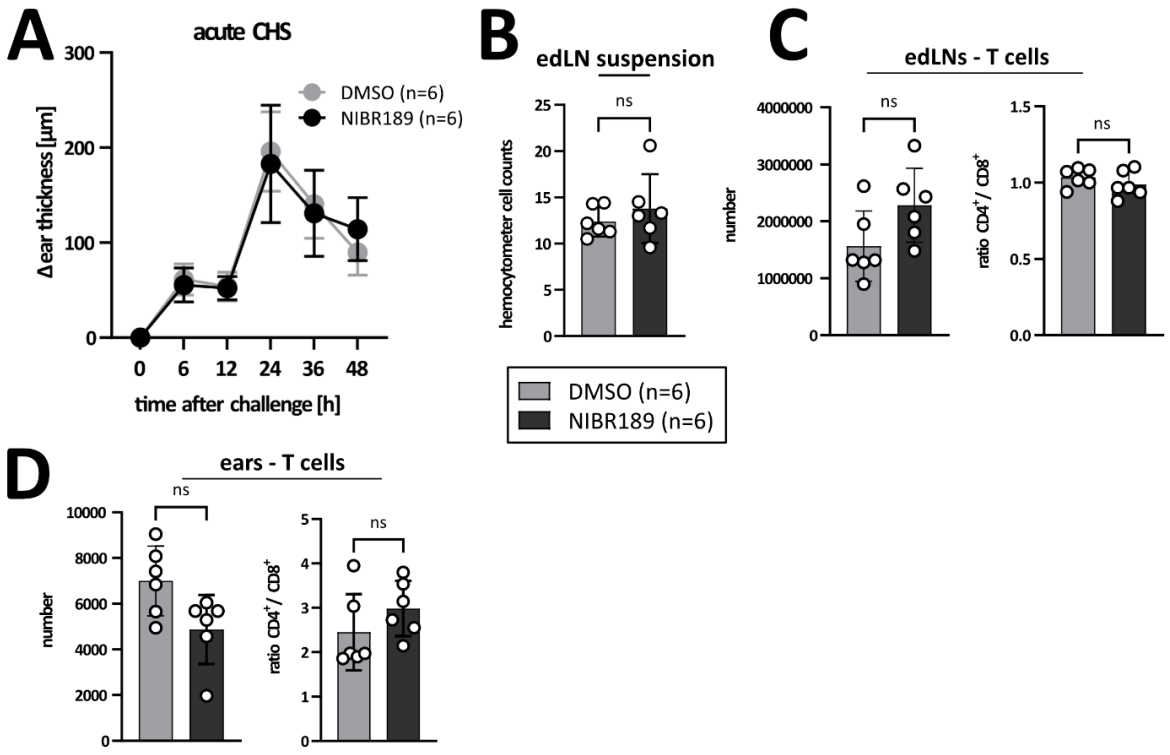

Figure 13. Effect of the EBI2-inhibitor NIBR189 on acute TNCB-induced CHS. A Ear swelling reaction in acute CHS of EBI2 WT mice, treated with DMSO (n = 6) or EBI2-inhibitor NIBR189 (n = 6) i.p. For acute CHS, mice were sensitized on d-5 with 1 % TNCB on the shaved abdomens and challenged with 0.5 % TNCB on the ears on d0. In addition, the mice were injected with 2 mg/ kg NIBR189 or corresponding amounts of DMSO i.p. every 12 h, starting 1 h before the challenge. Shown is the mean ± SD. **B** Number of live edLN single-cell suspension cells from at 48 h post challenge. **C-D** Flow cytometric analysis of T cells from **C** edLN pairs and **D** ears from **A** at 48 h post challenge. Shown are the number of T cells (left) and the ratio of $CD4^+$ to $CD8^+$ T cells (right). Dots represent individual mice ± SD. Two-tailed Mann-Whitney test. ns: not significant.

In conclusion, EBI2 deficiency did not show a major impact on the exacerbation of the TNCB-induced CHS reaction. Neither the full-body KO nor pharmacological inhibition of EBI2 led to a diminished CHS flare-up response. Interestingly though, there was a reduction in the cell number of the draining lymph nodes in the chronic model, for which one explanation could be the role of EBI2 in the priming of lymphocytes that was reported previously[150]. However, this was only apparent after repeated antigen challenges and seemed to have no further effect on the ear swelling response.

3.2.3 The role of EBI2 in the IMQ-induced psoriasis-like dermatitis as a model for psoriasis.

Human lesional psoriasis skin shows significantly different expression of the *GPR183* and *CYP7B1* genes, where both genes are slightly higher expressed in lesional vs non-lesional skin (Figure 8 E). Furthermore, a gain-of-function mutation in the EBI2 gene is associated with an increased onset of psoriasis in an IBD cohort[172]. A preclinical mouse model was used to investigate whether the EBI2-oxysterol axis is involved in the pathogenesis of psoriasis. For

this, the IMQ-induced psoriasis-like dermatitis model was used, which is induced by repeated daily application of a 5 % IMQ-containing cream (Aldara®) onto the shaved back skin and on the ears of the mice. IMQ is a TLR-7 agonist and daily application onto the skin of mice induces a dermatitis that shares many of the hallmark features of human plaque-type psoriasis like scaling and increased epidermal proliferation, neutrophil, pDC, $CD11b^+$ DC and $CD4^+$ T cell infiltration and an increased T_H17 response[189]. The model also critically depends on the IL-23/ IL-17 axis and the inflammation is mediated by T cells[189].

Of high interest, a recent study by Frascoli *et al*. found that EBI2 was critical for the IMQ-induced psoriasis-like dermatitis model[154]. In more detail, they showed that EBI2 was required for the thymic development of γδ T cells, where CH25H was expressed by mTEC1 in the thymus. Moreover, they observed reduced numbers of $V\gamma4^+V\delta4^+$ T cells (Heilig and Tonegawa nomenclature[190]) in the skin of EBI2 KO mice, which they attributed to the impaired thymic development. Furthermore, they could show a reduced exacerbation of the IMQ-induced psoriasis-like dermatitis model in EBI2 KO mice, where $V\gamma4^+V\delta4^+$ T cells are known to be one the key mediators for this model[191]. The authors claimed also that CH25H expressing basal keratinocytes maintained dermal γδT17 cells in the skin. High-fat diet increased the inflammation in the model, but not in EBI2 KO mice, suggesting that dietary cholesterol is sensed by components of the EBI2-oxysterol axis and enhances inflammation through it.

The IMQ-induced psoriasis-like dermatitis worsened over time in mice that were treated daily with Aldara® cream (Figure 14 A, B), whereas sham cream (cream formulated to resemble Aldara® cream as closely as possible, but lacking IMQ) treated mice did not develop dermatitis. However, I was unable to reproduce the published results. In this experiment, the model was not dependent on EBI2 expression as all scores were comparable between $EBI2^{EGFP/EGFP}$, $EBI2^{+/EGFP}$, and $EBI2^{+/+}$ mice. Analysis of the ear skin infiltrate after six days of treatment revealed no significant differences in the αβ T cell or neutrophil infiltration (Figure 14 C-E). There were also no differences in the proportion of γδ T cells in the skin and specifically of $V\gamma4^+V\delta4^+$ T cells, which have been shown to expand in this model and produce large amounts of IL-17A, critical for progression of the model[191].

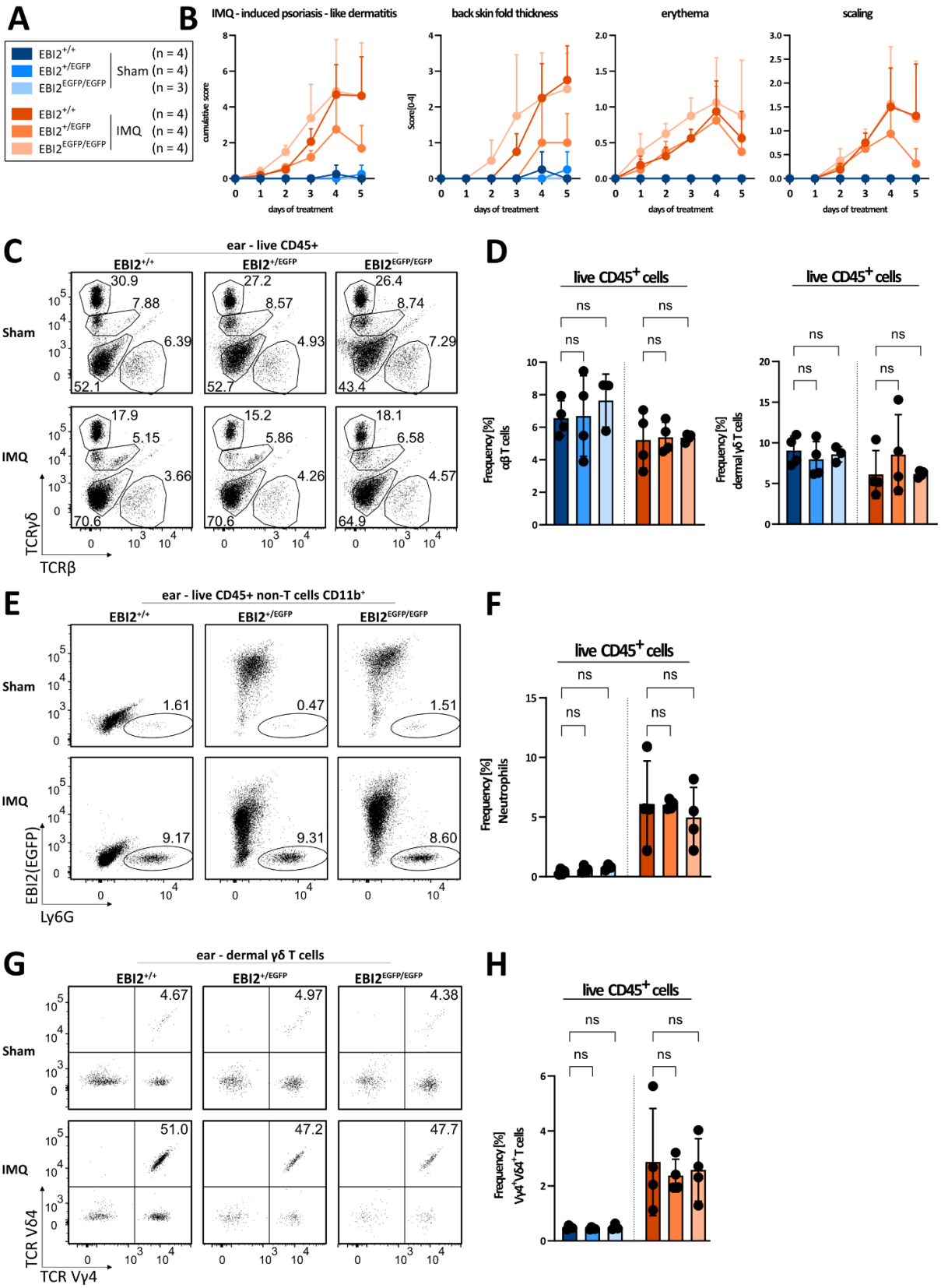

Figure 14. Role of EBI2 in IMQ-induced psoriasis-like dermatitis. A Legend for **B**. **B** Cumulative score and single scores for the IMQ-induced psoriasis-like dermatitis model. EBI2^{EGFP} mice were shaved and depilated on the lower back on d-2 and received treatment every 24 h from d0 on. For this, the mice were creamed with 5 % IMQ-containing Aldara® cream or sham cream on the shaved back skin as well as on both ears. The cumulative score resulted from the addition of the single scores from back skin

fold thickness change, erythema, and scaling of the back skin lesion. Dots represent the mean of n = 3-4 mice per group + SD. **C** Flow cytometric analysis of the ears of mice from **B**, analyzed after six days of treatment (d5). Shown are representative dot plots analyzing TCRβ- vs TCRγδ-expression of live CD45$^+$ cells. Gates indicate (from top left to bottom right) DETCs, TCRγδ^{high}TCRβ$^-$), dermal γδ T cells (TCRγδ^{dim}TCRβ$^-$), non-T cells (TCRγδ$^-$TCRβ$^-$), and αβ T cells (TCRγδ$^-$TCRβ$^+$). **E** Showing TCRβ$^-$ TCRγδ$^-$ CD11b$^+$ cells with gates indicating neutrophils. **G** Showing dermal γδ T cells with gates dissecting them for TCR Vδ4- and TCR Vγ4 expression (after Heilig & Tonegawa, 1986). **D, F, H** Bar plots showing the proportion of indicated populations from live CD45$^+$ cells with dots representing individual mice and bars representing the mean ± SD. One-Way ANOVA with Holm-Šídák correction for multiple testing. ns: not significant.

Additionally, to circumvent possible genetic compensatory mechanisms, an approach analogous to the CHS model was used, where EBI2 WT mice were treated with the EBI2-inhibitor NIBR189 during the IMQ-induced psoriasis-like dermatitis model. But also here, pharmacological inhibition of EBI2 showed no significant impact on the exacerbation of the model (Figure 15 A, B). The cumulative score and the back skin fold thickness were even slightly, but not significantly elevated in NIBR189 treated mice, compared to DMSO. This was reflected in the significantly increased proportion of γδ T cells in the ears of the Aldara® treated mice.

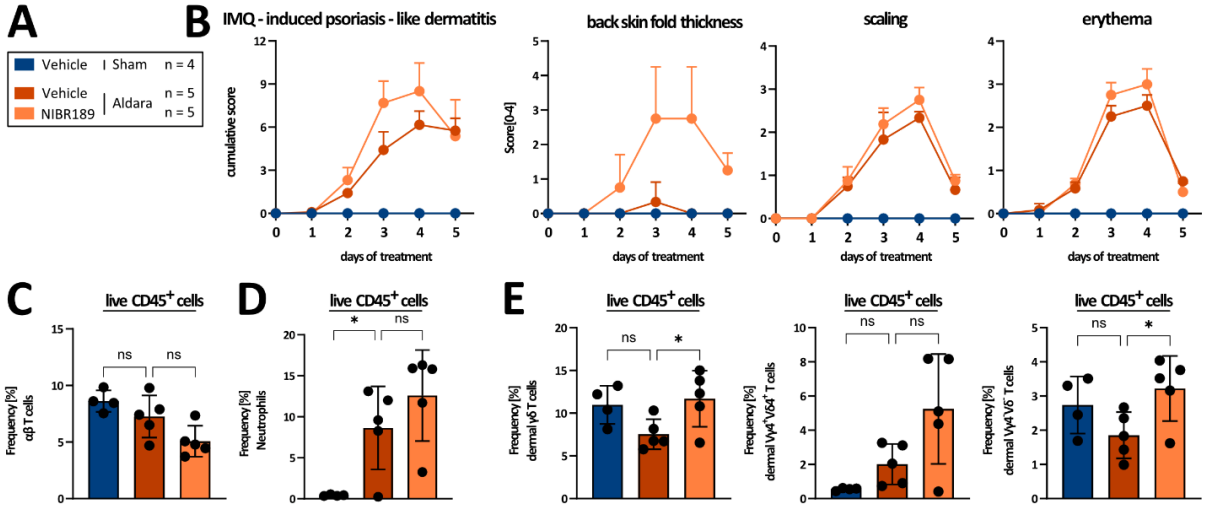

Figure 15. Effect of the EBI2-inhibitor NIBR189 on the IMQ-induced psoriasis-like dermatitis. **A** Legend. **B** EBI2 WT mice were shaved and depilated on the lower back on d-2 and received treatment every 24 h from d0 on. For this, the mice were creamed with 5 % IMQ-containing Aldara® cream or sham cream on the shaved back skin as well as on both ears. Mice additionally received twice daily i.p. injections of NIBR189 (2 mg/ kg) or DMSO (vehicle) as control, starting 1 h before the cream treatment, every 12 h. The cumulative score resulted from the addition of the single scores from back skin fold thickness change, erythema, and scaling of the back skin lesion. **C-E** Flow cytometric analysis of ear infiltrates of mice from **B.** Bars represent mean ± SD and dots represent individual mice. Showing **C** αβ T cells, **D** Neutrophils, **E** dermal γδ T cells, and indicated subtypes. Gating strategy and cell type differentiation, including discrimination of dermal and epidermal γδ T cells as in Figure 14. One-Way ANOVA with Holm-Šídák correction for multiple testing. ns: not significant, * $p < 0.05$.

In conclusion, in my hands, EBI2 deficiency had no impact on the exacerbation of the IMQ-induced psoriasis-like dermatitis model. Neither the clinical appearance after Aldara® treatment nor the cellular infiltration differed between EBI2$^{EGFP/EGFP}$ and control mice or between NIBR189 treated and control mice. Moreover, no reduction in the Vγ4^{+}Vδ4^{+} T cell frequency was observed. Therefore, I could show that the IMQ-induced psoriasis-like dermatitis was not dependent on EBI2.

3.3. T cell priming and T_{RM} cell generation capabilities of EBI2$^{EGFP/EGFP}$ mice.

3.3.1 The impact of EBI2 deficiency on the priming of B- and T cells.

The importance of the EBI2-oxysterol axis for the priming of B cells was demonstrated in 2009 simultaneously by two groups[122,123]. In 2019, Baptista *et al.* found that T cell priming is also partially dependent on the EBI2-oxysterol axis. They could show that especially CD4^{+} T cell priming and in general CD4^{+} T cell immunity was impaired in the absence of EBI2, while CD8^{+} T cells did not rely on the EBI2-oxysterol axis. In line with this, only cytotoxic lymphocyte (CTL) responses that relied on CD4^{+} T_H help were compromised.

No impact of EBI2 deficiency on the CHS or the IMQ-induced psoriasis-like dermatitis model was observed, even though an impaired T cell priming, as reported for EBI2$^{EGFP/EGFP}$ mice, should result in diminished inflammation. One hint in this direction was observed in the chronic CHS model, where, on d9 after 5 challenges, the draining lymph node cell counts were reduced in EBI2$^{EGFP/EGFP}$ mice compared to controls (Figure 12 D). To test whether EBI2$^{EGFP/EGFP}$ mice also had a defect in priming lymphocytes in the CHS model, EBI2$^{EGFP/EGFP}$ and EBI2$^{+/EGFP}$ mice were sensitized with TNCB, and lymphocyte activation in the dLNs was assessed three days later by flow cytometry. Parameters for activation were expression of CD69 and CD44, two of the most prominent activation markers for B- and T cells[6,192], as well as Ki-67 expression, a cell cycle protein expressed by proliferating cells[193], and IFN-γ expression, a cytokine expressed by type 1 effector and memory T cells[194].

Induction of all activation and memory markers was visible in T cells and B cells at d3 post challenge, comparing solvent treated with TNCB immunized mice (Figure 16 A-C). For further analysis, the individual values from immunized mice were normalized to the mean of solvent-sensitized mice of the same genotype. As expected, B cell numbers were significantly reduced in primed EBI2$^{EGFP/EGFP}$ LNs compared to LNs from EBI2$^{+/EGFP}$ mice (Figure 16 D). In line with this, the number of CD69-expressing B cells was also reduced, however, there was no reduction in the fraction of CD69-expressing B cells of all B cells. This demonstrated the reported priming deficiency in B cells. EBI2$^{EGFP/EGFP}$ CD4^{+} T cells in general as well as CD69 expressing ones were also reduced in numbers compared to control. Even though no difference was observed in Ki-67, CD44, or IFN-γ expression, this was an indication of the reduced priming capacity of EBI2-deficient CD4^{+} T cells. Also in line with expectations, CD8^{+} T cell priming was not reduced in EBI2$^{EGFP/EGFP}$ mice. Despite significantly reduced numbers of CD8^{+} T cells, no difference in activation marker expression could be observed and EBI2$^{EGFP/EGFP}$ CD8^{+} T cells showed even elevated Ki-67 expression.

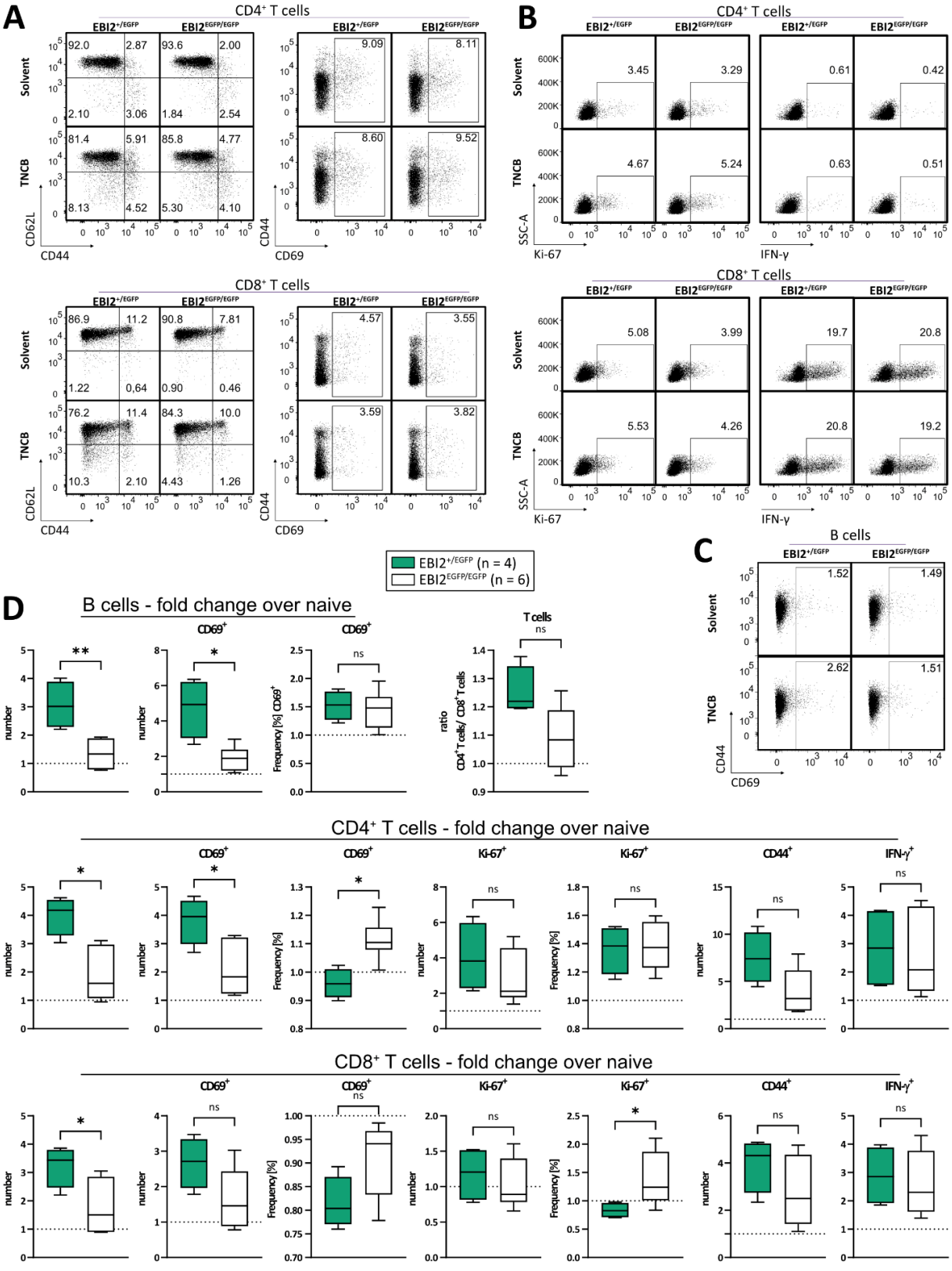

Figure 16. T cell priming capabilities of EBI2$^{EGFP/EGFP}$ mice in acute TNCB-induced CHS. Flow cytometric analysis of **A-B** CD4$^+$ T cell- (upper panels) and CD8$^+$ T cell- (lower panels) activation and differentiation and **C** B cell activation in the edLNs after TNCB sensitization. EBI2$^{+/EGFP}$ and EBI2$^{EGFP/EGFP}$ mice were sensitized on the shaved abdomen and ears with 1 % TNCB (EBI2$^{+/EGFP}$ n = 4, EBI2$^{EGFP/EGFP}$ n = 6) or solvent (EBI2$^{+/EGFP}$ n = 4, EBI2$^{EGFP/EGFP}$ n = 2) and the edLNs were analyzed on d5 post sensitization. **A** Surface marker analysis of CD62L vs CD44 and CD44 vs CD69. T_N: naïve T cells (CD62L$^+$CD44$^+$), T_{CM}: central

memory T cells ($CD62L^+CD44^+$), T_{EM}: effector- or effector memory T cells ($CD62L^-CD44^+$). **B** Intracellular and intranuclear marker analysis of Ki-67 and IFN-γ vs SSC-A. **C** Surface marker analysis of CD44 vs CD69. **D** Box plots comparing $EBI2^{+/EGFP}$ vs $EBI2^{EGFP/EGFP}$ lymphocyte activation after TNCB sensitization. Data for each mouse was normalized to the mean of solvent-sensitized mice of the respective genotype. Boxes range from the 25 % to 75 % quartile, the horizontal lines indicate the mean and the whiskers range to the min and max. Two-tailed Mann-Whitney test. ns: not significant, * $p < 0.05$, ** $p < 0.01$, *** $p < 0.001$, **** $p < 0.0001$.

In conclusion, I showed that the $EBI2^{EGFP/EGFP}$ mice used in this dissertation demonstrated the lymphocyte priming behavior that was previously reported and that should have led to a diminished immune response in the inflammatory skin disease models. This was apparent through the analysis of the lymphocytes in the dLNs on d3 post sensitization by cell counts but also by the expression of activation markers.

3.3.2 The role of tissue-resident and circulatory T cells in acute and memory CHS.

T_{RM} cells are a memory T cell subset, that constitutes the first line of defense in peripheral tissues, such as the skin, lung, gut, liver, female reproductive tract, and brain[17,45]. Although they have also been described in secondary lymphoid organs, such as the spleen and lymph nodes[17,45], they were originally found in the periphery and were associated with enhanced defense capabilities against secondary infections[39]. Nowadays, T_{RM} cells have also been recognized as key players in the pathogenesis of many inflammatory diseases, in particular chronic inflammatory skin diseases, such as fixed drug eruption (FDE)[195], ACD[108,64], AD[196], vitiligo[77], and psoriasis[173]. FTY720 is an inhibitor of the $S1P_1$, that inhibits the egress from lymphocytes from SLOs. This, among other tools, has been used to study the role of T_{RM} cells in many scenarios, as it allows separation of the circulatory and peripheral immune systems from each other[43].

Historically, my group observed rather consistently an impact of EBI2 deficiency on the memory phase of the TNCB-induced CHS model, where the EBI2 KO animals developed less severe skin inflammation after re-challenge compared to controls (unpublished data). As shown earlier, the results from me (Figure 9) and from Julius Schwingen (dissertation submitted for review, 2023) indicate an accumulation of the EBI2 ligand 7α,25-OHC in inflamed skin early in the inflammatory response across species. T_{RM} cells are present in peripheral tissues and able to readily sense and respond to inflammation and -associated mediators. Even though I did not observe an impact of EBI2 deficiency on the memory CHS model, it was interesting to investigate this potential link in more detail.

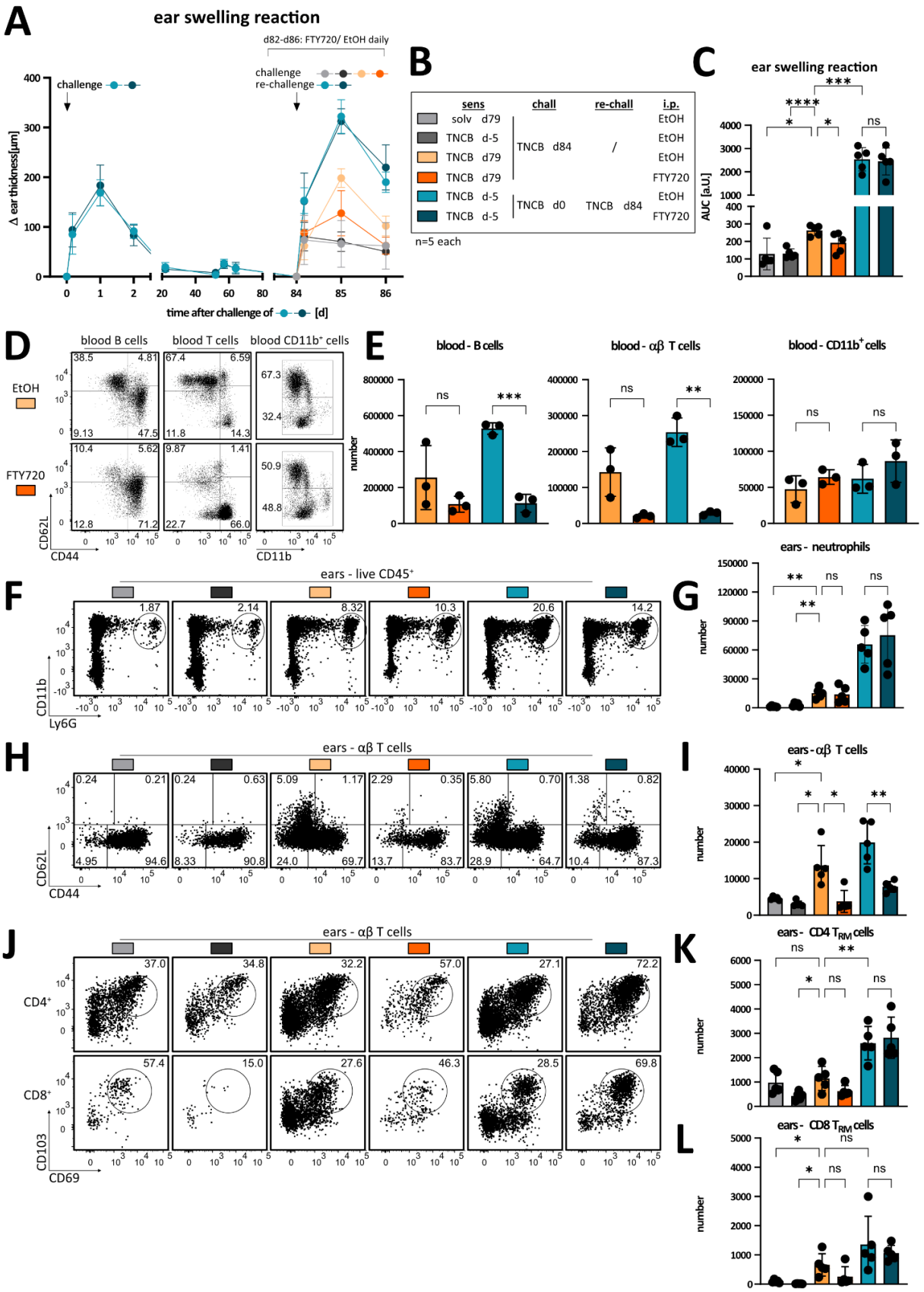

Figure 17. The role of skin-resident vs circulatory lymphocytes in the exacerbation of the CHS reaction. A Ear swelling reaction of WT mice in acute and memory CHS, treated with FTY720 or EtOH as control. Mice were sensitized on d-5 with 1 % TNCB on the shaved abdomen and challenged on d0 (light blue and dark blue) or left unchallenged (dark grey). The ear swelling reaction was monitored on

the indicated days. On d79, two additional groups of mice were sensitized with 1 % TNCB (light orange and dark orange) on the shaved abdomen. All groups were injected with FTY720 or EtOH from d82 until analysis. Injections were done i.p. every 24 h with 2.4 mg/ kg FTY720 or equivalent amounts of EtOH. All groups were treated on d84 with 0.5 % TNCB on both ears, this represents the memory re-challenge for the groups light blue and dark blue, the acute challenge for the groups light orange and dark orange, and the late challenge for group dark grey. Dots represent the mean of n = 5 per group ± SD. **B** Treatment legend. **C** AUCs as a.U. of the different groups from **A**. One-Way ANOVA with Brown-Forsythe and Welch correction. **D** Flow cytometric analysis of peripheral blood leukocytes, isolated via density gradient centrifugation from whole blood of mice from **A** on d86. Shown are dot plots of representative examples. **E** Bar plots showing the cell counts of B cells ($CD11b^-TCR\beta^-CD19^+$, left), T cells ($CD11b^-TCR\beta^+CD19^-$, center), and myeloid cells ($CD11b^+TCR\beta^-CD19^-$, right) from **D**. Bars indicate mean ± SD and dots represent individual mice. Dots represent individual mice with n = 3 per group, randomly chosen from the n = 5 total per group. One-way ANOVA with Brown-Forsythe and Welch correction. **F-L** Flow cytometric analysis of the ear infiltrate of pooled ears of mice from **A**, analyzed on d86. **F, H, J** Shown are dot plots of **F** live $CD45^+$ cells, gated for $CD11b^+Ly6G^+$ - neutrophils, **H** all αβ T cells, gated for CD62L vs CD44, with $CD62L^-CD44^+$ being T_{EM} cells, **J** all αβ T cells, gated for CD69 vs CD103, with $CD69^+CD103^+$ being T_{RM} cells. Shown are representative examples. **G, I, K, L** Bar plots showing the number of indicated cells with dots representing individual mice, the bar representing the mean ± SD. One-way ANOVA with Brown-Forsythe and Welch correction. ns: not significant, * $p < 0.05$, ** $p < 0.01$, *** $p < 0.001$, **** $p < 0.0001$.

For this, a proof-of-concept experiment using the TNCB-induced CHS model was conducted. WT mice were sensitized, challenged, and re-challenged 12 weeks later with TNCB and injected with FTY720 or control just before the challenge or re-challenge to demonstrate the role of the sessile peripheral immune system on the different phases of the CHS model. To enable a direct comparison of the magnitudes of the acute and memory response, the mice were treated in a way that challenge or re-challenge respectively were performed on the same day using the same TNCB solution and all mice were analyzed on the same day.

The acute and memory ear swelling response peaked at 24 h after challenge and re-challenge respectively, independent of FTY720 treatment (Figure 17 A-C). The memory response showed a higher magnitude of the ear swelling reaction at peak. Of note, the acute ear swelling reaction between different groups of mice at different time points without FTY720 treatment (light green, dark green, light orange) was comparable. Interestingly, mice that were sensitized but only challenged 84 days afterward, as opposed to five days in the traditional model, developed an ear swelling reaction similar to solvent-sensitized mice. This suggested that effector and memory cells generated by priming in the sensitization phase die off over the next two to three months when a second antigenic stimulus does not follow right away.

Acute TNCB challenge with or without prior TNCB sensitization led to a comparable ear swelling reaction for acutely challenged mice after 6 h. This was in line with the fact, that innate immune cells and keratinocytes react to the irritant properties of the TNCB and the solvent solution and thereby mediate early inflammation independent of the adaptive immune response initiated by the sensitization[88,95,197]. The peak ear swelling at 24 h after challenge was significantly reduced in mice treated with FTY720 compared to the control. However, this was not the case for the re-challenge which demonstrates, that the memory

and acute CHS reactions underly different immune responses and that the memory response is independent of the immune cells in the circulation, whereas the acute response depends on it.

FTY720 treatment of mice led to a strong reduction in B- and T cell numbers in the blood 48 h after the re-challenge, with a similar trend for the acute challenge, but did not have an impact on the abundance of $CD11b^+$ cells at either timepoint (Figure 17 C-D). Lymphocytes were not completely absent in the blood of FTY720 treated mice, because $S1P_1$ inhibition is known to block the egress of B- and T cells that recirculate through the SLOs and therefore affects mostly naïve and central memory T cells [198]. Recirculating populations are marked by the expression of CD62L, a feature of approx. 80-85 % of T cells[198]. Interestingly, although 67 % of $CD11b^+$ cells expressed CD62L, FTY720 treatment did not significantly reduce the abundance of $CD11b^+$ cells in the blood, likely because they do not recirculate through the SLOs despite CD62L expression, as much as lymphocytes do. This established that FTY720 treatment had the desired effect and that only lymphocytes were retained in the SLOs, but myeloid cells like neutrophils and monocytes were free to infiltrate the site of inflammation. In fact, neutrophil numbers in the ears were not significantly changed upon FTY720 treatment but correlated with the strength of the inflammation, with neutrophil numbers elevated in acute challenge compared to solvent challenge and in re-challenge compared to acute challenge (Figure 17 E-F). Expectedly, T cell numbers were significantly reduced in the ears of FTY720-treated mice in the acute and memory response, especially missing the $CD62L^+$ populations (Figure 17 G-H).

Numbers of T_{RM} cells in the ears of mice were differently distributed at steady state when comparing the $CD4^+$ and $CD8^+$ lineage (Figure 17 I-J). $CD4^+$ T_{RM} cells were abundant in steady-state ear skin, whereas $CD8^+$ T_{RM} cells were nearly absent. Because T_{EM} cells take approx. 30 days to differentiate into T_{RM} cells [39], CD69- and CD103-expressing T cells present in the skin at 48 h after challenge cannot be declared bona fide T_{RM} cells. Despite not constituting T_{RM} cells, $CD8^+$ T cells expressing those markers increased significantly in numbers after the acute challenge. Interestingly, even though general T cell numbers were reduced in the ears of FTY720-treated acutely challenged mice, the $CD69^+CD103^+$ T cell numbers were not significantly reduced. Moreover, the number of $CD69^+CD103^+$ T cells in the ears of the memory re-challenged mice was highly enriched compared to the acutely challenged mice and controls, suggesting robust memory formation through the challenge but only after a certain period of time.

In previous experiments by my group, $EBI2^{EGFP/EGFP}$ mice showed less ear swelling in the memory CHS response, which was not the case when I tried to reproduce the data. Having established that the T_{RM} cells are the key players in mediating this response and that the $EBI2^{EGFP/EGFP}$ mice showed a deficiency in $CD4^+$ T cell priming, it was investigated whether the $EBI2^{EGFP/EGFP}$ mice had a reduced capacity to generate T_{RM} cells. To investigate this, an acute CHS was conducted with $EBI2^{EGFP/EGFP}$ and $EBI2^{+/EGFP}$ mice, and the healed ears were analyzed on d30 post challenge.

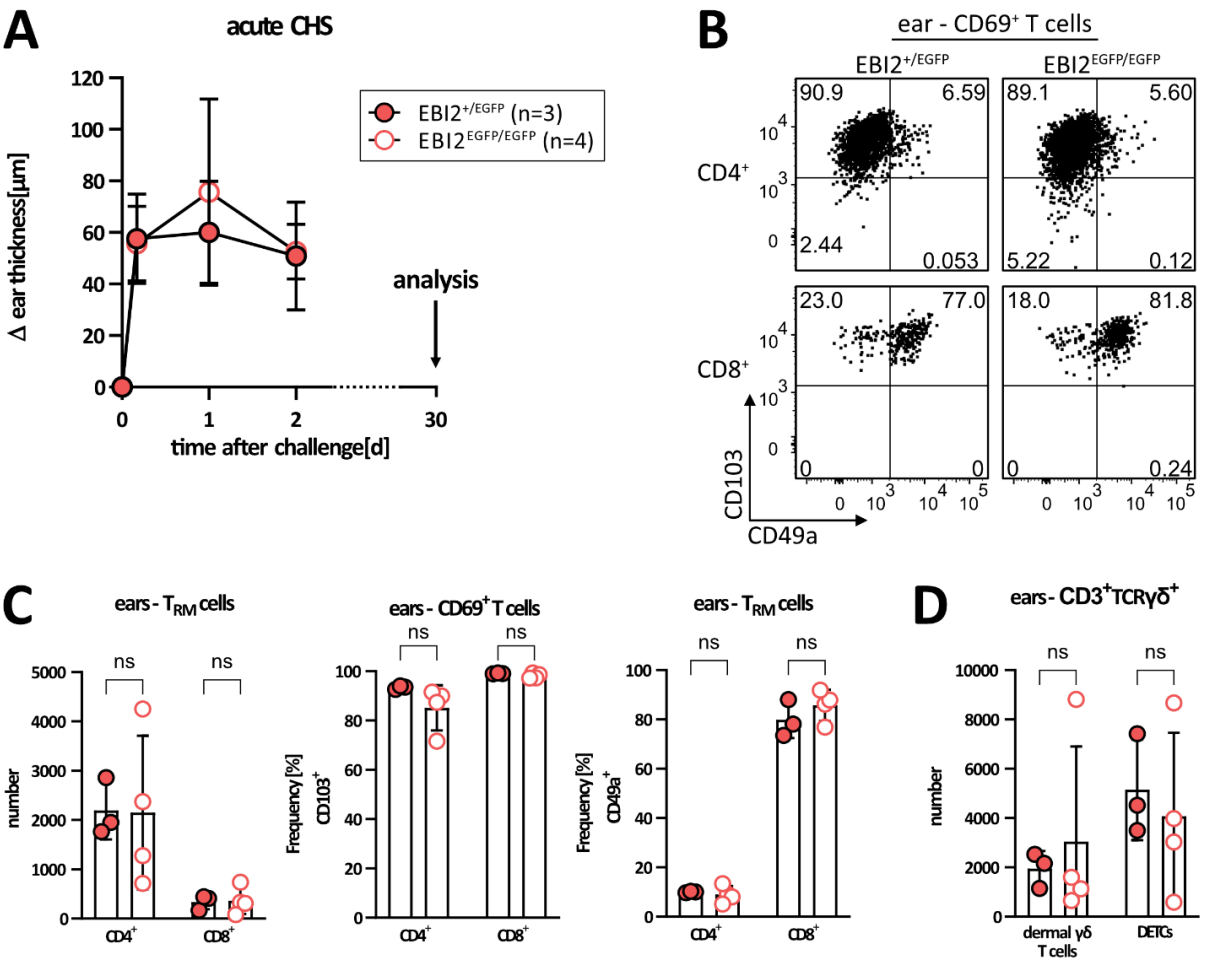

Figure 18. T_{RM} cell generation capabilities of EBI2$^{EGFP/EGFP}$ mice. A Ear swelling reaction of EBI2$^{+/EGFP}$ (n = 3) and EBI2$^{EGFP/EGFP}$ mice (n = 4) sensitized with 1 % TNCB on the shaved abdomen and challenged with 0.5 % TNCB on the ears. The ear swelling reaction was monitored for 48 h. Dots represent mean ± SD. **B** Flow cytometric analysis of CD69$^+$ T cells from the pooled ears of indicated mice. Depicted are CD4$^+$ (top) and CD8$^+$ (bottom) CD69$^+$ T cells and their expression of CD103 and CD49a. **C-D** Bar plots of flow cytometric analysis of **A**. Depicted are numbers of CD69$^+$CD103$^+$ T_{RM} cells (left), and their respective proportions of CD103$^+$ (center) and CD49a$^+$ cells (right). **D** Quantification of γδ T cells in the pooled ears of the mice from **A**. Dermal γδ T cells were gated as CD3^{high}TCRγδ^{high}TCRVβ$^-$ and DETCs as CD3$^{very\ high}$TCRγδ$^{very\ high}$TCRVβ$^-$. Bars represent the mean ± SD and dots represent individual mice. Unpaired student's t-test. ns: not significant.

As seen before, there was no difference in the ear swelling reaction during the acute CHS between EBI2$^{EGFP/EGFP}$ and EBI2$^{+/EGFP}$ mice (Figure 18 A). No differences between the genotypes were observed, when comparing the number of CD69$^+$CD103$^+$ T_{RM} cells in the ears of the mice, nor when comparing the quality of the T_{RM} cells generated by assessing the expression of CD103 on CD69$^+$ cell and the expression of CD49a on T_{RM} cells. Of note, as previously reported[59], CD49a expression was a feature of CD8$^+$ but not of CD4$^+$ T_{RM} cells. There were also no differences in the abundance of other skin-resident T cell populations, as the numbers of dermal γδ T cells and DETCs were comparable between EBI2$^{+/EGFP}$ and EBI2$^{EGFP/EGFP}$ mice.

Taken together, the memory CHS response to TNCB was stronger than the acute CHS response and the FTY720 treatment reduced the magnitude of the acute, but not of the memory response. This shows that at least the ear swelling reaction of the memory response is independent of circulating lymphocytes and highlights the role of T_{RM} cells as the first line of defense against previously encountered pathogens. However, T_{RM} cells were induced in the ear skin of mice only after appropriate sensitization and challenge. They then mediated a faster and stronger response against a secondary antigenic stimulus. $EBI2^{EGFP/EGFP}$ mice showed no reduced ability to generate T_{RM} cells or to maintain them in the skin, which was in line with the fact, that no differences in the magnitude of the memory CHS response were observed.

3.4. Differential regulation of EBI2 expression in peripheral T cells.

3.4.1 High EBI2 expression marks established T_{RM} cells in murine skin.

EBI2 expression was described as a feature of naïve and memory B cells as well as a feature of $CD4^+$ T_N, T_{CM}, and T_{EM} cells and of $CD8^+$ T_{CM} cells[120,122,149]. However, EBI2 has not been investigated in the context of T_{RM} cells as of yet. This is of particular interest, because of the importance of T_{RM} cells in the pathogenesis of many diseases, as described above, and because they have been recognized as an attractive target for new therapies.

Using the $EBI2^{EGFP}$ mice as a unique tool to investigate EBI2 expression, T_{RM} cells were generated by TNCB sensitization of the shaved abdomen and challenge of the ears of mice. Thirty days later, the ears were analyzed by flow cytometry (Figure 19 A, B). Strikingly, we found very strong EBI2 expression in both T cell lineages in the ear (Figure 19 C). Even more striking was the difference in EBI2 expression of circulating vs resident peripheral T cells. I found a drastic difference between the circulation and the periphery in the $CD8^+$ lineage. Approx. 15 % of memory T cells of the edLNs expressed EBI2, whereas memory T cells in the ear were almost completely positive, and again nearly all of them expressed CD69, which was not the case for circulating T cells, as expected. For $CD4^+$ T cells EBI2 expression was between 70-80 % for whole in the periphery and approx. 80 % in the ear, resulting also in a significant increase in EBI2 expression in $CD4^+$ T cells and especially memory $CD4^+$ T cells comparing the circulation with the periphery (edLNs and PBLs vs ear). Again, solvent-sensitized mice did not develop a repertoire of T_{RM} cells after the challenge, highlighting the need for priming and the generation of T_{EM} cells that infiltrate the ear upon challenge and then differentiate towards T_{RM} cells.

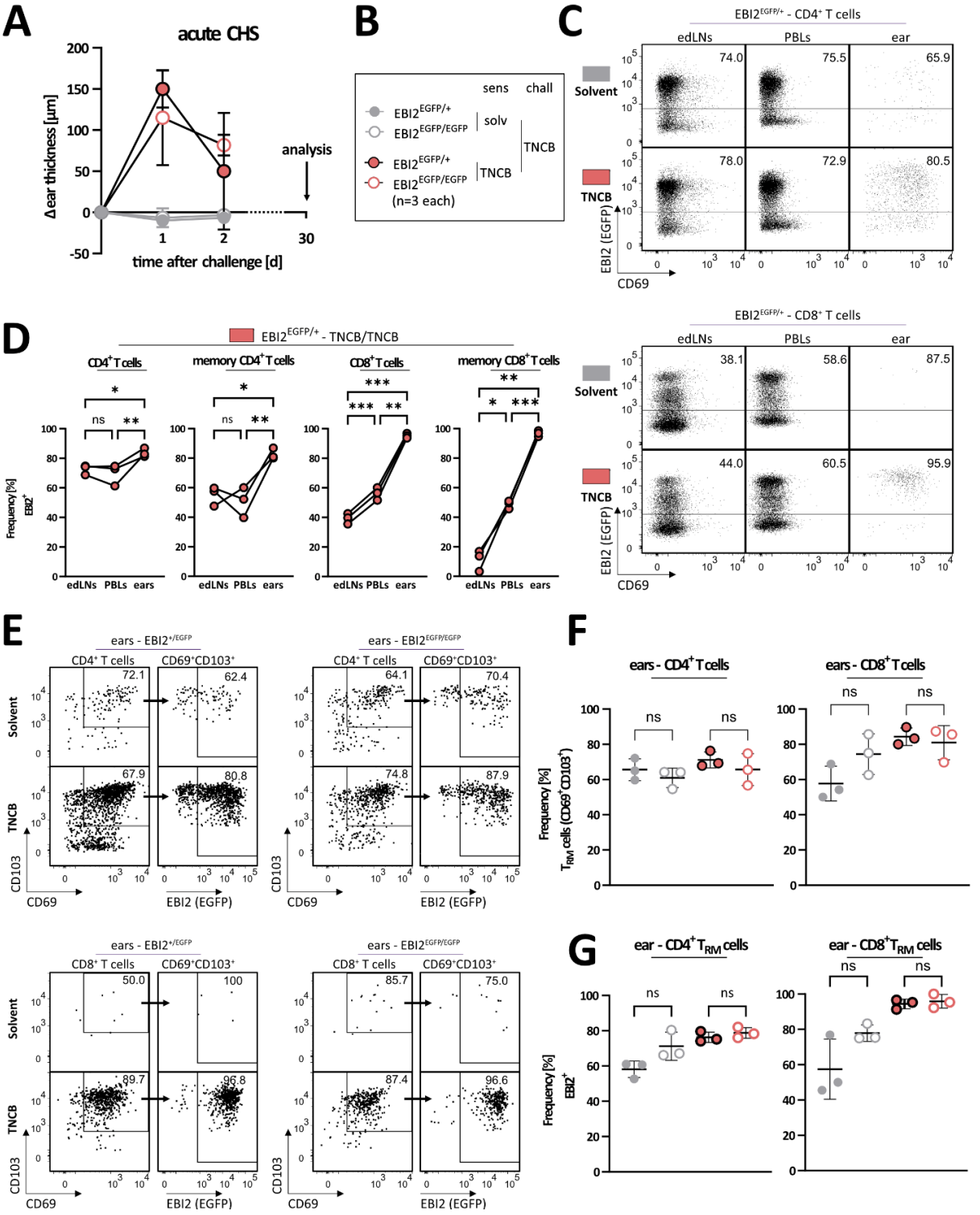

Figure 19. EBI2 (EGFP) expression is highly enriched in peripheral T cells and constitutes a feature of T_{RM} cells. A Ear swelling reaction in acute CHS of EBI2$^{+/EGFP}$ (full circles) and EBI2$^{EGFP/EGFP}$ (hollow circles) mice sensitized on d-5 with either solvent (grey circles) or 1 % TNCB (black circles) on the shaved abdomen and challenged with 0.5 % TNCB on d0 on one ear (n = 3 each). **B** Legend for **A-G**. **C** Flow cytometric analysis of mice from **A** on d30 post challenge of CD4$^+$ (top) or CD8$^+$ (bottom) T cells from solvent or TNCB-sensitized and TNCB-challenged EBI2$^{+/EGFP}$ mice. **D** As **C**, PBLs: peripheral blood lymphocytes (prepared from whole blood by density gradient centrifugation), memory T cells: CD44$^+$. Dots represent individual mice and connecting lines indicate matched samples. One-Way ANOVA with Geisser-Greenhouse correction. **E** As **C**, showing dot plots of CD69 or EBI2 (EGFP) vs CD103-expression in ears in indicated populations of CD4$^+$ (top) and CD8$^+$ (bottom) T cells from the ears of EBI2$^{+/EGFP}$ (left)

or EBI2$^{EGFP/EGFP}$ (right) mice. Arrows symbolize gating strategy and gates indicate EBI2-positive T_{RM} cells. **F-G** As **C**, scatter plots comparing **F** T_{RM} cell-frequency and **G** EBI2-expressing T_{RM} cell fraction of CD4$^+$ (left) and CD8$^+$ (right) indicated T cell populations. One-Way ANOVA with Brown-Forsythe and Welch correction and Dunett's T3 correction for multiple comparisons. Dots represent individual mice with mean as horizontal bar ± SD. ns: not significant, * $p < 0.05$, ** $p < 0.01$, *** $p < 0.001$.

Gating on CD69$^+$CD103$^+$ T cells in the ears revealed that, indeed, T_{RM} cells expressed EBI2 on a very high level (Figure 19 E-G). Especially CD8$^+$ T_{RM} cells were nearly ubiquitously positive for EBI2, which was in strong contrast to circulatory CD8$^+$ T cells. This constitutes the first evidence of EBI2 expression in T_{RM} cells on the protein level. In 2017, Cheuck *et al.* observed that *GPR183* gene expression was significantly enriched in CD49a$^+$ vs CD49a$^-$ CD69$^+$CD103$^+$ T_{RM} cells [59]. However, this was neither further investigated nor proven on protein level, nor could this be attributed to overall T_{RM} cells as only T_{RM} cell populations were compared, and the gene expression change is relative. Moreover, no conclusion could be drawn as to how strong the expression in CD49a$^+$ T_{RM} cells was, merely an upregulation compared to a reference was observed. Of note, no significant difference in the frequency of T_{RM} cells or the EBI2-expressing fraction of T_{RM} cells was observed when comparing EBI2$^{+/EGFP}$ with EBI2$^{EGFP/EGFP}$ (Figure 19 E-G), suggesting that T_{RM} cell generation is not critically dependent on the EBI2-oxysterol axis.

Since T_{RM} cells are generated and replenished from circulating progenitor cells[20,21] and blood T_{EM} cells express EBI2 on a lower level than peripheral T_{RM} cells (especially in the CD8$^+$ lineage), I hypothesized that T_{EM} cells, which are recruited to the site of inflammation and have not yet differentiated into T_{RM} cells, express less EBI2 than established T_{RM} cells do. To test this hypothesis, EBI2 expression of established T_{RM} cells was compared with freshly recruited T_{EM} cells in the same tissue. For this, EBI2$^{+/EGFP}$ mice were sensitized with TNCB and subsequently challenged on the ear to generate local T_{RM} cells (Figure 20 A-B). A group of mice was then re-challenged to recruit T_{RM} cell progenitors (T_{EM} cells) into the previously challenged site, where the T_{RM} cells had been generated. This made it possible to compare their phenotype via flow cytometry.

Analyzing T_{RM} cell development, naive ear skin contained few T_{RM} cells and their proportion increased significantly in healed ears (Figure 20 C-D). As expected, CD69$^+$CD103$^+$ T_{RM} cell frequency decreased again when the ears were re-challenged due to the infiltrating T cells. This was true for CD4$^+$ and CD8$^+$ T cells and frequencies of CD69$^-$CD103$^-$ non-T_{RM} cells behaved reciprocally. Interestingly, analyzing EBI2 expression, the fraction of EBI2-positive non-T_{RM} cells and the EBI2 MFI of those cells were comparable across all conditions. This showed that the T_{EM} cells expressed EBI2 at a stable level, irrespective of an ongoing inflammatory response. In contrast, the fraction of EBI2-positive T_{RM} cells was different across conditions. CD4$^+$ T_{RM} cells from healed ears expressed more EBI2 than T_{RM} cells from naïve ears. Finally, in line with the hypothesis, T_{RM} cells in the re-challenged ear expressed less EBI2 (CD4$^+$) or showed lower EBI2 MFI (CD8$^+$) compared to T_{RM} cells in the healed ear. Again, this was true for CD4$^+$ and CD8$^+$ showing either significant differences or strong trends.

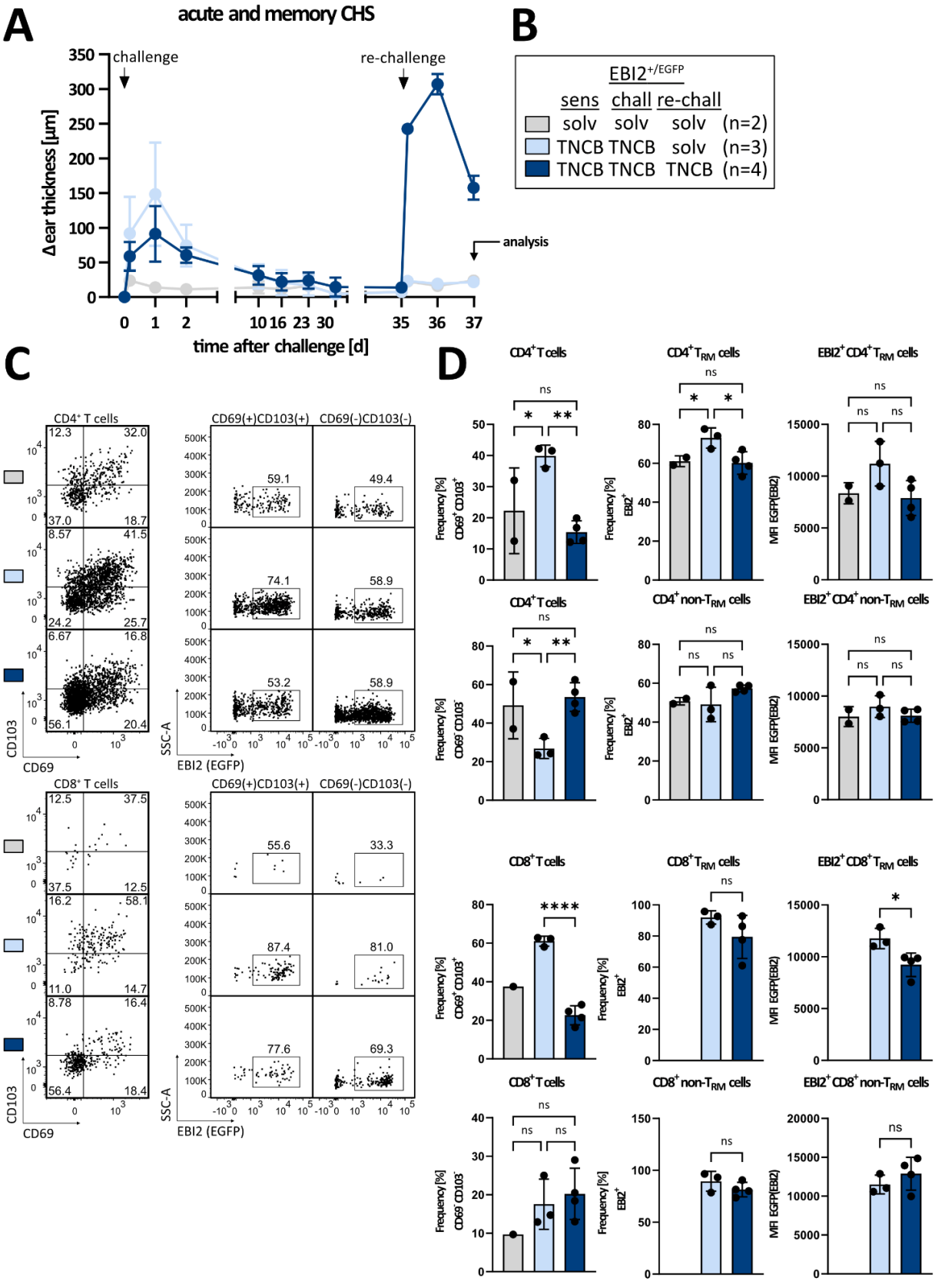

Figure 20. EBI2 expression in T_{RM} cells and newly infiltrating T_{EM} cells. A Ear swelling reaction of EBI2$^{+/EGFP}$ mice in acute and memory CHS. Mice were either sensitized, challenged, and re-challenged with solvent (n = 2), sensitized and challenged with 1 % TNCB on the shaved abdomen and re-challenged with solvent (n = 3), or sensitized, challenged, and re-challenged with 1 % TNCB (n = 4). Dots represent mean ± SD. **B** Legend for **A-D**. **C** Flow cytometric analysis of ears of mice from **A** on d37 post

challenge/ d2 post re-challenge. Shown are representative dot plots of $CD4^+$ (top) and $CD8^+$ (bottom) T cells, analyzing the expression of T_{RM} cell markers CD69 vs CD103 (left). Dot plots of $CD69^+CD103^+$ cells (fully differentiated T_{RM} cells) and $CD69^-CD103^-$ cells (T_{EM} cells and potential T_{RM} cell precursor cells) with gates indicating the EBI2-positive fraction. **D** Bar plot quantifying indicated population with bars indicating the mean ± SD and dots representing individual mice. T_{RM} cells: $CD69^+CD103^+$, non-T_{RM} cells: $CD69^-CD103^-$. One-Way ANOVA for comparisons of three groups, unpaired two-tailed student's t-test for comparisons of two groups. ns: not significant, * $p < 0.05$, ** $p < 0.01$, *** $p < 0.001$, **** $p < 0.0001$.

In conclusion, I here discovered EBI2 expression as a feature of established T_{RM} cells in the skin of mice. I could show that EBI2 expression is stronger in T_{RM} cells than in comparable T cell populations in the circulation. Moreover, I was able to demonstrate that T_{RM} cells in healed ears of mice express more EBI2 than those from ears that were recently re-challenged. This is likely because cells termed T_{RM} cells in this context (gated as $CD69^+CD103^+$) consisted of previously established bona fide T_{RM} cells and recently recruited progenitor cells. These expressed the hallmark markers of T_{RM} cells but have not undergone full differentiation over the course of 30 days. This highlights the caveat of using marker expression to define bona fide cell types. T_{RM} cells are characterized by their long-term tissue residency, in addition to the expression of CD69 and CD103 in mice.

3.4.2 EBI2 expression gradually increases over time during T_{RM} cell maturation.

Acknowledging the discrepancy in EBI2 expression between T_{RM} cells in healed ears and 'T_{RM} cells' in recently challenged ears, it was interesting to follow up on the dynamics of EBI2 expression in the development of T_{RM} cells in the skin. For this, $EBI2^{+/EGFP}$ mice were sensitized and then challenged with TNCB on one ear or with solvent on the other ear. Close monitoring of the ear swelling reaction over 30 days revealed typical peak swelling of the TNCB-challenged ear at 24 h post challenge and then further gradual asymptotic decrease until d30 (Figure 21 A).

Flow cytometric analysis of the ears on d0, d2, d6, d10, d21, and d30 showed an infiltration of $CD4^+$ and $CD8^+$ T cells into the ears, initially with a peak at d2 and a subsequent decline in numbers, but with another unsuspected peak at d21 (Figure 21 B). Analysis of T_{RM} cell markers CD69 and CD103 on skin T cells confirmed previous results with $CD4^+$ T_{RM} cells being present in naïve ears, but $CD8^+$ T_{RM} cells being virtually absent (Figure 21 C, E, G). Also in line with previous results, only up to 50 % of T_{EM} cells expressed EBI2 in the blood at steady state, but skin T_{EM} cells (before gating on $CD69^+CD103^+$ cells) and specifically T_{RM} cells (after gating on $CD69^+CD103^+$ T_{EM} cells) showed ubiquitous EBI2 expression (> 90 % for $CD4^+$ and 100 % for $CD8^+$ cells) (Figure 21 D, F, G). Due to technical issues at d2, T cell numbers displayed on the dot plots appear low, but actual numbers increased dramatically and the frequency of T_{RM} cells from all skin T cells dropped for $CD4^+$ T cells, due to infiltration of non-T_{RM} cells. T_{EM} cells gradually gained expression of tissue-residency markers CD69 and CD103 from d6 on and approx. reached baseline levels by d30. This resulted in a significant increase in the frequency of T_{RM} cells throughout the resolution of the inflammation (Figure 21 G).

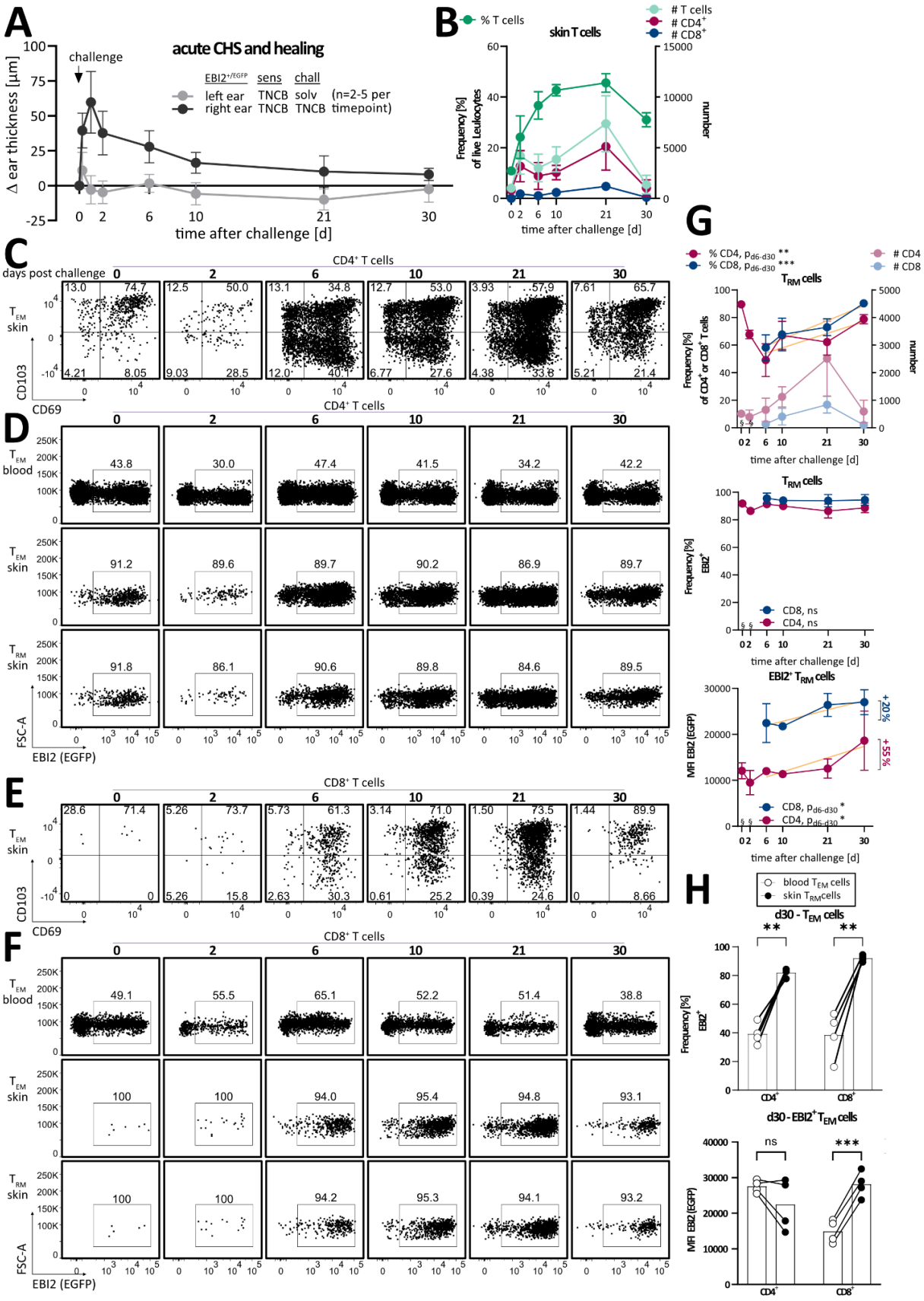

Figure 21. EBI2 is upregulated in skin T_{EM} cells during their differentiation to T_{RM} cells. A Ear swelling reaction of EBI2$^{+/EGFP}$ mice in acute CHS and during healing. Mice were sensitized with 1 % TNCB on the shaved abdomen on d-5 and challenged on d0 on the left ear with solvent and on the right ear with 0.5 % TNCB (n = 2-5 per timepoint). Biotin-labeled anti-mouse CD45.2 mAb was injected through the

tail vein 3 min before sacrifice. Cells labeled as such were excluded from the analysis of ear skin. **B** Flow cytometric analysis of ears of mice from **A** on indicated days after challenge. Left y-axis: Frequency of T cells of $CD45^+$ live $dump^-$ cells (dark green). Right y-axis: number of indicated T cell populations (#: number). Dots represent mean ± SD. **C-F** Flow cytometric analysis of T cells from skin or PBLs (blood) of mice from **A**, shown are dot plots of $CD4^+$ (**C-D**) and $CD8^+$ (**E-F**) T cell populations - indicated on the left, on days post challenge - indicated on top. Dot plots show all mice per timepoint concatenated. **C, E** T_{EM} cells ($CD62L^-CD44^+$) from skin, CD69 vs CD103. **D, F** T_{EM} cells from blood and skin and T_{RM} cells ($CD69^+CD103^+$) from skin, forward scatter (FSC-A) vs EBI2 (EGFP). **G** As **B**, top: left y-axis: fraction of T_{RM} cells in $CD4^+$ or $CD8^+$ T cells. Right y-axis: number of whole $CD4^+$ and $CD8^+$ T cells. Center: fraction of EBI2-expressing T_{RM} cells. Bottom: MFI of $EBI2^+$ T_{RM} cells. Numbers show change of EBI2-expression from d6-d30 [%]. §: too few cells for analysis. Golden lines show linear regression. Statistical analysis ($p_{d6\text{-}d30}$) indicates whether the slope of the linear regression differs significantly from 0, i.e., statistically significantly rises or drops over time from d6-d30. Dots represent mean ± SD. **H** As **C-F**, shown are the frequency of EBI2-expressing cells on d30 (top) and MFI thereof (bottom) from circulating T_{EM} cells (blood) and resident ones (skin). Lines indicate matched samples. Bars represent the mean, dots represent individual mice. Paired two-tailed student's t-test. ns: not significant, * $p < 0.05$, ** $p < 0.01$, *** $p < 0.001$.

Interestingly, even though T_{RM} cell maturation was apparent by the acquisition of tissue-residency markers, the fraction of EBI2-expressing T_{RM} cells remained stable across all investigated time points (Figure 21 G center). However, the EBI2 MFI increased significantly from d6 (the onset of T_{RM} cell maturation) to d30 (the end of T_{RM} cell maturation) (Figure 21 G bottom). This aligned with expectations and confirmed the hypothesis that EBI2 is upregulated during T_{EM} cell differentiation to T_{RM} cells and validated that EBI2 expression is a feature of established T_{RM} cells. This is highlighted by the comparison of EBI2 expression in circulating T_{EM} cells and skin T_{RM} cells on d30 (Figure 21 H). Of note, EBI2 expression in blood T_{EM} cells did not change significantly throughout the whole inflammatory response and resolution.

Only 11 years ago in 2013, Laura Mackay from the Gebhardt Lab, which had originally introduced the concept of T_{RM} cells in 2009, showed that $CD8^+$ T_{RM} cells are derived from tissue infiltrating $KLRG1^-$ T_{EM} cells. The group of Ton Schumacher verified $CD127^+KLRG1^-$ effector cells to be T_{RM} cell progenitor cells in 2020 by single-cell lineage tracing and found that T_{RM} cell fate decision is imprinted in individual cells before entry into the skin[20]. In 2021, the Gebhardt lab demonstrated that KLRG1 downregulation is even mandatory for $CD8^+$ T_{RM} cell differentiation and that forced expression of KLRG1 impeded the formation of $CD8^+$ T_{RM} cells in the skin[199]. To investigate whether EBI2 expression is already present in T_{RM} cell progenitors, the ears of mice from the time course experiment in Figure 21 were also analyzed for $CD127^+KLRG1^-$ effector cells. Since established T_{RM} cells are also $CD127^+KLRG1^-$, it was mandatory to differentiate between T_{RM} cells and sole T_{EM} cells. Reportedly, CD103 expression is a feature of T_{RM} cells that is only acquired after lodgment in the epidermis, which is a pivotal step and a requirement for the successful differentiation into T_{RM} cells[21]. Therefore, the analysis for Figure 22 was targeted at $CD62L^-CD44^+$ T_{EM} cells with the $CD127^+KLRG1^-$ phenotype and a lack of CD103 expression (non-memory).

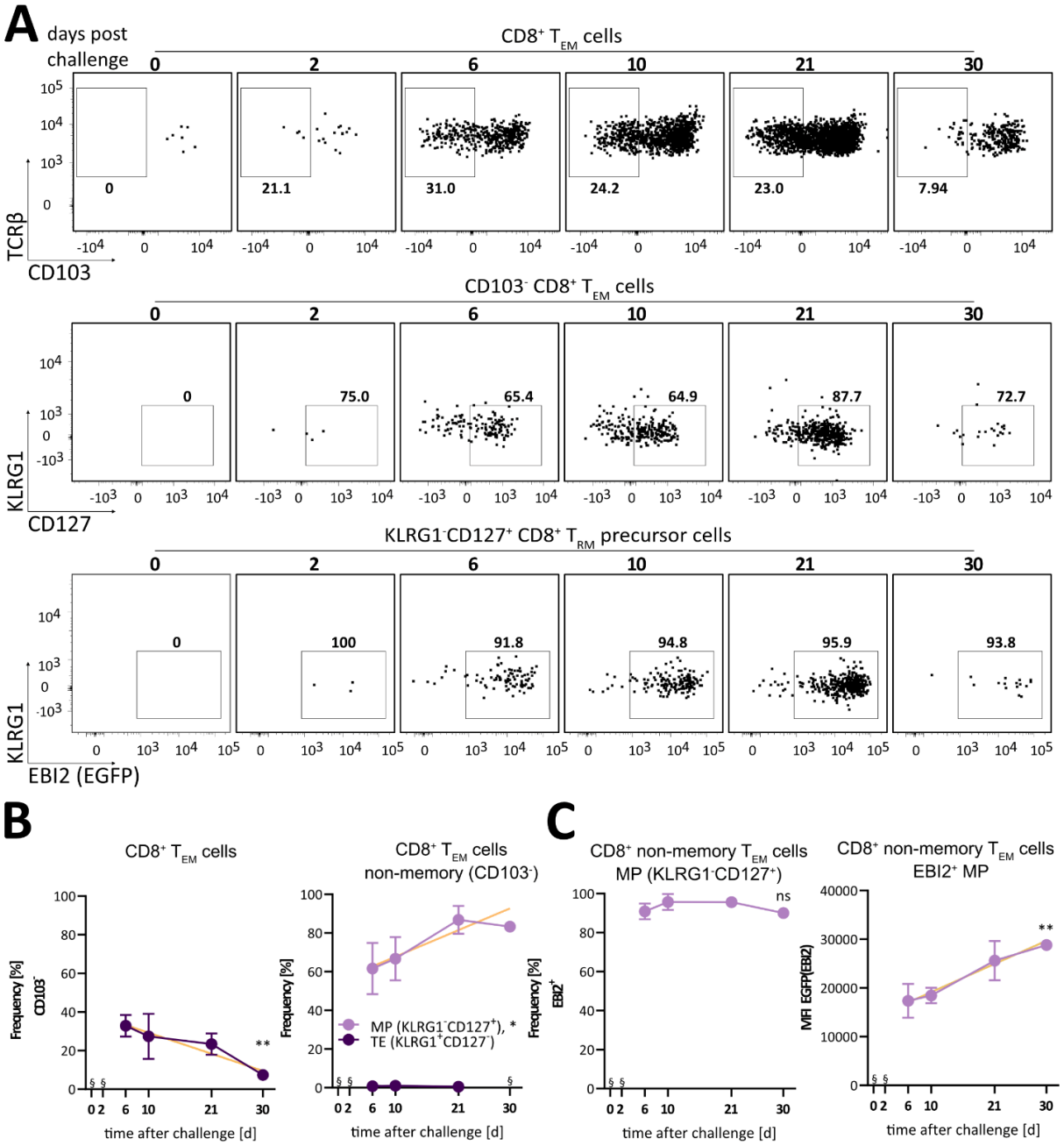

Figure 22. EBI2 expression in skin infiltrating T_{RM} cell precursors. Further flow cytometric analysis of the time course experiment in Figure 21. **A** Dot plots of (top) TCRβ- vs CD103-expression of $CD8^+$ $T_{EF\text{-}EM}$ cells of the ears; (center) KLRG1- vs CD127 (IL-7R)-expression of $CD103^-$ $CD8^+$ $T_{EF\text{-}EM}$ cells, here T_{RM} cell precursors; (bottom) EBI2-expression of $KLRG1^-CD127^+$ T_{RM} cell precursors. Dot plots show all mice per timepoint concatenated. **B** Frequency of $CD103^-$ not fully differentiated T_{RM} cell precursors in the ears (left), frequency of memory progenitor cells (MP), and terminal effector cells (TE) of $CD103^-$ $T_{EF\text{-}EM}$ cells (right). **C** Frequency of EBI2-expressing MPs (left) and EBI2 (EGFP) MFI thereof (right). §: too few cells for analysis. Golden lines show linear regression. Statistical analysis indicates whether the slope of the linear regression differs significantly from 0. Dots represent mean ± SD. ns: not significant, * $p < 0.05$, ** $p < 0.01$.

The abundance of non-memory $CD8^+$ T_{EM} cells showed a peak at d6 post challenge and thereafter declined gradually throughout healing (Figure 22 A, B). This was of course inverse to T_{RM} cell differentiation with the acquisition of CD103. Interestingly, non-memory T_{EM} cells only persisted when they expressed CD127, as the skin was largely devoid of $CD8^+$ $CD127^-$ non-memory T_{EM} cells at d30. This agrees with the fact that CD127 (IL-7Rα chain) is expressed on $CD8^+$ effector T cells that do not contract after the initial effector phase expansion in an infection and that become long-lived memory cells[200]. IL7Rα expressing cells become susceptible to IL-7 signaling, which is largely responsible for memory T cell survival, with contributions of IL-15[200]. Strikingly, similar to T_{RM} cells, almost all T_{RM} cell progenitors at d6 expressed EBI2 (Figure 22 A, C). This was stable throughout T_{RM} cell differentiation. However, also similar to T_{RM} cells, EBI2 MFI increased significantly from d6 to d30 on $CD8^+$ $CD127^+KLRG1^-$ $CD103^-$ memory progenitor cells.

Taken together, I discovered that EBI2 expression is not only a feature of murine skin T_{RM} cells, but that EBI2 expression is also already imprinted in their progeny. This raises the question whether EBI2 expression marks T_{EM} cells that are poised to become T_{RM} cells.

3.4.3 EBI2 is differentially expressed in T_{RM} cells subsets that are characterized by CD103- and CD49a expression.

I found that EBI2 is a feature of murine skin T_{RM} cells and that EBI2 expression is regulated in T_{RM} cells. This seems to happen mostly in the skin, as T_{RM} cell progenitors express less EBI2 than established T_{RM} cells and upregulate it during differentiation. Originally described as one population of memory T cells, it rapidly became clear that there are different T_{RM} cell subpopulations and that those are specialized to perform different functions. They coexist in the skin and produce specialized effector molecules of conventional type 1, 2, and 3 immunity[201]. $T_{RM}1$ cells produce IFN-γ and are associated with type 1 dermatopathies[59] and $T_{RM}17$ cells produce IL-17 and promote type 3 dermatopathies[59,69]. These subsets are also differentially involved in wound healing and the defense against viruses, bacteria, and tumors[202].

To investigate whether EBI2 expression in murine T_{RM} cells is associated with a specific T_{RM} cell subset, T_{RM} cells in recently challenged murine skin were analyzed for their expression of EBI2, CD103, and CD49a (Figure 21). As mentioned previously, $CD103^+CD49a^+$ $CD8^+$ T_{RM} cells (corresponding to $T_{RM}1$ cells) express higher amounts of EBI2 mRNA compared to $CD103^+CD49a^-$ $CD8^+$ T_{RM} cells (corresponding to $T_{RM}17$ cells)[59]. Analysis of protein expression by flow cytometry revealed that CD103 and CD49a were both significantly upregulated on $CD8^+CD69^+$ T_{EM} cells throughout the resolution of the inflammation and that the largest portion of $CD8^+CD69^+$ T_{EM} cells co-expressed both markers (Figure 23 A, C). Expectedly, CD49a expression was restricted to the $CD8^+$ lineage. Similar to previous findings, the frequency of EBI2-expressing cells in $CD8^+$ T_{RM} cell subsets, defined by CD103- and CD49a expression, remained stable over time (Figure 23 D left). Interestingly though, the EBI2 MFI increased significantly for the $T_{RM}1$ cell subset, but not for the others (Figure 23 D right). At d30,

CD103$^+$CD49a$^+$ (T_{RM}1 cells) CD8$^+$ T_{RM} cells expressed the most EBI2, compared to single CD103$^+$ or single CD49a$^+$ ones. This was in line with the reported enriched EBI2 mRNA expression in the T_{RM}1 cell subset compared to the T_{RM}17 cells.

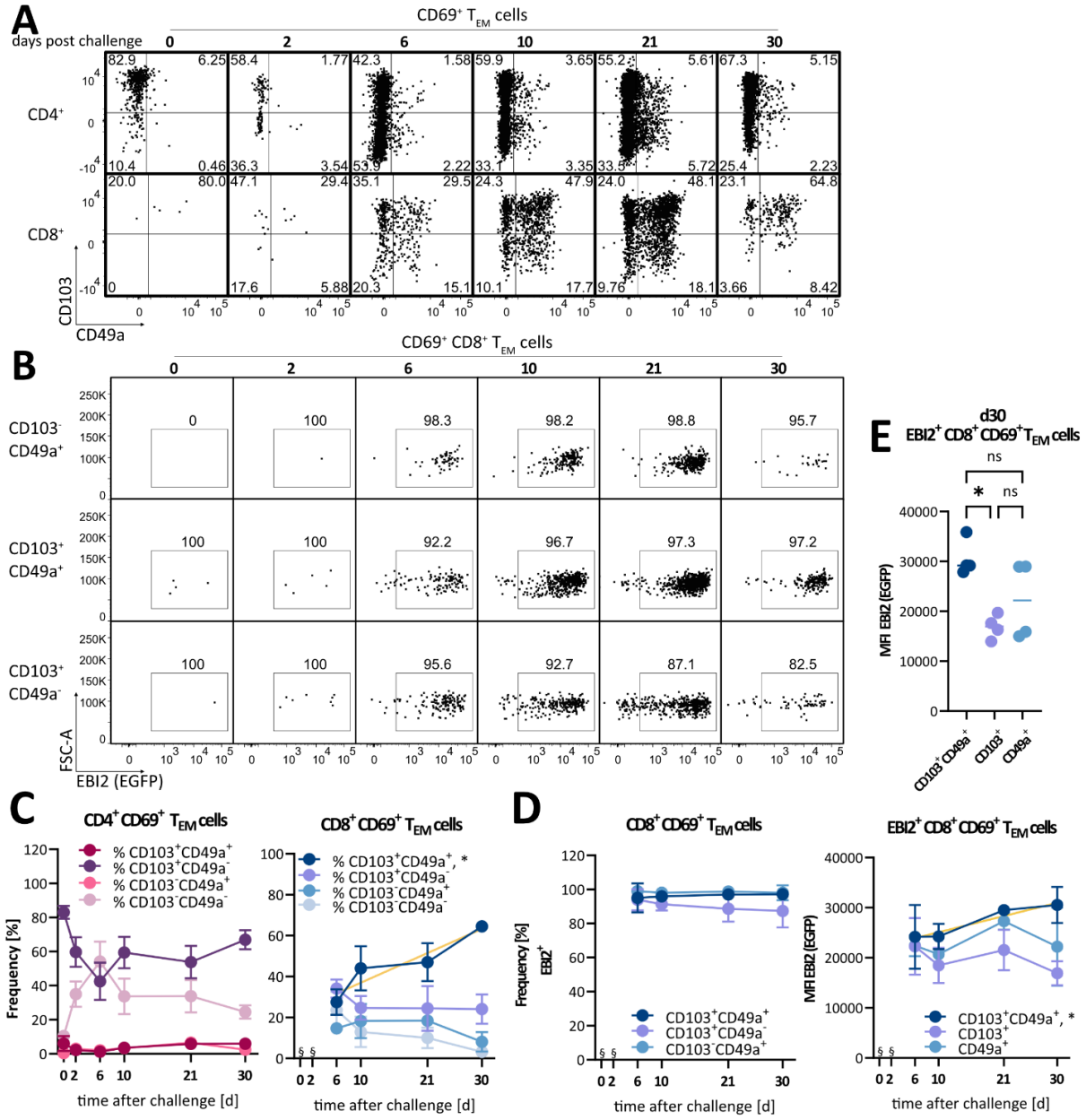

Figure 23. EBI2 is differentially expressed by CD8$^+$ T_{RM} cell subsets. Further analysis of the time course experiment in Figure 21. **A-B** Dot plots of **A** CD49a- vs CD103 expression of CD8$^+$ CD69$^+$ T_{EM} cells of the ears and **B** EBI2 expression of indicated subpopulations of CD8$^+$ CD69$^+$ T_{EM} cells of the ears. Dot plots show all mice per timepoint concatenated. **C** Frequencies of indicated populations of CD69$^+$ T_{EM} cells of the CD4$^+$ lineage (left) and CD8-lineage (right). **D** Frequencies of EBI2-expressing cells of the indicated subpopulations (left) and the MFI of the EBI2-expressing cells (right). **E** data from **D** (right), comparing EBI2 (EGFP) MFI on d30 post challenge. Golden line represents linear regression. Statistical analysis indicates whether the slope of the linear regression differs significantly from 0. Only significant regression lines are shown. Dots represent means ± SD. One-Way ANOVA with Geisser-Greenhouse correction. ns: not significant, * $p < 0.05$, ** $p < 0.01$, *** $p < 0.001$, **** $p < 0.0001$.

In summary, I found that EBI2 expression was significantly upregulated in the $CD8^+$ $T_{RM}1$ cell subset from d6 to d30. After bona fide T_{RM} cell differentiation at d30, this subset had the highest EBI2 expression which indicates that EBI2 and the EBI2-oxysterol axis could be involved in inflammatory skin diseases with underlying type 1 immunopathology like vitiligo. As of yet, no association between vitiligo pathology and the EBI2-oxysterol axis has been made.

3.4.4 T_{RM} cells in murine skin do not change tissue tropism during an inflammatory response.

My findings clearly show that EBI2 is present on T cells in the skin of mice. Julius Schwingen also found that the EBI2-oxysterol axis enzymes are upregulated in inflamed skin (dissertation submitted for review, 2023). Together, this presents a strong indication that the EBI2-oxysterol axis could play a role in inflammatory skin diseases. However, mechanistic insights are still missing. Since inflammation in the skin induces the upregulation of CH25H and CYP7B1, this results in the synthesis of 7α,25-OHC, creating a gradient from the center of the insult.

T_{RM} cells and other EBI2-expressing cells would be able to sense the ligand gradient, follow it, and find the center of the inflammation faster than EBI2-deficient cells would. In case of infection, this could lead to a faster recognition of the insulting agent and a faster triggering of the immune response. This proposed function of the EBI2-oxysterol axis in the skin is similar to the original function described in SLOs, where it would guide B- and T cells to very specific microanatomical niches to facilitate their activation[122,123,150]. Previous data from my group suggests that dermal fibroblasts could be a source of CH25H (and thereby 7α,25-OHC) during an inflammation. *Ex vivo* stimulation of murine dermal fibroblasts with pro-inflammatory cytokines induced expression of CH25H (data not shown). If fibroblasts, residing in the dermis, produce a 7α,25-OHC gradient, EBI2-expressing-T_{RM} cells could sense and follow the gradient. As introduced earlier (section 1.3.1), $CD4^+$ T_{RM} cells preferentially reside in the dermis, while $CD8^+$ T_{RM} cells are preferentially located in the epidermis. It was therefore hypothesized that epidermal $CD8^+$ T_{RM} cells would change their tissue tropism in case of inflammation and migrate into the dermis. Since edema formation in the memory CHS re-activation model starts already at 6 h post re-challenge (earliest measurement), evaluation of T_{RM} cell localization took place at 6 h post re-challenge.

As previously shown, the memory CHS flare-up reaction was stronger and faster than the acute reaction, as the ear thickness 6 h post re-challenge was already similar to peak ear swelling 24 h post acute challenge (Figure 24 A, B). Separate flow cytometric analysis of the dermis and epidermis demonstrated the tissue tropism described for T_{RM} cells in naïve and healed ears. In naïve ear skin, $CD4^+$ T cells were more prevalent in the dermis than $CD8^+$ T cells (Figure 24 C). In healed skin, numbers were almost equal in the dermis. However, recently re-challenged dermis had a slight prevalence of $CD4^+$ T cells. As analysis of CD69- and CD103 expression revealed, almost all T cells showed expression of CD69 and most $CD4^+$ T cells but

almost all CD8⁺ T cells co-expressed CD103 and can be considered T_{RM} cells. Neither the number nor the frequency of T_{RM} cells changed significantly when comparing healed and recently re-challenged skin. This is due to the treatment with FTY720, which prevents circulating T cells from entering the skin upon re-challenge.

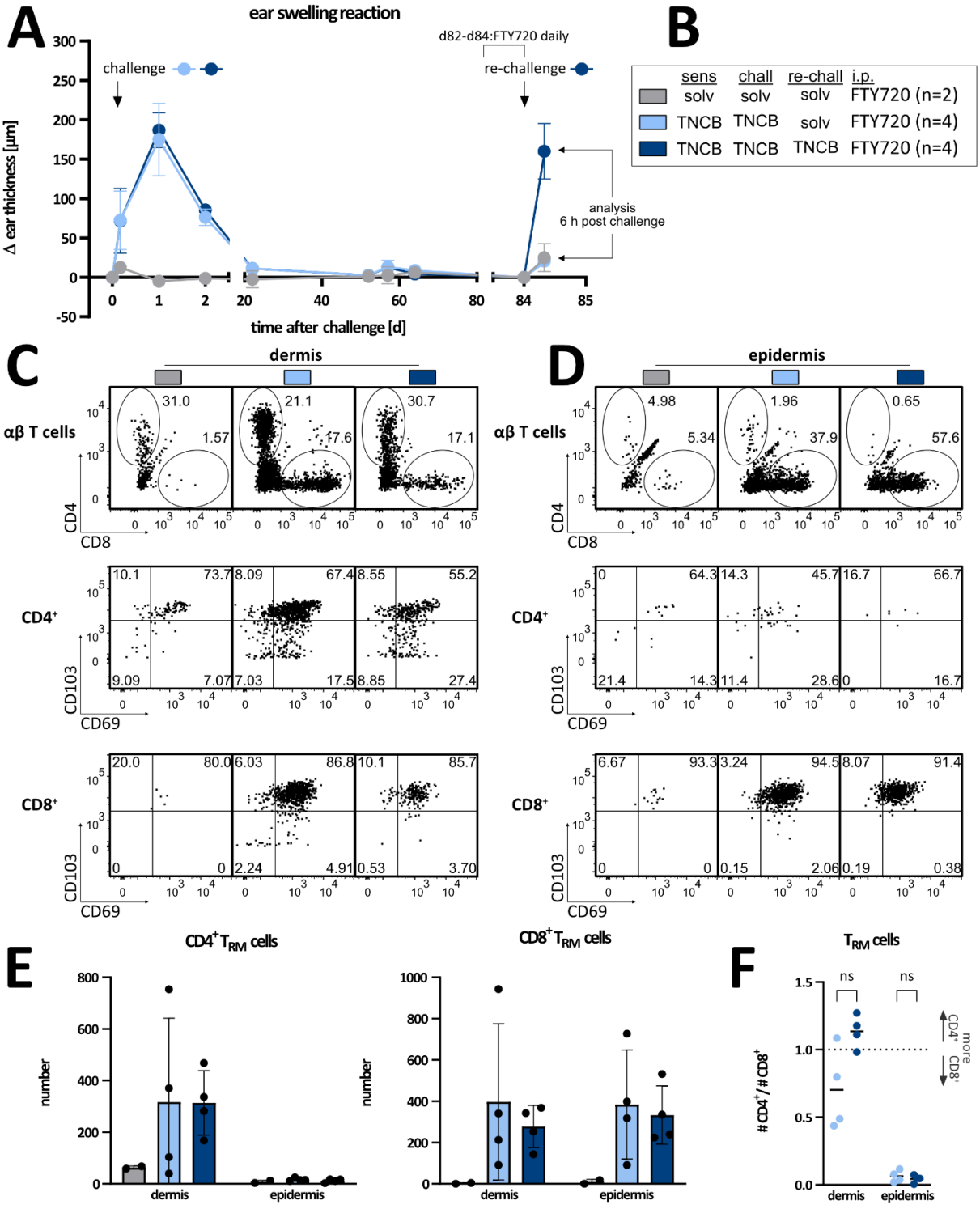

Figure 24. Ear tissue tropism of T_{RM} cells in naive, healed, and inflamed re-challenged skin. A Ear swelling reaction of WT mice in memory CHS. Mice were sensitized on d-5 with solvent (grey, n = 2) or 1 % TNCB (light blue and dark blue, n = 4) on the shaved abdomen and challenged on d0 with solvent

(grey) or 0.5 % TNCB (light blue and dark blue). The ear swelling reaction was monitored on the indicated days. All groups were injected daily with FTY720 from d82 until analysis (i.p., every 24 h with 2.4 mg/ kg FTY720). On d84 mice were re-challenged with solvent (grey and light blue) or 0.5 % TNCB on both ears. Dots represent the mean ± SD. **B** Legend for **A-F**. **C-F** Flow cytometric analysis of single ears of mice from **A**, 6 h after re-challenge. The epidermis and dermis were separated using trypsin/ EDTA. **C-D** Shown are dot plots of **C** dermis and **D** epidermis of αβ T cells (top), $CD4^+$ T cells (center), and $CD8^+$ T cells (bottom) showing the distribution of $CD4^+$ and $CD8^+$ T cells or the expression of CD69 and CD103. Shown are representative examples. **E** Bar plots showing the number of $CD4^+$ (left) and $CD8^+$ T_{RM} cells in the dermis or epidermis. Bars indicate the mean ± SD and dots represent individual mice. **F** Scatter plot showing the ratio of $CD4^+$ T_{RM} cells to $CD8^+$ T_{RM} cells in the dermis and epidermis. Dots represent the ratio calculated for the pair of T cells from within one Unpaired student's t-test with Welch's correction. ns: not significant.

Also, in line with previous findings, the naïve epidermis was mostly devoid of $CD8^+$ T cells (Figure 24 D). Agreeing with the literature, $CD8^+$ T cells populated the epidermis in healed and re-challenged skin. Moreover, no $CD4^+$ T_{RM} cells were found in the epidermis, which was according to expectations. Frequencies of $CD69^+CD103^+$ $CD8^+$ T cells were stable across all observed conditions. Upon inspection of the numbers of T_{RM} cells in the dermis and epidermis, no change in the mean abundance of either T_{RM} cell population was found. However, large standard deviations made it impossible to draw reliable clues. Analysis of T_{RM} cell ratios within each ear circumvented this problem for the most part as the interindividual variance was ignored. Furthermore, the T_{RM} cell ratios for the steady-state skin could not be calculated, since no $CD4^+$ T cells were present in the epidermis and $CD8^+$ T_{RM} cells were absent in general. Unexpectedly, the T_{RM} cell ratio in the dermis of healed skin was below 1, indicating a slightly higher prevalence of $CD8^+$ T_{RM} cells. Despite the considerable variation, a change of tropism was apparent 6 h post re-challenge, indicated by a change of the ratio of CD4 vs CD8 T_{RM} cells, although this did not reach statistical significance ($p = 0.056$). The T_{RM} cell ratio in the epidermis was heavily skewed towards $CD8^+$ T_{RM} cells and no change upon re-challenge was observed.

An increase in $CD4^+$ T_{RM} cells could only be attributed to *in situ* proliferation, because $CD4^+$ T_{RM} cells were absent in the epidermis and no shift of the T_{RM} cell ratio in the epidermis could be observed, and the treatment with FTY720 prevented circulating T cells from entering the re-challenged skin. This agrees with the results of a study by Park *et al*. The authors found that T_{RM} cells proliferate when restimulated by their antigen[24]. Moreover, the authors found no experimental evidence that $CD8^+$ T_{RM} cells would leave the epidermis after antigen encounter.

Reasons for the decrease in dermal $CD8^+$ T cells could have been that they had either migrated out of the skin, migrated into the epidermis, or undergone cell death. Migration of $CD8^+$ T_{RM} cells into the epidermis is a fundamental part of their biology and happens during the process of maturation[21], however, to change in the abundance of $CD8^+$ T_{RM} cells in the epidermis was observed here and therefore likely does not explain a decrease in $CD8^+$ T_{RM} cells in the dermis. T_{RM} cell emigration from the skin presents an intriguing and very recent topic of discussion. For mouse and human, research groups have shown that T_{RM} cells possess

plasticity and were observed to be able to emigrate from their tissue into the bloodstream and even into SLOs[203,204]. This phenomenon was observed after restimulation of T_{RM} cells in the skin and could therefore explain the change in the T_{RM} cell ratio in the dermis of re-challenged skin observed here.

Taken together, the tissue tropism of T_{RM} cells in the skin could be confirmed. I found indications that T_{RM} cells could change their tissue tropism in the early phase of an inflammation and migrate between the dermis and epidermis. However, due to large deviation in the data, this could only be interpreted as a tendency and no reliable conclusion could be drawn. Interestingly though, the trend observed would indicate that either dermal $CD4^+$ T_{RM} cells increase in number, or that dermal $CD8^+$ T_{RM} cells decrease in number.

3.5. EBI2 expression is a feature of human T_{RM} cells.

3.5.1 $CD8^+$ resident, rather than circulating memory T cells are marked by EBI2.

I established EBI2 expression to be a feature of murine T_{RM} cells in the skin. To study EBI2 expression on human T_{RM} cells, I initiated a collaboration with the surgical department of the dermatology clinic and was able to obtain healthy skin samples. Because T_{RM} cells are rare, blood was used as an FMO control and as a reference for comparison of EBI2 expression of skin T_{RM} cells. Two different skin sample types were obtained - full skin (Burow's Triangle) as well as split skin. Full skin is comprised of all layers of the skin, including the hypodermis, dermis, and epidermis, and therefore contains all types of skin immune cells. Split skin, however, contains the full epidermis and only a small margin of the dermis. This made it possible to compare T_{RM} cell phenotypes in different locations of the skin. Since only one split skin sample was obtained, analysis of this sample was indicated but should be viewed carefully and no reliable conclusions should be drawn from it. Of note, the anti-human EBI2 monoclonal antibody (clone: SA313E4, mouse IgG2a, κ light chain, Alexa Fluor 647 conjugate, from BioLegend™) was tested and validated on healthy human blood, according to published stainings[120,149] (data not shown).

Strikingly, EBI2 was expressed by T_{RM} cells of healthy human skin (Figure 25 A). In fact, 62 % of $CD4^+$ T_{RM} cells expressed EBI2, and 71 % of $CD8^+$ T_{RM} cells. Moreover, rather than separating in a clear positive and negative population, EBI2 expression displayed as a rather continuous pattern. The use of brighter fluorochromes or secondary stainings with e.g. biotin-streptavidin could theoretically enhance the signal and improve the separation of EBI2-positive from -negative cells. However, several other fluorochrome conjugates were tested, but none showed specific staining for EBI2 (data not shown).

Similar as in mice, more human $CD8^+$ T_{RM} cells in full skin expressed EBI2, compared to $CD8^+$ T cells in the circulation (Figure 25 B). Despite the fact that $CD8^+$ full-skin T_{RM} cells showed a strong tendency to express more EBI2 than memory $CD8^+$ T cells in the blood, this did not reach statistical significance ($p = 0.075$). Interestingly, full-skin $CD4^+$ T_{RM} cells expressed significantly less EBI2, compared to the circulating $CD4^+$ T cell population. This poses a

difference between mice and humans, as murine T_{RM} cells showed higher EBI2 expression as circulating T cell populations. Of note, it appears that in split skin (comprised mostly of epidermis) EBI2 expression is higher compared to full skin. Moreover, comparing EBI2 expression of $CD4^+$ and $CD8^+$ T cells in the blood highlights the fact that EBI2 is differentially regulated in both lineages, as was described in the literature[122], and shows comparable frequencies of EBI2-positive T cells to the ones published[120,149].

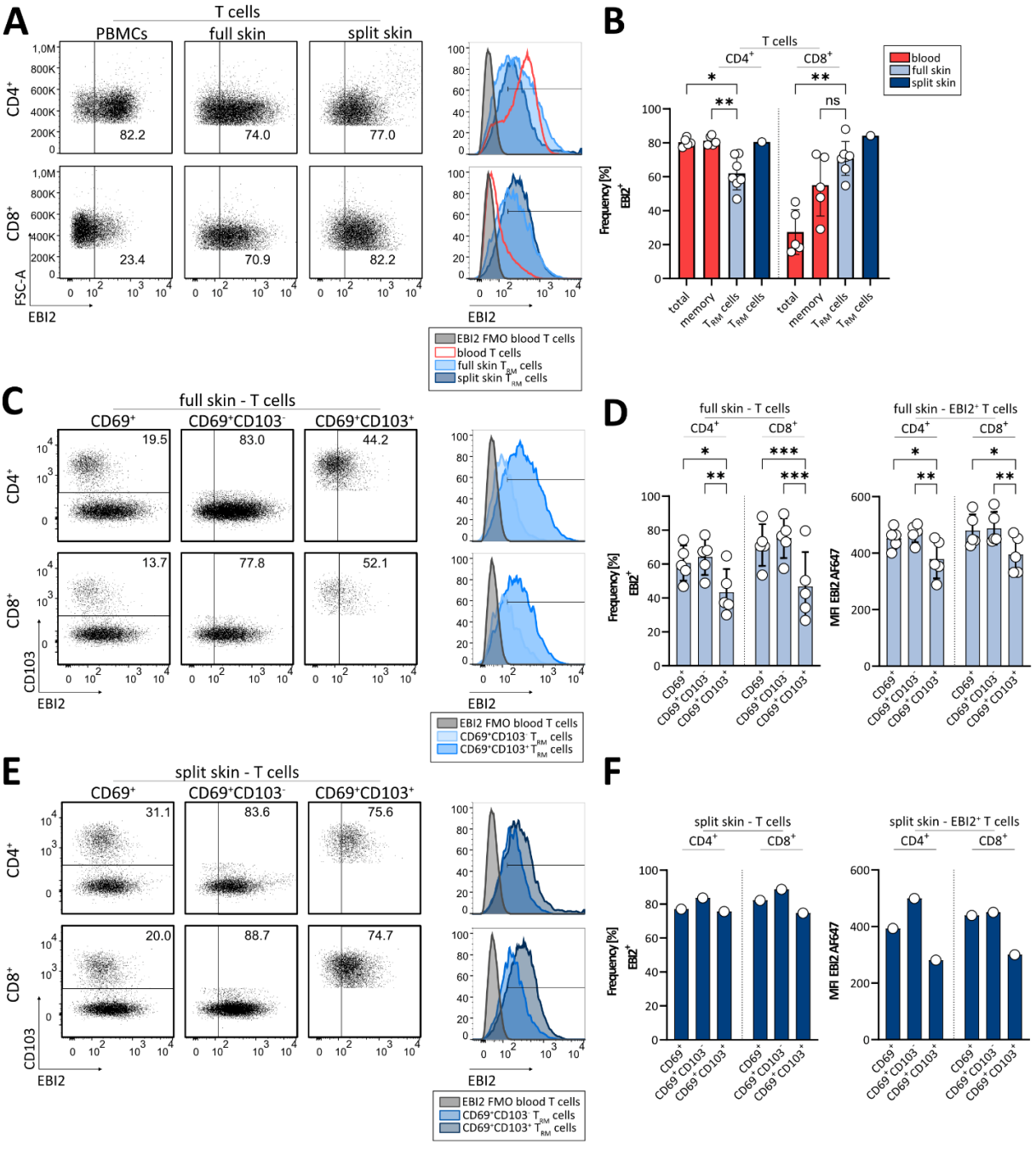

Figure 25. Comparison of EBI2 expression of human circulating (blood) T cells and skin T_{RM} cells. A-F Flow cytometric analysis of αβ T cells from healthy donors of blood (n = 5), full skin samples (n = 5), and a split skin sample (n = 1). Skin samples were obtained fresh from surgery. **A** Dot plots (left) of $CD4^+$ (top) and $CD8^+$ (bottom) T cells from indicated tissues, gated populations indicate EBI2-positive cells.

Right panel: EBI2 histogram overlays of indicated populations. T_{RM} cells: $CD45RA^{-}CD69^{+}$. Shown are representative examples. Horizontal bars indicate the EBI2-positive fraction. **B** Bar graphs showing EBI2 expression of indicated populations and tissues. Total: all αβ T cells, memory: $CD45RA^{-}$. Bars indicate mean ± SD and dots represent individual healthy donors. Mixed-effect analysis with Geisser-Greenhouse correction and uncorrected Fisher's test. **C** as **A**, left panel: gates indicate the frequency of CD103-expressing $CD4^{+}$ (top) and $CD8^{+}$ (bottom) T_{RM} cells (left). Comparison of EBI2-expression in $CD69^{+}CD103^{-}$ (center) vs $CD69^{+}CD103^{+}$ T_{RM} cells (right). **D** Bar plots showing the frequency of EBI2-expressing cells (left) and the EBI2 MFI of $EBI2^{+}$ cells. Bars indicate the mean ± SD. Dots represent individual donors and all populations from full skin or split skin are derived from the same five donors or the same one donor respectively (paired). Two-Way ANOVA with Tukey's correction for multiple testing. **E-F** as **C-D**, for split skin. ns: not significant, * $p < 0.05$, ** $p < 0.01$, *** $p < 0.001$.

To investigate whether EBI2 expression was different among T_{RM} cell subtypes, the frequencies of EBI2 expressing cells among human T_{RM} cells ($CD69^{+}$) and subsets thereof ($CD103^{-}$ or $CD103^{+}$) were analyzed (Figure 25 C-F). It stood out that EBI2 expression was significantly lower in $CD103^{+}$ T_{RM} cells compared to both other populations, in terms of frequency of positive cells and in terms of MFI of $EBI2^{+}$ cells. As CD103 expression is acquired after lodgment in the epidermis in mice[21], this is in contrast to the observation that split-skin T_{RM} cells appear to express EBI2 in a higher fashion compared to full-skin T_{RM} cells. Split skin tissue contains a much larger proportion of epidermis and should therefore contain more fully differentiated $CD103^{+}$ T_{RM} cells, which express less EBI2 than $CD103^{-}$ ones. Indeed, the split skin sample showed a higher proportion of CD103-expressing cells than the full skin samples (Figure 25 C, E), however, more split skin samples need to be investigated to draw reliable conclusions.

In conclusion, I found that EBI2 expression is also a feature of human T_{RM} cells in healthy skin and that EBI2 expression is differentially regulated between $CD103^{-}$ and $CD103^{+}$ T_{RM} cells. In humans similar to mice, EBI2 expression of $CD8^{+}$ T_{RM} cells was in strong contrast with EBI2 expression of circulating $CD8^{+}$ T cells, highlighting it as a feature of $CD8^{+}$ skin T_{RM} cells.

3.5.2 EBI2 expression is regulated differently between $CD4^{+}$ and $CD8^{+}$ T cells during memory formation but is similar across species.

Having established the EBI2 expression pattern across human and mouse throughout the circulation and the periphery made it possible to make comparisons across different memory subsets and between human and mouse (Figure 26). The analysis of the expression pattern during memory generation may yield insights into how EBI2 expression might be regulated and what could influence it.

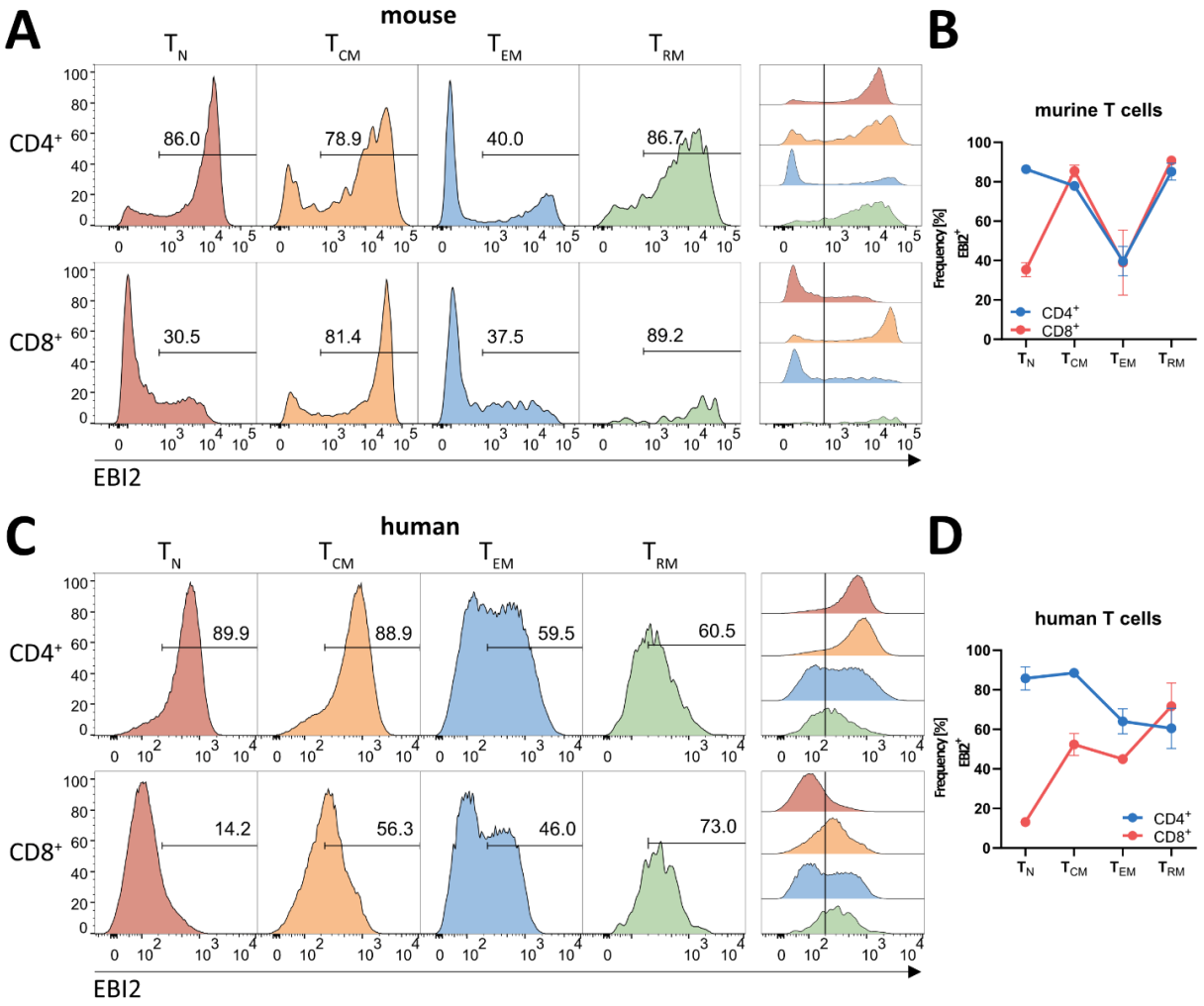

Figure 26. EBI2 expression pattern across different T cell subsets in mouse and human. A Flow cytometric analysis of EBI2 (EGFP) expression of indicated murine T cell subsets in the blood (T_N cells (naïve, $CD62L^+CD44^-$), T_{CM} cells (central memory, $CD62L^+CD44^+$), T_{EM} cells (effector memory, $CD62L^-CD44^+$)) and matched skin (T_{RM} cells, $TCR\alpha\beta^+CD62L^-CD44^+CD69^+CD103^+$). An acute CHS model was performed on $EBI2^{+/EGFP}$ mice (n = 4) and blood and healed skin were analyzed on d30 post challenge. Representative histograms show EBI2 expression and gates indicate the EBI2-positive fraction. The same histograms are overlaid by offset for better visualization of the differences. **B** X-Y diagram showing the frequency of EBI2-positive cells of indicated populations. Dots are connected to represent the differentiation path, assuming the linear differentiation model (Figure 1). Dots represent the mean ± SD. **C** As **A**, showing EBI2 expression in healthy human blood (T_N cells ($CD45RA^+CD127^+$), T_{CM} cells ($CD45RA^-CD127^+$), T_{EM} cells ($CD45RA^-CD127^-$) and not matched full skin (T_{RM} cells ($TCR\alpha\beta^+CD69^+$). Representative histograms are shown (n = 2 blood, n = 5 skin). **D** As **B**, visualizing data from **C**.

Using the $EBI2^{+/EGFP}$ mouse strain (Figure 26 A, B), it was confirmed that the EBI2 expression pattern in different murine T cell subsets, T_N cells ($CD62L^+CD44^-$), T_{CM} cells ($CD62L^+CD44^+$), and T_{EM} cells ($CD62L^-CD44^+$), was in line with published results[120]. Interestingly, following the linear model for memory T cell differentiation (Figure 1), $CD4^+$ and $CD8^+$ murine T cells start off with a drastic difference in EBI2 expression by T_N cells. They then, however, converge in all following memory T cell subsets. Intriguingly, T_{CM} cells express much more EBI2 than T_{EM} cells in both lineages. EBI2 expression increases from T_{EM} cells to T_{RM} cells again. This

highlights the fact that EBI2 expression is under tight and strict regulation, necessary for $CD4^+$ and $CD8^+$ T cells, and that it plays a crucial part in their biology. T_{EM} cells also represent the T cell with the least tissue tropism. They mostly localize in the bloodstream, with transient immigration into peripheral tissues, but not SLOs. The fact that T_{EM} cells express EBI2 the lowest among the compared T cell subsets, suggests that EBI2 expression is associated with tissue tropism, either SLOs (where the function of EBI2 was investigated in detail) or peripheral tissue (where less is known about the function of EBI2 on T cells).

It was especially interesting to see, that human T cells expressed EBI2 in a very similar pattern throughout memory T cell differentiation (Figure 26 C, D) compared to mouse. However, the difference in expression between subsets was not as drastic as seen for murine T cells. One reason for this might be that the investigated mice were homogenous in age and sex, free of specific pathogens, and inbred, whereas the human samples were much more diverse. Moreover, murine T_{RM} cells were characterized either in steady state or in a homogenous disease model. The discrepancy between $CD4^+$ and $CD8^+$ lineages was also more apparent, raising the question of how EBI2 expression is regulated and whether this is different for $CD4^+$ and $CD8^+$ T cells. Apart from that, the regulation of EBI2 expression on $CD4^+$ and $CD8^+$ T cells appeared to be conserved across these two species.

3.6. Pro-inflammatory T_{RM} cells in the skin of psoriasis patients express higher levels of EBI2.

3.6.1 Deep phenotyping of the T cell response in the skin of psoriasis patients.

Psoriasis is widely regarded as a chronic immune-mediated disease and its pathogenesis is directly linked to T cells[67]. This is highlighted by the fact that effective treatments aim to impair DC-T cell interactions by blocking DC-derived cytokines that polarize and / or activate T cells[113], neutralize the effector mechanisms of T cells, and neutralize T cell-derived cytokines[68,71]. Especially IL-17, which is produced by T cells, drives psoriasis lesions by activating keratinocytes[32,72], thereby recruiting neutrophils and inducing neovascularization[32]. It has been shown that dermal γδ T cells are the main mediators in some of the most widely used psoriasis mouse models[33,205,206]. This was attributed largely, but not exclusively, to their ability to produce large amounts of IL-17. However, in human skin, γδ T cells are rare and are not regarded to play impactful roles in the pathogenesis of psoriasis[32]. In humans, αβ T cells and DCs (conventional and plasmacytoid) are the main mediators of plaque psoriasis[68,71]. These T cells were shown to phenotypically resemble T_{RM} cells and to be still present in healed psoriatic lesions, which classifies them as bona fide T_{RM} cells[69,207,208].

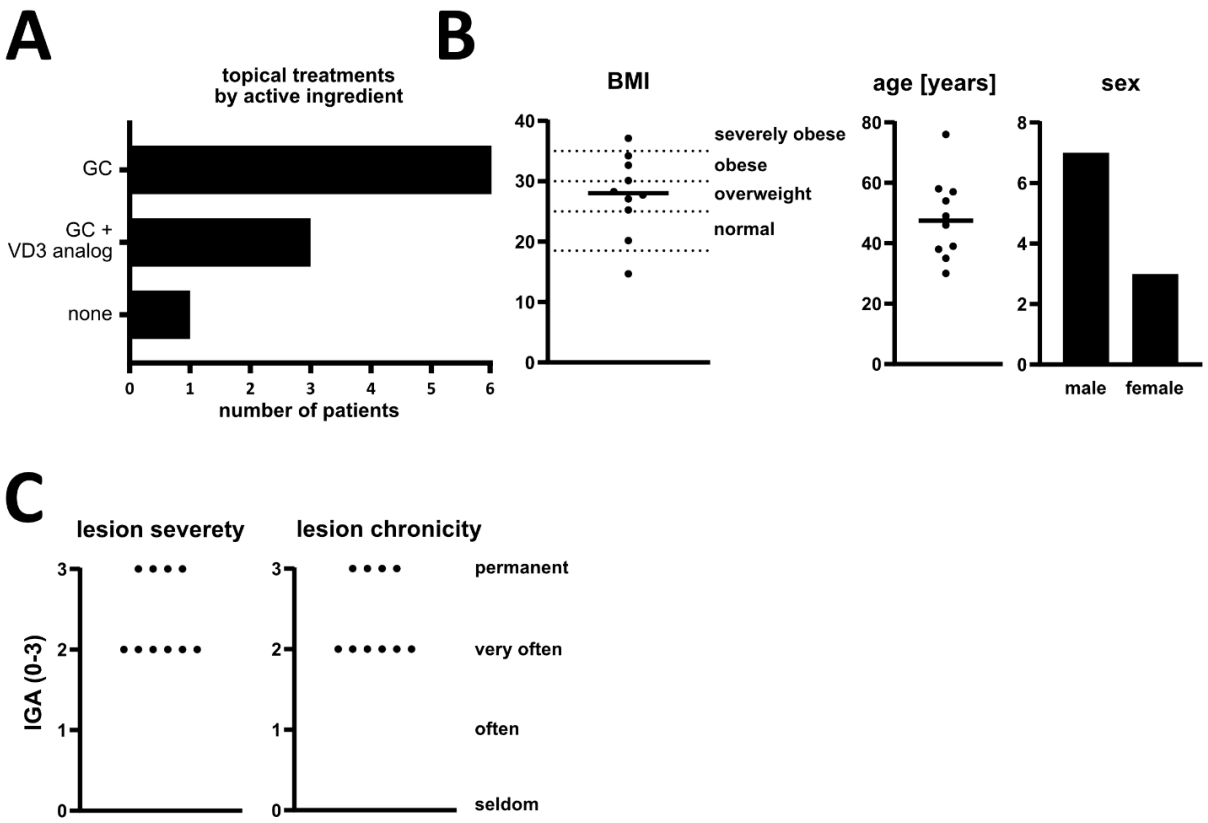

Figure 27. Study details and patient metadata from my clinical trial. A Bar graph showing the active ingredients of the topical treatment of the patients included in the study and the number of patients receiving it. GC: glucocorticoid, VD3: vitamin D3. **B** Left: scatter plots of body mass index (BMI), including thresholds for severely obese, obese, overweight, and normal weight[209]. Center: scatter plot showing age distribution in years. Right: bar graph showing sex distribution. **C** Measurements of disease severity given by dermatologists as investigators global assessment (IGA) score: lesion severity - intensity of the current flare (left) and lesion chronicity - frequency of this lesion flaring up (right).

To study the role of EBI2 on human skin T_{RM} cells in psoriasis, I initiated my clinical study and got approval from the local ethics committee. This made it possible to collect patient skin samples (6 mm punch biopsies, n = 10) from lesional skin and non-lesional skin (> 10 cm distance to the lesion) and to utilize a 23-parameter flow cytometry panel for deep phenotyping of T_{RM} cells in non-lesional and lesional psoriatic skin.

Patients were excluded from the study when they were or have been in the last 2 months under treatment of systemic immunomodulatory drugs. Since almost all patients that present in the clinic are under topical immunomodulatory drugs (here 90 %), it was not possible to account for this factor. Patients included in the study were treated with glucocorticoids (GCs) or with GCs + vitamin d3 (VD3) analogs (Figure 27 A). One patient was completely therapy naïve. These topical treatments can influence the immune response and need to be considered in the analysis. Furthermore, it is known that obesity is a risk factor for psoriasis[210]. Indeed, the mean BMI for patients in the study was 27.7 (Figure 27 B), which is considered overweighed by German health insurances[209]. Further, 40 % of the patients were even obese

or severely obese while only one patient was of normal weight and one patient was underweight. The mean age was 48.2 years and 70 % of the patients were male. Expectedly, since the patients presented at the hospital, the lesions were quite severe with an IGA (investigator's global assessment score) of 2 or 3 (Figure 27 C) and chronic with patients stating that the lesions from which the samples were obtained flared up very often up to permanently.

To analyze such high-dimensional data, uniform manifold approximation and projection (UMAP) was applied. UMAP dimensionality reduction made it possible to visualize the data in a two-dimensional space (UMAP1 vs UMAP2), where similarities and dissimilarities of cell clusters can be compared. Exploration of the UMAP revealed that the dominant cell type in the skin of psoriasis patients was T_{RM} cells (Figure 28 A). Interestingly, the second most common cell type was T_{CM} cells. Peripheral tissue tropism is typically attributed to T_{RM} cells and T_{EM} cells. Detected T_{CM} cells and T_N cells therefore either have transiently entered the tissue or were located in the blood vessel of the biopsy during the time of excision.

Heatmaps were created from all relevant parameters to explore the UMAP clusters (Figure 28 B). This revealed that EBI2 was expressed by most T cells and only a few highly or lowly expressing cells were apparent. This ubiquitous expression on T cells is in line with the results obtained from healthy skin (Figure 25). The two major clusters were made up of $CD4^+$ and $CD8^+$ T cells respectively (Figure 28 B). Smaller clusters to the bottom right constituted non-T_{RM} cells and one group of clusters high in CD69 was located even more distant from the two major clusters. Interestingly, cells in these $CD69^{high}$ clusters seemed particularly low in terms of EBI2 expression. CD103 and CD49a positive cells were enriched in the top of the UMAP and overlapped for $CD8^+$ T cells, indicating co-expression. Interestingly, the exhaustion markers CD101 and PD-1 did not cluster together, but the expression patterns of PD-1 and CD69 appeared rather similar. This highlighted the fact that PD-1 is a core-marker of T_{RM} cells[56,57].

There were separate clusters of IFN-γ and granzyme B-expressing cells in both T cell lineages (Figure 28 B). For the most part, these clusters overlapped, indicating bona fide type 1 T cells. Interestingly, IL-$17A^+$ cells formed one cluster, and $CD4^+$ and $CD8^+$ IL-$17A^+$ T cells were located very close together, suggesting strong similarity despite the different lineages. IL-22 and IL-4 expressing cells were located predominantly on the $CD4^+$ clusters. Only very few cells expressed IL-13 and IL-10 and Ki-67 expression was modest as well. Interestingly, the cells with the highest Ki-67 expression were located in the IL-$17A^+$ cluster, suggesting that these cells were actively proliferating (Ki-67 expressing) and likely contributing to disease maintenance.

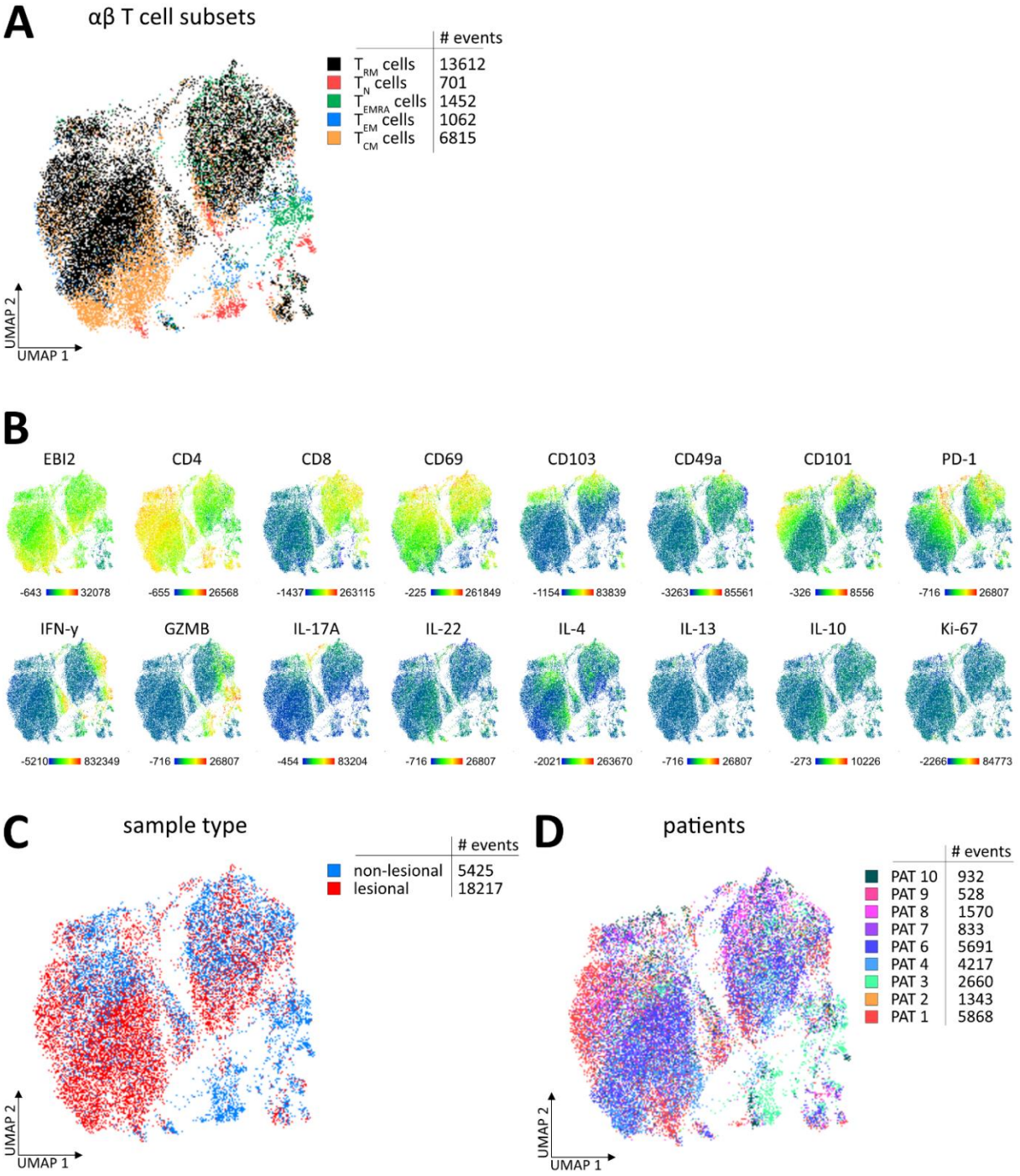

Figure 28. UMAP of high dimensional flow cytometry of psoriasis patient skin samples. Flow cytometric analysis of 6 mm skin punch biopsies from psoriasis patients (n = 9). Donor 6 was excluded from statistical analysis due to low cell numbers. Uniform Manifold Approximation and Projection (UMAP) was created in FlowJo™ Treestar on ViaDye$^-$CD45$^+$TCRβ$^+$ from all patients and skin samples (non-lesional and lesional) using Euclidian clustering with 10 neighbors. Overlays of **A** T cell subsets, **B** heatmaps of relative expression of indicated parameters, **C** sample types (non-lesional and lesional skin samples), and **D** individual patients. Indicated are the number (#) of flow cytometry events per parameter. Patient 5 was excluded due to low cell numbers. T_{RM} cells (CD69$^+$), T_N cells (CD45RA$^+$CCR7$^+$), T_{EMRA} cells (effector memory T cells re-expressing CD45RA CD45RA$^+$CCR7$^-$), T_{EM} cells (CD45RA$^-$CCR7$^-$), T_{CM} cells (CD45RA$^-$CCR7$^+$), PAT: patient.

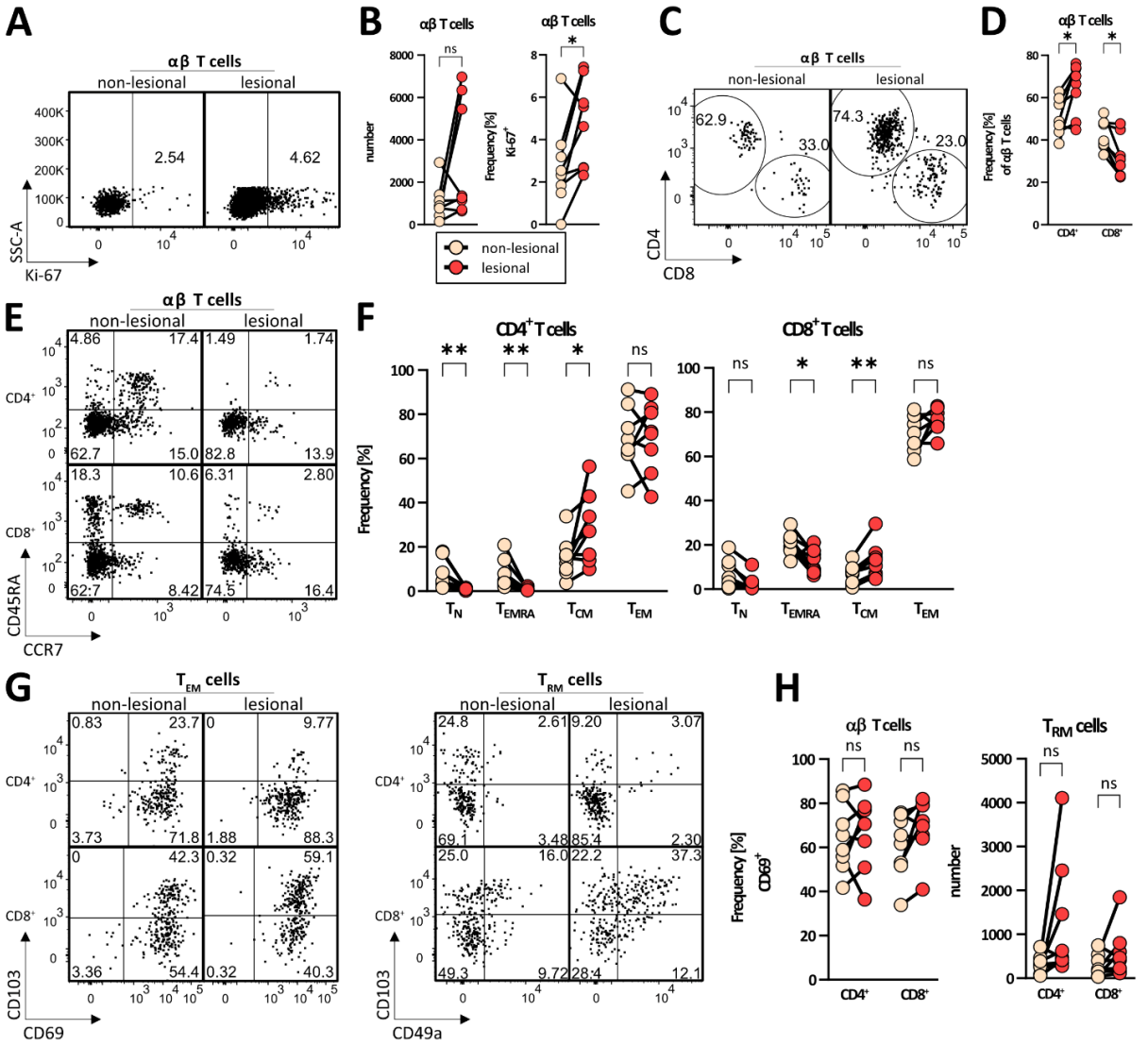

Figure 29. Characterization of skin biopsies from psoriasis patients for disease characteristics of T cells. Flow cytometric analysis of 6 mm skin punch biopsies from psoriasis patients (n = 8). **A** Dot plots of skin αβ T cells of non-lesional and lesional skin, gates indicate Ki-67-positive fraction. Shown is a representative example of matched samples. **B** Scatterplots of indicated populations from matched non-lesional and lesional skin biopsies. Wilcoxon matched-pairs signed-rank test. **C** As **A**, showing frequencies of $CD4^+$ and $CD8^+$ αβ T cells. **D** As **B**, showing frequencies for $CD4^+$ (left) and $CD8^+$ (right) αβ T cells. **E** As **A**, showing CCR7- vs CD45RA expression of $CD4^+$ (top) and $CD8^+$ (bottom) T_{EM} cells. **F** As **B**, comparing the proportion of naïve T cells (T_N, $CD45RA^+CCR7^+$), effector memory T cells re-expressing CD45RA (T_{EMRA}, $CD45RA^+CCR7^-$), central memory T cells (T_{CM}, $CD45RA^-CCR7^+$) and effector memory T cells (T_{EM}, $CD45RA^-CCR7^-$) in $CD4^+$ T cells (left) and $CD8^+$ T cells (right) in non-lesional vs lesional skin. **G** As **A**, showing CD69- vs CD103 expression of T_{EM} cells (left) and CD49a- vs CD103 expression of T_{RM} cells ($CD69^+$ T_{EM} cells) (right). **H** As **B**, comparing the proportion of T_{RM} cells of T_{EM} cells and cell counts thereof. ns: not significant, * $p < 0.05$, ** $p < 0.01$.

Discriminating non-lesional and lesional skin samples (Figure 28 C), it became apparent that cells from non-lesional skin and cells from lesional skin preferentially clustered together respectively. This highlighted the difference in the T cell landscape between the two skin sample types. Additionally, the IL17-A$^+$Ki-67$^+$ cluster in the top center seemed to consist mostly of cells from the lesional skin samples. Clusters that consisted mostly of non-lesional cells were the two non-T_{RM} cell clusters described above. This was intriguing, as it showed, that there existed specific populations of T cells (CD4$^+$ and CD8$^+$) that were present almost exclusively in the non-lesional skin but still expressed high amounts of pro-inflammatory granzyme B and IFN-γ. Additionally, cells with high IL-4 expression also seemed to be enriched in regions with a high density of cells from non-lesional skin. Moreover, those clusters expressed high amounts of GZMB and IFN-γ and consisted in large parts of cells from patient 3 (Figure 28 D). Apart from these the clusters showed little to no patient bias.

The non-lesional and lesional skin biopsies were compared and analyzed for characteristics of inflammation regarding T cells. T cells were found to proliferate more in the lesional skin, marked by expression of Ki-67 (Figure 29 A, B). Moreover, CD4$^+$ T cells were increased significantly in proportion, while, unexpectedly, overall numbers of T cells did not change significantly (Figure 29 C, D). Interestingly, T_N cells and T_{EMRA} (effector memory T cells re-expressing CD45RA) cells were less abundant in lesional compared to non-lesional skin and T_{CM} cells were more abundant, while the proportion of T_{EM} cells did not change (Figure 29 E, F). This is in line with the ability of T_{RM} cells to recruit T_{CM} cells into the skin, following reactivation[17]. Unexpectedly, the overall number and proportion of T_{RM} cells of all T cells in the skin did not change significantly, while at least the proportion was expected to be less in lesional skin, due to the constant recruitment of T_{EM} cells and T_{CM} cells (Figure 29 G, H). In conclusion, the T cell landscape of the lesional skin showed characteristics of chronic inflammation, however it was less pronounced than expected.

This was also reflected in the cytokines produced by T_{RM} (CD45RA$^-$CCR7$^-$CD69$^+$) cells. IL-17A-producing CD8$^+$ T_{RM} cells were significantly more abundant in the lesional skin of psoriasis patients, however, this was not the case for CD4$^+$ T_{RM} cells, even though a strong tendency was observable both in terms of number and proportion (Figure 30 A, B). This increase in the proportion of IL-17A-producing T_{RM} cells was accompanied by a diminished fraction of T_{RM} cells producing other cytokines, including IL-22, IL-13, IL-4, and IL-10 (Figure 30 C-H). Also unexpectedly, the expression of markers associated with T cell exhaustion, CD101, and PD-1, was reduced in lesional skin, for CD101 even significantly (Figure 30 I, J).

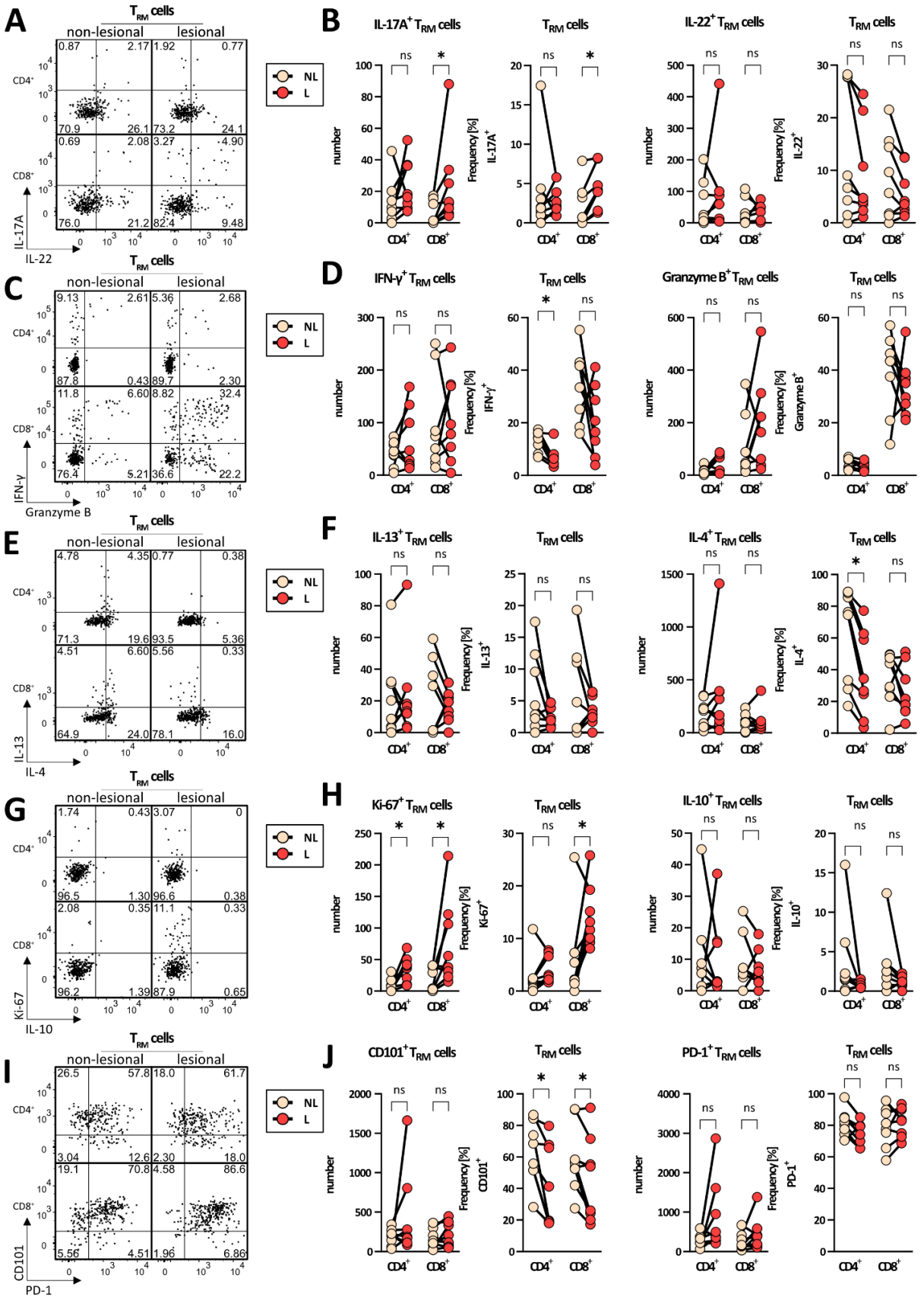

Figure 30. Overview of the T cell landscape in psoriasis patient skin biopsies. Flow cytometric analysis of 6 mm skin punch biopsies from psoriasis patients (n = 8). Left panels: dot plots of skin T_{RM} cells of non-lesional and lesional skin. Shown is a representative example of matched samples. Right panels: scatterplots of indicated populations from matched non-lesional and lesional skin biopsies. Left: $CD4^+$

T_{RM} cells, right: $CD8^+$ T_{RM} cells. Wilcoxon matched-pairs signed-rank test. **A-B** IL-17-A and IL-22, **C-D** granzyme B and IFN-γ, **E-F** IL-13 and IL-4, **G-H**, Ki-67 and IL-10, **I-J** CD101 and PD-1. Wilcoxon matched-pairs signed-rank test. ns: not significant, * $p < 0.05$.

Altogether, all cytokines included in the analysis were detectable in T_{RM} cells from the skin biopsies of psoriasis patients after PMA/ionomycin restimulation. Five out of eight patients showed very strong expression of IL-4, which is uncharacteristic for psoriasis, where IL-4 is even explored as a treatment option[211]. Also, no characteristic increase of IL-22, IFN-γ, and granzyme B-producing cells was observed. While the lesional skin was assessed as severe or even very severe, the molecular differences to non-lesional skin (at least 10 cm apart from a lesion) were mild, which could be due to the topical treatment 9/10 patients were under.

3.7. EBI2 expression functionally segregates T_{RM} cells of psoriatic skin.

3.7.1 EBI2 is enriched in T_{RM} cells with a pro-inflammatory signature in psoriatic skin.

To study the role of EBI2 on T_{RM} cells in general and in the pathogenesis of chronic inflammatory skin diseases, high-parameter flow cytometry provides a powerful tool. It makes it possible to investigate the expression and co-expression of markers associated with disease pathogenesis and/or -progression on a protein level. Harnessing this power, EBI2 expression of T_{RM} cells from skin biopsies of psoriasis patients was studied, alongside the expression of cytokines, effector molecules, and exhaustion markers. This enabled the construction of hypotheses on how EBI2 could be involved in the complex disease network.

Although I found clues by analysis of published transcriptome sequencing datasets (Figure 8), it is not known whether EBI2 is expressed on human T_{RM} cells residing in the skin affected by chronic inflammatory skin diseases as of yet. I discovered that, indeed, EBI2 is expressed on $CD4^+$ and $CD8^+$ T_{RM} cells of non-lesional and lesional skin biopsies from psoriasis patients (Figure 31 A). However, similar to healthy skin, the EBI2 expression did not appear as strong as in murine T_{RM} cells. Since a shift of the whole T_{RM} cell population compared to the FMO control was apparent, it was likely that 100 % of the T_{RM} cells in the skin of psoriasis patients expressed EBI2. Similar to healthy skin, an improvement of the staining intensity was not possible. The T_{RM} cells were divided into $EBI2^{low}$ and $EBI2^{high}$ ones based on EBI2 expression in relation to the FMO control, in order to investigate whether EBI2 expression was associated with a specific immune response phenotype. Quantifying these two populations, it was observed that the frequency and the total number of $EBI2^{high}$ T_{RM} cells are similar comparing non-lesional and lesional skin (Figure 31 B, C). However, a significant downregulation of the EBI2 MFI on $EBI2^{high}$ $CD8^+$ T_{RM} cells from lesional skin was observed, and a similar trend for $EBI2^{high}$ $CD4^+$ T_{RM} cells.

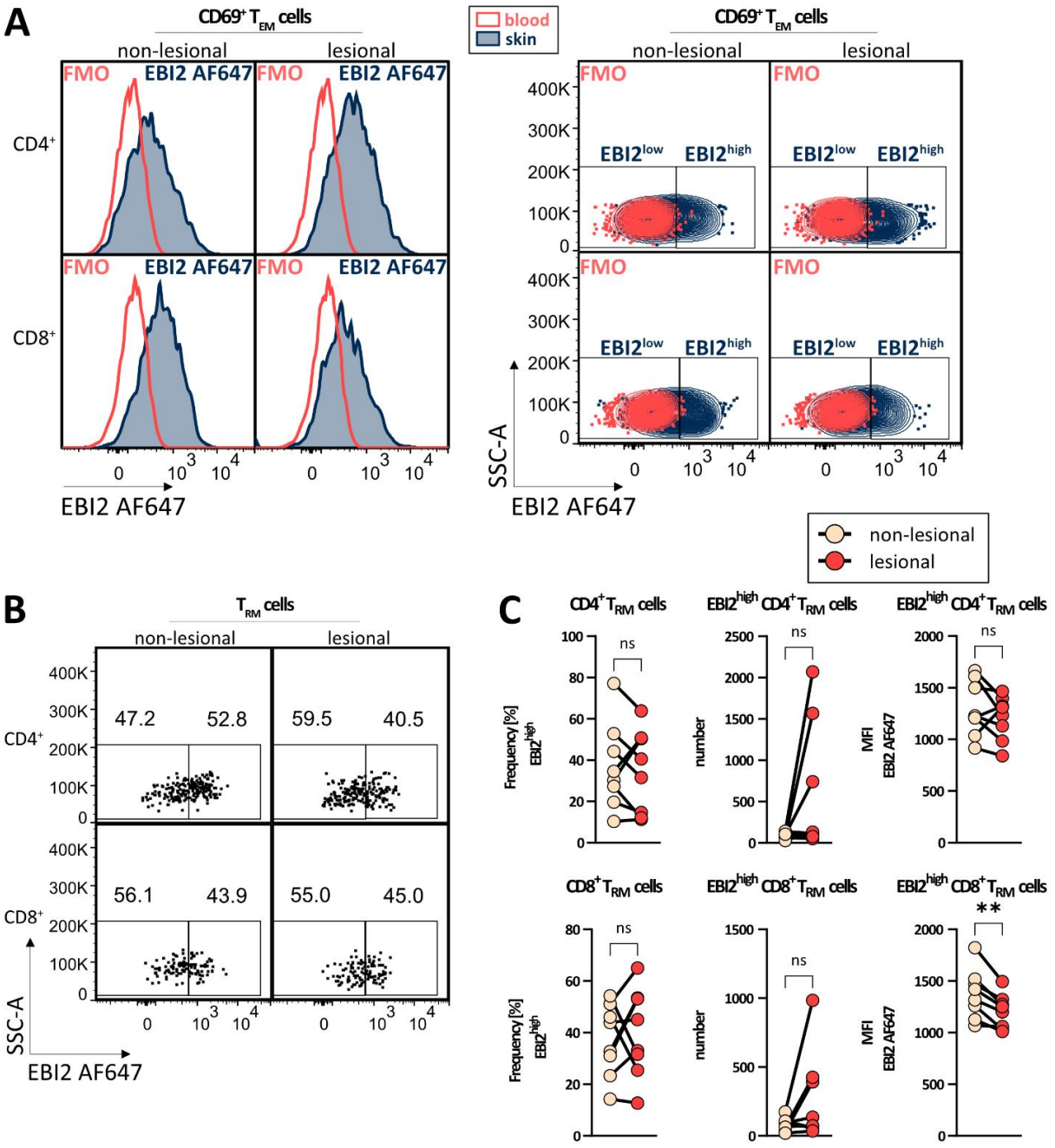

Figure 31. EBI2 expression of T_{RM} cells in psoriasis patient skin. Flow cytometric analysis of 6 mm skin punch biopsies from psoriasis patients (n = 8). **A** EBI2 expression of CD69$^+$ T_{EM} cells of the blood (red, FMO (fluorescence minus one)) and in CD69$^+$ T_{EM} cells of the skin (T_{RM} cells, blue, full stain) in non-lesional and lesional skin of CD4$^+$ (top) or CD8$^+$ (bottom) cells. Left: EBI2 histogram overlays, right: Contour plot overlays. Skin T_{RM} cells were segregated into EBI2^{low} and EBI2^{high}, according to the FMO control. **B** Dot plots showing EBI2 expression of CD4$^+$ (top) and CD8$^+$ (bottom) T_{RM} cells of non-lesional and lesional skin. Shown is a representative example of matched samples. **C** Quantification of EBI2^{high} CD4$^+$ (top) and CD8$^+$ (bottom) T_{RM} cells. From left to right showing cell counts, frequency, and EBI2 MFI of EBI2^{high} T_{RM} cells, comparing non-lesional and lesional skin. Wilcoxon matched-pairs signed-rank test. ns: not significant, ** $p < 0.01$.

A significant downregulation of the EBI2 MFI on EBI2^{high} CD8^{+} T_{RM} cells was observed, and a similar trend for EBI2^{high} CD4^{+} T_{RM} cells (Figure 31 C). One reason for this could be GPCR desensitization and downregulation, as discussed previously. I found hints that the EBI2 ligand-generating enzymes are upregulated in the inflamed skin of psoriasis patients (Figure 8). Local T_{RM} cells would be able to sense 7α,25-OHC and downregulate EBI2 consequently. Another possibility, which does not contradict the first one, could be that the lower EBI2 expression in the lesional skin is due to higher T_{RM} cell turnover. I found that EBI2 is upregulated by T_{RM} cells upon initiation of the differentiation process in murine skin, with cells expressing T_{RM} cell markers early after inflammation but only upregulating EBI2 during the differentiation to T_{RM} cells (section 3.4). Therefore, a lower MFI could also indicate T_{RM} cells in their early differentiation stage.

UMAP analysis was used to help identify the co-localization (indicating co-expression) of EBI2^{high} T_{RM} cells with T_{RM} cells gated positively for all other relevant markers (Figure 32). This made it possible to gain a broad overview of this high-dimensional data and to ascertain whether EBI2 expression was associated with a general phenotype of cells. Interestingly, even though EBI2 showed a continuous expression pattern on T_{RM} cells (Figure 31 A), as opposed to separation into a clear positive and negative population, certain areas of the UMAP were enriched for EBI2^{high} T_{RM} cells, and others were enriched in EBI2^{low} T_{RM} cells (Figure 32 A, C).

Most prominent was the cluster of cells located to the bottom right of the UMAP, away from the two main clusters, which was exclusively negative for EBI2. Additionally, a cluster to the center bottom of the UMAP, also distant from the two main clusters, appeared exclusively positive for EBI2 (Figure 32 C). Judging by the expression of other markers (Figure 32 B) the EBI2^{-} cluster appeared to consist of CD4^{+} and CD8^{+} T_{RM} cells. Expression of CD103 and CD49a for the CD4^{+} T_{RM} cells in the clusters varied, while most CD8^{+} T_{RM} cells seemed to co-express these markers. Additionally, these clusters showed a high proportion of PD-1 and CD101-expressing cells and a low proportion of cells expressing most other effector molecules and markers. This suggested that T cells in these clusters might be exhausted. However, a more detailed characterization of these populations would be necessary to demonstrate bona fide T-cell exhaustion.

It was also interesting, that regions at the top of the two main clusters, which were enriched in CD103^{+} T_{RM} cells, were less dense in EBI2^{high} T_{RM} cells. This was in line with the previous findings that CD103^{+} T_{RM} cells expressed less EBI2 than CD103^{-} ones (Figure 25). EBI2^{high} T_{RM} cell dense regions of the UMAP were enriched in Ki-67^{+}, granzyme B^{+}, IFN-γ^{+}, IL-17A^{+}, IL-22^{+}, and IL-10^{+} cells and decreased in CD101^{+} cells. This was especially intriguing, as it suggested either a type 1 or type 17 (or mixed) phenotype of EBI2^{high} T_{RM} cells. This would link EBI2 expression to a general T cell phenotype associated with pro-inflammatory characteristics and with psoriasis pathogenesis. Additionally, the enrichment of Ki-67^{+} T_{RM} cells and the absence of CD101 further suggests that EBI2^{high} T_{RM} cells are actively proliferating, non-exhausted, and pro-inflammatory.

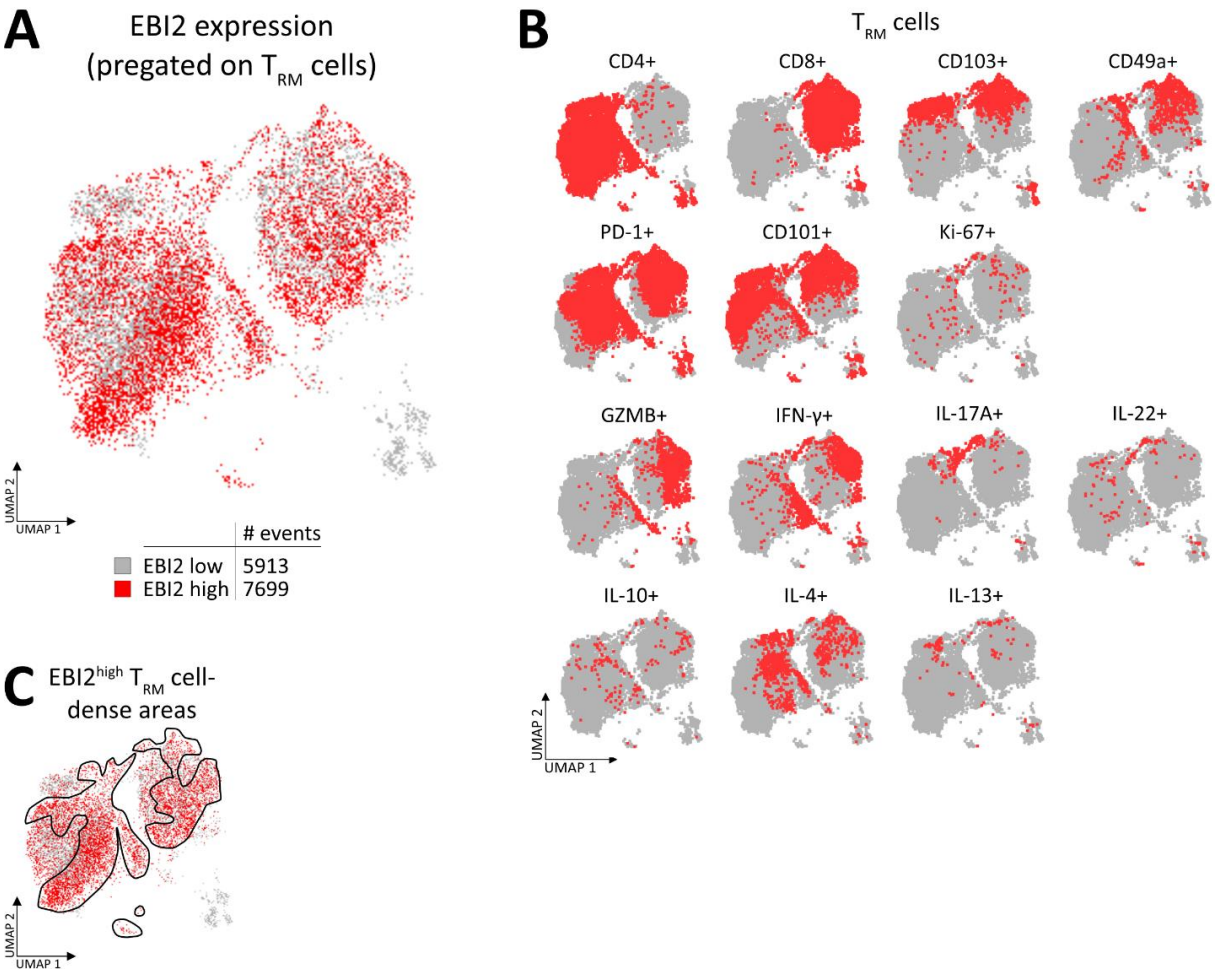

Figure 32. EBI2 and cytokine and effector molecule expression by T_{RM} cells in human skin. Flow cytometric analysis of 6 mm skin punch biopsies from psoriasis patients (n = 9). Donor 6 was excluded from statistical analysis due to low cell numbers. UMAP was created in FlowJo™ Treestar on ViaDye$^-$ CD45$^+$TCRβ$^+$ from all patients and skin samples (non-lesional and lesional) using Euclidian clustering with 10 neighbors. UMAP shows only CD69$^+$ T_{RM} cells. **A** Overlay of EBI2 low (grey) and high (red) T_{RM} cells (gated as in Figure **31** A, left panel). **B** Overlay of T_{RM} cells gated as positive for each indicated marker respectively (red).

Analyzing the proportions of type 1 effector molecule (granzyme B and IFN-γ)-producing cells between the EBI2^{low} and EBI2^{high} T_{RM} cells in greater detail (Figure 33 A-C) confirmed the observations made using the UMAP (Figure 32). Significant enrichment of granzyme B-producing cells was apparent in the EBI2^{high} population in both the CD4$^+$ and the CD8$^+$ lineage. Interestingly, the enrichment was only seen in the non-lesional skin. A similar but not significant trend could be observed in the lesional skin. However, a strong enrichment of IFN-γ producing cells in EBI2^{high} CD4$^+$ T_{RM} cells was observed in both types of skin, but not for the CD8$^+$ lineage. This correlation of high EBI2 expression and type 1 effector molecule expression suggests a bias towards the $T_{RM}1$ cell phenotype of EBI2^{high} T_{RM} cells. No enrichment of type 17 (IL-17 and IL-22) or type 2 (IL-4 and IL-13) cytokine-expressing cells was observed in the EBI2^{high} T_{RM} cells.

In concordance with a pro-inflammatory phenotype of EBI2^{high} T_{RM} cells, there was a significantly lower number of cells expressing the exhaustion marker CD101 in the EBI2^{high} vs the EBI2^{low} compartment (Figure 33 D-F). Interestingly, no difference was observed for the expression of PD-1. Since PD-1 was discovered in 1992 as a protein upregulated during T cell apoptosis[212], several other characteristics have been attributed to it. Among those, its application as a target in cancer therapy and T cell exhaustion[213] and its function as a T_{RM} cell marker and member in the core tissue-residency transcriptional signature on T_{RM} cells in mice and humans[56,57]. Despite this universal expression on T_{RM} cells, PD-1 has been shown to mediate T_{RM} cell function in the CHS mouse model[94].

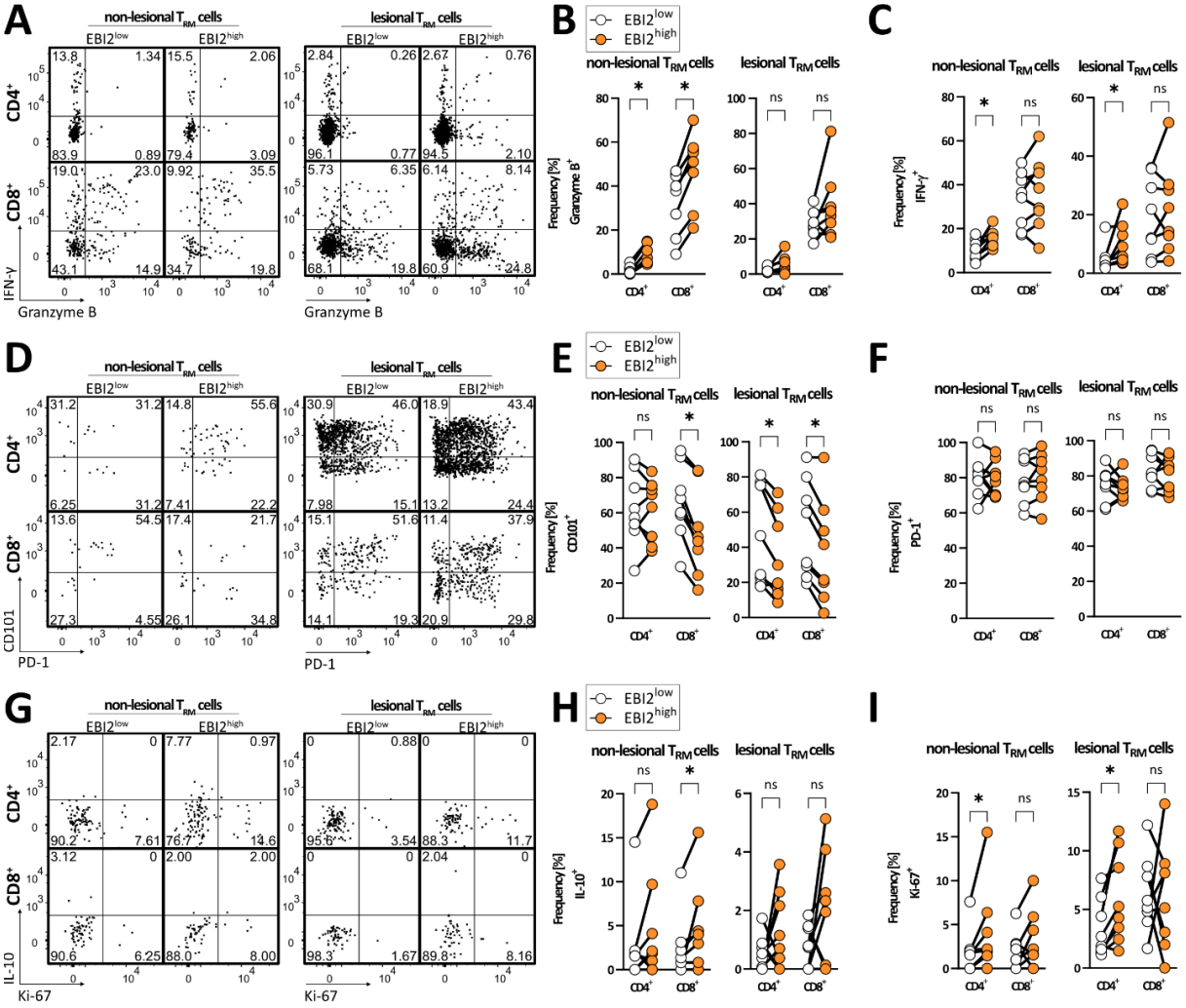

Figure 33. EBI2 expression segregates T_{RM} cells of psoriasis patient skin functionally. Flow cytometric analysis of 6 mm skin punch biopsies from psoriasis patients (n = 8). Left panels: dot plots of skin T_{RM} cells of non-lesional and lesional skin and EBI2^{low} and EBI2^{high} T_{RM} cells respectively. All plots are derived from a representative example of matched samples. Right panels: scatterplots of indicated populations from matched non-lesional and lesional skin biopsies. Left: $CD4^+$ T_{RM} cells, right: $CD8^+$ T_{RM} cells. Wilcoxon matched-pairs signed-rank test. **A-C** Granzyme B and IFN-γ, **D-F** CD101 and PD-1, **G-I** IL-10, and Ki-67. ns: not significant, * $p < 0.05$.

Moreover, IL-10-producing cells were significantly enriched in EBI2^{high} T_{RM} cells of the CD8^{+} lineage although only in non-lesional skin biopsies (Figure 33 G-I). However, a similar trend was observed for CD4^{+} EBI2^{high} T_{RM} cells and in lesional skin. This is in line with the discovery that IFN-γ secreting FoxP3^{-} bona fide T_H1 cells are the major source of IL-10 in a murine protozoan infection model and that this T_H1-derived IL-10 was crucial to dampen the immune response and improve survival[214]. IL-10 is therefore regarded to be secreted by T_H1 cells as a mechanism of autoregulation[215]. Its enrichment in EBI2^{high} T_{RM} cells in the skin of psoriasis patients therefore supports the indications for a $T_{RM}1$ phenotype. Despite this increased production of IL-10, CD4^{+} EBI2^{high} T_{RM} cells were also enriched in Ki-67^{+} cells (Figure 33 I). This indicated that CD4^{+} EBI2^{high} T_{RM} cells proliferated significantly more than CD4^{+} EBI2^{low} T_{RM} cells in the non-lesional skin and is in line with observations made using the UMAP (Figure 32).

In summary, using high-dimensional flow cytometry and dimensionality reduction algorithms on psoriasis skin samples, I discovered that EBI2 is not only expressed on a high proportion of human T_{RM} cells from psoriasis patient skin biopsies but also that EBI2 expression functionally segregates them. EBI2^{high} T_{RM} cells produced significantly more IFN-γ, granzyme B, and IL-10 than EBI2^{low} T_{RM} cells, which identifies them as $T_{RM}1$ cells. They also expressed less CD101 and more Ki-67. Hence, I discovered elevated EBI2 expression in pro-inflammatory, potentially lesion-driving T_{RM} cells in psoriatic skin.

3.7.2 EBI2 expression in human T_{RM} cells is associated with low CD103 expression.

As introduced in section 3.4.3, EBI2 was found differently expressed in human skin CD8^{+} T_{RM} cell subsets, defined by the expression of CD103 and CD49a. CD103^{+}CD49a^{-} T_{RM} cells expressed less EBI2 than CD103^{+}CD49a^{+} T_{RM} cells and were shown to preferentially produce IL-17 and to be enriched in psoriasis lesions, while CD103^{+}CD49a^{+} T_{RM} cells were shown to produce granzyme B and to be enriched in vitiligo lesions[59]. Utilizing psoriasis skin samples from my clinical study, this phenomenon was studied and EBI2 expression was determined on a protein level as opposed to the transcriptional level in the described study.

Interestingly, there was no difference in the CD103 expression of T_{RM} cells in non-lesional and lesional skin (Figure 34 A). It was expected that CD103 expression, which marks murine CD8^{+} T_{RM} cells located in the epidermis that are further advanced in their differentiation, would be enriched in non-lesional skin with less T_{RM} cell turnover and less T cell influx. However, there was a significant reduction in EBI2 expression in CD103^{+} vs CD103^{-} T_{RM} cells of the CD4^{+} lineage in the non-lesional skin, but with similar trends for the CD8^{+} lineage and in the lesional skin. Furthermore, focusing on the CD8^{+} lineage, the lowest frequency of EBI2^{high} cells was found in the CD103^{+}CD49a^{-} T_{RM} cell subset, with its frequency of EBI2^{high} cells being significantly lower than the frequency of CD103^{+}CD49a^{+}. This is in line with the findings from Cheuk *et al*. and the first proof of this finding on a protein level (Figure 34 B). This was also reflected in the MFI, but not significantly. Interestingly, all subpopulations in lesional skin displayed similar frequencies of EBI2^{high} T_{RM} cells and similar MFI.

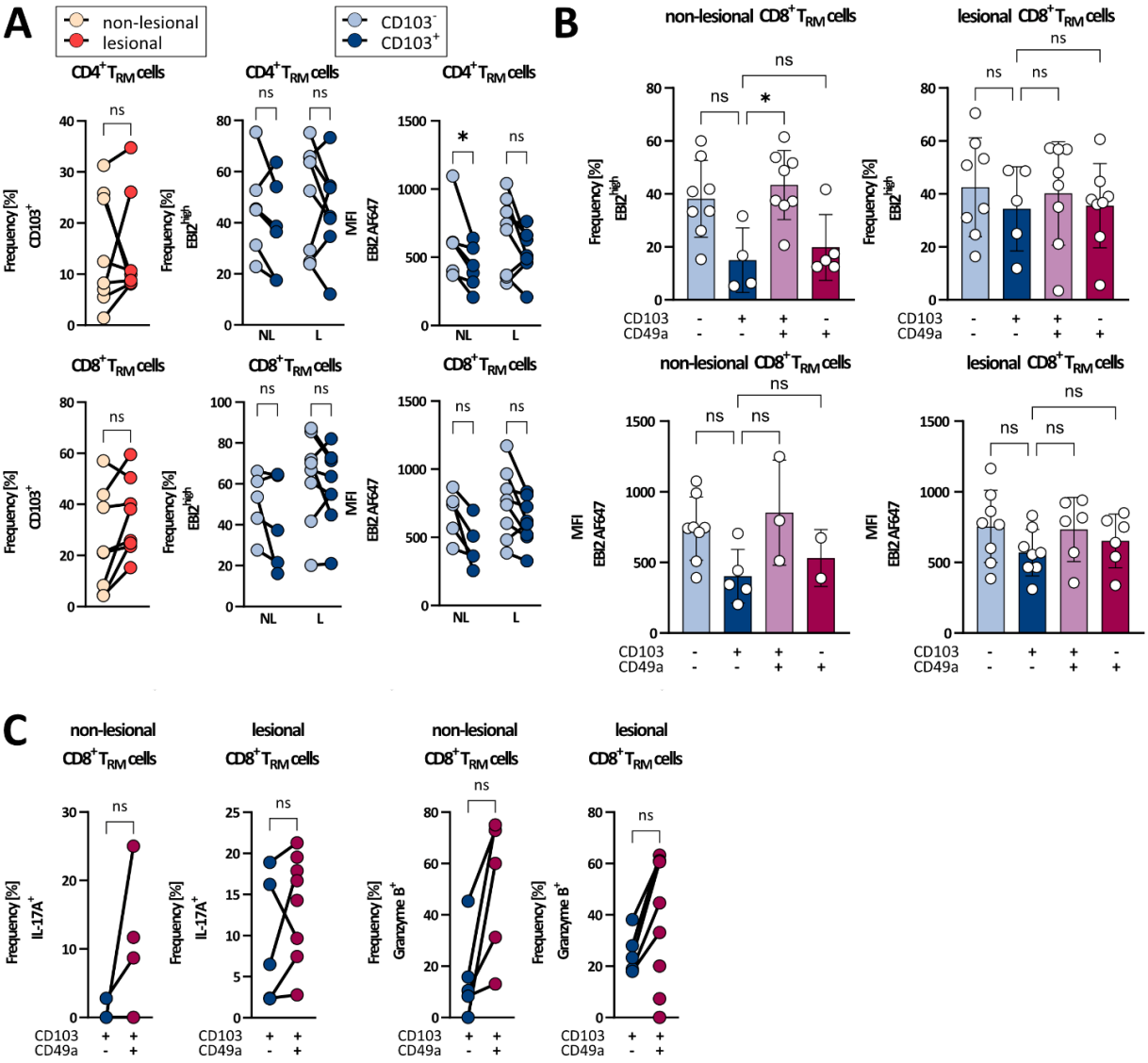

Figure 34. EBI2 expression on human skin T_{RM} cell subsets. Flow cytometric analysis of 6 mm skin punch biopsies from psoriasis patients (n = 8). Samples with < 10 cells of the indicated populations were excluded. **A** Scatterplots of matched non-lesional (NL) and lesional (L) skin biopsies, quantifying the frequency of $CD103^+$ T_{RM} cells (left) and analyzing EBI2 expression (frequency: center, MFI: right) of $CD103^-$ vs $CD103^+$ T_{RM} cells. $CD4^+$ T_{RM} cells: top, $CD8^+$ T_{RM} cells: bottom. Wilcoxon matched-pairs signed-rank test. **B** Bar plots showing the proportion (top) and EBI2 MFI (bottom) of $EBI2^{high}$ $CD8^+$ T_{RM} cells of either non-lesional (left) or lesional skin (right). Unpaired Kruskal-Wallis test. **C** Paired scatter plots of non-lesional or lesional $CD8^+$ T_{RM} cells showing IL-17A- (left) and granzyme B expression (right) of $CD103^+CD49a^-$ vs $CD103^+CD49a^+$ $CD8^+$ T_{RM} cells. Wilcoxon matched-pairs signed-rank test. ns: not significant, * $p < 0.05$.

The IL-17 bias of $CD103^+CD49a^-$ $CD8^+$ T_{RM} cells and the granzyme B bias of $CD103^+CD49a^+$ $CD8^+$ T_{RM} cells were investigated irrespective of EBI2 expression (Figure 34 C). In line with the reports from Cheuk *et al.*, $CD49a^+$ $CD8^+$ T_{RM} cells did display a heightened capacity over $CD49a^-$ ones to produce granzyme B. Due to the low numbers of cells per biopsy, some donors were excluded from this analysis, which is likely the reason why the results did not reach statistical significance but show a clear trend. No reliable conclusion could be drawn as to whether

CD49a$^-$ CD8$^+$ T_{RM} cells also display a heightened capacity to produce IL-17A, due to similar issues.

Overall, the analysis indicated that, indeed, CD103$^+$CD49a$^+$ CD8$^+$ T_{RM} cells were more capable of producing granzyme B than CD103$^+$CD49a$^-$ ones were. Additionally, I found EBI2 expression was significantly higher on this T_{RM} cell subtype, further strengthening the point that EBI2 expression marks $T_{RM}1$ cells in human psoriatic skin.

3.8. EBI2 expression is a ubiquitous feature of human T_{RM} cells in multiple peripheral organs.

I discovered EBI2 expression on T_{RM} cells and established this as a core feature of mouse and human T_{RM} cells in health and disease. The question of whether EBI2 expression is a ubiquitous feature of T_{RM} cells in all organs or only confined to the skin microenvironment, however, remains unanswered.

A connection between the EBI2-oxysterol axis and the lung was already made upon discovery of EBI2 in the original article, describing the expression of large amounts of the *Gpr183* gene in lung[113]. Furthermore, 25 years later, EBI2 was connected to several lung disease pathologies, like COPD[160] and Covid-19[162,216]. Following up on this, I reached out to Tonia Bargmann from the Fraunhofer Institute for Toxicology and Experimental Medicine (ITEM) for collaboration. She investigated EBI2 expression on lung T_{RM} cells of PCLS (precision-cut lung slices) from tumor-free lung tissue obtained from resected tumor-burdened lungs. Coordination, reagent provision, scientific strategy, and flow cytometric analysis were done by me.

Strikingly, human T_{RM} cells in tumor-free lung tissue uniformly expressed EBI2 (Figure 35 A, B). This was true for both lineages, CD4$^+$ and CD8$^+$. However, in contrast to the skin, lung T_{RM} cell subsets based on the expression of CD103 and CD49a did not differ in EBI2 expression (Figure 35 C, D). Interestingly, Kumar *et al*. established a core T_{RM} cell transcriptional signature in their study from 2017[56]. Among other techniques, they sequenced lung and spleen (periphery and circulation) CD69$^+$ vs CD69$^-$ T cells, with CD69$^+$ T cells representing T_{RM} cells in the lung and activated T cells in the spleen. This approach identified EBI2 to be significantly upregulated in CD8$^+$ T_{RM} cells, compared to CD69$^-$ cells (Figure 35 E). Interestingly, no significant changes in EBI2 expression were observed for CD8$^+$ T cells in the spleen nor for CD4$^+$ T cells in either lung or spleen. This highlights the role of EBI2 on CD8$^+$ T_{RM} cells and is in line with my findings that especially CD8$^+$ T cells upregulate EBI2 during T_{RM} cell differentiation. However, analyzing this aspect on the protein level showed small but not statistically significant differences in the frequency of EBI2$^+$ cells (CD8$^+$ CD69$^+$ vs CD69$^-$: p-value 0.78) or in the EBI2 MFI (CD4$^+$ CD69$^+$ vs CD69$^-$: p-value 0.54) thereof in either lineage, leaving no reliable to conclusion left to be drawn at this point.

in cooperation with Tonia Bargmann - Fraunhofer ITEM

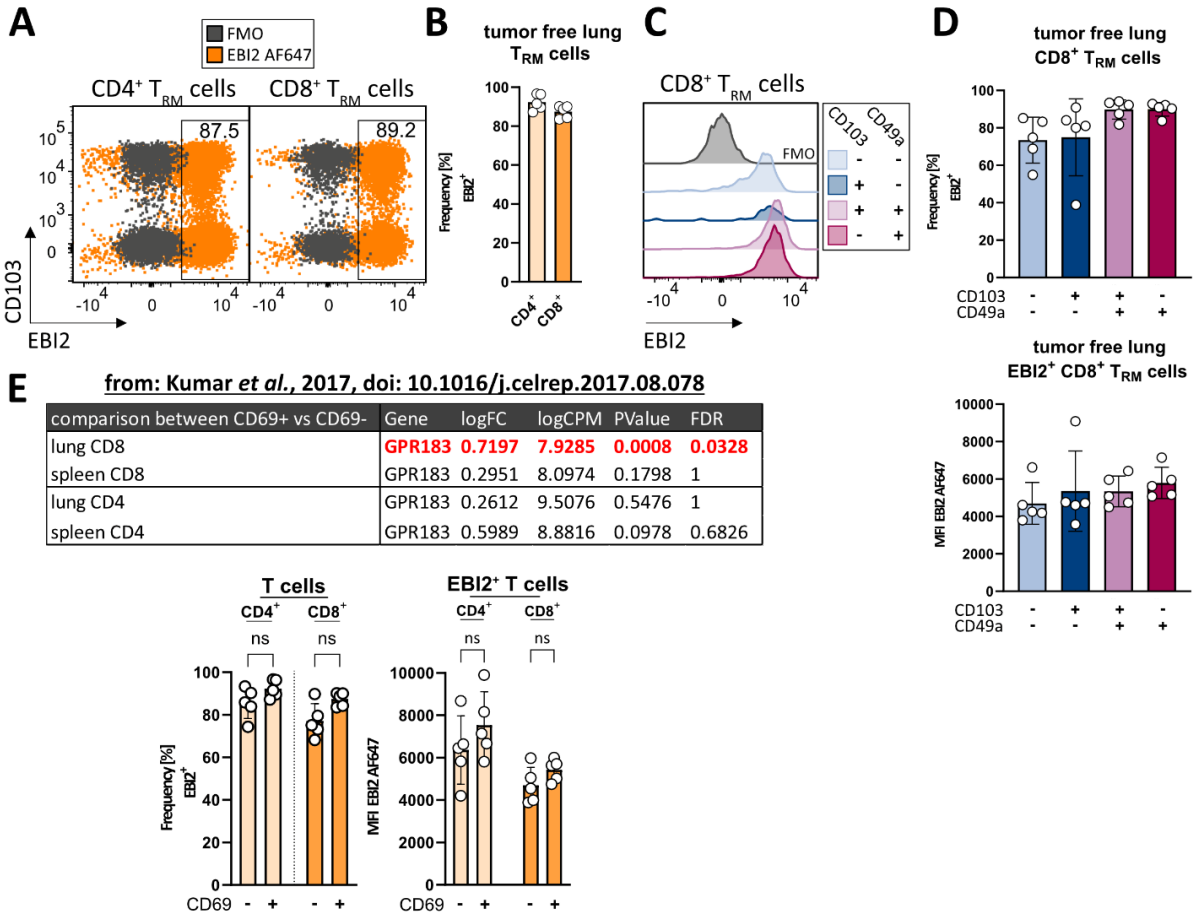

comparison between CD69+ vs CD69-	Gene	logFC	logCPM	PValue	FDR
lung CD8	**GPR183**	**0.7197**	**7.9285**	**0.0008**	**0.0328**
spleen CD8	GPR183	0.2951	8.0974	0.1798	1
lung CD4	GPR183	0.2612	9.5076	0.5476	1
spleen CD4	GPR183	0.5989	8.8816	0.0978	0.6826

Figure 35. EBI2 is highly expressed by human lung T_{RM} cells. A-D Flow cytometric analysis of T_{RM} cells from PCLS (precision-cut lung slices). Preparation of tumor-free lung tissue, isolation of single-cell suspension and antibody staining, and flow cytometric acquisition were performed by Tonia Bargmann from the Fraunhofer ITEM in Hannover, Germany. **A** Dot plot overlay of EBI2 FMO and full stain from a representative donor. Gates set on the full stain sample indicate the EBI2-positive fraction. **B** Bar plots quantifying the frequency of $EBI2^+$ T_{RM} cells of the indicated T cell populations (n = 5) with bars indicating the mean ± SD and dots representing individual donors. **C-D** Analysis of EBI2 expression on T_{RM} cell subsets defined by CD103 and CD49a expression. **C** EBI2 histogram overlays of EBI2 FMO (grey) and full-stain lung T_{RM} cell subsets. **D** Bar plots showing the frequency of $EBI2^+$ T_{RM} cells (top) and EBI2 MFI thereof of the indicated T_{RM} cell subsets, with bars representing the mean ± SD and dots representing individual donors. **E** Table rows were extracted from supplemental material from Kumar *et al*. (doi: 10.1016/j.celrep.2017.08.078). In this study by Kumar *et al*., circulatory (CD69-) and tissue-resident memory T cells (CD69+) from matched lung and spleen of deceased organ donors (n = 3) were compared by bulk RNA-sequencing. Cells were isolated from tissues and sorted as $CD4^+$ or $CD8^+$ T_{EM} cells ($CD3^+CD45RA^-CCR7^-$). The table shown depicts values from differential gene expression analysis of indicated comparisons. Highlighted in red: FDR < 0.05. Bar plots (bottom) show flow cytometric analysis of the T cells from PCLS again. Shown is the frequency of $EBI2^+$ T cells comparing $CD69^-$ and $CD69^+$ and the MFI thereof, with bars representing the mean ± SD and dots representing individual donors. Paired student's t-test. logFC: log2 fold-change, logCPM: log counts per million, FDR: false discovery rate. ns: not significant.

The EBI2-oxysterol axis has also been linked to the pathology of inflammatory bowel diseases colitis and Crohn's disease[171,172] and a gain of function SNP in the *GPR183* gene was even associated with an increased onset of IBD and psoriasis in IBD patients[172]. Because of this highly interesting connection, I established another cooperation with Valerie Beneke and Klaudia Grieger, also from the Fraunhofer ITEM in Hannover, Germany. Coordination, reagent provision, scientific strategy, and flow cytometric analysis were done by me.

in cooperation with Tonia Bargmann, Valerie Beneke and Klaudia Maria Grieger - Fraunhofer ITEM

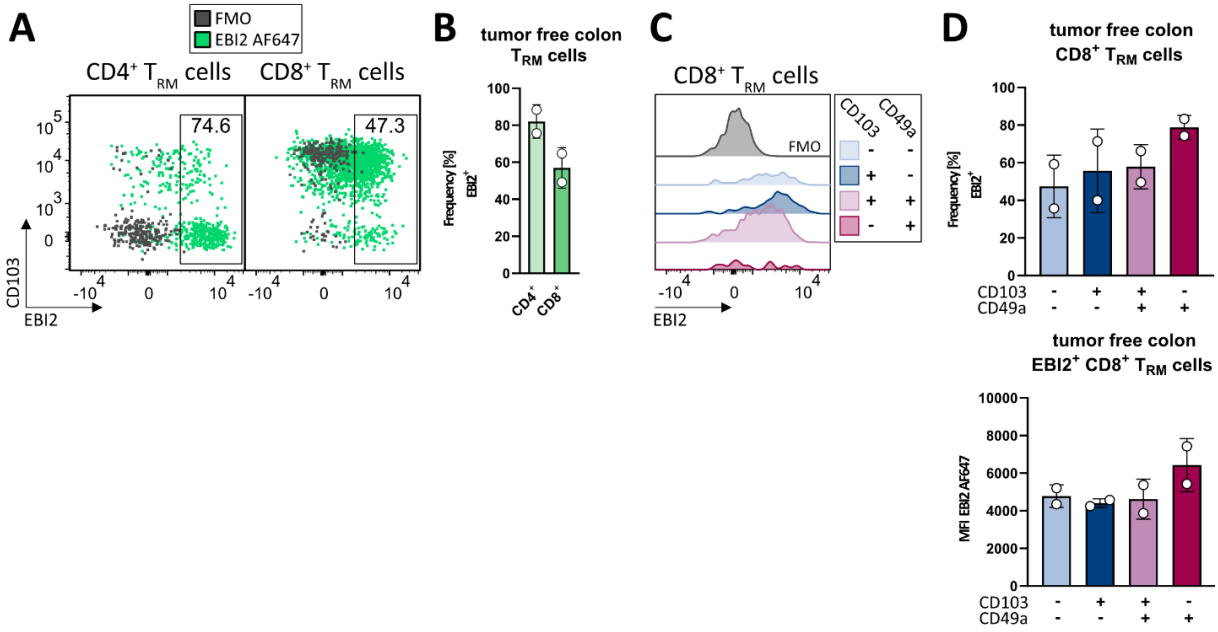

Figure 36. EBI2 is expressed by human colon T_{RM} cells. A-D Flow cytometric analysis of T_{RM} cells from tumor-free human colon. Preparation of tumor-free colon tissue, isolation of single-cell suspension and antibody staining, and flow cytometric acquisition were performed by Valerie Beneke and Klaudia Grieger from the Fraunhofer ITEM in Hannover, Germany. **A** Dot plot overlay of EBI2 FMO and full stain from a representative donor. **B** Bar plot quantifying the frequency of $EBI2^+$ T_{RM} cells of the indicated T cell populations (n = 2), with bars representing the mean ± SD and dots representing individual donors. **C-D** Analysis of EBI2 expression on T_{RM} cell subsets defined by CD103 and CD49a expression. **C** EBI2 histogram overlays of EBI2 FMO (grey) and full-stain lung T_{RM} cell subsets. **D** Bar plots showing the frequency of $EBI2^+$ T_{RM} cells (top) and EBI2 MFI thereof of the indicated T_{RM} cell subsets, with bars representing the mean ± SD and dots representing individual donors.

Interestingly, flow cytometric analysis of T_{RM} cells of human tumor-free colon posed a different pattern of EBI2 expression as the lung and the skin T_{RM} cells. While lung T_{RM} cells expressed EBI2 uniformly ($CD4^+$ and $CD8^+$ T_{RM} cells), only about 60 % of $CD8^+$ colon T_{RM} cells were positive for EBI2 (Figure 36 A, B). About 80 % of colon $CD4^+$ T_{RM} cells expressed EBI2. This showed that EBI2 expression was also a feature of human colon T_{RM} cells and therefore detectable in all investigated human tissues. However, colon T_{RM} cells are the first instance, where EBI2 expression appears to be differently regulated between $CD4^+$ and $CD8^+$ T_{RM} cells. However, these results can only be interpreted as preliminary ones, since only two donors

could be observed. Similar to the lung but again different from the skin, T_{RM} cell subsets defined by CD103 and CD49a expression did not show differentially regulated EBI2 expression. This phenomenon therefore seems to be confined to the skin; however, other organs need to be investigated for this matter (Figure 36 C, D).

A direct comparison of EBI2 expression between the different organs needs to be done carefully due to the use of different flow cytometers, different staining panels, and different methods of cell isolation. However, comparing the EBI2 expression in all investigated human organs (Figure 37), it became apparent that EBI2 expression is under fine regulation and there are considerable differences between the $CD4^+$ and the $CD8^+$ lineage, between the circulation (blood) and the periphery, in-between the peripheral organs (i.e. T_{RM} cells of different tissue origins) and between healthy and diseased skin.

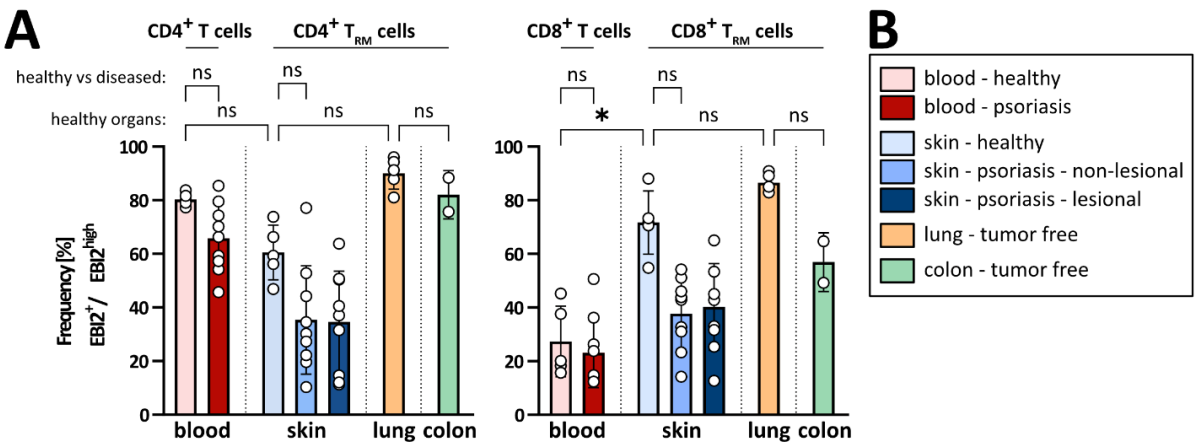

Figure 37. Comparison of EBI2 expression of human circulatory and T_{RM} cells of different peripheral organs and health states. A-B Flow cytometric analysis of EBI2 expression as described previously. Blood was collected from healthy volunteers (n = 5) and psoriasis patients (n = 9). Skin samples were derived from healthy full skin (n = 5) and psoriasis patient 6 mm punch biopsies of non-lesional and lesional skin (n = 9 each). Lung samples were derived from PCLS (precision-cut lung slices) from resected tumor-burdened lungs from tumor-free areas and prepared by Tonia Bargmann from the Fraunhofer ITEM in Hannover, Germany (n = 5). Colon samples were derived from resected tumor-burdened colons from tumor-free areas and prepared by Valerie Beneke and Klaudia Grieger from the Fraunhofer ITEM in Hannover, Germany (n = 2). Bars represent the mean ± SD and dots represent individual donors. Kruskal-Wallis test with Dunn's correction for multiple testing. ns: not significant, * $p < 0.05$.

Due to a large standard deviation, the EBI2 expression in circulating $CD4^+$ T cells between healthy volunteers (mean = 80.3 %) and psoriasis patients (mean = 65.8 %) was not significantly different, however, a strong trend was observed, that EBI2 expression was lower in the blood of psoriasis patients. In contrast, EBI2 expression of $CD8^+$ T cells in the blood of healthy volunteers (mean = 27.3 %) and psoriasis patients (mean = 23 %) was comparable. As described previously comparing circulating T cells with peripheral T_{RM} cells, a large discrepancy was observed in the $CD8^+$ lineage (mean = 23 % vs 71.6 %). EBI2 expression by T_{RM} cells of

different healthy tissue origins was apparent for $CD4^+$ and $CD8^+$ cells, but their magnitude differed and was highest in healthy lung tissue in both lineages (mean $CD4^+$ = 90 %, mean $CD8^+$ = 86.5 %). Healthy colon $CD4^+$ T_{RM} cells expressed EBI2 comparable to their lung counterpart (mean = 82 %), while $CD8^+$ T_{RM} cells expressed drastically lower amounts of EBI2 in the colon (mean = 56.9 %) compared to the lung. EBI2 expression in psoriatic skin was comparable between non-lesional and lesional skin, but always lower compared to healthy skin (mean $CD4^+$ non-lesional = 35.5 %, lesional = 34.6 %, mean $CD8^+$ non-lesional = 37.7 %, lesional = 40.2 %).

In conclusion, I defined EBI2 expression as a novel core feature of human T_{RM} cells in the skin, lungs, and colon. These tissues are characterized by fundamentally different interactions with the environment in terms of mechanical stress, air contact, mucus presence, bacterial load, and many more. Likely because of these fundamentally different properties of the tissues, EBI2 expression is also differentially regulated and the T_{RM} cells with the highest EBI2 expression reside in the lung. Interestingly, non-lesional and lesional skin of psoriasis patients displayed the lowest amount of $EBI2^{high}$ T_{RM} cells compared to all other peripheral organs investigated, which could be connected to the disease nature, but needs to be investigated in more detail.

4. Discussion

The aim of my thesis was to elucidate the role of EBI2 in inflammatory skin diseases. Bioinformatical expression analysis of EBI2 and the cholesterol converting enzymes showed that lesions of inflammatory human skin diseases such as psoriasis and AD are associated with expression of these proteins. However, while I confirmed that EBI2-deficient mice are impaired in $CD4^+$ T cell and B cell priming after TNCB sensitization, I did not observe an impact of EBI2 deficiency on the exacerbation of the TNCB-induced CHS or on the IMQ-induced psoriasis-like dermatitis model. Nevertheless, I discovered that EBI2 expression is strongly associated with T cells residing in peripheral tissues, i.e., T_{RM} cells. Moreover, I found that EBI2 expression is induced in T_{RM} cell precursor cells upon differentiation into T_{RM} cells in the skin and that this expression is a universal feature of not only murine but also human T_{RM} cells. In addition to skin, collaboration partners found that human T_{RM} cells from lung and colon also express EBI2. Utilizing high parameter flow cytometry, I showed that EBI2 expressing-T_{RM} cells are present in the skin of psoriasis patients and that high EBI2 expression levels are associated with a pro-inflammatory $T_{RM}1$ phenotype. My data therefore established EBI2 as a prominent feature of T_{RM} cells and suggests a functional relevance thereof. Despite a lack of impact of EBI2 deficiency on the investigated animal models, this supports an involvement of EBI2 in inflammatory skin diseases.

4.1. Regulation of EBI2 expression is an intricate part of T cell biology.

I discovered that EBI2 is highly expressed on T_{RM} cells, which are terminally differentiated T cells (Figure 19). This allowed to characterize the EBI2 expression of mature T cells of all known major differentiation stages (Figure 26), flowing the linear differentiation model (Figure 1). There was a drastic discrepancy in EBI2 expression between $CD4^+$ and $CD8^+$ T_N cells, which was not apparent for the following differentiation stages, and EBI2 was even shown to be differentially expressed between the two lineages[150]. However, $CD4^+$ and $CD8^+$ T cells converged in terms of EBI2 expression in all memory subsets. This demonstrates that differential EBI2 expression at the T_N cell stage is important for efficient LN organization. $CD4^+$ T cells were shown to regulate EBI2 expression in response to TCR-mediated activation[120,151]. They upregulate EBI2 12 h after activation by cognate antigen or anti-CD3 and anti-CD28 stimulation. EBI2 levels remain high until downregulation to base level by 72 h post activation[151].

Differentiated T_{CM} cells express high levels of EBI2, much in contrast to T_{EM} cells (Figure 26). Because trafficking to SLOs is a major hallmark of and restricted to T_{CM} cells in comparison to T_{EM} cells, this could hint towards a need for EBI2 expression of T_{CM} cells in SLOs. However, a role of the EBI2-oxysterol axis T_{CM} cell reactivation in the SLOs has not been investigated. It will be interesting to elucidate this connection, as not only $CD4^+$ but also $CD8^+$ T_{CM} cells are highly positive for EBI2. This should lead to co-localization of both populations in the SLOs during an immune response, which is in contrast to their naïve cell stages and may facilitate

$CD4^+$ T_{CM} cell help for $CD8^+$ T_{CM} cells. On the other hand, T_{EM} cells' blood-confined tropism might eliminate a need for EBI2 expression.

Low EBI2 expression by T_{EM} cells is then followed by upregulation of EBI2 by T_{RM} cells (Figure 26). Furthermore, I found evidence for its upregulation in T_{RM} cell progenitors during differentiation (Figure 21 and Figure 22). T_{RM} cell progenitor cells in the skin expressed EBI2 on the first timepoint of investigation (d2 post challenge). EBI2 was then further upregulated upon T_{RM} cell differentiation over the course of 30 days. Importantly, EBI2 deficiency did not impair T_{RM} cell generation or their subset distribution (Figure 18). This was evaluated by analysis of healed murine skin, 30 days post challenge. These results therefore exclude a contribution of the EBI2-oxysterol axis to T_{RM} cell development and retention in the skin of TNCB-challenged mice. However, my data does not exclude a functional relevance of EBI2 expression by T_{RM} cells in host defense or pathologies.

The differential expression of EBI2 in different T cell stages (Figure 26) and different tissues (Figure 37) raises an important question as to which signals drive its expression. While it was already discussed that BCR and TCR stimulation upregulate EBI2 *in vivo* and *in vitro*[151], it is less well-studied what influences different cytokine milieus and other tissue factors have on EBI2 expression. Increasing extent of antigen interaction, which drives the memory T cell progression in the linear model (Figure 1), however, does not lead to increasing expression of EBI2. In fact, reactivation of EBI2-high expressing T_{CM} cells is followed by low EBI2 expression in T_{EM} cells (Figure 26). Wanke with Kurschus and colleagues showed that the presence of the EBI2 ligand 7α,25-OHC did not affect the *in vitro* generation of either of the subsets[120]. In line with this, the authors also observed that EBI2 deficiency did not alter the generation of T_H1, T_H17, or T_{reg} cells *in vitro* and *in vivo*. This is in line with my results that show no impact of EBI2 deficiency on T_{RM} cell generation and their subset distribution *in vivo* (Figure 18). Moreover, it shows that, although EBI2 expression is tightly regulated in T cells, it is not required for memory T cell differentiation after priming was initiated. Wanke *et al*. also showed that EBI2 expression was reduced in *in vitro*-differentiated T_{reg} cells in the presence vs absence of IL-2[120]. This represents evidence that cytokines can be involved in the regulation of EBI2 expression by T cells. Other inflammatory mediators might also modulate its expression, since EBI2 is significantly induced in T_{EM} cells upon tissue entry and upon differentiation towards T_{RM} cells, which typically follows infection or flare ups of chronic diseases (Figure 21). Inflammation is generally accompanied by a drastic shift in the cytokine and inflammatory mediator milieu, which could induce changes in EBI2 expression[116]. However, the signals that modulate peripheral EBI2 expression remain to be elucidated and targeting them could have therapeutical potential.

EBI2 expression is tightly regulated at different stages of the B cell (section 1.6.1) and T cell response (section 1.6.3, Figure 26). Similarly, the expression of the 7α,25-OHC-synthetizing enzymes CH25H and CYP7B1 is drastically elevated in the spleen when mice are injected with LPS[116]. This shows that the regulation of EBI2 and its ligand-producing enzymes is deeply implemented in the orchestration of the immune response against pathogens. Altogether, the

present data demonstrates that B- and T cells rely on EBI2 expression for efficient priming, and suggest a role in many other aspects of their biology and during an immune response. The physiological role of the EBI2-oxysterol axis described in SLOs highlights the need for tight regulation. Hence, disturbances of the EBI2-oxysterol axis are associated with many disease pathologies[120,149,154,159,162,169,171,172,217].

4.2. EBI2 expression is a feature of T_{RM} cells conserved across species and organs.

By analysis of the naïve and immunized skin of mice, I found that EBI2 is ubiquitously expressed on T_{RM} cells (Figure 19). Already KLRG1$^-$CD127$^+$ T_{RM} cell progenitors express EBI2 (Figure 22) and upregulated it during their differentiation to T_{RM} cells over the course of 30 days (Figure 21). The fact that EBI2 is expressed on nearly 100 % of CD4$^+$ and CD8$^+$ murine T_{RM} cells and that their circulating progenitors (T_{EM} cells) express EBI2 at a much lower frequency, makes this especially intriguing. This ubiquitous and rather extreme upregulation of EBI2 makes it tempting to speculate that EBI2 could be a fundamental part of the biology of T_{RM} cells of the skin.

In any case, I found EBI2 expression to be a feature of T_{RM} cells in the skin. Its ubiquitous expression qualifies EBI2 as a marker for T_{RM} cells. More specifically, I observed that the differentiation progress of T_{RM} cell progenitors was reflected in their EBI2 MFI. Therefore, I propose that EBI2 expression could even be used as a marker to identify T_{RM} cell progenitors and their status of differentiation. Used in flow cytometry, a comparison of the EBI2 MFI of single cells that are part of a mixture (tissue) could even identify recently established T_{RM} cells vs long resident ones. I was able to show this in mouse skin during the resolution of the CHS reaction (Figure 20). With this, it could be possible to identify T_{RM} cells that are relevant for disease progression. Recently infiltrated T_{RM} cell progenitors in inflamed tissue, like in inflammatory skin diseases (e.g. psoriasis), are likely to have been specifically recruited in the context of the inflammation and therefore be antigen-specific. These would express EBI2 on a lower level compared to established T_{RM} cells in the same tissue and location.

It is unknown which signals induce EBI2 expression in skin infiltrating T_{RM} cell progenitors. The infiltration of T cells into a peripheral tissue from the blood (e.g. in the context of an infection) poses a considerable change in the microenvironment of a T cell that can lead to the induction of many molecular changes (such as tissue-residency programs). Cells adapt to their current microenvironment by sensing it and responding to these signals by adjusting gene- and consequently protein expression. One of many examples of how (tissue) microenvironment shapes a cell was published in 2019. The study by Matthias *et al*. showed how high salt concentrations in the skin shaped the development of T cell memory[218]. Especially human atopic skin presented with the highest salt concentration, which ultimately induced a type 2 phenotype of memory T cells that contributed to pathological events. Another constituent of the tissue microenvironment are cytokines. IL-7, IL-15 and TGF-β have been shown to have a

major influence on T cells and to induce tissue-residency programs, as introduced before in section 1.3. Bioinformatic analysis could answer the question of whether EBI2 is upregulated as part of residency programs initiated through these cytokines. It is possible to predict binding sites in the EBI2 gene and its regulatory elements of transcription factors that are part of the signaling cascade downstream of IL-7, IL-15, and TGF-β[219].

Whether the regulation of EBI2 expression underlies similar mechanisms in humans and mice is an unaddressed question. My results suggest analogous regulatory means. I observed a similar expression pattern during T cell differentiation in mouse and human (Figure 26). EBI2 expression appears to be a generalized feature of T_{RM} cells and to be conserved across species, at least among humans and mice. This evolutionarily conserved feature further suggests a functional role of EBI2 on T_{RM} cells. This is supported by the expression of EBI2 on human T_{RM} cells, not only in the skin but also in the lungs (Figure 35) and colon (Figure 36). These findings have important implications because they show that EBI2 expression is not confined to skin T_{RM} cells, where I had originally discovered it. Moreover, it seems to be a universal feature of T_{RM} cells in potentially all tissues, which raises even more questions. Are the signals that induce EBI2 expression on T_{RM} cells the same across the different tissues? Furthermore, the proportions of EBI2 expressing T_{RM} cells slightly vary between skin, lung, and colon. And while this needs to be interpreted with caution, due to the measurements being done on different flow cytometers, and with different tissue preparation methods and staining panels, it still raises even more interesting questions that need to be addressed. For example, it will be interesting to investigate whether different signals in the respective organs drive EBI2 expression and whether these are equally potent in inducing EBI2. If the same agent or agents regulate EBI2 expression in the different organs, it would furthermore be interesting to elucidate whether they are present in different quantities in each organ. Perhaps the most important question to address would be whether such differential expression of EBI2 by T_{RM} cells in different organs also reflects a different biological function of the EBI2-oxysterol axis in the respective tissues. As seen in LNs, regulation of EBI2 expression spatially distributes $CD4^+$ and $CD8^+$ T_N cells which optimizes priming for both populations. Regulation of EBI2 expression in peripheral tissues could therefore be a means of spatially distributing cells into different niches.

4.3. Different EBI2 expression levels are associated with different functional properties of peripheral T cells.

The importance of the tight regulation of EBI2 expression during T cell differentiation was discussed in section 4.1. However, I found evidence that EBI2 expression levels of rather terminally differentiated T_{RM} cells are associated with certain phenotypical characteristics. By performing high-parameter flow cytometry on T_{RM} cells from the skin of psoriasis patients, I discovered that those T_{RM} cells with high EBI2 expression were associated with a pro-inflammatory $T_{RM}1$ phenotype, marked by expression of IFN-γ, granzyme B, and Ki-67. Cheuk *et al*. presented similar findings in their study, where they found EBI2 upregulated in

$CD103^+CD49a^+$ T_{RM} cells in the skin. This population was furthermore shown to preferentially produce granzyme B and the authors characterized them as $T_{RM}1$ cells. In contrast, low EBI2 expression was a feature of $CD103^+CD49a^-$ $T_{RM}17$ cells in the skin, which produced IL-17. However, despite being among the top differentially expressed genes between the two subsets the authors did not further discuss EBI2 in their study. I found strong trends, but no statistically significant evidence of the presence of these two T_{RM} cell populations in my data (Figure 34). Moreover, in the study by Cheuk *et al*., the authors found $T_{RM}1$ cells to be enriched in vitiligo lesions (a type 1 immune-mediated disease) and $T_{RM}17$ cells to be enriched in psoriasis skin (a type 17 immune-mediated disease). This poses the question of whether EBI2 could be involved in the pathogenesis of vitiligo or other type 1-mediated dermatopathies. However, no vitiligo patients partook in my study and I was therefore unable to address this question.

Table 14. Query results for *GPR183* in differential gene expression analysis from Park *et al*., 2023. Average fold-change was calculated from the provided average $\log_2$ fold-change with the formula: fold-change = $2^{(\log2 \text{ fold-change})}$. T_{CIRCM}: circulatory memory T cells, avg.: average, adj.: adjusted.

compared $CD8^+$ T cell populations	adj. p-value	avg. $\log_2$ fold-change	avg. fold-change
skin $T_{RM}1$ vs skin $T_{RM}17$	1	0.019045	1.0133
skin $T_{RM}1$ vs T_{CIRCM}	**1.93×10^{-177}**	**0.554108**	**1.4683**
skin $T_{RM}17$ vs T_{CIRCM}	**1.59×10^{-72}**	**0.532343**	**1.4463**
skin $T_{RM}1$ WT vs Hobit KO	1	0.013090	1.0091
skin $T_{RM}17$ WT vs c-Maf KO	1	0.150613	1.1100

I found that IL-10 production is also associated with a high EBI2 expression in skin T_{RM} cells of psoriasis patients (Figure 33). This further supports an association of high EBI2 expression with a type 1 phenotype of T_{RM} cells, as IL-10 production is a known feature of T_H1 cells[214,215]. Very recently, a study by Park *et al*. was published, where they characterized $CD8^+$ $T_{RM}1$ and $T_{RM}17$ cells[82]. Through transcriptome sequencing and experimental validation, they found that the transcription factor Hobit was controlling the $T_{RM}1$ cell residency program and that the transcription factor c-Maf induced residency in $T_{RM}17$ cells. They also found EBI2 to be highly significantly upregulated when comparing both populations with circulating T cells (Table 14), further manifesting EBI2 expression to be a feature of specifically tissue-resident rather than circulating $CD8^+$ T cells. Of note, EBI2 was not differentially expressed when comparing $T_{RM}1$ with $T_{RM}17$ cells, or when comparing the respective WT with Hobit or c-Maf KO T_{RM} cells. It can be deduced from this, that EBI2 expression is not under control of either Hobit or c-Maf. In line with this, I did not observe an enrichment of IL-17A-producing cells in the $EBI2^{low}$ T_{RM} cell population. Moreover, this challenges the suspected association of high EBI2 expression and bona fide $T_{RM}1$ cells. However, the average $\log_2$ fold change observed by Park *et al*. of EBI2 mRNA expression between T_{RM} cells and circulating T cells was slightly higher for $T_{RM}1$ than for $T_{RM}17$ cells (Table 14)[82]. Whether this small difference in mRNA expression

would lead to a difference in expression of the protein, detectable by flow cytometry is unknown.

Furthermore, as discussed previously, Ruiz *et al*. found that a mutation in the EBI2 gene, which led to increased surface expression, was associated with an increased rate of psoriasis onset in an IBD cohort[172]. Two GWAS had already identified the same mutation in the EBI2 gene and a mutation in the CH25H gene to be linked to an increased risk of developing IBD[170,169]. These studies represent direct links between the EBI2 expression level and disturbances in the regulation of its expression to be a risk factor for inflammatory diseases mediated by T cells.

Another study, that found EBI2 expression to be associated with a particular T cell phenotype, was recently published by Meng *et al*. The authors discovered transcriptomic signatures of pancreas cancer TILs that enabled them to reliably identify pancreas carcinoma-reactive TILs and bystander TILs (not reactive against the pancreas carcinoma)[178]. Among other genes, they identified high EBI2 expression to be a hallmark feature of bystander TILs. This raises the question of whether high EBI2 expression would be linked to a worse outcome in cancer scenarios. However, this has not been investigated yet.

In conclusion, there exists profound experimental evidence that EBI2 expression is associated with different functional properties of T cells. In general, high EBI2 expression was associated with an increased risk for inflammatory disease development, with non-tumor-reactive T cells and with T_{RM} cells that preferentially produce granzyme B in vitiligo lesions. In addition, I found high EBI2 expression to correlate with a $T_{RM}1$ cell phenotype in psoriatic skin. This clearly demonstrates the potential of addressing the EBI2-oxysterol axis as a target for new therapeutical strategies.

However, it needs to be considered that almost all patients included in my study were under topical immunomodulatory drug treatment and that these treatments likely had an impact on the T cell phenotype in the treated (lesional) skin. Therefore, these results need to be clearly stated to be associated with topically treated and not with treatment-naïve psoriatic skin. However, as topical immunomodulatory drugs are the first line of treatment, which is also reflected in the number of patients enrolled in the study that received them, my results are still clinically valid and represent the state of the immune system under these common conditions.

The topical treatments were confined to two active ingredients: GCs and a combination of GCs and vitamin D analogs (Figure 27). Two types of GCs were used as active ingredients: betamethasone and clobetasol; both of which are categorized as 'superpotent GCs'[220]. GCs signal via the transcription factor glucocorticoid receptor (GR) and signaling induces the expression of genes with wide immunosuppressive functions, such as IL-1R antagonist, β-adrenergic receptor, and IL-10[220]. Interestingly, the GR was also shown to inhibit NF-κB, which is known to regulate EBI2 expression[136,220]. Therefore, it needs to be considered, that the topical treatment with GCs might have altered EBI2 expression in the lesional skin. This issue needs to be further investigated. Vitamin D3 analogs are used in combination therapy and the

most common combination is calcipotriol-betamethasone dipropionate, which was also what the patients enrolled in the study received[220–222]. These GC and the vitamin D3 analog showed additive inhibitory effects in murine and human studies. In human psoriasis biopsies, the combination therapy inhibited *ex vivo* keratinocyte proliferation, secretion of IL-17A and TNF-α by T cells and of IL-23 and TNF-α by DCs and enhanced IL-10 production by T cells[221,222]. Altogether, the topical therapies are assumed to have modulated the effector function of T cells in the lesional skin biopsies of the patients in my study, specifically, enhanced IL-10 production and reduced IL-17A and IL-23 production could be the result of it.

4.4. Proposed functions of the EBI2-oxysterol axis in peripheral inflammation.

Despite its potential use as a T_{RM} cell marker, no functional contribution of EBI2 expression by T_{RM} cells is known yet. Importantly, I did not find an impact of EBI2 deficiency on the quantity, quality (expression of CD103 and CD49a), or function (as investigated by the memory CHS model) of murine skin T_{RM} cells. Therefore, it needs to be taken into consideration that EBI2 could be a sort of 'bystander gene', i.e. EBI2 is upregulated as part of a larger genetic program but has no actual relevance. NF-κB, whose induction also induces EBI2 gene expression[136], controls many more target genes[223]. Next to EBI2, this includes anti-apoptotic factors, adhesion molecules, chemokines, cell cycle regulators, cell fate modulators, and a wide range of different pro-inflammatory cytokines[223]. Induction of e.g. NF-κB in T_{RM} cell progenitors could therefore lead to the upregulation of EBI2 but would serve different purposes.

I did not observe differences in terms of EBI2 expression in psoriatic non-lesional vs lesional skin. Therefore, I did not find a direct indication that dysregulation of the EBI2-oxysterol axis would be involved in psoriasis lesion exacerbation and psoriasis pathogenesis. However, more targeted investigations are needed to answer this question. Moreover, non-lesional psoriatic skin shares considerable similarities with lesional skin and dissimilarities with healthy skin. In a mouse model of psoriasis, engraftment of non-lesional skin from human psoriasis patients was sufficient to elicit a psoriatic phenotype in those mice[173]. Moreover, the epidermis of non-lesional skin from human psoriasis patients is enriched in IL-17 and IFN-γ producing T_{RM} cells, compared to healthy skin[224]. Therefore, a comparison of EBI2 expression between non-lesional and lesional psoriatic skin might not be suitable to elucidate whether the EBI2-oxysterol axis is involved in disease pathogenesis. A more detailed characterization of the EBI2-oxysterol axis in lesional, non-lesional, healthy skin is needed to answer this question.

Still, there exist clear indications for a role of EBI2 in the pathogenesis of psoriasis. Genetically caused heightened EBI2 expression on peripheral T cells was shown to be associated with psoriasis onset in an IBD cohort[172], and EBI2 deficiency led to a weaker exacerbation of the IMQ-induced psoriasis-like dermatitis model in mice[154]. In line with this, I found that the transcripts of *GPR183* and *CYP7B1* are upregulated in lesional vs non-lesional skin of psoriatic patients (Figure 9). However, in my hands, EBI2 deficiency had no impact on either the IMQ-

induced psoriasis-like dermatitis model (section 3.2.3) or on the CHS model in different variations (section 3.2.2). Julius Schwingen, from my group, showed a significant upregulation of CH25H early after treating mouse ear skin with TNCB. Other supporting data from my group show that treating mouse skin-derived fibroblasts with combinations of proinflammatory cytokines (IL-17A/F, IFN-γ, and TNF-α) induces the upregulation of CH25H and CYP7B1 mRNA (data not shown). It is therefore likely that fibroblasts react to the induction of an inflammation and that they are at least partially responsible for the rapid upregulation of CH25H in the skin. However, it remains to be investigated whether and which other cell types are also capable of doing so. Recently, Frascoli *et al*. showed supporting data for basal keratinocytes to be important CH25H expressing cells in inflammation[154]. This and EBI2 expression by skin T_{RM} cells clearly demonstrate that the EBI2-oxysterol axis is present in the skin and is induced at the beginning of the inflammatory response. Additionally, since CH25H was among the highest upregulated genes in lesional vs non-lesional AD skin (Figure 9), it will be interesting to investigate whether the EBI2-oxysterol axis contributes to disease pathogenesis in the skin of AD patients and mechanistically in mouse models for AD.

When Fibroblasts and/or other cells in the skin upregulate CH25H in response to an inflammatory trigger, 7α,25-OHC is synthesized around them, creating a gradient from the center of the inflammation. Since EBI2-expressing cells can sense this gradient, they should be able to migrate toward the center of the inflammation, thereby either aiding in eliminating the infection or amplifying a pathogenic inflammatory response. Based on this, I propose two models that could explain the role of the EBI2-oxysterol axis in the skin and of EBI2 on T_{RM} cells. Importantly, these models do not exclude each other and both hypothesized mechanisms could occur at the same time or in succession. However, they both propose the EBI2-oxysterol axis as a guiding system for microanatomical localization of immune cells to enhance skin immunity, analogous to what has been shown in the SLOs[122,123], lung[160], and intestine[142].

4.4.1 The peripheral re-activation model.

The first model is the peripheral re-activation model (Figure 38). There, a trigger, such as environmental or endogenous factors (like in autoimmune settings), or an infection, starts an inflammation in the skin. Rapidly responding to it, fibroblasts and potentially other skin cells would upregulate CH25H and CYP7B1 and synthesize 7α,25-OHC. As a result, a 7α,25-OHC gradient would be generated, originating from and with the highest concentration at the origin of the trigger. EBI2-expressing cells like B cells, T cells, and professional APCs would consequently follow the gradient and co-localize, essentially forming TLS. This would lead to a faster and more efficient re-activation of B- and T cells in the periphery and therefore be of advantage in, e.g., fighting off an infection. The model proposes a mechanism similar to the function that was described for the EBI2-oxysterol axis in SLOs, where $CD4^+$ DCs, cDC2s, B cells, and T cells are all guided by chemotactic cues (including the EBI2-oxysterol axis), in order to efficiently co-localize and interact[122,123,144,150]. Also there, injection of LPS induces strong

upregulation of CH25H in murine spleen[116], which suggests that contact with microbiota in the skin would result in a similar induction.

The peripheral reactivation model is supported by a study that investigated a cigarette-smoke-induced model of COPD in mice[160]. The authors describe TLS, called iBALT, in the lungs of COPD-affected mice that were essential for disease progression. Moreover, they found that the EBI2-oxysterol axis was critical for the formation of the iBALT. In line with this, EBI2 or CH25H deficiency resulted in less iBALT and protected the mice from COPD[160]. Such TLS are known to be important for T cell activation in the skin and have been reported by Japanese scientists that observed inducible skin-associated lymphoid tissue (iSALT) formation in inflamed skin[225,226]. Similar structures termed memory lymphocyte clusters (MLCs) were also found in the vaginal mucosa upon herpes simplex virus (HSV) infection and they contained $CD4^+$ T_{RM} cells reactive to HSV[44]. However, no link to the EBI2-oxysterol axis was made in either study. In fact, both TLS were shown to be, at least partially mediated by other chemokine-receptor systems. However, it was not excluded that the EBI2-oxysterol axis could contribute to their formation.

Studies show that, indeed, such TLS form in the skin of CHS mice upon challenge[227]. The authors initially termed them perivascular leukocyte clusters and then introduced the term iSALT. They found that these iSALTs promoted local activation of effector T cells. When the formation of these clusters was inhibited, the CHS reaction was alleviated and IFN-γ production was reduced. Interestingly, the authors found similar clusters of $CD3^+$ T cells and $CD11c^+$ DCs in a patch-test (controlled elicitation of allergic contact dermatitis to test for allergens) skin biopsy of a patient[225,227]. Moreover, they found that M2 macrophages mediated the formation of these clusters[227]. The skin macrophages responded to IL-1α stimulation by producing CXCL2, which attracted CXCR2 expressing DCs. Blocking of either the IL-1R or CXCR2 inhibited the formation of iSALTs in mice. Whether the EBI2-oxysterol axis might at least partially contribute to the formation of these clusters remains to be investigated. Furthermore, the authors did not address the question of how T cells were attracted to these clusters, as CXCR2 expression was mainly attributed to DCs. Different cells could utilize different attractant-receptor systems to form these clusters. Moreover, other forms of antigen or other triggers may induce different forms of these clusters. After all, haptens induce distinct immune responses, which are not fully understood and are different from e.g. infection[226]. Another interesting question that arises is whether professional APCs, such as Langerhans cells and DCs, and macrophages express EBI2 or CH25H. This could give hints as to whether they would be guided to the same place in case of infection or a trigger.

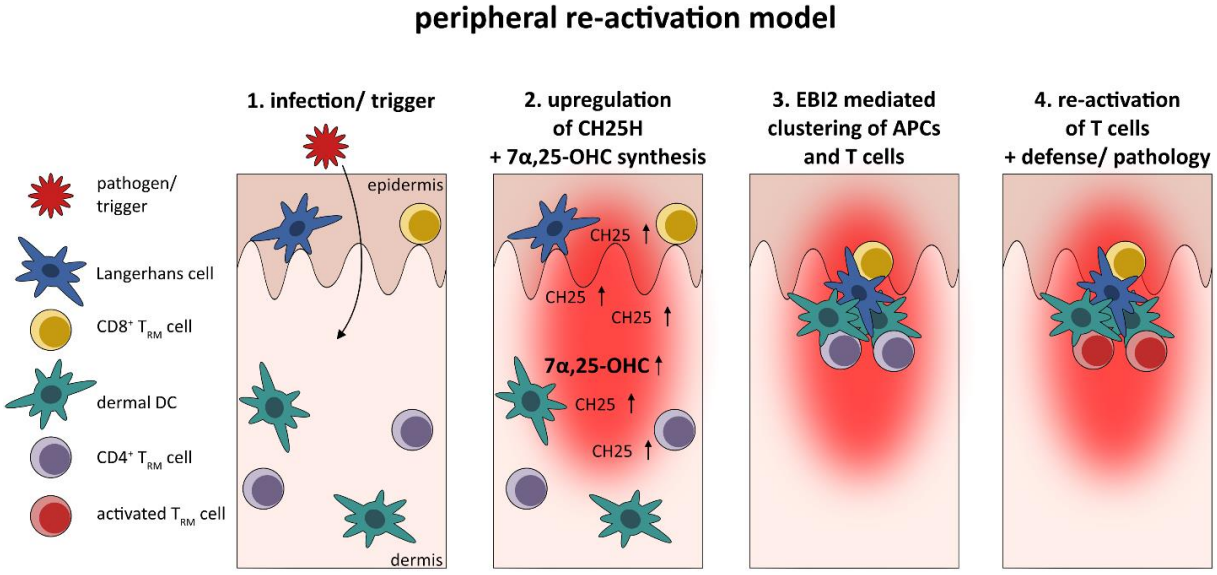

Figure 38. The peripheral activation model. 1. An environmental or endogenous trigger, or an infection starts an inflammation in the skin. 2. Skin cells (fibroblasts and other cells) respond to the infection/ trigger by upregulating CH25H, which leads to the synthesis of 7α,25-OHC and the formation of a gradient thereof, centered around the origin of the infection/ trigger. 3. EBI2-expressing skin cells (T cells, T_{RM} cells, and APCs) sense and follow the gradient and co-localize. 4. Co-localization facilitates efficient peripheral re-activation of skin T cells by APCs, leading to host defense or pathology.

Taken together, the existence of peripheral immune cell clusters is known and their importance in host defense and pathology is acknowledged. However, they show great diversity in their structure and means of attractants. While iSALTs in the skin of CHS mice relied on CXCL2 and CXCR2, the MLCs in the vaginal mucosa, to fight against HSV infection, relied on CCL5, and the iBALT formation in the lungs relied on the EBI2-oxysterol axis. Whether these differences are due to the different organs or to the different types of immune challenges is an interesting point of further investigation. In line with this, it remains to be investigated whether EBI2 might play a role in other skin inflammation models than the TNCB-induced CHS and the IMQ-induced psoriasis-like dermatitis model, e.g. bacterial or viral infection.

4.4.2 The emergency call model.

The peripheral re-activation model (Figure 38) is suited to explain how the EBI2-oxysterol axis might aid T cells in being re-activated in peripheral tissues. Interestingly, contradictory studies were published, claiming that either T_{RM} cell re-activation is dependent on or independent of professional APCs. The study by Low *et al*. described that lung T_{RM} cells do not rely on professional APCs to be re-activated[111]. Rather, T_{RM} cells can even be activated by non-hematopoietic cells. Furthermore, the functional properties acquired by T_{RM} cells after cognate activation differ depending on the type of APC, they encounter their antigen on. Interestingly, the authors did not mention any advantage for T_{RM} cells to encounter their antigen on hematopoietic APCs compared to non-hematopoietic APCs[111]. In contrast, Kamenjarin *et al*. demonstrated that epidermal Langerhans cells were required for $CD8^+$

T_{RM} cell re-activation in the skin[228]. Cross-presentation of keratinocyte-derived viral antigens was necessary to induce TCR triggering in T_{RM} cells. The authors referred to the aforementioned study and mentioned that antigen load (which was limited and restricted to keratinocytes in their setting) might dictate whether professional APCs are necessary for this process.

T_{RM} cells constantly migrate through the skin in a random fashion[40]. They scan the skin to quickly recognize foreign agents and immediately trigger a wide-ranging state of alert in the surrounding tissue[42]. Due to the random patrolling movement that they perform, T_{RM} cells surveil large areas of the tissue, without leaving their general location. The emergency call model (Figure 39) presents a mechanism, in which the EBI2-oxysterol axis is involved in aiding a T_{RM} cell to efficiently encounter an infected cell. Given the rapid upregulation of CH25H in the skin when antigen is applied, this model assumes that CH25H would also be rapidly upregulated in a cell when it becomes infected or senses an infection otherwise. This is supported by the fact that LPS is a potent inducer of CH25H in murine spleen[116].

Upregulation of CH25H upon infection would lead to the synthesis of 7α,25-OHC and the generation of a gradient thereof. EBI2-expressing T_{RM} cells would be able to sense the gradient and change their random patrolling into a directed migration. They would follow the 7α,25-OHC gradient centered around the infected cell, and thereby encounter it more efficiently than in the case of continuous random patrolling. EBI2 expression would therefore confer an advantage to the T_{RM} cells, to find the infecting agent more rapidly and to have a greater chance of containing the infection. This could be investigated in e.g. an HSV skin infection experiment, utilizing the $EBI2^{EGFP/EGFP}$ vs $EBI2^{+/+}$ mice and inducing the infected in a very limited area, preferably in a few cells only. An advantage of $EBI2^{+/+}$ T_{RM} cells over $EBI2^{EGFP/EGFP}$ T_{RM} cells in the defense against this infection would show that EBI2 expression is necessary for T_{RM} cell function. This could explain the upregulation of EBI2 on T_{RM} cell precursors during their differentiation, essentially arming the T_{RM} cells.

The emergency call model, moreover, also holds an explanation as to why EBI2 was dispensable in the IMQ-induced psoriasis-like dermatitis and the CHS model. The emergency call model proposes the EBI2-oxysterol axis as a guiding system for T_{RM} cells, essentially optimizing microanatomical migration. In both skin inflammation models applied, the antigen (TNCB in solvent solution and IMQ in a cream) is applied over a large area of the skin. This leads to a distribution of the antigen and the CH25H triggering agent over the whole area, and T_{RM} cells present at any site of the skin would be able to readily respond to it. High antigen load and ubiquitous availability essentially eliminate the need for optimization of T_{RM} cell migration and consequently for the proposed function of EBI2. An additional possibility is that EBI2 signaling in tissues might confer a rather anti-inflammatory state as was suggested previously[146,147]. A stronger inflammation in murine EBI2 KO tissues in combination with an impaired directed T cell migration might lead to a functional neutralization of effects of the full body knockout in the used models.

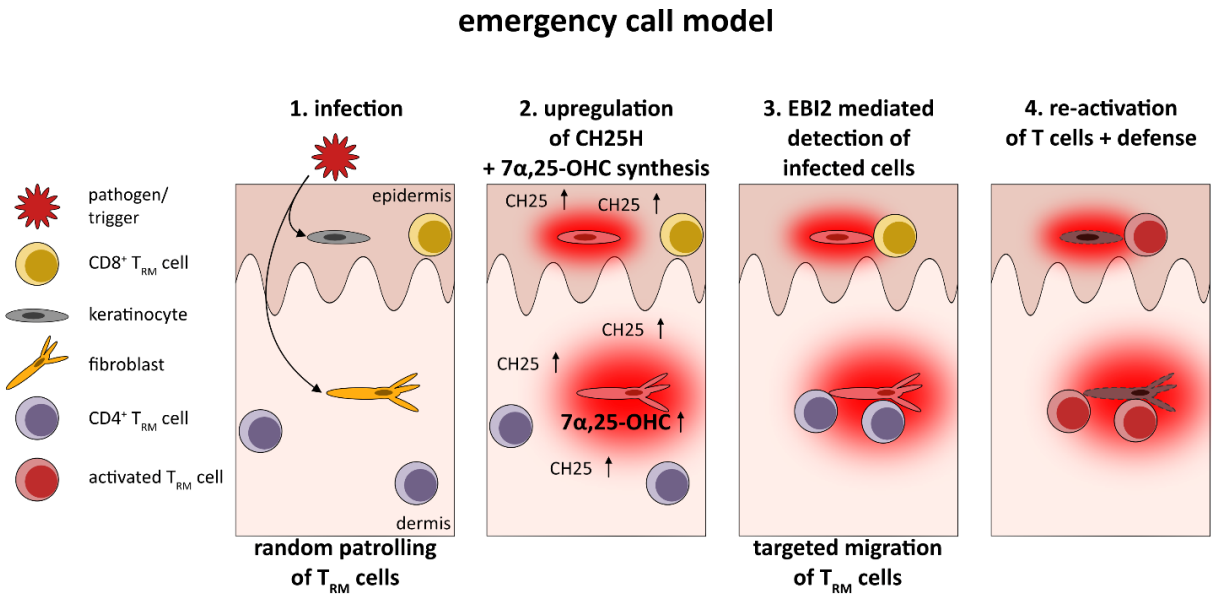

Figure 39. The emergency call model. In steady-state, T_{RM} cells randomly patrol the skin to defend against secondary infections. 1. Skin cells become infected. Keratinocyte and fibroblast are depicted, but any cell capable of expressing CH25H in response to infection could start this cascade. 2. The infected cell or cells upregulate CH25H which leads to the synthesis of 7α,25-OHC and the formation of a gradient thereof, centered around the origin of the infection. Thereby, sending out a metaphorical emergency call. 3. EBI2 expressing T_{RM} cells (and other cells) can sense the gradient and respond to the emergency call by targeted migrating towards the center of the gradient, changing their random patrolling behavior. 4. T_{RM} cells then readily become activated and contribute to host defense.

Of note, my group previously described a tissue recruiting function of EBI2 on T cells. In the study, EBI2-expressing pathogenic T cells showed an advantage over EBI2-deficient T cells to cross the blood-brain barrier and to cause EAE[120]. However, considering a similar mechanism in the skin, I did not observe a reduced infiltration of T cells into the skin in the CHS model (Figure 13). A detailed time course analysis of the very early events (minute to few hours) in the skin during the CHS model might give more insight into this matter, as especially the EAE onset was delayed when EBI2 deficient T cells were transferred compared to EBI2 expressing ones.

In summary, I discovered that EBI2 is a ubiquitous feature of T_{RM} cells. I demonstrated that human and murine $CD4^+$ and $CD8^+$ T_{RM} cells express EBI2 in the skin and that human T_{RM} cells of the lung and colon are also EBI2-positive. While I did not observe indications for a functional role of EBI2 on T_{RM} cells or the general impact in the elicitation of inflammatory skin disease models, I suggest investigating this matter using a different model, based on the proposed function as an emergency guiding system (Figure 39). This model should require potential fine-positioning of T_{RM} cells in the skin. This could involve viral infection models, as viral infection typically affects only a few keratinocytes as a point of entry. In contrast, the two models applied affected large skin areas and might make EBI2-mediated migration obsolete. I also suggest live *in vivo* imaging as a method for detailed analysis of migratory behavior. Co-

transfer of fluorescent EBI2 WT (e.g. tdTomato) and EBI2 KO T cells (e.g. EGFP) into a non-fluorescent WT host would allow the comparison of functional and migrational parameters of the transferred cells in the same microenvironment and the same infection. Moreover, live imaging would allow direct monitoring and comparisons of migrational properties like speed and medium turning angles respective to the origin of infection This experimental approach would be suitable to elucidate whether there exists a functional role of EBI2 on T_{RM} cells in the skin and to characterize it in a clinical setting.

In addition, I found that the EBI2-oxysterol axis is potentially involved in human inflammatory skin diseases. CH25H and CYP7B1 are upregulated in the lesional skin of patients (Figure 9) and $EBI2^{high}$ expressing T_{RM} cells show a pro-inflammatory phenotype by enrichment in granzyme B, IFN-γ, and Ki-67 expressing cells, compared to $EBI2^{low}$ T_{RM} cells (Figure 32). These $T_{RM}1$-like cells clearly showed a phenotype that could potentially contribute to lesion exacerbation; however, this remains to be experimentally proven. To further elucidate the role of EBI2 in inflammatory skin diseases, I suggest also investigating skin diseases other than psoriasis. I found indications, that the EBI2-oxysterol axis could also play a role in AD lesion formation (Figure 9). Lastly, the $T_{RM}1$ subsets of T_{RM} cells were shown to be involved in vitiligo pathogenesis[59]. Investigating the EBI2-oxysterol axis in these two additional diseases and mouse models thereof might provide more insights into the role of EBI2 in inflammatory skin diseases.

5. Ethics Statements

5.1. Animal ethics committee approval

All animal procedures were carried out in accordance with the guidelines and regulations for animal welfare and were approved by the regional administrative authority in Karlsruhe, Germany. All efforts were made to comply with the 3R principle. Approval number: G-1/19 and amendments.

5.2. Human ethics committee approval

Skin biopsies and blood from psoriasis patients were obtained after informed written consent. The study was approved by the Ethics Committee of the Medical Faculty Heidelberg and conducted in accordance with the declaration of Helsinki. Approval number: S-791/2022.

6. Literature References

1. Blanchard, L. & Girard, J.-P. High endothelial venules (HEVs) in immunity, inflammation and cancer. *Angiogenesis* 24, 719–753; 10.1007/s10456-021-09792-8 (2021).
2. Alon, R. *et al.* Leukocyte trafficking to the lungs and beyond: lessons from influenza for COVID-19. *Nature reviews. Immunology* 21, 49–64; 10.1038/s41577-020-00470-2 (2021).
3. Saxena, V. *et al.* Role of lymph node stroma and microenvironment in T cell tolerance. *Immunological reviews* 292, 9–23; 10.1111/imr.12799 (2019).
4. Cyster, J. G. & Allen, C. D. C. B Cell Responses: Cell Interaction Dynamics and Decisions. *Cell* 177, 524–540; 10.1016/j.cell.2019.03.016 (2019).
5. Dustin, M. L. & Depoil, D. New insights into the T cell synapse from single molecule techniques. *Nature reviews. Immunology* 11, 672–684; 10.1038/nri3066 (2011).
6. Cebrián M *et al.* Triggering of T cell proliferation through AIM, an activation inducer molecule expressed on activated human lymphocytes. *Journal of Experimental Medicine,* 1621–1637; 10.1084/jem.168.5.1621 (1988).
7. Shiow, L. R. *et al.* CD69 acts downstream of interferon-alpha/beta to inhibit S1P1 and lymphocyte egress from lymphoid organs. *Nature* 440, 540–544; 10.1038/nature04606 (2006).
8. Farber, D. L., Yudanin, N. A. & Restifo, N. P. Human memory T cells: generation, compartmentalization and homeostasis. *Nature reviews. Immunology* 14, 24–35; 10.1038/nri3567 (2014).
9. Jameson, S. C. & Masopust, D. Understanding Subset Diversity in T Cell Memory. *Immunity* 48, 214–226; 10.1016/j.immuni.2018.02.010 (2018).
10. Kakaradov, B. *et al.* Early transcriptional and epigenetic regulation of CD8+ T cell differentiation revealed by single-cell RNA sequencing. *Nature immunology* 18, 422–432; 10.1038/ni.3688 (2017).
11. Teijaro, J. R. *et al.* Cutting edge: Tissue-retentive lung memory CD4 T cells mediate optimal protection to respiratory virus infection. *Journal of immunology (Baltimore, Md. : 1950)* 187, 5510–5514; 10.4049/jimmunol.1102243 (2011).
12. Künzli, M. & Masopust, D. CD4+ T cell memory. *Nature immunology* 24, 903–914; 10.1038/s41590-023-01510-4 (2023).
13. Schenkel, J. M., Fraser, K. A. & Masopust, D. Cutting edge: resident memory CD8 T cells occupy frontline niches in secondary lymphoid organs. *Journal of immunology (Baltimore, Md. : 1950)* 192, 2961–2964; 10.4049/jimmunol.1400003 (2014).
14. Gattinoni, L., Speiser, D. E., Lichterfeld, M. & Bonini, C. T memory stem cells in health and disease. *Nature medicine* 23, 18–27; 10.1038/nm.4241 (2017).
15. Ahmed, R., Bevan, M. J., Reiner, S. L. & Fearon, D. T. The precursors of memory: models and controversies. *Nature reviews. Immunology* 9, 662–668; 10.1038/nri2619 (2009).
16. Lanzavecchia, A. & Sallusto, F. Progressive differentiation and selection of the fittest in the immune response. *Nature reviews. Immunology* 2, 982–987; 10.1038/nri959 (2002).
17. Mueller, S. N. & Mackay, L. K. Tissue-resident memory T cells: local specialists in immune defence. *Nature reviews. Immunology* 16, 79–89; 10.1038/nri.2015.3 (2016).

18. Sallusto, F., Geginat, J. & Lanzavecchia, A. Central memory and effector memory T cell subsets: function, generation, and maintenance. *Annual review of immunology* 22, 745–763; 10.1146/annurev.immunol.22.012703.104702 (2004).

19. Masopust, D., Vezys, V., Marzo, A. L. & Lefrançois, L. Preferential localization of effector memory cells in nonlymphoid tissue. *Science (New York, N.Y.)* 291, 2413–2417; 10.1126/science.1058867 (2001).

20. Kok, L. *et al.* A committed tissue-resident memory T cell precursor within the circulating CD8+ effector T cell pool. *The Journal of experimental medicine* 217; 10.1084/jem.20191711 (2020).

21. Mackay, L. K. *et al.* The developmental pathway for CD103(+)CD8+ tissue-resident memory T cells of skin. *Nature immunology* 14, 1294–1301; 10.1038/ni.2744 (2013).

22. Kok, L., Masopust, D. & Schumacher, T. N. The precursors of CD8+ tissue resident memory T cells: from lymphoid organs to infected tissues. *Nature reviews. Immunology* 22, 283–293; 10.1038/s41577-021-00590-3 (2022).

23. Skon, C. N. *et al.* Transcriptional downregulation of S1pr1 is required for the establishment of resident memory CD8+ T cells. *Nature immunology* 14, 1285–1293; 10.1038/ni.2745 (2013).

24. Park, S. L. *et al.* Local proliferation maintains a stable pool of tissue-resident memory T cells after antiviral recall responses. *Nature immunology* 19, 183–191; 10.1038/s41590-017-0027-5 (2018).

25. Kaech, S. M. & Wherry, E. J. Heterogeneity and cell-fate decisions in effector and memory CD8+ T cell differentiation during viral infection. *Immunity* 27, 393–405; 10.1016/j.immuni.2007.08.007 (2007).

26. Clark, R. A. *et al.* The vast majority of CLA+ T cells are resident in normal skin. *Journal of immunology (Baltimore, Md. : 1950)* 176, 4431–4439; 10.4049/jimmunol.176.7.4431 (2006).

27. Zhang, C., Merana, G. R., Harris-Tryon, T. & Scharschmidt, T. C. Skin immunity: dissecting the complex biology of our body's outer barrier. *Mucosal immunology* 15, 551–561; 10.1038/s41385-022-00505-y (2022).

28. Tajima, S. & Pinnell, S. R. Collagen synthesis by human skin fibroblasts in culture: studies of fibroblasts explanted from papillary and reticular dermis. *Journal of Investigative Dermatology* 77, 410–412; 10.1111/1523-1747.ep12494614 (1981).

29. Driskell, R. R. *et al.* Distinct fibroblast lineages determine dermal architecture in skin development and repair. *Nature* 504, 277–281; 10.1038/nature12783 (2013).

30. Cruz, M. S., Diamond, A., Russell, A. & Jameson, J. M. Human αβ and γδ T Cells in Skin Immunity and Disease. *Frontiers in immunology* 9, 1304; 10.3389/fimmu.2018.01304 (2018).

31. Byrd, A. L., Belkaid, Y. & Segre, J. A. The human skin microbiome. *Nature reviews. Microbiology* 16, 143–155; 10.1038/nrmicro.2017.157 (2018).

32. Kurschus, F. C. & Moos, S. IL-17 for therapy. *Journal of dermatological science* 87, 221–227; 10.1016/j.jdermsci.2017.06.010 (2017).

33. Cai, Y. *et al.* Pivotal role of dermal IL-17-producing γδ T cells in skin inflammation. *Immunity* 35, 596–610; 10.1016/j.immuni.2011.08.001 (2011).

34. Sanchez Rodriguez, R. *et al.* Memory regulatory T cells reside in human skin. *The Journal of clinical investigation* 124, 1027–1036; 10.1172/JCI72932 (2014).

35. Scharschmidt, T. C. *et al.* A Wave of Regulatory T Cells into Neonatal Skin Mediates Tolerance to Commensal Microbes. *Immunity* 43, 1011–1021; 10.1016/j.immuni.2015.10.016 (2015).

36. Thelen, F. & Witherden, D. A. Get in Touch With Dendritic Epithelial T Cells! *Frontiers in immunology* 11, 1656; 10.3389/fimmu.2020.01656 (2020).

37. McCarthy, K. N., Hone, S., McLoughlin, R. M. & Mills, K. H. G. IL-17 and IFN-γ-producing respiratory tissue resident memory CD4 T cells persist for decades in adults immunized as children with whole cell pertussis vaccines. *The Journal of infectious diseases*; 10.1093/infdis/jiae034 (2024).

38. Pan, Y. *et al.* Epicutaneous immunization with modified vaccinia Ankara viral vectors generates superior T cell immunity against a respiratory viral challenge. *NPJ vaccines* 6, 1; 10.1038/s41541-020-00265-5 (2021).

39. Gebhardt, T. *et al.* Memory T cells in nonlymphoid tissue that provide enhanced local immunity during infection with herpes simplex virus. *Nature immunology* 10, 524–530; 10.1038/ni.1718 (2009).

40. Ariotti, S. *et al.* Tissue-resident memory CD8+ T cells continuously patrol skin epithelia to quickly recognize local antigen. *Proceedings of the National Academy of Sciences of the United States of America* 109, 19739–19744; 10.1073/pnas.1208927109 (2012).

41. Schenkel, J. M., Fraser, K. A., Vezys, V. & Masopust, D. Sensing and alarm function of resident memory $CD8^+$ T cells. *Nature immunology* 14, 509–513; 10.1038/ni.2568 (2013).

42. Ariotti, S. *et al.* T cell memory. Skin-resident memory $CD8^+$ T cells trigger a state of tissue-wide pathogen alert. *Science (New York, N.Y.)* 346, 101–105; 10.1126/science.1254803 (2014).

43. Jiang, X. *et al.* Skin infection generates non-migratory memory CD8+ T(RM) cells providing global skin immunity. *Nature* 483, 227–231; 10.1038/nature10851 (2012).

44. Iijima, N. & Iwasaki, A. A local macrophage chemokine network sustains protective tissue-resident memory CD4 T cells. *Science (New York, N.Y.)* 346, 93–98; 10.1126/science.1257530 (2014).

45. Szabo P, Miron M, Farber D. Location, location, location: Tissue resident memory T cells in mice and humans. Review. *Science immunology* (2019).

46. Mackay, L. K. *et al.* Long-lived epithelial immunity by tissue-resident memory T (TRM) cells in the absence of persisting local antigen presentation. *Proceedings of the National Academy of Sciences of the United States of America* 109, 7037–7042; 10.1073/pnas.1202288109 (2012).

47. FitzPatrick, M. E. B. *et al.* Human intestinal tissue-resident memory T cells comprise transcriptionally and functionally distinct subsets. *Cell reports* 34, 108661; 10.1016/j.celrep.2020.108661 (2021).

48. Corgnac, S., Boutet, M., Kfoury, M., Naltet, C. & Mami-Chouaib, F. The Emerging Role of CD8+ Tissue Resident Memory T (TRM) Cells in Antitumor Immunity: A Unique Functional Contribution of the CD103 Integrin. *Frontiers in immunology* 9, 1904; 10.3389/fimmu.2018.01904 (2018).

49. Watanabe, R. *et al.* Human skin is protected by four functionally and phenotypically discrete populations of resident and recirculating memory T cells. *Science Translational Medicine* 7; 10.1126/scitranslmed.3010302 (2015).

50. Dijkgraaf, F. E. *et al.* Tissue patrol by resident memory CD8+ T cells in human skin. *Nature immunology* 20, 756–764; 10.1038/s41590-019-0404-3 (2019).

51. Rosato, P. C., Beura, L. K. & Masopust, D. Tissue resident memory T cells and viral immunity. *Current opinion in virology* 22, 44–50; 10.1016/j.coviro.2016.11.011 (2017).

52. Mackay, L. K. *et al.* Cutting edge: CD69 interference with sphingosine-1-phosphate receptor function regulates peripheral T cell retention. *Journal of immunology (Baltimore, Md. : 1950)* 194, 2059–2063; 10.4049/jimmunol.1402256 (2015).

53. Mackay, L. K. *et al.* T-box Transcription Factors Combine with the Cytokines TGF-β and IL-15 to Control Tissue-Resident Memory T Cell Fate. *Immunity* 43, 1101–1111; 10.1016/j.immuni.2015.11.008 (2015).

54. Yu, C. I. *et al.* Human CD1c+ dendritic cells drive the differentiation of CD103+ CD8+ mucosal effector T cells via the cytokine TGF-β. *Immunity* 38, 818–830; 10.1016/j.immuni.2013.03.004 (2013).

55. Nath, A. P. *et al.* Comparative analysis reveals a role for TGF-β in shaping the residency-related transcriptional signature in tissue-resident memory CD8+ T cells. *PloS one* 14, e0210495; 10.1371/journal.pone.0210495 (2019).

56. Kumar, B. V. *et al.* Human Tissue-Resident Memory T Cells Are Defined by Core Transcriptional and Functional Signatures in Lymphoid and Mucosal Sites. *Cell reports* 20, 2921–2934; 10.1016/j.celrep.2017.08.078 (2017).

57. Mackay, L. K. *et al.* Hobit and Blimp1 instruct a universal transcriptional program of tissue residency in lymphocytes. *Science (New York, N.Y.)* 352, 459–463; 10.1126/science.aad2035 (2016).

58. Fonseca, R. *et al.* Runx3 drives a CD8+ T cell tissue residency program that is absent in CD4+ T cells. *Nature immunology* 23, 1236–1245; 10.1038/s41590-022-01273-4 (2022).

59. Cheuk, S. *et al.* CD49a Expression Defines Tissue-Resident CD8+ T Cells Poised for Cytotoxic Function in Human Skin. *Immunity* 46, 287–300; 10.1016/j.immuni.2017.01.009 (2017).

60. Harrison, O. J. *et al.* Commensal-specific T cell plasticity promotes rapid tissue adaptation to injury. *Science (New York, N.Y.)* 363; 10.1126/science.aat6280 (2019).

61. Brunner, P. M. *et al.* Nonlesional atopic dermatitis skin shares similar T-cell clones with lesional tissues. *Allergy* 72, 2017–2025; 10.1111/all.13223 (2017).

62. Sasson, S. C., Gordon, C. L., Christo, S. N., Klenerman, P. & Mackay, L. K. Local heroes or villains: tissue-resident memory T cells in human health and disease. *Cellular & molecular immunology* 17, 113–122; 10.1038/s41423-019-0359-1 (2020).

63. Samat, A. A. K., van der Geest, J., Vastert, S. J., van Loosdregt, J. & van Wijk, F. Tissue-Resident Memory T Cells in Chronic Inflammation-Local Cells with Systemic Effects? *Cells* 10; 10.3390/cells10020409 (2021).

64. Lefevre, M.-A., Vocanson, M. & Nosbaum, A. Role of tissue-resident memory T cells in the pathophysiology of allergic contact dermatitis. *Current opinion in allergy and clinical immunology* 21, 355–360; 10.1097/ACI.0000000000000763 (2021).

65. Trubiano, J. A. *et al.* Analysis of Skin-Resident Memory T Cells Following Drug Hypersensitivity Reactions. *The Journal of investigative dermatology* 140, 1442-1445.e4; 10.1016/j.jid.2019.11.020 (2020).

66. Ho, A. W. & Kupper, T. S. T cells and the skin: from protective immunity to inflammatory skin disorders. *Nature reviews. Immunology* 19, 490–502; 10.1038/s41577-019-0162-3 (2019).

67. Menssen, A. *et al.* Evidence for an antigen-specific cellular immune response in skin lesions of patients with psoriasis vulgaris. *The Journal of Immunology* 155, 4078–4083; 10.4049/jimmunol.155.8.4078 (1995).

68. Nestle Frank O., Kaplan Daniel H. & Barker Jonathan. Psoriasis. *The New England Journal of Medicine* 361, 496–509; 10.1056/NEJMra0804595 (2009).

69. Cheuk, S. *et al.* Epidermal Th22 and Tc17 cells form a localized disease memory in clinically healed psoriasis. *Journal of immunology (Baltimore, Md. : 1950)* 192, 3111–3120; 10.4049/jimmunol.1302313 (2014).

70. Prinz, J. C. Autoimmune aspects of psoriasis: Heritability and autoantigens. *Autoimmunity reviews* 16, 970–979; 10.1016/j.autrev.2017.07.011 (2017).

71. Armstrong, A. W. & Read, C. Pathophysiology, Clinical Presentation, and Treatment of Psoriasis: A Review. *JAMA* 323, 1945–1960; 10.1001/jama.2020.4006 (2020).

72. Moos, S., Mohebiany, A. N., Waisman, A. & Kurschus, F. C. Imiquimod-Induced Psoriasis in Mice Depends on the IL-17 Signaling of Keratinocytes. *The Journal of investigative dermatology* 139, 1110–1117; 10.1016/j.jid.2019.01.006 (2019).

73. Matos, T. R. *et al.* Clinically resolved psoriatic lesions contain psoriasis-specific IL-17-producing αβ T cell clones. *The Journal of clinical investigation* 127, 4031–4041; 10.1172/JCI93396 (2017).

74. Zhang, Y. Y. *et al.* CD8αα+T cells exert a pro-inflammatory role in patients with psoriasis. *Skin health and disease* 1, e64; 10.1002/ski2.64 (2021).

75. Whitley, S. K. *et al.* Local IL-23 is required for proliferation and retention of skin-resident memory TH17 cells. *Science immunology* 7, eabq3254; 10.1126/sciimmunol.abq3254 (2022).

76. Chang, W.-L., Lee, W.-R., Kuo, Y.-C. & Huang, Y.-H. Vitiligo: An Autoimmune Skin Disease and its Immunomodulatory Therapeutic Intervention. *Frontiers in cell and developmental biology* 9, 797026; 10.3389/fcell.2021.797026 (2021).

77. Richmond, J. M. *et al.* Resident Memory and Recirculating Memory T Cells Cooperate to Maintain Disease in a Mouse Model of Vitiligo. *The Journal of investigative dermatology* 139, 769–778; 10.1016/j.jid.2018.10.032 (2019).

78. Tokura, Y., Phadungsaksawasdi, P., Kurihara, K., Fujiyama, T. & Honda, T. Pathophysiology of Skin Resident Memory T Cells. *Frontiers in immunology* 11, 618897; 10.3389/fimmu.2020.618897 (2020).

79. Kubelis-López, D. E. *et al.* Updates and new medical treatments for vitiligo (Review). *Experimental and therapeutic medicine* 22, 797; 10.3892/etm.2021.10229 (2021).

80. Facheris, P., Jeffery, J., Del Duca, E. & Guttman-Yassky, E. The translational revolution in atopic dermatitis: the paradigm shift from pathogenesis to treatment. *Cellular & molecular immunology* 20, 448–474; 10.1038/s41423-023-00992-4 (2023).

81. Tsakok, T., Woolf, R., Smith, C. H., Weidinger, S. & Flohr, C. Atopic dermatitis: the skin barrier and beyond. *The British journal of dermatology* 180, 464–474; 10.1111/bjd.16934 (2019).

82. Park, S. L. *et al.* Divergent molecular networks program functionally distinct CD8+ skin-resident memory T cells. *Science (New York, N.Y.)* 382, 1073–1079; 10.1126/science.adi8885 (2023).

83. Zheng, C., Cao, T., Ye, C. & Zou, Y. Neutrophil recruitment by CD4 tissue-resident memory T cells induces chronic recurrent inflammation in atopic dermatitis. *Clinical immunology (Orlando, Fla.)* 256, 109805; 10.1016/j.clim.2023.109805 (2023).

84. Tampa, M., Mitran, C. I., Mitran, M. I. & Georgescu, S. R. A New Horizon for Atopic Dermatitis Treatments: JAK Inhibitors. *Journal of personalized medicine* 13; 10.3390/jpm13030384 (2023).

85. Gell, P. & Coombs, R. *Clinical Aspects of Immunology. The classification of allergic reactions underlying disease.* (Blackwell Scientific Pulications, Blackwell, Oxford, 1963).

86. van Loveren, H., Meade, R. & Askenase, P. W. An early component of delayed-type hypersensitivity mediated by T cells and mast cells. *Journal of Experimental Medicine* 157, 1604–1617; 10.1084/jem.157.5.1604 (1983).

87. Scheper, R. J. *et al.* Induction of immunological memory in the skin. Role of local T cell retention. *Clinical & Experimental Immunology* 51, 141–148 (1983).

88. Christensen, A. D. & Haase, C. Immunological mechanisms of contact hypersensitivity in mice. *APMIS : acta pathologica, microbiologica, et immunologica Scandinavica* 120, 1–27; 10.1111/j.1600-0463.2011.02832.x (2012).

89. Gadsbøll, A.-S. Ø. *et al.* Pathogenic CD8+ Epidermis-Resident Memory T Cells Displace Dendritic Epidermal T Cells in Allergic Dermatitis. *The Journal of investigative dermatology* 140, 806-815.e5; 10.1016/j.jid.2019.07.722 (2020).

90. Brar, K. K. A review of contact dermatitis. *Annals of allergy, asthma & immunology : official publication of the American College of Allergy, Asthma, & Immunology* 126, 32–39; 10.1016/j.anai.2020.10.003 (2021).

91. Richmond, J. M. *et al.* Antibody blockade of IL-15 signaling has the potential to durably reverse vitiligo. *Science Translational Medicine* 10; 10.1126/scitranslmed.aam7710 (2018).

92. Descotes, J. & Choquet-Kastylevsky, G. Gell and Coombs's classification: is it still valid? *Toxicology,* 43–49 (2001).

93. Jankovic, D. & Waksman, H. Delayed sensitization to purified blood group substances in the guinea pig. *Journal of immunology (Baltimore, Md. : 1950)* 89, 598–607 (1962).

94. Gamradt, P. *et al.* Inhibitory checkpoint receptors control CD8+ resident memory T cells to prevent skin allergy. *The Journal of allergy and clinical immunology* 143, 2147-2157.e9; 10.1016/j.jaci.2018.11.048 (2019).

95. Yamaguchi, H. L., Yamaguchi, Y. & Peeva, E. Role of Innate Immunity in Allergic Contact Dermatitis: An Update. *International journal of molecular sciences* 24; 10.3390/ijms241612975 (2023).

96. Clausen, B. E. & Stoitzner, P. Functional Specialization of Skin Dendritic Cell Subsets in Regulating T Cell Responses. *Frontiers in immunology* 6, 534; 10.3389/fimmu.2015.00534 (2015).

97. Honda, T. *et al.* Compensatory role of Langerhans cells and langerin-positive dermal dendritic cells in the sensitization phase of murine contact hypersensitivity. *The Journal of allergy and clinical immunology* 125, 1154-1156.e2; 10.1016/j.jaci.2009.12.005 (2010).

98. Ohl, L. *et al.* CCR7 governs skin dendritic cell migration under inflammatory and steady-state conditions. *Immunity* 21, 279–288; 10.1016/j.immuni.2004.06.014 (2004).

99. Kripke, M. L., Munn, C. G., Jeevan, A., Tang, J. M. & Bucana, C. Evidence that cutaneous antigen-presenting cells migrate to regional lymph nodes during contact sensitization. *Journal of immunology (Baltimore, Md. : 1950)* 145, 2833–2838; 10.4049/jimmunol.145.9.2833 (1990).

100. Kohler, J., Hartmann, U., Grimm, R., Pflugfelder, U. & Weltzien, H. U. Carrier-independent hapten recognition and promiscuous MHC restriction by CD4 T cells induced by trinitrophenylated peptides. *The Journal of Immunology* 158, 591–597; 10.4049/jimmunol.158.2.591 (1997).

101. Nakashima, D. *et al.* Impaired initiation of contact hypersensitivity by FTY720. *The Journal of investigative dermatology* 128, 2833–2841; 10.1038/jid.2008.174 (2008).

102. Chiba, K. *et al.* FTY720, a novel immunosuppressant, induces sequestration of circulating mature lymphocytes by acceleration of lymphocyte homing in rats. I. FTY720 selectively decreases the number of circulating mature lymphocytes by acceleration of lymphocyte homing. *Journal of immunology (Baltimore, Md. : 1950)* 160, 5037–5044 (1998).

103. Pinschewer, D. D. *et al.* FTY720 immunosuppression impairs effector T cell peripheral homing without affecting induction, expansion, and memory. *Journal of immunology (Baltimore, Md. : 1950)* 164, 5761–5770; 10.4049/jimmunol.164.11.5761 (2000).

104. van den Broeck, W., Derore, A. & Simoens, P. Anatomy and nomenclature of murine lymph nodes: Descriptive study and nomenclatory standardization in BALB/cAnNCrl mice. *Journal of immunological methods* 312, 12–19; 10.1016/j.jim.2006.01.022 (2006).

105. Barker, J., Mitra, R. S., Griffiths, C., Dixit, V. M. & Nickoloff, B. J. Keratinocytes as initiators of inflammation. *Lancet,* 221-214; 10.1016/0140-6736(91)92168-2 (1991).

106. Grabbe, S., Steinbrink, K., Steinert, M., Luger, T. A. & Schwarz, T. Removal of the majority of epidermal Langerhans cells by topical or systemic steroid application enhances the effector phase of murine contact hypersensitivity. *Journal of immunology (Baltimore, Md. : 1950)* 155, 4207–4217; 10.4049/jimmunol.155.9.4207 (1995).

107. Grabbe, S. & Schwarz, T. Immunoregulatory mechanisms involved in elicitation of allergic contact hypersensitivity. *Immunology Today,* 37–44; 10.1016/S0167-5699(97)01186-9 (1998).

108. Schmidt, J. D. *et al.* Rapid allergen-induced interleukin-17 and interferon-γ secretion by skin-resident memory CD8+ T cells. *Contact dermatitis* 76, 218–227; 10.1111/cod.12715 (2017).

109. Murata, A. & Hayashi, S.-I. CD4+ Resident Memory T Cells Mediate Long-Term Local Skin Immune Memory of Contact Hypersensitivity in BALB/c Mice. *Frontiers in immunology* 11, 775; 10.3389/fimmu.2020.00775 (2020).

110. Iborra, S. *et al.* Optimal Generation of Tissue-Resident but Not Circulating Memory T Cells during Viral Infection Requires Crosspriming by DNGR-1+ Dendritic Cells. *Immunity* 45, 847–860; 10.1016/j.immuni.2016.08.019 (2016).

111. Low, J. S. *et al.* Tissue-resident memory T cell reactivation by diverse antigen-presenting cells imparts distinct functional responses. *The Journal of experimental medicine* 217; 10.1084/jem.20192291 (2020).

112. Rosenkilde, M. M. *et al.* Molecular pharmacological phenotyping of EBI2. An orphan seven-transmembrane receptor with constitutive activity. *The Journal of biological chemistry* 281, 13199–13208; 10.1074/jbc.M602245200 (2006).

113. Birkenbach, M., Josefsen, K., Yalamanchili, R., Lenoir, G. & Kieff, E. Epstein-Barr virus-induced genes: first lymphocyte-specific G protein-coupled peptide receptors. *Journal of virology* 67, 2209–2220; 10.1128/JVI.67.4.2209-2220.1993 (1993).

114. Chen, H., Huang, W. & Li, X. Structures of oxysterol sensor EBI2/GPR183, a key regulator of the immune response. *Structure (London, England : 1993)* 30, 1016-1024.e5; 10.1016/j.str.2022.04.006 (2022).

115. Hannedouche, S. *et al.* Oxysterols direct immune cell migration via EBI2. *Nature* 475, 524–527; 10.1038/nature10280 (2011).

116. Liu, C. *et al.* Oxysterols direct B-cell migration through EBI2. *Nature* 475, 519–523; 10.1038/nature10226 (2011).

117. Russell, D. W. The enzymes, regulation, and genetics of bile acid synthesis. *Annual review of biochemistry* 72, 137–174; 10.1146/annurev.biochem.72.121801.161712 (2003).

118. Shi, Q., Chen, J., Zou, X. & Tang, X. Intracellular Cholesterol Synthesis and Transport. *Frontiers in cell and developmental biology* 10, 819281; 10.3389/fcell.2022.819281 (2022).

119. Maxfield, F. R. & van Meer, G. Cholesterol, the central lipid of mammalian cells. *Current opinion in cell biology* 22, 422–429; 10.1016/j.ceb.2010.05.004 (2010).

120. Wanke, F. *et al.* EBI2 Is Highly Expressed in Multiple Sclerosis Lesions and Promotes Early CNS Migration of Encephalitogenic CD4 T Cells. *Cell reports* 18, 1270–1284; 10.1016/j.celrep.2017.01.020 (2017).

121. Yi, T. *et al.* Oxysterol gradient generation by lymphoid stromal cells guides activated B cell movement during humoral responses. *Immunity* 37, 535–548; 10.1016/j.immuni.2012.06.015 (2012).

122. Pereira, J. P., Kelly, L. M., Xu, Y. & Cyster, J. G. EBI2 mediates B cell segregation between the outer and centre follicle. *Nature* 460, 1122–1126; 10.1038/nature08226 (2009).

123. Gatto, D., Paus, D., Basten, A., Mackay, C. R. & Brink, R. Guidance of B cells by the orphan G protein-coupled receptor EBI2 shapes humoral immune responses. *Immunity* 31, 259–269; 10.1016/j.immuni.2009.06.016 (2009).

124. Benned-Jensen, T. *et al.* Small molecule antagonism of oxysterol-induced Epstein-Barr virus induced gene 2 (EBI2) activation. *FEBS Open Bio* 3, 156–160; 10.1016/j.fob.2013.02.003 (2013).

125. Gessier, F. *et al.* Identification and characterization of small molecule modulators of the Epstein-Barr virus-induced gene 2 (EBI2) receptor. *Journal of medicinal chemistry* 57, 3358–3368; 10.1021/jm4019355 (2014).

126. Yang, D. *et al.* G protein-coupled receptors: structure- and function-based drug discovery. *Signal transduction and targeted therapy* 6, 7; 10.1038/s41392-020-00435-w (2021).

127. Weis, W. I. & Kobilka, B. K. The Molecular Basis of G Protein-Coupled Receptor Activation. *Annual review of biochemistry* 87, 897–919; 10.1146/annurev-biochem-060614-033910 (2018).

128. Wootten, D., Christopoulos, A., Marti-Solano, M., Babu, M. M. & Sexton, P. M. Mechanisms of signalling and biased agonism in G protein-coupled receptors. *Nature reviews. Molecular cell biology* 19, 638–653; 10.1038/s41580-018-0049-3 (2018).

129. Benned-Jensen, T. & Rosenkilde, M. M. Structural motifs of importance for the constitutive activity of the orphan 7TM receptor EBI2: analysis of receptor activation in the absence of an agonist. *Molecular pharmacology* 74, 1008–1021; 10.1124/mol.108.049676 (2008).

130. Fields, T. A. & Casey, P. J. Signalling functions and biochemical properties of pertussis toxin-resistant G-proteins. *The Biochemical journal* 321 (Pt 3), 561–571; 10.1042/bj3210561 (1997).

131. Pedro, M. P., Salinas Parra, N., Gutkind, J. S. & Iglesias-Bartolome, R. Activation of G-Protein Coupled Receptor-Gαi Signaling Increases Keratinocyte Proliferation and Reduces Differentiation, Leading to Epidermal Hyperplasia. *The Journal of investigative dermatology* 140, 1195-1203.e3; 10.1016/j.jid.2019.10.012 (2020).

132. Gainetdinov, R. R., Premont, R. T., Bohn, L. M., Lefkowitz, R. J. & Caron, M. G. Desensitization of G protein-coupled receptors and neuronal functions. *Annual review of neuroscience* 27, 107–144; 10.1146/annurev.neuro.27.070203.144206 (2004).

133. Reif, K. *et al.* Balanced responsiveness to chemoattractants from adjacent zones determines B-cell position. *Nature* 416, 94–99; 10.1038/416094a (2002).

134. Legler, D. F. *et al.* B cell-attracting chemokine 1, a human CXC chemokine expressed in lymphoid tissues, selectively attracts B lymphocytes via BLR1/CXCR5. *Journal of Experimental Medicine* 187, 655–660; 10.1084/jem.187.4.655 (1998).

135. Cyster, J. G. B cell follicles and antigen encounters of the third kind. *Nature immunology* 11, 989–996; 10.1038/ni.1946 (2010).

136. Cahir-McFarland, E. D. *et al.* Role of NF-kappa B in cell survival and transcription of latent membrane protein 1-expressing or Epstein-Barr virus latency III-infected cells. *Journal of virology* 78, 4108–4119; 10.1128/jvi.78.8.4108-4119.2004 (2004).

137. Barroso, R. *et al.* EBI2 regulates CXCL13-mediated responses by heterodimerization with CXCR5. *FASEB journal : official publication of the Federation of American Societies for Experimental Biology* 26, 4841–4854; 10.1096/fj.12-208876 (2012).

138. Rodda, L. B. *et al.* Single-Cell RNA Sequencing of Lymph Node Stromal Cells Reveals Niche-Associated Heterogeneity. *Immunity* 48, 1014-1028.e6; 10.1016/j.immuni.2018.04.006 (2018).

139. Diczfalusy, U. *et al.* Marked upregulation of cholesterol 25-hydroxylase expression by lipopolysaccharide. *Journal of lipid research* 50, 2258–2264; 10.1194/jlr.M900107-JLR200 (2009).

140. Shaffer AL, Yu X, He Y. BCL-6 Represses Genes that Function in Lymphocyte Differentiation, Inflammation, and Cell Cycle Control. *Immunity,* 199–212 (2000).

141. Lu, E. & Cyster, J. G. G-protein coupled receptors and ligands that organize humoral immune responses. *Immunological reviews* 289, 158–172; 10.1111/imr.12743 (2019).

142. Ceglia, S. *et al.* An epithelial cell-derived metabolite tunes immunoglobulin A secretion by gut-resident plasma cells. *Nature immunology* 24, 531–544; 10.1038/s41590-022-01413-w (2023).

143. Gatto, D. *et al.* The chemotactic receptor EBI2 regulates the homeostasis, localization and immunological function of splenic dendritic cells. *Nature immunology* 14, 446–453; 10.1038/ni.2555 (2013).

144. Yi, T. & Cyster, J. G. EBI2-mediated bridging channel positioning supports splenic dendritic cell homeostasis and particulate antigen capture. *eLife* 2, e00757; 10.7554/eLife.00757 (2013).

145. Reizis, B. Plasmacytoid Dendritic Cells: Development, Regulation, and Function. *Immunity* 50, 37–50; 10.1016/j.immuni.2018.12.027 (2019).

146. Chiang, E. Y., Johnston, R. J. & Grogan, J. L. EBI2 is a negative regulator of type I interferons in plasmacytoid and myeloid dendritic cells. *PloS one* 8, e83457; 10.1371/journal.pone.0083457 (2013).

147. Reboldi, A. *et al.* 25-Hydroxycholesterol suppresses interleukin-1–driven inflammation downstream of type I interferon. *Science (New York, N.Y.)* 345, 679-648; 10.1126/science.1254790 (2014).

148. Benned-Jensen, T. *et al.* Ligand modulation of the Epstein-Barr virus-induced seven-transmembrane receptor EBI2: identification of a potent and efficacious inverse agonist. *The Journal of biological chemistry* 286, 29292–29302; 10.1074/jbc.M110.196345 (2011).

149. Clottu, A. S. *et al.* EBI2 Expression and Function: Robust in Memory Lymphocytes and Increased by Natalizumab in Multiple Sclerosis. *Cell reports* 18, 213–224; 10.1016/j.celrep.2016.12.006. (2017).

150. Baptista, A. P. *et al.* The Chemoattractant Receptor Ebi2 Drives Intranodal Naive CD4+ T Cell Peripheralization to Promote Effective Adaptive Immunity. *Immunity* 50, 1188-1201.e6; 10.1016/j.immuni.2019.04.001 (2019).

151. Li, J., Lu, E., Yi, T. & Cyster, J. G. EBI2 augments Tfh cell fate by promoting interaction with IL-2-quenching dendritic cells. *Nature* 533, 110–114; 10.1038/nature17947 (2016).

152. Lu, E., Dang, E. V., McDonald, J. G. & Cyster, J. G. Distinct oxysterol requirements for positioning naïve and activated dendritic cells in the spleen. *Science immunology* 2; 10.1126/sciimmunol.aal5237 (2017).

153. Ki, S., Thyagarajan, H. M., Hu, Z., Lancaster, J. N. & Ehrlich, L. I. R. EBI2 contributes to the induction of thymic central tolerance in mice by promoting rapid motility of medullary thymocytes. *European Journal of Immunology* 47, 1906–1917; 10.1002/eji.201747020 (2017).

154. Frascoli, M. *et al.* Skin γδ T cell inflammatory responses are hardwired in the thymus by oxysterol sensing via GPR183 and calibrated by dietary cholesterol. *Immunity* 56, 562-575.e6; 10.1016/j.immuni.2023.01.025 (2023).

155. Takahashi, H. *et al.* Cholesterol 25-hydroxylase is a metabolic switch to constrain T cell-mediated inflammation in the skin. *Science immunology* 6, eabb6444; 10.1126/sciimmunol.abb6444 (2021).

156. Chalmin, F. *et al.* Oxysterols regulate encephalitogenic CD4(+) T cell trafficking during central nervous system autoimmunity. *Journal of autoimmunity* 56, 45–55; 10.1016/j.jaut.2014.10.001 (2015).

157. Papassotiropoulos, A. *et al.* Cholesterol 25-hydroxylase on chromosome 10q is a susceptibility gene for sporadic Alzheimer's disease. *Neuro-degenerative diseases* 2, 233–241; 10.1159/000090362 (2005).

158. Laumet, G. *et al.* Systematic analysis of candidate genes for Alzheimer's disease in a French, genome-wide association study. *Journal of Alzheimer's disease : JAD* 20, 1181–1188; 10.3233/JAD-2010-100126 (2010).

159. Nevius, E. *et al.* Oxysterols and EBI2 promote osteoclast precursor migration to bone surfaces and regulate bone mass homeostasis. *Journal of Experimental Medicine* 212, 1931–1946; 10.1084/jem.20150088 (2015).

160. Jia, J. *et al.* Cholesterol metabolism promotes B-cell positioning during immune pathogenesis of chronic obstructive pulmonary disease. *EMBO molecular medicine* 10; 10.15252/emmm.201708349 (2018).

161. Shi, W. *et al.* Bioinformatics approach to identify the hub gene associated with COVID-19 and idiopathic pulmonary fibrosis. *IET systems biology* 17, 336–351; 10.1049/syb2.12080 (2023).

162. Foo, C. X. *et al.* GPR183 antagonism reduces macrophage infiltration in influenza and SARS-CoV-2 infection. *The European respiratory journal* 61; 10.1183/13993003.01306-2022 (2023).

163. Conlon, T. M. & Yildirim, A. Ö. Oxysterol metabolism dictates macrophage influx during SARS-CoV-2 infection. *The European respiratory journal* 61; 10.1183/13993003.02417-2022 (2023).

164. Bohrer, A. C. *et al.* Rapid GPR183-mediated recruitment of eosinophils to the lung after Mycobacterium tuberculosis infection. *Cell reports* 40, 111144; 10.1016/j.celrep.2022.111144 (2022).

165. Ngo, M. D. *et al.* A Blunted GPR183/Oxysterol Axis During Dysglycemia Results in Delayed Recruitment of Macrophages to the Lung During Mycobacterium tuberculosis Infection. *The Journal of infectious diseases* 225, 2219–2228; 10.1093/infdis/jiac102 (2022).

166. Bartlett, S. *et al.* GPR183 Regulates Interferons, Autophagy, and Bacterial Growth During Mycobacterium tuberculosis Infection and Is Associated With TB Disease Severity. *Frontiers in immunology* 11, 601534; 10.3389/fimmu.2020.601534 (2020).

167. Shen, Z.-J. *et al.* Epstein-Barr Virus-induced Gene 2 Mediates Allergen-induced Leukocyte Migration into Airways. *American journal of respiratory and critical care medicine* 195, 1576–1585; 10.1164/rccm.201608-1580OC (2017).

168. Fricker, M. *et al.* An altered sputum macrophage transcriptome contributes to the neutrophilic asthma endotype. *Allergy* 77, 1204–1215; 10.1111/all.15087 (2022).

169. Wu, Y. *et al.* GWAS of peptic ulcer disease implicates Helicobacter pylori infection, other gastrointestinal disorders and depression. *Nature communications* 12, 1146; 10.1038/s41467-021-21280-7 (2021).

170. Jostins, L. *et al.* Host-microbe interactions have shaped the genetic architecture of inflammatory bowel disease. *Nature* 491, 119–124; 10.1038/nature11582 (2012).

171. Wyss, A. *et al.* The EBI2-oxysterol axis promotes the development of intestinal lymphoid structures and colitis. *Mucosal immunology* 12, 733–745; 10.1038/s41385-019-0140-x (2019).

172. Ruiz, F. *et al.* A single nucleotide polymorphism in the gene for GPR183 increases its surface expression on blood lymphocytes of patients with inflammatory bowel disease. *British journal of pharmacology* 178, 3157–3175; 10.1111/bph.15395 (2021).

173. Boyman, O. *et al.* Spontaneous development of psoriasis in a new animal model shows an essential role for resident T cells and tumor necrosis factor-alpha. *The Journal of experimental medicine* 199, 731–736; 10.1084/jem.20031482 (2004).

174. Kurschus, F. C. & Wanke, F. EBI2 - Sensor for dihydroxycholesterol gradients in neuroinflammation. *Biochimie* 153, 52–55; 10.1016/j.biochi.2018.04.014 (2018).

175. Barington, L. *et al.* EBI2 in splenic and local immune responses and in autoimmunity. *Journal of leukocyte biology* 104, 313–322; 10.1002/JLB.2VMR1217-510R (2018).

176. Nevius, E., Gomes, A. C. & Pereira, J. P. Inflammatory Cell Migration in Rheumatoid Arthritis: A Comprehensive Review. *Clinical reviews in allergy & immunology* 51, 59–78; 10.1007/s12016-015-8520-9 (2016).

177. Rutkowska, A., Dev, K. K. & Sailer, A. W. The Role of the Oxysterol/EBI2 Pathway in the Immune and Central Nervous Systems. *Current drug targets* 17, 1851–1860; 10.2174/1389450117666160217123042 (2016).

178. Meng, Z. *et al.* Transcriptome-based identification of tumor-reactive and bystander CD8+ T cell receptor clonotypes in human pancreatic cancer. *Science Translational Medicine* 722; 10.1126/scitranslmed.adh9562 (2023).

179. Heinen, A. P. *et al.* Improved method to retain cytosolic reporter protein fluorescence while staining for nuclear proteins. *Cytometry. Part A : the journal of the International Society for Analytical Cytology* 85, 621–627; 10.1002/cyto.a.22451 (2014).

180. Tsoi, L. C. *et al.* Atopic Dermatitis Is an IL-13-Dominant Disease with Greater Molecular Heterogeneity Compared to Psoriasis. *The Journal of investigative dermatology* 139, 1480–1489; 10.1016/j.jid.2018.12.018 (2019).

181. Love, M. I., Huber, W. & Anders, S. Moderated estimation of fold change and dispersion for RNA-seq data with DESeq2. *Genome biology* 15, 550; 10.1186/s13059-014-0550-8 (2014).

182. Leek JT *et al. sva: Surrogate Variable Analysis* (2022).

183. Harris, C. R. *et al.* Array programming with NumPy. *Nature* 585, 357–362; 10.1038/s41586-020-2649-2 (2020).

184. Kitagaki, H., Fujisawa, S., Watanabe, K., Hayakawa, K. & Shiohara, T. Immediate-type hypersensitivity response followed by a late reaction is induced by repeated epicutaneous application of contact sensitizing agents in mice. *Journal of Investigative Dermatology* 105, 749–755; 10.1111/1523-1747.ep12325538 (1995).

185. Pichler, B. J. *et al.* Imaging of delayed-type hypersensitivity reaction by PET and 18F-galacto-RGD. *Journal of nuclear medicine : official publication, Society of Nuclear Medicine* 46, 184–189 (2005).

186. Mather, K. Genetical control of stability in development. *Heredity* 7, 297–336; 10.1038/hdy.1953.41 (1953).

187. El-Brolosy, M. A. *et al.* Genetic compensation triggered by mutant mRNA degradation. *Nature* 568, 193–197; 10.1038/s41586-019-1064-z (2019).

188. Ma, Z. *et al.* PTC-bearing mRNA elicits a genetic compensation response via Upf3a and COMPASS components. *Nature* 568, 259–263; 10.1038/s41586-019-1057-y (2019).

189. van der Fits, L. *et al.* Imiquimod-induced psoriasis-like skin inflammation in mice is mediated via the IL-23/IL-17 axis. *Journal of immunology (Baltimore, Md. : 1950)* 182, 5836–5845; 10.4049/jimmunol.0802999 (2009).

190. Heilig, J. S. & Tonegawa, S. Diversity of murine gamma genes and expression in fetal and adult T lymphocytes. *Nature* 322, 836–840; 10.1038/322836a0 (1986).

191. Ramírez-Valle, F., Gray, E. E. & Cyster, J. G. Inflammation induces dermal Vγ4+ γδT17 memory-like cells that travel to distant skin and accelerate secondary IL-17-driven responses. *Proceedings of the National Academy of Sciences of the United States of America* 112, 8046–8051; 10.1073/pnas.1508990112 (2015).

192. Budd, R. C. *et al.* Distinction of virgin and memory T lymphocytes. Stable acquisition of the Pgp-1 glycoprotein concomitant with antigenic stimulation. *The Journal of Immunology* 138, 3120–3129; 10.4049/jimmunol.138.10.3120 (1987).

193. Gerdes, J., Schwab, U., Lemke, H. & Stein, H. Production of a mouse monoclonal antibody reactive with a human nuclear antigen associated with cell proliferation. *International journal of cancer* 31, 13–20; 10.1002/ijc.2910310104 (1983).

194. Sanders M *et al.* Human memory T lymphocytes express increased levels of three cell adhesion molecules 8LFA-3, CD3 and LFA-1) and three other molecules (UCHL1, CDw29, AND Pgp-1) and have enhanced IFN-y production. *The Journal of Immunology,* 1401–1407 (1988).

195. Shiohara T, Mizukawa Y, Teraki Y. Pathophysiology of fixed drug eruption: the role of skin-resident T cells. *Current opinion in allergy and clinical immunology,* 317–323 (2002).

196. Brunner, P. M. *et al.* Nonlesional atopic dermatitis skin shares similar T-cell clones with lesional tissues. *Allergy* 72, 2017–2025; 10.1111/all.13223 (2017).

197. Kish, D. D., Li, X. & Fairchild, R. L. CD8 T cells producing IL-17 and IFN-gamma initiate the innate immune response required for responses to antigen skin challenge. *Journal of immunology (Baltimore, Md. : 1950)* 182, 5949–5959; 10.4049/jimmunol.0802830 (2009).

198. Hofmann, M., Brinkmann, V. & Zerwes, H.-G. FTY720 preferentially depletes naive T cells from peripheral and lymphoid organs. *International immunopharmacology* 6, 1902–1910; 10.1016/j.intimp.2006.07.030 (2006).

199. Hochheiser, K. *et al.* Ptpn2 and KLRG1 regulate the generation and function of tissue-resident memory CD8+ T cells in skin. *The Journal of experimental medicine* 218; 10.1084/jem.20200940 (2021).

200. Kaech, S. M. *et al.* Selective expression of the interleukin 7 receptor identifies effector CD8 T cells that give rise to long-lived memory cells. *Nature immunology* 4, 1191–1198; 10.1038/ni1009 (2003).

201. Naik, S. *et al.* Commensal-dendritic-cell interaction specifies a unique protective skin immune signature. *Nature* 520, 104–108; 10.1038/nature14052 (2015).

202. Linehan, J. L. *et al.* Non-classical Immunity Controls Microbiota Impact on Skin Immunity and Tissue Repair. *Cell* 172, 784-796.e18; 10.1016/j.cell.2017.12.033 (2018).

203. Fonseca, R. *et al.* Developmental plasticity allows outside-in immune responses by resident memory T cells. *Nature immunology* 21, 412–421; 10.1038/s41590-020-0607-7 (2020).

204. Strobl, J. *et al.* Human resident memory T cells exit the skin and mediate systemic Th2-driven inflammation. *The Journal of experimental medicine* 218; 10.1084/jem.20210417 (2021).

205. El Malki, K. *et al.* An alternative pathway of imiquimod-induced psoriasis-like skin inflammation in the absence of interleukin-17 receptor a signaling. *The Journal of investigative dermatology* 133, 441–451; 10.1038/jid.2012.318 (2013).

206. Mabuchi, T., Takekoshi, T. & Hwang, S. T. Epidermal CCR6+ γδ T cells are major producers of IL-22 and IL-17 in a murine model of psoriasiform dermatitis. *Journal of immunology (Baltimore, Md. : 1950)* 187, 5026–5031; 10.4049/jimmunol.1101817 (2011).

207. Beura, L. K. *et al.* T Cells in Nonlymphoid Tissues Give Rise to Lymph-Node-Resident Memory T Cells. *Immunity* 48, 327-338.e5; 10.1016/j.immuni.2018.01.015 (2018).

208. Phadungsaksawasdi, P. *et al.* PD-1 Expression Defines Epidermal CD8+CD103+ T Cells Preferentially Producing IL-17A and Using Skewed TCR Repertoire in Psoriasis. *The Journal of investigative dermatology* 141, 2426-2435.e5; 10.1016/j.jid.2021.03.011 (2021).

209. Salima Coy. Was ist Fett-lei-big-keit (Adi-po-si-tas)? Available at https://www.tk.de/techniker/gesundheit-und-medizin/behandlungen-und-medizin/stoffwechselerkrankungen/was-ist-fettleibigkeit-adipositas-2017418?tkcm=ab (2022).

210. Naldi, L. *et al.* Cigarette smoking, body mass index, and stressful life events as risk factors for psoriasis: results from an Italian case-control study. *Journal of Investigative Dermatology* 125, 61–67; 10.1111/j.0022-202X.2005.23681.x (2005).

211. Hahn, M. & Ghoreschi, K. The role of IL-4 in psoriasis. *Expert review of clinical immunology* 13, 171–173; 10.1080/1744666X.2017.1279054 (2017).

212. Ishida, Y., Agata, Y., Shibahara, K. & Honjo, T. Induced expression of PD-1, a novel member of the immunoglobulin gene superfamily, upon programmed cell death. *The EMBO journal* 11, 3887–3895; 10.1002/j.1460-2075.1992.tb05481.x (1992).

213. Iwai Y *et al.* Involvement of PD-L1 on tumor cells in the escape from host immune system and tumor immunotherapy by PD-L1 blockade. *Proceedings of the National Academy of Sciences of the United States of America* 99, 12293–12297; 10.1073/pnas.192461099 (2002).

214. Jankovic, D. *et al.* Conventional T-bet(+)Foxp3(-) Th1 cells are the major source of host-protective regulatory IL-10 during intracellular protozoan infection. *The Journal of experimental medicine* 204, 273–283; 10.1084/jem.20062175 (2007).

215. O'Garra, A. & Vieira, P. T(H)1 cells control themselves by producing interleukin-10. *Nature reviews. Immunology* 7, 425–428; 10.1038/nri2097 (2007).

216. Fessler, M. B. *et al.* Endogenous and Therapeutic 25-Hydroxycholesterols May Worsen Early SARS-CoV-2 Pathogenesis in Mice. *American journal of respiratory cell and molecular biology* 69, 638–648; 10.1165/rcmb.2023-0007OC (2023).

217. Klejbor, I. *et al.* EBI2 is expressed in glial cells in multiple sclerosis lesions, and its knock-out modulates remyelination in the cuprizone model. *The European journal of neuroscience* 54, 5173–5188; 10.1111/ejn.15359 (2021).

218. Matthias J *et al.* Sodium chloride is an ionic checkpoint for human TH2 cells and shapes the atopic skin microenvironment. *Science Translational Medicine* 11, 1–11; 10.1126/scitranslmed.aau0683 (2019).

219. Ying-Yin Chao *et al.* Human TH17 cells engage gasdermin E pores to release IL-1α on NLRP3 inflammasome activation, 295–308; 10.1038/s41590-022-01386-w (2023).

220. Uva, L. *et al.* Mechanisms of action of topical corticosteroids in psoriasis. *International journal of endocrinology* 2012, 561018; 10.1155/2012/561018 (2012).

221. Fujiyama, T. *et al.* Topical application of a vitamin D3 analogue and corticosteroid to psoriasis plaques decreases skin infiltration of TH17 cells and their ex vivo expansion. *The Journal of allergy and clinical immunology* 138, 517-528.e5; 10.1016/j.jaci.2016.03.048 (2016).

222. Lovato, P., Norsgaard, H., Tokura, Y. & Røpke, M. A. Calcipotriol and betamethasone dipropionate exert additive inhibitory effects on the cytokine expression of inflammatory dendritic cell-Th17 cell axis in psoriasis. *Journal of dermatological science* 81, 153–164; 10.1016/j.jdermsci.2015.12.009 (2016).

223. Liu, T., Zhang, L., Joo, D. & Sun, S.-C. NF-κB signaling in inflammation. *Signal transduction and targeted therapy* 2, 17023-; 10.1038/sigtrans.2017.23 (2017).

224. Gallais Sérézal, I. *et al.* A skewed pool of resident T cells triggers psoriasis-associated tissue responses in never-lesional skin from patients with psoriasis. *The Journal of allergy and clinical immunology* 143, 1444–1454; 10.1016/j.jaci.2018.08.048 (2019).

225. Honda, T. & Kabashima, K. Novel concept of iSALT (inducible skin-associated lymphoid tissue) in the elicitation of allergic contact dermatitis. *Proceedings of the Japan Academy. Series B, Physical and biological sciences* 92, 20–28; 10.2183/pjab.92.20 (2016).

226. Honda, T., Egawa, G. & Kabashima, K. Antigen presentation and adaptive immune responses in skin. *International immunology* 31, 423–429; 10.1093/intimm/dxz005 (2019).

227. Natsuaki, Y. *et al.* Perivascular leukocyte clusters are essential for efficient activation of effector T cells in the skin. *Nature immunology* 15, 1064–1069; 10.1038/ni.2992 (2014).

228. Kamenjarin, N. *et al.* Cross-presenting Langerhans cells are required for the early reactivation of resident CD8+ memory T cells in the epidermis. *Proceedings of the National Academy of Sciences of the United States of America* 120, e2219932120; 10.1073/pnas.2219932120 (2023).

7. Software References

7.1. R packages

pacman: Rinker, T. W. & Kurkiewicz, D. (2017). pacman: Package Management for R. version 0.5.0. Buffalo, New York. http://github.com/trinker/pacman

BiocParallel: Morgan M, Wang J, Obenchain V, Lang M, Thompson R, Turaga N (2022). _BiocParallel: Bioconductor facilities for parallel evaluation_. R package version 1.30.4, <https://github.com/Bioconductor/BiocParallel>.

DESeq2: Love, M.I., Huber, W., Anders, S. Moderated estimation of fold change and dispersion for RNA-seq data with DESeq2 Genome Biology 15(12):550 (2014)

apeglm: Zhu, A., Ibrahim, J.G., Love, M.I. Heavy-tailed prior distributions for sequence count data: removing the noise and preserving large differences Bioinformatics (2018)

sva: Leek JT, Johnson WE, Parker HS, Fertig EJ, Jaffe AE, Zhang Y, Storey JD, Torres LC (2022). _sva: Surrogate Variable Analysis_. R package version 3.44.0.

vsn: Wolfgang Huber, Anja von Heydebreck, Holger Sueltmann, Annemarie Poustka and Martin Vingron. Variance Stabilization Applied to Microarray Data Calibration and to the Quantification of Differential Expression. Bioinformatics 18, S96-S104 (2002).

dplyr: Wickham H, François R, Henry L, Müller K, Vaughan D (2023). _dplyr: A Grammar of Data Manipulation_. R package version 1.1.2, <https://CRAN.R-project.org/package=dplyr>.

stats: R Core Team (2022). R: A language and environment for statistical computing. R Foundation for Statistical Computing, Vienna, Austria. URL https://www.R-project.org/.

dfidx: Croissant Y (2022). _dfidx: Indexed Data Frames_. R package version 0.0-5, <https://CRAN.R-project.org/package=dfidx>.

ggplot2: H. Wickham. ggplot2: Elegant Graphics for Data Analysis. Springer-Verlag New York, 2016.

ggpubr: Kassambara A (2023). _ggpubr: 'ggplot2' Based Publication Ready Plots_. R package version 0.6.0, <https://CRAN.R-project.org/package=ggpubr>.

ggfortify: Yuan Tang, Masaaki Horikoshi, and Wenxuan Li. ‘ggfortify: Unified Interface to Visualize Statistical Result of Popular R Packages.’ The R Journal 8.2 (2016): 478-489. | Masaaki Horikoshi and Yuan Tang (2016).

ggfortify: Data Visualization Tools for Statistical Analysis Results. https://CRAN.R-project.org/package=ggfortify

pheatmap: Kolde R (2019). _pheatmap: Pretty Heatmaps_. R package version 1.0.12, <https://CRAN.R-project.org/package=pheatmap>.

rmarkdown: Allaire J, Xie Y, Dervieux C, McPherson J, Luraschi J, Ushey K, Atkins A, Wickham H, Cheng J, Chang W, Iannone R (2023). _rmarkdown: Dynamic Documents for R_. R package version 2.25, <https://github.com/rstudio/rmarkdown>. | Xie Y, Allaire J, Grolemund G (2018). _R Markdown: The Definitive Guide_. Chapman and Hall/CRC, Boca Raton, Florida. ISBN 9781138359338, <https://bookdown.org/yihui/rmarkdown>. | Xie Y, Dervieux C, Riederer E (2020). _R Markdown Cookbook_. Chapman and Hall/CRC, Boca Raton, Florida. ISBN 9780367563837, <https://bookdown.org/yihui/rmarkdown-cookbook>.

7.2. Python libraries

pandas: McKinney W, others. Data structures for statistical computing in Python. In: Proceedings of the 9th Python in Science Conference. 2010. p. 51–6.

numpy: Harris CR, Millman KJ, van der Walt SJ, Gommers R, Virtanen P, Cournapeau D, et al. Array programming with NumPy. Nature. 2020;585:357–62.

matplotlib: Hunter JD. Matplotlib: A 2D graphics environment. Computing in science & engineering. 2007;9(3):90–5.

seaborn: Waskom M, Botvinnik O, Kane D, Hobson P, Lukauskas S, Gemperline DC, et al. mwaskom/seaborn: v0.8.1 (September 2017) [Internet]. Zenodo; 2017. Available from: https://doi.org/10.5281/zenodo.883859

8. Acknowledgements

First of all, I want to thank Prof. Dr. Alexander Enk for allowing me to conduct my PhD thesis research in your institute and for being my supervisor. I am grateful for this opportunity and for the valuable discussions in the lab and during the TAC meetings.

I would also like to thank HBIGS, the Heidelberg Bioscience Graduate School, and personally, the people involved: Rolf Lutz, Sandara Martini, and Martina Galvan. You all have made all the administrative tasks a breeze and were kind and personal from the very beginning. I visited many courses and events organized by you and value all the effort that you put in to help us grow as PhD students. Especially the TAC meeting is a great asset in that.

I want to say special thanks to all the members of my TAC meeting. Prof. Dr. Ana Martin-Villalba, Prof. Dr. Viktor Umansky, and Prof. Dr. Alexander Enk. Thanks for making time for me and listening to my talks. Your scientific advice has been invaluable for the development of my thesis and your personal advice for my development as well. Also, thanks to Prof. Dr. Ana Martin-Villalba and Prof. Dr. Alexander Enk for taking over the responsibility of functioning as the first and second reviewer for my dissertation.

I also want to thank the animal caretakers in the IBF. You took a lot of responsibility and work off my shoulders and did a fantastic job. Especially the people in the KEB: Ulrike, Silvio, Ilona, and Svenja. You were always kind to me and looked after my mice. I could always ask for help and advice during experiments.

Next, I would like to thank the people in the clinic who have helped me gather the psoriasis patient skin samples. Prof. Dr. Knut Schäkel, you were a great help when I was writing my first ethics proposal. Thank you for your critical review and input. Many thanks also to Dr. Franziska Keidel and Dr. Mina Raahimi, you did most of the work in patient acquisition, informing, and sample taking. Thank you for all your effort, I really enjoyed our collaboration. I would also like to thank the surgeons and nurses who have helped me many times when I was in need of materials and especially in supplying me with healthy resected skin. Much of this work would not have been possible without you.

Many thanks also to my collaboration partners in Hannover. Tonia Bargmann, Valerie Beneke, and Klaudia Grieger, getting to know you during the DGfI and Fraunhofer events was really a coincidence. However, for some reason, I could convince you that EBI2 is an interesting target to look at and you were immediately ready to jump into the lab to do some science on it. Thank you so much for your valuable collaboration and for taking time for our uncomplicated and friendly meetings. Hope to see you back at some science events in the future!

I am also incredibly grateful to have worked in such a friendly lab. Thank you to all my colleagues for all the countless lunch breaks that I enjoyed so much. Thanks, Vanessa, for all the emotional support especially in our starting times, and the meme wall. I will take it with me and cherish it. Forever. Meme thanks also go out to Lisa, Sonja, and Yizhu. Thanks, Lisa, for all the valuable information about dogs and the cool BBQ parties. Thanks, Sophi for being

the best sports partner, I will especially remember our dodgeball session. Thanks also to Michi. You made so many lab and office days brighter and funnier. Thanks also for the countless brainstorming sessions about our projects, hang in there, you almost got it too! Get it? HANG in there, because you are a boulder nerd. Thanks also to Jin, our language discussions were always really fun, and you were a great desk neighbor, ganbatte! Thanks also to Karsten for organizing everything in the lab, for the help with mice, and some great discussions.

Special thanks to Sonja and Yizhu. We, the Kurschus Group, are small but maybe that is why we stick together so well. I will always remember all of us sitting there mincing mouse ears and chatting. Well, Yizhu and Sonja never at the same time but you get me. Thank you so much for your help in some of these crazy big experiments and for your input and critique. It has been amazing working with you both! Also, many thanks to our HiWis Nina, Greta, and Lena. You were all really bright students and your help with the genotyping was incredibly valuable. I really, really enjoyed our lab events like the Christmas markets every year and just us as the Kurschus group at Yangda and Vetter's. Thanks so much and best of luck in your further studies!

Moreover, I want to thank my family. Thank you, Mama, Papa, and Alicia, for your emotional support and bearing having your son/ brother hours of train ride away. Of course, you were with me from kindergarten, all the way through elementary school, high school, university, and now my PhD thesis. Thank you for everything you have done for me. I know I can always rely on you. Of course, big thanks also to Vivi. Thank you for being the best partner in crime. Traveling between Heidelberg, Rostock, and Leipzig sure was not easy and has put its mark on my PhD journey, but we made it work. Thanks for always looking out for me and for making the little bit of free time I had so special. The time of thesis writing was especially difficult but thanks to you and endless patience and good sleep through my nightly writing adventures, its finally over. Who would have thought that?

And Florian, you are the person who I would like to thank the most. First of all, thank you so much for being my wet lab supervisor and also my mentor. Of course, I learned from you how to do science, but you were also an incredible role model as a person. Your passion for science sure is contagious and I definitely caught some of it. Why else would I be so crazy to go continue as a PostDoc? You took care of my experiments by always having a critical look at my experimental plans, and sometimes even jumped back into the lab yourself. But you also took care of me as a person. Without you, long-distance would likely not have been possible in this way. You also never pushed me too hard and always believed in me, even in dark, dark, so very dark, times of data and PhD thesis. You allowed me to develop and pursue my own scientific interests and always supported me in everything I did. I would always come to you with so many ideas for the project and I do not remember a single 'No'. You also showed me that antibodies and chemicals can still work, even if you bought them 20 years and three labs ago, amazing. In all seriousness, thank you for everything you have done for me. Thank you for being such a great lab leader and mentor. And thank you for guiding me through my PhD thesis.